Errata

Page	Line†	for:	read:
Contents	3.2	'of the Approximation'	'of Approximations'
1.5	27	'on from calculational'	'on calculational'
2.1	17	'[Aitchson]'	'[Aitchison]'
3.1	45	'straight-forward'	'straightforward'
3.8	61	'which, acting on'	'which, when acting on'
3.10	22	'techniques which allows'	'techniques which allow'
3.11	43	'self-consitent'	'self-consistent'
3.13	40	'we have redefined'	'we have defined'
3.14	1	'a $p\frac{1}{2}$ orbital'	'a $p\frac{1}{2}$ pnc orbital'
3.17	27	'counter-part'	'counterpart'
4.2	23	'there by by prefixing'	'there by prefixing'
5.2	44	' + c^2 (β-I)'	' - c^2 (β-I)'
7.13	53	'inluding'	'including'
7.19	3	'systemmatic'	'systematic'
8.2	37	'were neglected'	'were neglected.'
8.13	25	'effectively doing are'	'effectively doing is'
8.15	55	'[Mckoy]'	'[McKoy]'
A.3	42	'$<\kappa_1 \mid C^k \mid \kappa_2>$'	'$<-\kappa_1 \mid C^k \mid \kappa_2>$'
A.5	12	'<v|a+>'	'$<v \mid a^+>$'
Credits	9	'was origianlly'	'was originally'
Credits	11	'was written by my'	'was written by myself'
References			
p1	28	'Bleany B.I., Bleany B.'	'Bleaney B.I., Bleaney B.'
p2	11	'Parpia *et al.*'....is out of order	

References Update

Amaldi U. *et al.*, 1987, *Phys Rev. D*, 36, 1385

Noecker M.C., Masterson B.P., Weiman C.E., 1988, *Phys. Rev. Lett.* , 61, 310

† single line spacing

The Theory of Parity Non-Conservation in Atoms

A.C. Hartley

Balliol College

Thesis submitted for the degree of Doctor of Philosophy in the University of Oxford

Hiliary Term 1989

ॐ परमात्मने नमः

अथ

'It is by standing on the shoulders

of giants that we see furthest'

A. Einstein

Whilst this thesis does not claim to see furthest it is hoped that it will at least provide a shoulder to stand on. It is dedicated to the never ending quest for understanding.

Abstract

A.C. Hartley
Balliol College

D.Phil.
Hilary 1989

The Theory of Parity Non-Conservation in Atoms

In this thesis we are concerned with calculating the parity non-conserving (PNC) E1 transition matrix elements for the caesium $6s_{\frac{1}{2}} \rightarrow 7s_{\frac{1}{2}}$ transition and the thallium $6p_{\frac{1}{2}} \rightarrow 7p_{\frac{1}{2}}$ and $6p_{\frac{1}{2}} \rightarrow 6p_{3/2}$ transitions using the Equations of Motion (EOM) formalism. We add the weak interaction Hamiltonian to derive the PNC EOM. Taking a subset of the EOM terms gives the Random Phase Approximation equations and their PNC counterpart. Solving these, we obtain good agreement with similar calculations by other groups.

In order to estimate correlation effects we use a parameterised semi-empirical potential which is adjusted to give the best fit with experimental data for the valence and excited state energy levels. Including the potential in the EOM and PNC EOM gives us very accurate values for the parity conserving transitions. For the PNC transitions we obtain

Caesium	$6s_{\frac{1}{2}} \rightarrow 7s_{\frac{1}{2}}$	$0.895\ (1\pm0.03) \times 10^{-11}\ (-iea_0Q_W/N)$
Thallium	$6p_{\frac{1}{2}} \rightarrow 7p_{\frac{1}{2}}$	$-7.85\ (1\pm0.05) \times 10^{-11}\ (-iea_0Q_W/N)$
Thallium	$6p_{\frac{1}{2}} \rightarrow 6p_{3/2}$	$-28.4\ (1\pm0.07) \times 10^{-11}\ (-iea_0Q_W/N)$

These are in very good agreement with the most extensive Many-Body Perturbation Theory calculations performed. Using our value for the caesium transition matrix element and the latest experimental results gives a value of $Q_W = -71.8 \pm 1.8 \pm 2.1$ where the first error is experimental and the second is theoretical. This corresponds to a value of the standard model $\sin^2\Theta_W = 0.230 \pm 0.009$ which is to be compared with the current world average value of 0.230 ± 0.005.

We investigate the single particle EOM terms that were not included in the above calculation and find that they are concerned with the Exclusion Principle violating terms that are implicitly included in an RPA calculation. Other terms represent the valence contribution to certain two particle effects. Since the main two particle terms have not been included however, these correction terms do not lead to a significant increase in the accuracy of the calculation.

Acknowledgements

First of all I must thank Pat Sandars my supervisor. He has managed to steer me successfully through a troubled start to my post-graduate career and through his knowledge and experience I have come to appreciate the subject enough to want to continue studying it after my D.Phil. His 'black box' approach to computing has meant that he is able to suggest all sorts of tests and pitfalls of the numerical calculations and which I would otherwise have over-looked. I look forward to many more years in collaboration and consultation with him.

Secondly I must thank Ann-Marie Martensson-Pendrill who was the original author of many of the programs that are used in this thesis. Her wealth of experience in the field of computational theoretical atomic physics has been of great help, especially when faced with one of the Professor's black-box tests! I hope to spend much fruitful time working with her on the relativistic pair equation. My thanks go also to Eva Lindroth for her help in her year here. She was a great help in providing a 'sounding board' for ideas that I wanted to try out before confronting the Professor with them.

Thanks must also go to Steve Blundell (though now he has defected to the 'other side') for teaching me the art of structured, disciplined programming. I feel that I have nearly earnt the award of SABCPP[†]. Also special thanks must go to 'wee Malkie' Macpherson as the lab computer guru. Without him I would never have come to terms with the intricacies of the world of autosketch, VW and QDOS. He has taught me many 'computing tricks' over the years so that I can 'write FORTRAN in any language'! He has also provided a very useful data base of diagrams and references which has made writing this thesis easier! I look forward to many more late night poker sessions with him so that he can take more of my money from me.

Special thanks go to Ms. Sandie Clemas who effectively runs this lab! She has put up with my constant interruptions to use her laser printer remarkably well. I have enjoyed many an hour spent gossiping with her in her room when I should be working. She has also given up her spare time to proof read 'my boring thesis'. I am greatly indebted to her.

Thanks must also go to all my colleagues in the Clarendon who provide such a pleasant work environment. Special thanks go to: Liz Boston for being such a tolerant room companion, for finding many vital flaws in my equations and for introducing me to Kung Fu!; Mark Plimmer whose enthusiasm and dedication to his subject has been an example to us all; Ken Zetie for sending me junk on the computer mail and all the other experimental people (though I've never quite understood what they actually do!) for making coffee and tea breaks so pleasant.

I would like to thank 'the gang' at the Manor, especially Lucy for looking after me during the difficult writing up period, everyone at Waterperry for keeping me sane and most of all my parents who have done so much for me without any thanks in return.

Lastly I would like to thank the SERC for my D.Phil. grant and the heads of department.

[†]The S.A. Blundell Certificate of Perfect Programming

Contents

Appendices

Layout of this Thesis

In this thesis we shall start in chapter one with an overview of parity non–conserving phenomena and show how their measurement can give important insights into the fundamental nature of the weak force. The different approaches to making parity measurements are discussed and comparisons between high energy methods and those of atomic physics are made. The need for accurate theory calculations to compliment precise experimental measurements is explained.

Chapter two gives a brief history of the theory of weak interactions leading up to the standard model. The chief points of the model are discussed and the nature of the Hamiltonian investigated with the most important contributing terms identified.

In chapter three we give the background to the atomic theory necessary for the calculation of the parity non–conserving electric dipole matrix elements. We also discuss how the spin independent PNC Hamiltonian can be included in the equations.

Chapter four gives a detailed discussion of the Equations of Motion method which is the particular approach that we have adopted in this thesis.

We discuss the numerical methods used for solving the derived equations in chapter five and we give the full radial equations used. The results are presented in chapter six and the limitations of the methods used so far are discussed.

In chapter seven we give a method for improving the calculations done so far in a simple, semi–empirical way. The results of this method are given.

In chapter eight the remaining terms from the Equations of Motion method that were disregarded as an initial approximation are discussed and the equivalent many–body perturbation theory terms given. The calculations are repeated with the terms added and the results are discussed.

Finally in chapter nine we give a summary of the work done in this thesis. We also discuss the results in the context of the other work done in this field and give the latest experimental and theoretical results obtained.

CHAPTER 1: Introduction to Parity Non-Conservation

1.1. Introduction

Physicists throughout the years have always been searching for fundamental principles and symmetries that simplify their understanding of the physical world. The idea that the basic laws of physics should remain unchanged when the co-ordinate system undergoes a parity transformation was a widely held belief until 1957 when [Wu] discovered a parity non-conserving (PNC) effect in Colbalt 60. It was observed that the angular distribution of β decay emitted electrons was not symmetric in the way that it should be if parity was conserved. It was this discovery of PNC in the weak force that was the impetus for the succession of experiments and calculations throughout the physics community. Even today, thirty two years later, they are still been carried out with as much importance being attached to them as ever.

The parity operator in quantum mechanics is an operator which changes the radial vector $\underline{r}$ to $-\underline{r}$, i.e. it amounts to a reflection through the origin of the co-ordinate system. Since the laws of physics are unchanged under a rotation (it is this symmetry law which leads to the conservation of angular momentum) and the parity operation is equivalent to a reflection in a plane and a rotation it is often described as being merely the operation of a reflection in a plane. The parity of a function is how it behaves under this transformation: if the function (e.g. a wavefunction) just has a sign change but is otherwise the same (e.g. $\underline{r}$) then it is said to have a parity of minus one; if it is unchanged (e.g. $|\underline{r}|$) then plus one; if it is neither of these then it is not an eigenfunction of the parity operator.

How various physical properties change under a parity transformation can easily be worked out. Polar vectors such as $\underline{r}$ have parities of -1. Since velocity is the differential of $\underline{r}$ with respect to time then that has a parity of -1 also, as will linear momentum. Axial vectors, such as angular momentum which is given by $\underline{l} = \underline{r} \times \underline{p}$, will not change under parity as both the constituent vectors change. Scalar quantities might or might not change: $\underline{p} \cdot \underline{p}$ will not change whereas $\underline{p} \cdot \underline{l}$ will change. Quantities of this type are called pseudo-scalars. In table 1.1 we give the transformation properties of various physical quantities.

Table 1.1

Transformation Properties Under Parity

Quantity	Under P	
$\underline{r}$	$-\underline{r}$	Vector
$\underline{p}$	$-\underline{p}$	Polar Vector
$\underline{\sigma}$	$\underline{\sigma}$	Axial Vector
$\underline{E}$	$-\underline{E}$	($= \partial V/\partial \underline{r}$)
$\underline{B}$	$\underline{B}$	as for $\underline{\sigma}$
$\underline{\sigma}.\underline{B}$	$\underline{\sigma}.\underline{B}$	Magnetic Dipole Moment
$\underline{\sigma}.\underline{E}$	$-\underline{\sigma}.\underline{E}$	Electric Dipole Moment
$\underline{\sigma}.\underline{p}$	$-\underline{\sigma}.\underline{p}$	Longitudinal Polarisation
$\underline{\sigma}.(\underline{p}_1 \times \underline{p}_2)$	$\underline{\sigma}.(\underline{p}_1 \times \underline{p}_2)$	Transverse Polarisation

If there are no parity violating phenomena associated with an experiment, say, then one would expect there to be a mirror symmetry to the system: i.e. the mirror image of the experiment and its results are physically correct. The presence of a parity violating effect associated with the weak force will manifest itself as an asymmetry in the layout. For example the presence of the weak force can lead to optical rotations of the plane of polarised light passing through heavy metal vapours. The mirror image of this experiment would produce a rotation in the opposite direction to the observed one and the mirror image result would not constitute a physically possible outcome in a real experiment.

1.2 The Standard Model: Motivation for the Experiments

What is being sought in physics at the moment is a theory that unifies the four fundamental forces in nature (strong, electro-magnetic, weak and gravity). The Glashow-Weinberg-Salam model or 'standard model' as it is usually referred to, has managed to unify the weak and the electro-magnetic forces. Though all the evidence so far accumulated does not contradict the standard model it has by no means been fully tested and there are other models and theories which could equally well be correct. More fundamental theories than the standard one which attempt to unify all the forces are currently being worked on. For example quantum chromo-dynamics (QCD) deals with the strong force; one theory which attempts to unify all the forces is string theory, but there are other contenders. All these theories make predictions which have to be tested; what is needed are measurements of the physical constants that are predicted by the models to as great a precision as possible.

The origin of the PNC nature of the weak force is dealt with in detail in chapter two. The basic principle is the requirement of gauge invariance under the $SU(2) \otimes U(1)$ gauge transformation which leads to the electro-weak Hamiltonian. There are four intermediate fields involved which are required to avoid unphysically large reaction cross sections and renormalisation problems: two charged particles W^+ and W^-, a neutral Z^0 and the photon field $A\mu$. The three basic fundamental parameters that determine the masses of the W's and Z's and the interaction coupling strengths are the mixing angle Θ_W, the Fermi constant G_F and the electric charge e.

These have to be determined experimentally.

Most tests and experiments on weak force phenomena are done using high energy particle techniques which are described in the next section. However these tests are all carried out at high momentum transfers or q's and these methods cannot test the low q end of the reactions. This is where atomic physics comes in. Within an atom there will be weak force interactions between the electrons and between the electrons and the nucleus. The relative sizes of these interactions are dealt with in chapter two. By the nature of the main interaction Hamiltonian the observable effect of this will be to mix each orbital with a small amount of wavefunction with opposite parity. The mechanism of this is dealt with in chapter three. Since these effects are of minute size compared to normal atomic interactions, which are all electro-magnetic, one might think that these weak force effects could not be measured in practice. But they can be distinguished from the electro-magnetic interactions because of their PNC property and certain ingenious experiments have been devised to obtain measurements of their magnitude. However the nature of the experiments are such that the information about the fundamental physical constants cannot be obtained directly from what is measured. What is also needed is a theoretical matrix element. It is the calculation of these matrix elements that this thesis is primarily concerned with.

1.3 The Weak Force Experiments

1.3.1. High Energy Tests

1. The existence of the neutral Z^0 currents has been specifically looked for using neutrinos at CERN [Hasert *et al.*]. The signature for these type of reactions is the absence of charged leptons in the final state. Both pure leptonic reactions of this type and semi-leptonic ones involving hadrons were observed.
2. The PNC nature of the weak force was observed using deep inelastic scattering of left- and right-circularly polarised electrons from hydrogen and deuterium targets at SLAC [Prescott *et al.*] The parity violating asymmetry in the cross sections for the two polarisations was measured and found to be consistent with a value of $\sin^2 \theta_W = 0.224 \pm 0.02$.

3. W and Z bosons have recently been produced directly at CERN ([Rubbia *et al.*]) by colliding a 270 GeV/c proton beam with a similar anti-proton beam and looking for the leptonic decay of the resulting boson. Some 100 such charged events have been observed and 17 neutral ones. The resulting masses for the M_W and M_Z are in excellent agreement with those obtained from the standard model using the value of $\sin^2 \theta_W$ obtained in 2 above. Alternatively, using the masses to determine $\sin^2 \theta_W$ gives 0.226 ± 0.0015 and 0.216 ± 0.01 from two separate experiments that were performed.
4. In the near future a new e^+e^- collider at LEP will come on line that should produce a more accurate value for $\sin^2 \theta_W$ than has been hitherto obtained.

1.3.2 The Atomic Physics Tests

Obviously there can be no direct measurements of the weak force in the atom. However the presence of this force can be detected due to the PNC nature of the Hamiltonian. Interactions principally between the nucleons and the electrons that involve the Z^0 boson produce parity-mixed orbitals so that dipole transitions that would nominally be parity forbidden do in fact occur with very small amplitudes. All atomic physics experiments rely on interference between the parity forbidden transition and parity allowed ones; one usually looks at M1 transitions that acquire PNC E1 amplitudes because the former are intrinsically of smaller amplitude than E1 transitions by a factor of order α. There are two main approaches to measuring this effect experimentally: optical rotation experiments and fluorescence experiments. The experimental details will be discussed in chapter nine. The current atomic PNC experiments are all on high Z atoms: this is because of the approximately Z^3 enhancement of PNC effects, first pointed out by [Bouchiat and Bouchiat 1974].

Due to the small size of the weak force the effect will be linear in the weak charge Q_W, a parameter first used by [Bouchiat and Bouchiat 1974] to quantify the strength of the force. Q_W is a function of θ_W and it is the determination of the value of Q_W and hence θ_W that atomic PNC experiments are concerned with. Because the PNC effects are linear in Q_W they can be written as Q_W multiplied by an atomic structure factor. It is not possible to determine this structure factor

experimentally, one can only measure the overall effect. Therefore in order to obtain a value for Q_W the atomic part of the PNC E1 matrix element has to be calculated. This is the role of the theoretical calculations in the atomic PNC determination of Θ_W. This thesis is concerned with the calculation of E1 PNC matrix elements for the caesium $6s_{\frac{1}{2}}$ to $7s_{\frac{1}{2}}$ transition and for the thallium $6p_{\frac{1}{2}}$ to $7p_{\frac{1}{2}}$ and $6p_{\frac{1}{2}}$ to $6p_{3/2}$ transitions.

There are some other experiments that are possible that do not rely on the atomic theory. Atomic hydrogen and deuterium are exactly calculable in theory so the only errors in the determination of Θ_W will be experimental ones. The experiments are concerned with the PNC $2s_{\frac{1}{2}}$ to $1s_{\frac{1}{2}}$ transition; the parity mixing of the upper state with the $2p_{\frac{1}{2}}$ orbital is greatly enhanced by the near degeneracy of the two states which leads to a large energy denominator in the expression for the mixing coefficient. The use of magnetic fields to shift the energy levels can further enhance this effect (see [Hinds]). Unfortunately there is no work on this experiment at present.

Another way of obtaining a measurement less dependent on from calculational uncertainties has been proposed for samarium ([Davies]) which has the possibility of anomalously close levels of opposite parity and the advantage of a high Z (see chapter two). There are ten isotopes on which a series of measurements could be made. By forming ratios of the optical rotations obtained the contribution of individual nucleons could be obtained and most of the atomic theoretical uncertainties could be removed.

As is shown in appendix four one can treat the weak force coupling constants as model independent parameters which are to be determined empirically. Experimental determination of the relationships between the up and down quark constants can be made for both atomic and high energy physics. The constraints on the possibilities as determined by atomic physics experiments are almost orthogonal to those of the high energy determinations. This is an added justification for atomic approach to PNC measurements as well as the high energy one.

At the moment the experimentalists are ahead of the theoreticians as far as errors are concerned: the latest atomic PNC experiment claims an accuracy of only 2% [Noecker *et al.*] and other experiments are at less than 10%, whereas the best theory is at about 5% though one group has claimed a 2% error for caesium. The

current status of the PNC experiments and the theory calculations will be reviewed in chapter nine.

1.4 Conclusion

Although the existence of PNC phenomena has now been well established the standard model for the electro-weak interaction has not yet been fully tested, though no evidence so far has contradicted it. The fundamental constant that determines the strength of the interactions and the masses of the intermediate vector bosons, Θ_W, has still to be measured with precision. Atomic physics provides a valuable test of electro-weak theory at very low energies but in order to do this it needs not only an experimental measurement but also a theoretical calculation of the PNC E1 transition matrix element. For a comprehensive review of the current status of the standard model tests see [Almaldi *et al*].

CHAPTER 2: Background to the Electro-Weak Theory

2.1 Introduction

To give a full description of the standard model (as first proposed by [Weinberg], [Salam], [Glashow]) and its derivation would require the full machinery of quantum field theory and would be outside the scope of this thesis. However in this chapter we give a brief history of weak interaction theory culminating with the unification of the electro-magnetic and weak forces in the standard model. For a more detailed description readers are referred to e.g. [Aitchison and Hey] and the references therein.

2.2 The Fermi Weak Interaction Theory

The first theory to explain the weak processes of β decay and K capture was proposed by [Fermi] in 1934. It successfully accounted for the changes in the numbers of protons and neutrons within the atom and also hypothesised the existence of the neutrino: a massless particle that was required to balance the energies in the equations. The interaction was considered to occur at a single space-time point (see figure 2.1)

$$n \rightarrow p + e^- + \bar{\nu} \qquad \beta \text{ decay} \qquad (2.1)$$

$$p + e^- \rightarrow n + \nu \qquad \text{K capture} \qquad (2.2)$$

The Hamiltonian was of the form

$$H = G_F \sum_i C_i \, (\bar{\Psi}_p \, \Gamma_i \, \Psi_n) \, (\bar{\Psi}_e \, \Gamma_i \, \Psi_\nu) \qquad (2.3)$$

where the Γ_i's are products of γ matrices describing the five possible interactions of the form scalar, vector, axial-vector, tensor and pseudoscalar and the C_i's are their associated coupling constants which give their relative strengths. G_F is the Fermi coupling constant which gives the overall size of the weak interaction. Its value has been accurately determined from muon lifetime measurements and equals $(1.16634 \pm 0.00002) \times 10^{-5}$ GeV^{-2} (see Review of Particle Properties 1980) which accounts for the 'weakness' of the force. Angular correlation experiments which measured the direction of emission of an electron and its recoiling nucleus later

Figure 2.1. Point-Like Fermi Weak Interaction

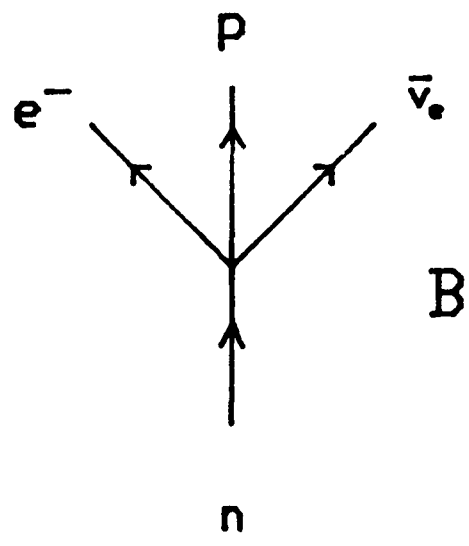

Beta Decay

Figure 2.2. Intermediate Vector Boson Diagram

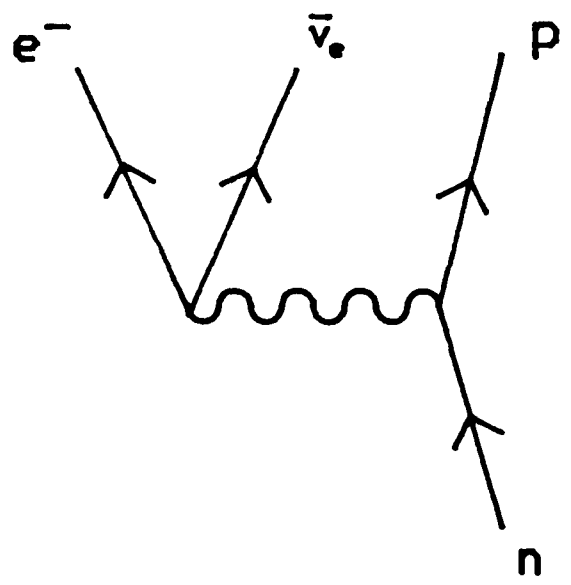

Beta Decay

showed that only the vector and axial-vector interactions had non-zero coupling constants.

With the proposal ([Lee,Yang]) and subsequent detection ([Wu]) of parity violation in the β decay of ^{60}Co it was shown that there was a fundamental difference between the electro-magnetic force and the weak one in that the former did not violate parity whereas the later one could. A series of celebrated experiments (see [Perkins]) demonstrated that only the negative 'left-handed' helicity state of the neutrino participates in the weak interaction. It was also shown that the charged weak interaction currents are vector and axial-vector in nature only. The interaction Hamiltonian was therefore modified to take this into account ([Macpherson]).

$$H = \frac{G_F}{\sqrt{2}} \left\{ \Psi_p \gamma_\mu \left(1 - \frac{C_A}{C_V} \gamma_5\right) \Psi_n \right\} \left\{ \Psi_e \gamma^\mu (1 - \gamma_5) \Psi_\nu \right\} \qquad (2.4)$$

The $(1 - \gamma_5)$ terms acts as a left-handed projection operator so that the lepton interaction only couples to left-handed leptons. The C_A and C_V refer to the relative strengths of the vector (V) and axial-vector (A) interactions. Their ratio is -1.26 so that both handed nucleons may interact.

2.3 Violation of Unitarity

It can be shown (see e.g. [Aitchison and Hey] p147) that the scattering cross section of the interaction has a dependence on E given by

$$\sigma_F \sim G_F{}^2 \, E^2 \qquad (2.5)$$

where E is the centre of mass energy of the interaction. The trouble with this is that there is an upper limit on the allowable cross section for a point-like interaction which is proportional to the de Broglie wavelength squared and at high energies the expression in (2.5) exceeds this. Thus unitarity would be violated by equation (2.5).

2.4 Addition of a Propagator Term to the Interaction

In order to cure this problem of the high energy violation of unitarity the idea of an intermediate virtual particle was proposed in analogy with the extremely successful quantum electro-dynamics (QED) theory which has a virtual photon propagator.

Whereas the photon is massless so that the electro-magnetic force has an infinite range, the weak force one would necessarily have to be massive and of spin one to preserve the V-A nature of the interaction (see figure 2.2). The cross section is now given by ([Macpherson])

$$\sigma_F = \frac{G_F^2\, q^2}{\pi} \frac{M_W^2}{(q^2 + M_W^2)} \rightarrow \frac{G_F^2\, M_W^2}{\pi} \quad \text{as } q \rightarrow \infty \qquad (2.6)$$

where q is the momentum transfer of the interaction. Thus the unitarity violation has successfully been removed. The interaction strength at each vertex is expressed in terms of a dimensionless weak coupling constant g_W in analogy with QED. By matching the low energy behaviour with the old theory the relationship between the G_F and g_W can be found:

$$\frac{G_F}{\sqrt{2}} = \left[\frac{g_W}{M_W} \right]^2 \qquad (2.7)$$

However even this modified theory has problems, though they only occur at higher orders. Certain diagrams such as those in figure 2.3 still diverge at high energies. The method of dealing with this is gauge invariance.

2.5 Gauge Invariance

Gauge invariance, i.e. that the physics of a system should remain unaltered if the Hamiltonian undergoes a gauge transformation (see [Aitchison and Hey]) has been very successfully applied to QED. In the case of the electro-magnetic field $A_\mu(x)$ the gauge transformation

$$A_\mu(x) \rightarrow A_\mu(x) + \partial_\mu f(x) \qquad (2.8)$$

leads to a corresponding phase transformation in the Dirac field

$$\Psi(x) \rightarrow \Psi(x) e^{-ief(x)} \qquad (2.9)$$

Under such a transformation (known as a local gauge transformation) the 'physical fields' $\underline{E}$ and $\underline{B}$ and hence the observable physics of the system, remain unchanged.

Instead of making a gauge transformation and observing the effect on the system one can require that the system be invariant with respect to local gauge

Figure 2.3 Diagrams That Show High Energy Divergence

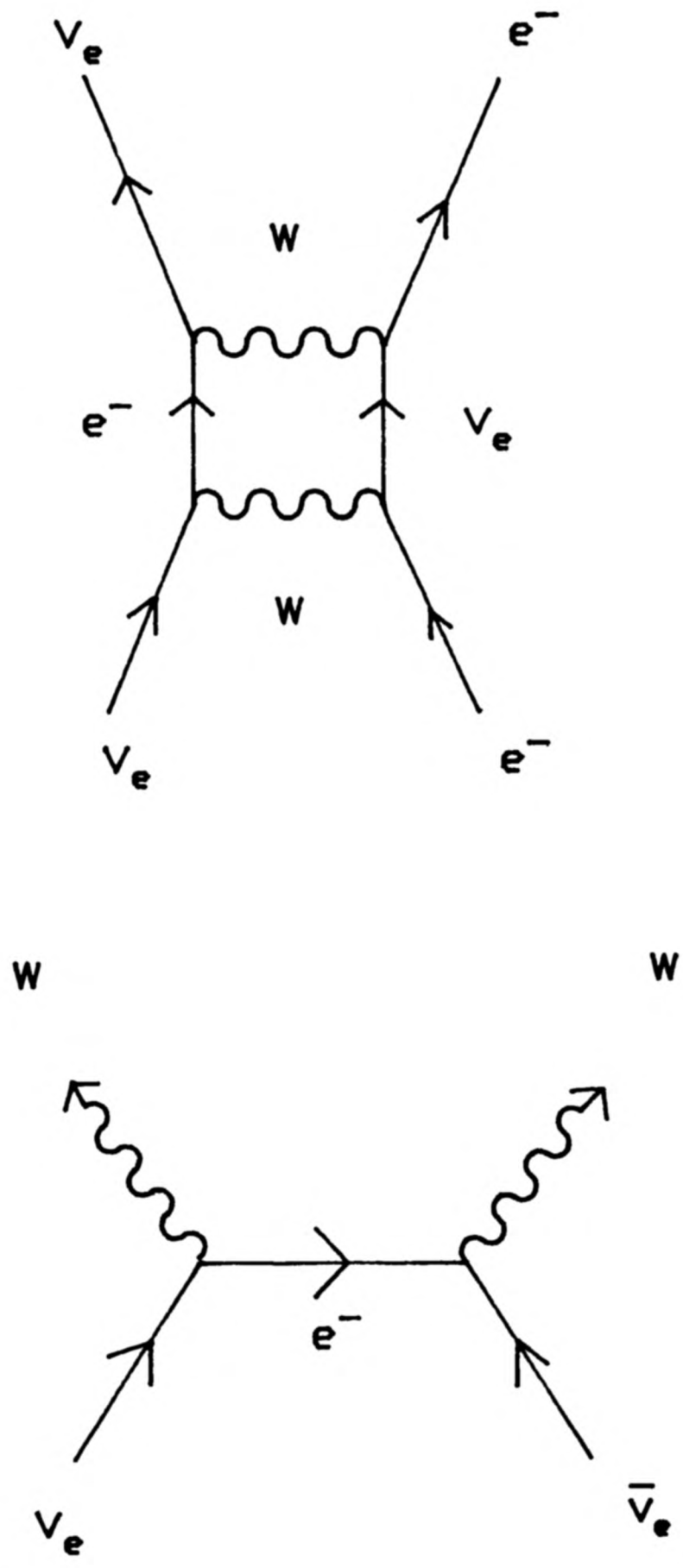

transformations. This leads to the requirement of the compensating field $A^{\mu}(x)$ in the free particle Dirac equation such that

$$\partial^{\mu} \rightarrow \partial^{\mu} + ieA^{\mu}(x) \qquad (2.10)$$

This compensating field that ensures local gauge invariance gives the electro-magnetic interaction in QED.

2.6 The Standard Model

In analogy with the previous section the standard model requires gauge invariance within the more general transformation group of [SU(2) ⊗ U(1)]. This will, as before, give rise to compensating fields in the expression for the differential operator.

$$\partial^{\mu} \rightarrow \partial^{\mu} + ig\, \underline{\tau}.\underline{W}^{\mu}(x) + ig'y\, B^{\mu}(x) \qquad (2.11)$$

The new fields are three vector fields $\underline{W}^{\mu}$ and a scalar field B^{μ}. $\underline{\tau}$ is the weak isospin and y the weak hypercharge (in analogy with their strong interaction counterparts). There are three fermion leptons associated with the weak force: the electron, muon and tauon. Each has an associated neutrino ν_e , ν_μ and ν_τ. In addition there are six quarks which come in isospin doublets: up and down; strangeness and charm; truth and beauty. Each particle can have an anti-particle as well which is identical apart from having the opposite charge. Due to the fact that handedness has to be taken into consideration, the particles have a left or right handedness assigned to them. Only left-handed particles have a non-zero isospin and can hence couple to the $\underline{W}$ fields.

Table 2.1 The Electro-Weak Family of Particles and theirWeak Quantum Numbers

Particle and Handedness	τ	τ_3	y	q $(=y+\tau_3)$
$\begin{bmatrix} \nu_e \\ e^- \end{bmatrix}_L$ $\begin{bmatrix} \nu_\mu \\ \mu^- \end{bmatrix}_L$ $\begin{bmatrix} \nu_\tau \\ \tau^- \end{bmatrix}_L$	$\frac{1}{2}$	$+\frac{1}{2}$ $-\frac{1}{2}$	$-\frac{1}{2}$	0 -1
$\begin{bmatrix} u \\ d \end{bmatrix}_L$ $\begin{bmatrix} s \\ c \end{bmatrix}_L$ $\begin{bmatrix} t \\ b \end{bmatrix}_L$	$\frac{1}{2}$	$+\frac{1}{2}$ $-\frac{1}{2}$	1/6	2/3 -1/3
e^-_R μ^-_R τ^-_R	0	0	-1	-1
$\begin{bmatrix} u \\ d \end{bmatrix}_R$ $\begin{bmatrix} s \\ c \end{bmatrix}_R$ $\begin{bmatrix} t \\ b \end{bmatrix}_R$	0	0	2/3 -1/3	2/3 -1/3

There are still problems with infinities: the theory is only renormalisable (infinity free) as it stands if the intermediate W's are massless so that they clearly cannot be the propagator terms that were introduced earlier. However, as shown by Higgs', they can acquire mass via a mechanism known as spontaneous symmetry breaking which is brought about by the inclusion of an additional gauge boson, the Higgs boson (see [Aitchison and Hey]). This theory with its five gauge particles is renormalisable and preserves gauge invariance.

The addition of the Higgs boson as well as creating the masses of the particles also produces mixing of the neutral gauge fields $W^0{}_\mu(x)$ and $B_\mu(x)$. The mixing angle is the all important electro-weak parameter the Weinberg angle θ_W.

$$\begin{aligned} Z^0{}_\mu(x) &= \cos\theta_W \; W^0{}_\mu(x) - \sin\theta_W \; B_\mu(x) \\ A_\mu(x) &= \sin\theta_W \; W^0{}_\mu(x) + \cos\theta_W \; B_\mu(x) \end{aligned} \qquad (2.12)$$

Thus the actual physical particles that result are the two charged W particles, the neutral Z^0 and the virtual photon field $A_\mu(x)$. The coupling strengths g and g' are related by

$$\tan\theta_W = \frac{g'}{g} \qquad (2.13)$$

and the masses of the W and Z particles by

$$\cos \theta_W = \frac{M_W}{M_Z} \tag{2.14}$$

Re-writing the covariant differential operator using equations (2.12) and (2.13) and the relationship between hypercharge and charge q we obtain

$$\partial\mu + ig(\tau_1 W\mu_1 + \tau_2 W\mu_2) + \frac{ig}{\cos\theta_W}(\tau_3 - q\sin\theta_W)\, Z\mu_0 + i\, g\, \sin\theta_W\, A\mu \tag{2.15}$$

The second term is the charged weak current interaction involving the W^+ and W^- particles, the third term is the neutral weak current interaction involving the Z^0 and the last term is the electro-magnetic interation term so that we immediately obtain the relationship that

$$e = g \sin \theta_W \tag{2.16}$$

By examining the expression for charged current interactions such as

$$\nu_\mu + e^- \rightarrow \mu^- + \nu_e \tag{2.17}$$

in the limit of low q^2 dependence we can compare the resulting expression with that obtained using the Fermi point-like interaction. Thus we obtain an expression relating G_F to the coupling strength g and the mass of the W intermediate boson.

$$\frac{G_F}{\sqrt{2}} = \frac{g^2}{8 M_W^2} \tag{2.18}$$

Comparing this with (2.7) we see that the same form is obtained with a rescaled coupling constant.

There are still problems with the standard model in the way the masses enter the theory. However it goes a long way towards the unification of the weak and electro-magnetic forces.

2.7 Summary of the Standard Model

The standard model comes about by requiring invariance under the gauge transformations of the SU(2) ⊗ U(1) group. This introduces four compensating fields. These fields acquire mass via spontaneous symmetry breaking which also mixes the

neutral fields so that we have two charged particles W^+ and W^-, a neutral Z^0 and the photon field $A\mu$. The field strengths are governed by three fundamental parameters e, G_F and Θ_W which have to be determined experimentally

2.8 The Neutral Current Interaction Term in the Atom

The weak force term in the modification of $\partial\mu$ (2.15) which does not involve charged propagators in lowest order and therefore does not change the chemical nature of the atom is the neutral current term. To obtain the Hamiltonian the replacement (2.15) is made in the free particle Dirac equation to give the neutral current interaction term:

$$-i\ \gamma_0\ \gamma_\mu\ \frac{i\ g}{\cos\Theta_W}\ (\ \tau_3\ -\ q\ \sin\Theta_W\ )\ Z^\mu{}_0 \qquad (2.19)$$

We are going to include this term in our atomic Hamiltonian. The effect of the $Z^\mu{}_0$ is replaced by the intermediate vector boson propagator multiplied by the transition current of the other particle (so we have for example a nucleon and an electronic interaction current). Since the effect of the τ_3 term depends on the handedness of the electrons, projection operators for the two handednesses should be used:

$$P_{L/R} = \tfrac{1}{2}\ (\ 1\ \pm\ \gamma_5\ ) \qquad (2.20)$$

where the plus sign gives the left-handed projector and the minus the right. Thus we shall get terms of two types: those with γ_μ in which are the vector terms; those with $\gamma_\mu\gamma_5$ in which are the axial vector terms. Since we require terms that are of negative overall parity we shall only keep terms that are vector in one interaction current and axial-vector in the other. At the atomic energies that we are interested in the q^2 dependence of the propagator has negligible effect and the interaction can be considered to be point-like. The interaction matrix element will therefore look like:

$$\frac{G_F}{2\sqrt{2}} \sum_{e,n} \Big[(\bar{e}|\gamma_\mu\gamma_5|e)\,(C_{1p}\ (\bar{p}|\gamma^\mu|p) + C_{1n}\ (\bar{n}|\gamma^\mu|n))$$

$$+ \quad (\bar{e}|\gamma_\mu|e)\ \ (C_{2p}\ (\bar{p}|\gamma^\mu\gamma_5|p) + C_{2n}\ (\bar{n}|\gamma^\mu\gamma_5|n))$$

$$+ \quad C_{3e}\ (\bar{e}|\gamma_\mu\gamma_5|e)\ (\bar{e}|\gamma^\mu\gamma_5|e) \quad \Big] \qquad (2.21)$$

where the e, p and n stand for the electron, proton and neutron wavefunctions respectively and the sum is over all electrons amd nucleons in the atom. By explicitly inserting the isospin and charge quantum numbers for each handedness of the interacting particles and rearranging the terms as products of vector and axial-vector interactions and comparing the coefficients with above we obtain the standard model predictions for the coupling constants. We have given their values below where radiative corrections have been included (these are of order of 10% [Lynn]) and quark-quark strong effects (which gives rise to the factor of 1.25 in some of the expressions); the value of $\sin^2\Theta_W \approx 0.23$.

$$\begin{aligned}
C_{1p} &= \quad\quad (1 - 4\sin^2\Theta_W)(1-\Delta r) + \Delta C_{1p} \simeq \quad 0.05 \\
C_{1n} &= \quad -1(1-\Delta r) \quad\quad\quad\quad\quad + \Delta C_{1n} \simeq -0.5 \\
C_{2p} &= -1.25\ (1 - 4\sin^2\Theta_W)(1-\Delta r) + \Delta C_{2p} \simeq -0.05 \qquad (2.22) \\
C_{2n} &= \quad 1.25\ (1 - 4\sin^2\Theta_W)(1-\Delta r) + \Delta C_{2n} \simeq \quad 0.05 \\
C_{3e} &= \quad\quad (1 - 4\sin^2\Theta_W)(1-\Delta r) + \Delta C_{3e} \simeq -0.05
\end{aligned}$$

In these expressions the subscripts $_{1-3}$ refer to the nature of the interaction: $_1$ means that the nucleon interaction is V in nature (with A type electronic interaction), $_2$ refers to the nucleon A and electronic V interaction and $_3$ is the electron-electron interaction. The first two terms in (2.21) are referred to as the spin independent and spin dependent terms respectively for reasons which we shall now investigate.

2.9 The Spin Independent Term

This is the term which is vector in nature in the nucleon bracket and axial-vector in the electronic bracket.

$$\sum_{e,n} (\Psi^{\dagger}_{e1}\ \gamma_0\ \gamma_\mu\ \gamma_5\ \Psi_{e2}).(\Psi^{\dagger}_{n1}\ \gamma_0\ \gamma^\mu\ \Psi_{n2})d\tau \qquad (2.23)$$

where the n's represent the nucleons and the e's are the electrons. The γ_μ has four components: a time-like component and three space-like ones that correspond to the vector $\underline{\alpha}$ multiplied by the Dirac matrix β. (We are using the notation of [Aitchison and Hey] Appendix D). Dividing the interaction up into its component parts we obtain:

$$\sum_{e,n} (\Psi^{\dagger}_{e1}\ \gamma_5\ \Psi_{e2}).(\Psi^{\dagger}_{n1}\Psi_{n2}) \quad - \quad (\Psi^{\dagger}_{e1}\ \underline{\alpha}\ \gamma_5\ \Psi_{e2}).(\Psi^{\dagger}_{n1}\ \underline{\alpha}\ \Psi_{n2}) \qquad (2.24)$$

We only require the first term because the second term is of even parity in the electronic part and so will not be detectable by atomic physics experiments. The subscripts $_1$ and $_2$ refer to the final and initial states in the interaction respectively. In the first term the initial and final nucleon states will be the same and the nucleon product is equivalent to a nucleon density which can be normalised to have a unit integral over all space.

With the nucleon product written as a nuclear density the nucleons will act coherently within the nucleus and the sum over the nucleons will be simply additive. Defining Q_W, the weak charge (as first done by [Bouchiat and Bouchiat 1974]) by

$$Q_W = Z\ C_{1p} + N\ C_{1n} \qquad (2.25)$$

and including all the multiplicative constants we finally obtain for the spin independent term

$$H_{spin\ indep.} = \frac{G_F\ Q_W}{2\sqrt{2}}\ \gamma_5\ \rho_n(r) \qquad (2.26)$$

where we have defined (N+Z) $\rho_n(r)$ to be the actual nuclear mass density.

A few things to note about equations (2.25) and (2.26)

1. By comparing the values of C_{1p} and C_{1n} it can be seen that the main contribution comes from the neutron interaction (because $1-4\sin^2\theta_W \simeq 0$) and Q_W approximately equals the number of neutrons in the nucleus.
2. As first pointed out by [Bouchiat and Bouchiat 1974] the spin-independent matrix element has a Z^3 dependence. The three contributions to this are:

   1: Q_W is approximately proportional to N which ~ 3Z/2 for heavy atoms

   2: The matrix element is proportional to the density of the electronic wavefunction at the origin which is proportional to Z for heavy atoms

   3: The matrix element is proportional to the velocity of the electron at the origin which gives an additional factor of Z
3. The γ_5 matrix swaps the parity of the upper and lower components (see chapter three) but does not effect the j value so that the effect is to mix $s_{\frac{1}{2}}$ and $p_{\frac{1}{2}}$ states. The amount of mixing of other orbitals, again diagonal in j, is very small due to their small amplitude at the nucleus.
4. The weak charge can be written as a function of the coupling parameters C_{1u} and C_{1d} which can be treated as model independent parameters to be determined (see Appendix 4). The standard model predicts them as functions of θ_W.

2.10 The Spin Dependent Term

The spin dependent term is so called because, unlike the spin independent term it does not scale with Z due to the weak charge, but depends on the nuclear spin which remains roughly constant across the periodic table and is only non-zero for nuclei with spin $I \neq 0$. The coupling constants are also far smaller due to the fact that $(1 - 4 \sin^2\theta_W)$ is about 0.1 times the spin independent contribution constant. As shown by [Flambaum *et al.* 1980] and [Novikov *et al.* 1977] the spin dependent term can be written approximately for a single particle as

$$H_{\text{spin dep.}} = \frac{G_F}{2\sqrt{2}} \mu_W \cdot \underline{\alpha}\, \delta^3(\underline{r}) \qquad (2.27)$$

where μ_W is the weak magnetic moment in analogy with the hyperfine interaction.

The spin dependent term can mix states with J's that differ by one so that it is possible to enhance its effect over the spin independent one by working with near degenerate levels of opposite parity with different J's.

2.11 The Electron–Electron Interaction

The non–relativistic reduction of the electron–electron interaction is

$$H_{ee} = -\frac{G_F\, C_{3e}}{2\sqrt{2}} \left(\underline{\sigma}_1 - \underline{\sigma}_2 + i(\underline{\sigma}_1 \times \underline{\sigma}_2).(\underline{p}_1 - \underline{p}_2)\, \delta^3(\underline{r}_1 - \underline{r}_2) + h.c. \right) \tag{2.28}$$

It involves a point–like interaction between two electrons that exchange a Z^0. The coupling constant is of the same order of magnitude as the spin dependent term. We shall not consider it further.

2.12 Anapole Moments

Within the nucleus there can be interactions between the nucleons that involve the exchange of the charged intermediate vector bosons W^+ and W^- as well as the Z_0. This leads to parity mixed nuclear orbitals which can then interact with the electrons via the usual virtual photon field to produce parity mixing in the electronic space. Such effects are attributed to what has been termed the nuclear anapole moment because of the nature of its current distribution. It is thought that the contributions from these anapoles are of the same order of magnitude as the spin dependent term and the electronic Hamiltonian is identical. For more details see [Flambaum *et al.* 1984].

2.13 Summary of Atomic PNC Effects

The spin independent term is the main electro–weak PNC effect that can be observed in an atom, partly due to the larger value of its coupling constant and partly due to the fact that in heavy atoms it has a Z^3 dependence. The other effects are about two orders of magnitude smaller than the spin independent effect and we shall not consider them further in this thesis.

The spin independent term is proportional to the weak charge Q_W which is given by the standard model as a function of Θ_W. It is also proportional to a nuclear density (mainly the neutron density as the C_{1n} coupling constant is the main contributor to Q_W). The Hamiltonian mixes states of the same J but opposite parity. This leads to parity mixed electronic wavefunctions in the atom.

CHAPTER 3: Background Atomic Theory

3.1. Introduction

The purpose of this chapter is to give a brief description of the background atomic theory behind the calculations undertaken in this thesis. For a hydrogenic system, the Dirac equation offers an analytical description of the atom (neglecting certain QED effects) but for any system more complicated than this no such solution is possible. The reason for this is that the problem is a 'many-body' one involving interactions between each of the constituent electrons and all of the others. In this case the solution has to be approached by making approximations so that the problem is manageable. One then gradually extends the calculation by reducing the approximations. The calculations are done numerically rather than analytically and a large amount of time and effort goes into optimising the computing side of the operation. It is only comparatively recently that the continuing improvement in computing resources has allowed atomic theory calculations on their present scale.

One of the usual first approximations that is made in order to make a many-body problem manageable is the 'independent-particle model' where each electron is assumed to interact with a mean field produced by the other electrons and the nucleus. Using the variational principle to minimise the total energy with respect to small changes in the wavefunctions leads to the (unrestricted) Hartree-Fock (HF) equations. Making the additional assumption that the field from other electrons is spherically symmetric leads to the 'central-field model' (CFM) and the restricted HF equations. These are straight-forward to solve and are often used as a convenient starting point in many calculations.

As an initial estimate the CFM provides a reasonable model of the atom, producing fairly accurate energy levels and wavefunctions. However, for accurate calculations, such as we require for PNC effects, this model is not good enough and refinements have to be made. One physical effect not included in it is the polarization of the core electron cloud by the open shell electrons. Although not included in the CFM, this effect is still within the framework of the independent-particle picture. Still omitted are some residual interactions which can be

described by two or more particle excitations (e.g. the interaction of the polarised core back on the valence electron). These are collectively known as correlation effects, of which the dominating ones are the two particle excitations.

The main methods of doing calculations that include correlation effects are: configuration interaction (CI), multi-configurational Dirac-Fock (MCDF), many-body perturbation theory (MBPT) and potentially the Equations of Motion method (EOM) for problems concerning atomic transitions. In the CI formalism the exact wavefunction is expressed as a sum of configurations of anti-symmetrised products of single particle wavefunctions where it is the coefficients in the sum which have to be determined. The configurations are all treated equally with the approximations being in which configurations are included. MBPT starts with an approximate determinantal wavefunction and derives an operator which when acting on the approximate wavefunction gives the exact one. The operator is expanded as a series of correction terms of decreasing size; these correction terms are given in terms of matrix elements of the perturbation and energy denominators. The correction terms are often classified according to the number of Coulomb interaction matrix elements in them. The EOM formalism starts with a ground state which is operated on by an excitation operator to obtain the excited state. The approximations are in the level of complexity of the excitation operator and the accuracy of the ground state.

To treat all two particle excitations, say, in a rigorous manner using these methods is 'non-trivial', involving an extremely large amount of time and effort. One alternative which is far simpler and which we have adopted is a semi-empirical approach which can give a good estimate of many of these effects.

If these various different methods were carried to all orders they should, of course, agree to within the initial approximations made. However, since this is impossible in practice, a comparison of the answers achieved by different methods gives an indication of the contributions of the various terms.

The latest calculations done in this field by other groups (e.g. W. Johnson and Dzuba) include in a rigorous manner many of the important correlation effects. However, the semi-empirical approach together with the Equations of Motion method gives a very useful check to these results.

3.1.1 The Relativistic Hamiltonian

As mentioned in the previous chapter the 'Z^3' enhancement factor means that our theoretical calculations need to be done for heavy atoms and hence must use a relativistic formalism. The correct Hamiltonian to start from can be found in the formalism of QED. Unfortunately this presents great difficulties: only charge is conserved and not the number of electron/positron pairs; also there are infinite sums of certain interactions which lead to 'renormalisation' of the electron mass and charge. In the Feynman gauge for example the full interaction virtual photon field consists of four kinds of photons: two transverse polarizations, one longitudinal polarization and one 'time-like' photon. When these last two are treated to all orders they can be shown to be equivalent to the standard $1/r_{12}$ static Coulomb interaction term. The transverse photons give retardation corrections and magnetic interactions. If all photon interactions are summed to all orders then the results will be gauge independent but if the sums are truncated then the results will depend on the chosen gauge.

The nature of the full QED Hamiltonian makes practical calculations using it impossible so that approximations have to be made. Since the transverse photon effects are usually of a far smaller magnitude than the other two the usual approach is to work in the Coulomb gauge with a $1/r_{12}$ static term and the transverse photon effects are treated as perturbations (e.g. the Breit interaction term, see [Bethe and Salpeter]).

There are additional difficulties associated with the Dirac equation: to prevent the theoretical possibility of transitions of electrons to the negative energy states it is necessary to assume that the latter are fully occupied so that the Pauli Exclusion Principle prevents the transitions. There should therefore be excitations from the sea of negative energy states as well as the positive energy core states; the former represent the creation of electron/positron pairs. However at the level of calculation pursued in this thesis the neglect of these considerations will have negligible effect. For a more detailed discussion of the relativistic Hamiltonian see [Lindroth] and the references therein.

Our initial Hamiltonian therefore is going to be (in atomic units: see Appendix 5):

$$H = \sum_i c\ \underline{\alpha}_i \cdot \underline{p}_i + c^2\ (\beta_i - I) + V_{nuc}(r_i) + \sum_{i>j} \frac{1}{r_{12}} \qquad (3.1)$$

V_{nuc} is the potential due to the nucleus and equals $-Z/r$ outside the nucleus. It has been written in this form so that different potential distributions within the nucleus can be used. α and β are the standard Dirac matrices (see e.g. [Aitchison and Hey]). It should be pointed out that whilst the Dirac equation is an exact equation for a single-electron system, treating many electron systems in a rigorous way is a very difficult problem. The difficulty comes from the last term which represents the interaction between the electrons in the atom. The usual approach is to write the Hamiltonian in the following form

$$H = H_0 + H_1 \qquad (3.2)$$

where

$$H_0 = \sum_i c\ \underline{\alpha}_i \cdot \underline{p}_i + c^2\ (\beta_i - I) + V(r_i) + V_{nuc}(r_i) \qquad (3.3)$$

and

$$H_1 = \sum_{i>j} \frac{1}{r_{12}} - \sum_i V(r_i) \qquad (3.4)$$

where $V(r_i)$ is a suitable central potential so that the eigenfunctions can be written as an anti-symmetrised product of single-particle wave functions. The corrections are then calculated by treating H_1 as a perturbation. This approach is used for many calculations.

3.2. The Hierarchy of Approximations

As mentioned above, one starts with a simple independent particle CFM such as in equation (3.3). One can then make successive improvements to this model using the correction Hamiltonian (3.4). In this thesis we use such a hierarchy of approximations, starting with the Relativistic Self-Consistent Field (RSCF) local potential.

3.3 Relativistic Self-Consistent Field Calculation

To obtain a convenient starting point in our calculations we have used the Relativistic Self-Consistent Field (RSCF) program originally written by Lindgren's group in Sweden. This consists in solving for the electrons moving independently in a local central field so that the Hamiltonian that is used is of the form of (3.3). It produces an approximate solution to the Hartree-Fock equations (q.v.). The exchange term is represented by the local potential

$$V_{loc}(r) = \frac{-3\ C}{2\ r}\left[\frac{3\ r^n\ \rho(r)^m}{4\ \pi^2}\right]^{1/3} \qquad (3.5)$$

where $\rho(r)$ is the electron density summed over occupied orbitals and C, n and m are input parameters for the program. There are various input options for the program including a 'LATTER' correction for matching the potential as seen by the unoccupied orbitals to 1/r for large r as the local potential above falls off too rapidly otherwise. The output from the program consists of the local RSCF wavefunctions and an effective charge Z_{eff} (r) such that the equation for each local orbital can be written

$$\left[\epsilon_i - h_D + \frac{Z_{eff}(r)}{r}\right] |i_{loc}> = 0 \qquad (3.6)$$

where $h_D = c\ \underline{\alpha}_i \cdot \underline{p}_i + c^2\ (\beta_i - I)$ and Z_{eff}/r is the positive absolute value of the potential energy of the electron.

It should be pointed out that the particular choice of the local RSCF wave functions is not essential: it is just a convenient starting point for more advanced calculations. However, in practice the ease of doing the numerical calculation depends on the choice of the RSCF wave functions being used.

3.4 Hartree-Fock Equations

The next stage in our hierarchy are the Hartree-Fock (HF) equations. The RSCF potential is an approximation to the HF potential.

The HF equations are used in nearly all calculations as a starting point before more detailed calculation is done. Strictly speaking HF should refer to the non-relativistic equations, the relativistic equations usually being called the Dirac-Fock

equations but we shall stick with the original name.

The derivation of the equations assumes a single particle anti-symmetrised wavefunction. It then requires the expectation value of the Hamiltonian (3.1) with this determinant to be a minimum. This leads to the HF equations (for details see e.g. [Lindgren and Morrison]). The HF equations are:

$$(h_D + V_{nuc}(r) + V_{hf}) \mid a > = \epsilon_a \mid a > \qquad (3.7)$$

where

$$V_{hf} \mid a > = \sum_b \left[<b|\frac{1}{r_{12}}|b>|a> - <b|\frac{1}{r_{12}}|a>|b> \right] \qquad (3.8)$$

which is often more conveniently written as

$$V_{hf} \mid a > = \sum_b <b|\frac{1}{r_{12}} (1 - P_{12})|b>|a> \qquad (3.9)$$

where P_{12} is the exchange operator that exchanges the states to be operated upon. The sum over *b* is over all occupied electron states.

Since there is no restriction on the single particle states these equations are referred to as the unrestricted HF equations. Requiring the potential to be spherically symmetric so that the orbitals can be written as a product of a radial function and an angular function gives the restricted HF equations which we shall be using. It also places restrictions on the orbitals *b* that contribute to the sum in (3.9) (see below).

Because the HF equations are so often used as a starting point and because in many cases they offer a fairly good description of the atom it is worth while noting some of the properties of the equations and of the potential itself.

3.4.1. Properties of the HF Equations

1. The direct part of the potential consists of a sum over the electrons *b* and represents the Coulomb interaction between the orbital *a* being solved for and all of the orbitals in the sum over *b*. When *a* is included in this sum then it would be interacting with itself but the exchange part of the potential exactly cancels out the 'self-interaction' term. If *a* is not in this sum then there is no cancellation and the potential has an unphysical asymptotic value as $r \rightarrow \infty$.

2. At large distances from the nucleus each direct radial contribution behaves as 1/r so for N electrons contributing to the potential it will go as N/r. The exchange term will cancel out one of these (provided there is a self-interaction cancellation term) so that the net dependence is (N-1)/r.

3. The restricted V_{hf} potential is required to be spherically symmetric. That is to say that the angular properties of $V_{hf} | a >$ are the same as the state $| a >$ itself.

4. The HF potential is chosen to be hermitian so the eigenfunctions of equation (3.7) form an orthonormal set. The orthonormal condition can be expressed formally as:

$$< i | j > = \delta_{ij}$$

where δ_{ij} is the Kroneker delta.

4. The eigenvalue ϵ_a of equation (3.7) can be shown by [Koopmans]' theorem to be related to the binding energy of the electron. However, it does not necessarily equal it because the initial and final configurations – after removal of the electron from a particular shell – have generally a term splitting and the work required to remove the electron depends on the final (as well as on the initial) state. However, if a configurational-averaged HF is performed (see [Lindgren and Morrison]) then the eigenvalue equals the negative of the average binding energy (the difference in average energy for the initial and final configurations).

5. For single valence systems such as we are interested in, if the HF potential is only contributed to by core orbitals (i.e. a V_{N-1} HF, see below) then the determinantal state formed by anti-symmetrising the product of HF eigenfunctions (*i.e.* a Slater determinant) will have no first order single excitation corrections when MBPT is performed to correct for the residual (non-central) Coulomb interactions. This reduces the number of perturbation diagrams to be calculated, which is why the V_{N-1} HF equations are used so widely as the first stage in a calculation.

3.4.1 Orbitals Contributing to the HF Potential

As mentioned in section 1 above the choice of which orbitals contribute to the HF potential is not obvious. For an atom with N electrons ideally each electron should interact with N−1 other electrons. If all N electrons were in the potential and were all closed shells then the self−interaction cancellation would ensure that each saw N−1 others. However for open shell atoms, such as the ones that we will be doing calculations on in this thesis, when the excited states are solved for they will see all N electrons and will hence be totally unrealistic. The excited states are of great physical importance as it is usually transitions between them and the valence states that we are interested in. What is commonly done for single valence systems is to perform a V_{N-1} HF calculation whereby only the N−1 core orbitals contribute to the HF potential. Thus the physically important excited and valence states see N−1 electrons but the less important core orbitals now see N−2 orbitals.

3.5 Beyond The Hartree−Fock

The next stage in our hierarchy is to go beyond the HF equations. In equation (3.2) we divided the Hamiltonian into a central part and a residual part. The central part is usually the core HF potential as described in the previous section. We now discuss how to go beyond the approximations of the HF equations and to calculate the effect of the residual Hamiltonian (3.4).

If one has a complete set of eigenfunctions of a Hamiltonian then it is always possible to express any corrections to a wavefunction in terms of an expansion of that complete set where the expansion coefficients have to be determined. There are several approaches to this. One which is often used is Many Body Perturbation Theory (MBPT).

3.5.1 Many Body Perturbation Theory

This is based around expanding the corrections to the wave functions and eigenvalues as a series of decreasingly important correction terms. Given an initial single particle approximation to the exact wavefunction, a wave operator is defined which, acting on this approximate wavefunction, generates the exact solution.

$$\Omega \Psi_0 = \Psi \qquad (3.10)$$

where Ψ_0 denotes the approximate wavefunction and Ψ the exact one. The correction terms in the expansion of Ω are given in terms of matrix elements of the perturbation and an energy denominator. Without any additional physical effects added the perturbation is given by (3.4). To aid the derivation of the MBPT correction terms diagrammatic techniques has been developed to represent the correction terms in terms of matrix elements of the perturbation, energy denominators, and creation and annihilation operators (see Appendix 1) which act on the single particle basis states. The matrix elements are represented by lines joining vertices with lines going into a vertex denoting an annihilation operator and lines going out a creation operator. Dotted lines represent Coulomb interactions and wavy lines the transition photon. Core orbitals point downwards and excited and valence orbitals upwards (valence orbitals are represented explicitly by two arrows).

MBPT corrections are often classified according to their order or number of Coulomb interaction matrix elements in them. In figure 3.1 we give examples of MBPT diagrams. For example diagram *a* represents

$$a^\dagger_{v2}\, a^\dagger_r\, a_a\, a_{v1}\, \frac{\langle v_2\, r | r_{12}^{-1} | v_1\, a\rangle}{(\epsilon_a + \epsilon_{v1} - \epsilon_r - \epsilon_{v2})} \qquad (3.11)$$

3.5.2 The RPA Diagrams

These are a certain set of MBPT diagrams, characterised by a series of loops or 'bubbles', which represent interactions with the core orbitals. It is possible to sum all such diagrams to all orders by solving a set of self-consistent equations called the RPA equations. Typical RPA diagrams are given in figure 3.2.

By way of illustration we shall describe the RPA equations for the hyperfine interation as we shall be calculating this at a later stage. The hyperfine interaction is given by $V_{hyp} = \underline{T}^1 . \mu_I$ ([Schwartz]) where μ_I is the nuclear magnetic moment and $\underline{T}^1$ is given by

$$\underline{T}^1 = - i \alpha r^{-2} (\underline{\alpha} . \underline{l}\, C^1) \qquad (3.12)$$

Figure 3.1 First Order MBPT Diagrams

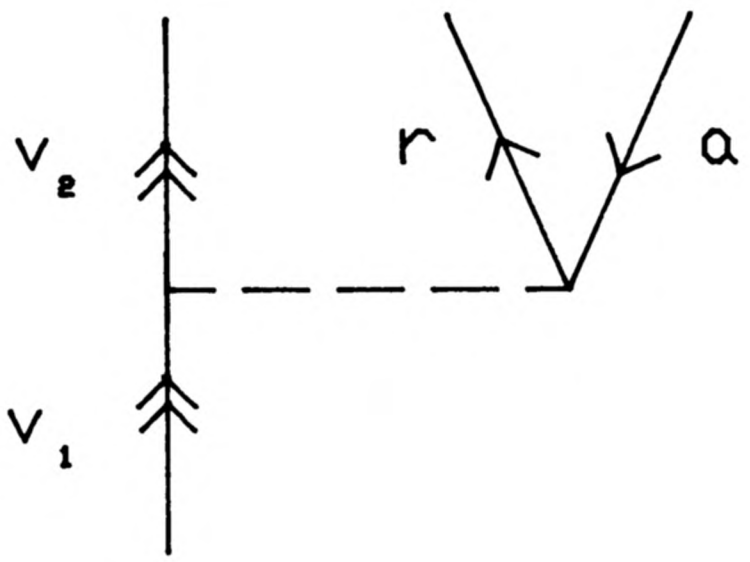

a

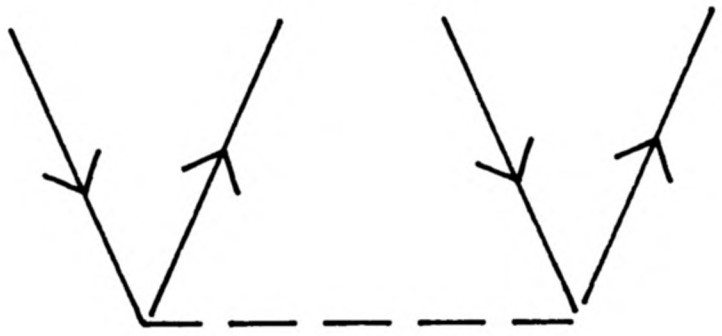

b

Figure 3.2 Some Third Order RPA Diagrams

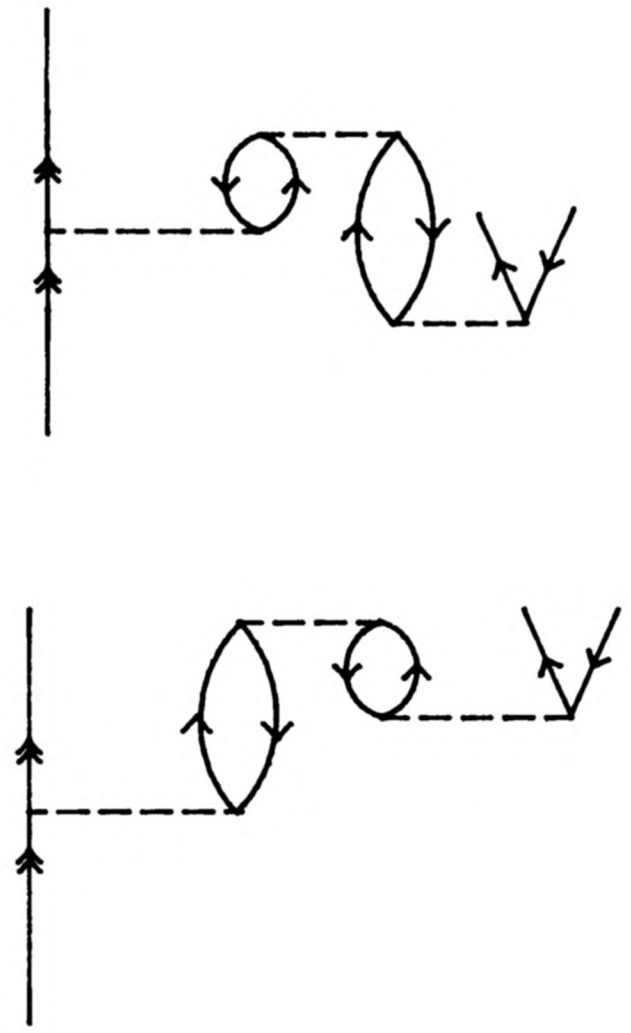

The zeroth order interaction term is given by

$$< v_2 \mid V_{hyp} \mid v_1 > \qquad (3.13)$$

where v_1 and v_2 are valence orbitals (usually the same one apart from the magnetic quantum number). This term is represented by diagram *a* in figure 3.3. A typical first order correction term is given by diagram *b* which represents:

$$\sum_r < a \mid V_{hyp} \mid r > \frac{<v_2\ r|r_{12}^{-1}|a\ v_1>}{(\epsilon_a + \epsilon_{v1} - \epsilon_r - \epsilon_{v2})} \qquad (3.14)$$

where the infinite sum over *r* can be can be carried out using Sternheimer techniques.

3.5.3 'Sternheimer' Technique

In this thesis we make extensive use of 'Sternheimer' techniques which allows the infinite summation over excited states to be converted to a finite sum. This is a very powerful method for manipulating MBPT corrections. Consider the function

$$|a^+> \equiv \sum_r |\ r > \frac{<v_2\ r|g_{12}|v_1\ a>}{(\epsilon_a - \epsilon_r)} \qquad (3.15)$$

where $g_{12} = r_{12}^{-1}\ (1-P_{12})$ and we have put $\epsilon_{v1} = \epsilon_{v2}$. This is a single particle function which is a solution of

$$(\epsilon_a - H_0^{HF})|a^+> = \sum_r |\ r > <v_2\ r|g_{12}|v_1\ a> \qquad (3.16)$$

where H_0^{HF} is the HF Hamiltonian. Using the closure relationship for the HF basis set we can write

$$\sum_r |r><r| = 1 - \sum_b |b><b| \qquad (3.17)$$

Putting this into (3.15) gives

$$(\epsilon_a - H_0^{HF})|a^+> = <v_2|g_{12}|v_1>|a > - \sum_b |b><v_2\ b|g_{12}|v_1\ a> \qquad (3.18)$$

Thus we have replaced the infinite sum with a finite one over the core states.

We can now evaluate the expression in (3.14) which is given by $<a|V_{hyp}|a^+>$.

Figure 3.3 MBPT Hyperfine Interaction Diagrams

a

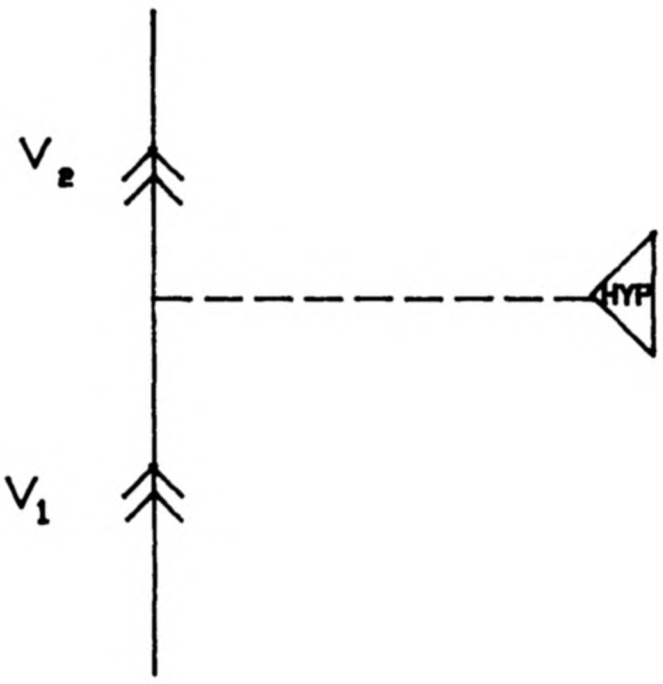

b

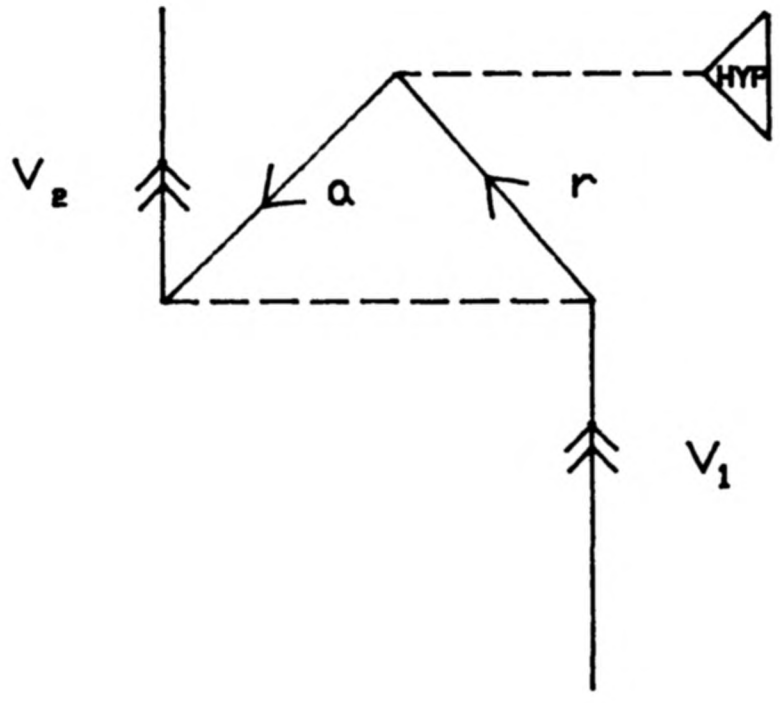

3.5.4. The Feedback Terms

The single particle function in (3.15) represents the modification of the core orbital *a* by a Coulomb interaction with the valence orbital. It is possible to derive an equation that evaluates the effect of this modification to the core orbitals back on the other core orbitals. To do this in a simple way we consider the HF potential with each core orbital replaced by the core orbital and its perturbed part

$$V_{hf}|a\rangle \rightarrow \sum_{b,b^+} \langle b + b^+|g_{12}|b + b^+\rangle|a + a^+\rangle \qquad (3.19)$$

If we only take terms linear in the modified orbitals and add this to the right-hand side of (3.18) we obtain

$$\begin{aligned}(\epsilon_a - H_0^{HF})|a^+\rangle &= \langle v_2|g_{12}|v_1\rangle|a\rangle \\ &\quad + \sum_b \langle b^+|g_{12}|b\rangle|a\rangle + \langle b|g_{12}|b^+\rangle|a\rangle \\ &\quad - \sum_b |b\rangle\langle b|rhs\rangle \end{aligned} \qquad (3.20)$$

where $|rhs\rangle$ represents the first three terms on the right-hand side of (3.20). The first term on the right-hand side is the driving term (the interaction with the valence electron); the second two terms are the feedback terms representing the effect of other core orbitals, having been modified by their driving terms, back on orbital *a*. The effect of this interaction is then fed back to the other core orbitals via their feedback terms. When solved numerically until self-consitent this method effectively sums all the RPA diagrams of figure 3.4. The RPA matrix element is given by terms such as $\langle a|V_{hyp}|a^+\rangle$ where $|a^+\rangle$ is now the iterated excitation.

A few things to note that are typical of RPA type equations:

1. The right-hand side consists of a driving term and feedback terms; the latter are initially zero but give a contribution once the equations are iterated.
2. We could equally have had the hyperfine interaction as the driving term and taken the interaction with the valence electron at the end. This 'reversibility' is typical of the RPA equations.

Figure 3.4 RPA Diagrams

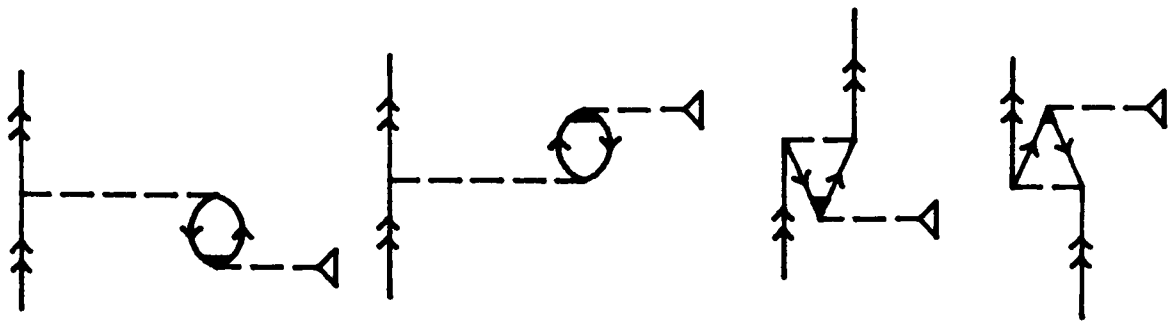

where the RPA vertex is given by

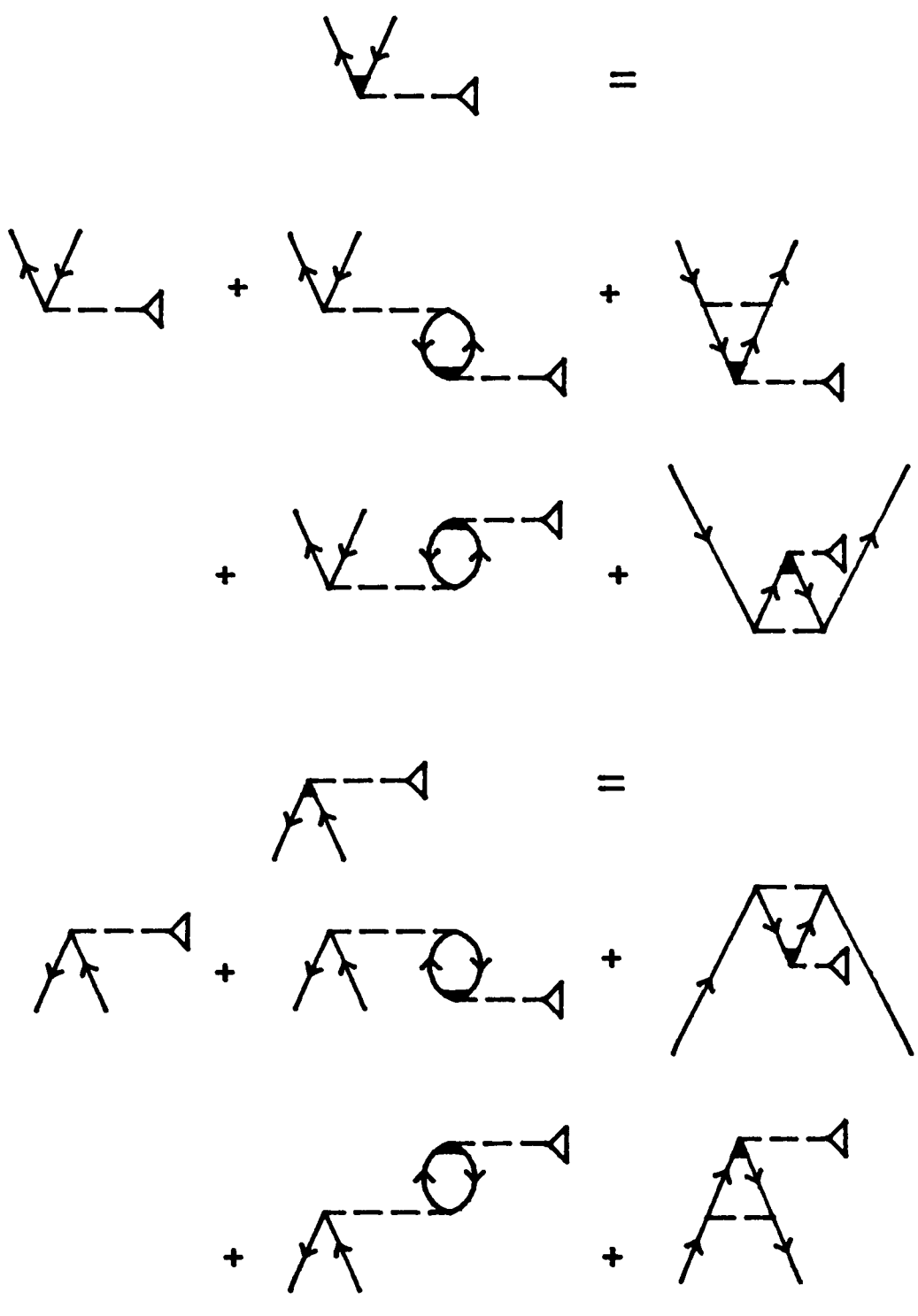

3. The last term in (3.18) is the orthogonality term that ensures that there are no admixtures of core orbitals in the core orbital excitations. However it can be shown that any admixture of core orbitals will cancel out overall and (3.20) need only be orthogonalised to the orbital *a* being solved for.

The details of the hyperfine equations are given in Appendix two. For a detailed discussion of hyperfine calculations see [J. Heully and A.M. Martensson-Pendrill] and the references therein.

An advantage of using RPA type equations for the calculation of E1 transition matrix elements (such as the EOM discussed in the next chapter) is that the RPA E1 matrix element is independent of whether the length or velocity gauge is used for the dipole operator expression. This provides a very useful check to the numerical solutions. This is discussed in more detail in Appendix 3.

3.6 The Introduction of Parity Non-Conservation to the Equations

We have described how starting with a CFM we can systematically extend the calculations to include more physical effects. As mentioned in chapter one the main purpose of this thesis is to calculate PNC E1 matrix elements which, when combined with atomic PNC measurements, allow a determination of the weak charge Q_W.

3.6.1. The PNC Hamiltonian

In the previous chapter we demonstrated that the most important part of the weak force Hamiltonian is the spin independent term which is given by:

$$h^{pnc} = \frac{G_F \; Q_w \; \gamma_5 \; \rho_n \; (r)}{2\sqrt{2}} \qquad (3.21)$$

$$\gamma_5 = \begin{bmatrix} 0 & 1 \\ 1 & 0 \end{bmatrix} \qquad (3.22)$$

The ρ_n (r) is a suitable nuclear density renormalised so that its integral over all space equals unity. Thus this Hamiltonian only acts within the nucleus and only has significant matrix elements between $s_{\frac{1}{2}}$ and $p_{\frac{1}{2}}$ orbitals. This is because only $s_{\frac{1}{2}}$ functions can have non-zero density at the origin and the γ_5 matrix mixes the upper

and lower components of the Dirac spinors (the lower component of the $p\frac{1}{2}$ orbital is '$s\frac{1}{2}$' like in character). The parity mixing for j values other than $\frac{1}{2}$ will be small due to their small amplitude at the nucleus. The size of the physical constants G_F and Q_w means that the effect is extremely small but it is important because of the parity mixing nature of the interaction.

When the Hamiltonian given in equation (3.22) acts on a Dirac orbital $|\Psi_a\rangle$ we obtain :

$$\frac{G_F\ Q_W\ \gamma_5\ \rho_n(r)}{2\sqrt{2}}\ |\Psi_a\rangle = \frac{G_F\ \ Q_W\ \ \rho_n(r)}{2\sqrt{2}} \begin{bmatrix} 0 & 1 \\ 1 & 0 \end{bmatrix} \frac{1}{r} \begin{bmatrix} P_a(r)\ X_{\kappa a} \\ i\ Q_a(r)\ X_{-\kappa a} \end{bmatrix}$$

$$= \frac{G_F\ Q_W}{2\sqrt{2}} \quad \frac{i}{r} \begin{bmatrix} \rho_n(r) Q_a(r)\ X_{-\kappa a} \\ -i\ \rho_n(r) P_a(r)\ X_{\kappa a} \end{bmatrix}$$

$$= \frac{G_F\ Q_W}{2\sqrt{2}} \quad \frac{i}{r} \begin{bmatrix} F_a(r)\ X_{\kappa'} \\ i\ G_a(r)\ X_{-\kappa'} \end{bmatrix} \qquad (3.23)$$

where we have redefined the parity non-conserving radial components F and G by

$$\begin{aligned} F_a(r)\ \ X_{\kappa'} &\equiv \rho(r)\ Q_a(r)\ X_{-\kappa a} \\ G_a(r)\ \ X_{-\kappa'} &\equiv -\rho(r) P_a(r)\ X_{\kappa a} \end{aligned} \qquad (3.24)$$

and κ' is the opposite parity to κ_a. Thus we see that when the weak interaction Hamiltonian (3.21) is present then the orbitals are no longer exact eigenstates of parity but have small admixtures of opposite parity.

Important things to note about the opposite parity wavefunctions:

1. The perturbation only acts over the nucleus but the PNC wavefunctions can extend beyond this: the first order perturbation correction is expressed as a sum of HF eigenstates with matrix elements of (3.21) determining the admixture coefficients.
2. The PNC orbitals will have the characteristics of their unperturbed opposite parity

counterparts, for example a $p_{\frac{1}{2}}$ orbital will have the characteristics of an $s_{\frac{1}{2}}$ orbital and *vice versa*.

3. The PNC functions are purely imaginary.

3.6.2. The Addition of PNC to Parity Conserving Equations

Performing first order perturbation theory with the weak Hamiltonian as a perturbation will give single particle wavefunction corrections such as:

$$|a^{pnc}\rangle = \sum_r |r\rangle \frac{\langle r|h^{pnc}|a\rangle}{\epsilon_a - \epsilon_r} \qquad (3.25)$$

where r is summed over the excited states.

If we write down the E1 transition matrix element between two parity mixed states such that the transition is nominally parity forbidden (e.g. the caesium 6s to 7s transition) then we can see how the admixture of opposite parities means that there is a non-zero transition amplitude. Here and in all the following we shall denote parity mixed orbitals by a tilde sign above the orbital.

$$\begin{aligned} \langle \tilde{a} \mid \underline{D} \mid \tilde{b} \rangle &= \langle a_0 + a^{pnc} \mid \underline{D} \mid b_0 + b^{pnc} \rangle \\ &= \langle a_0 \mid \underline{D} \mid b_0 \rangle + \langle a^{pnc} \mid \underline{D} \mid b^{pnc} \rangle \\ &+ \langle a^{pnc} \mid \underline{D} \mid b_0 \rangle + \langle a \mid \underline{D} \mid b^{pnc} \rangle \\ &= \langle a^{pnc} \mid \underline{D} \mid b_0 \rangle + \langle a \mid \underline{D} \mid b^{pnc} \rangle \qquad (3.26) \end{aligned}$$

since the other two transitions are parity forbidden in this case. To evaluate this we use MBPT to obtain the four diagrams of figure 3.5. The diagrams, when added, represent the terms:

$$\sum_i \frac{\langle a|h^{pnc}|i\rangle\langle i|\underline{D}|b\rangle}{\epsilon_a - \epsilon_i} + \sum_j \frac{\langle a|\underline{D}|j\rangle\langle j|h^{pnc}|b\rangle}{\epsilon_b - \epsilon_j} \qquad (3.27)$$

where the sums for *i* and *j* are over all orbitals. Using the Sternheimer technique outlined in section 3.5.3 we can evaluate $|a^{pnc}\rangle$ by solving the differential equation :

$$(\epsilon_a - H_0^{HF}) \; |a^{pnc}\rangle = h^{pnc} \; |a\rangle \qquad (3.28)$$

Figure 3.5 Lowest Order PNC E1 Transition Matrix Element

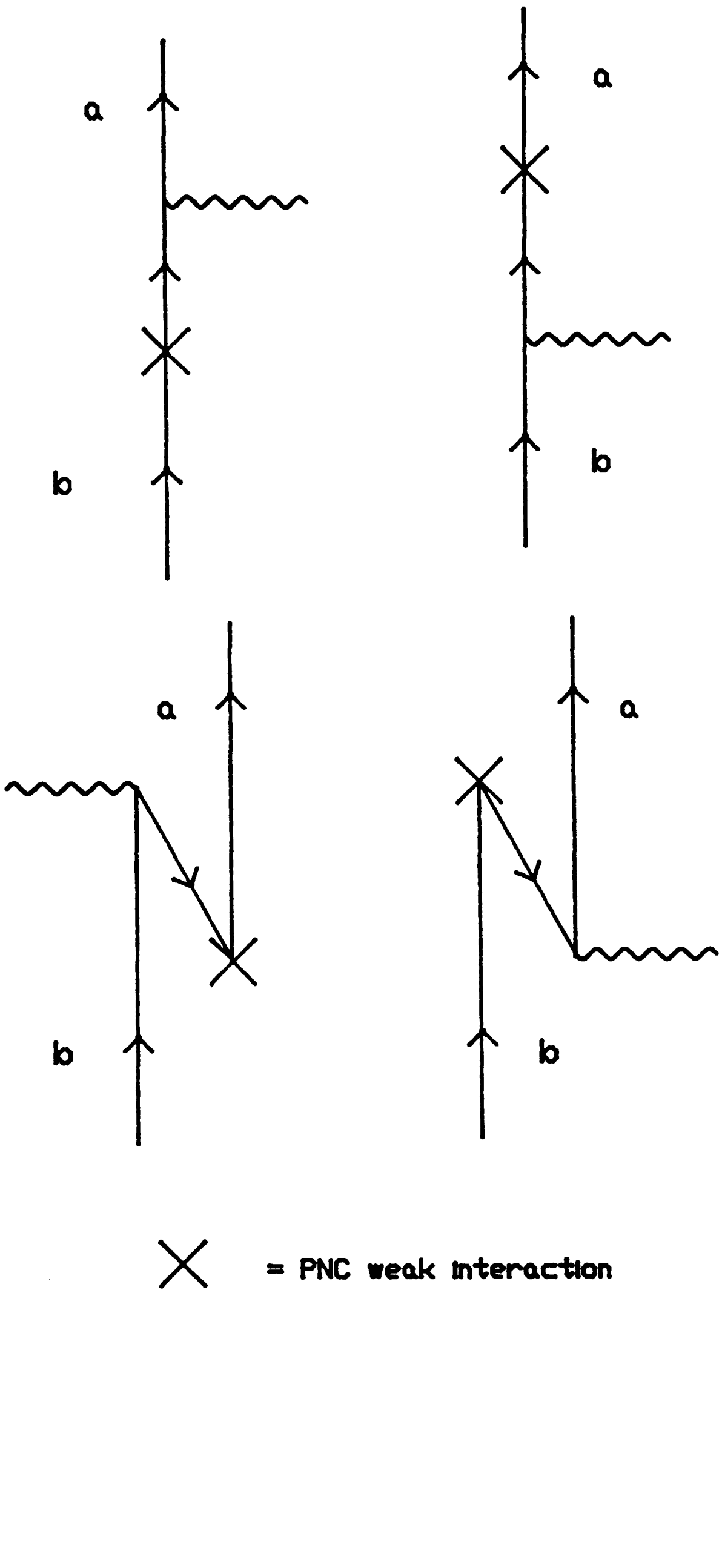

This can then simply be substituted into equation (3.26). This gives a simple demonstration of the use of Sternheimer techniques, in this case to evaluate the first order weak force induced parity forbidden E1 transition matrix element.

3.6.3 PNC Hartree–Fock Equations

So far we have just considered the weak Hamiltonian perturbing one orbital in isolation. The next stage is to determine the effect of one perturbed orbital on the other orbitals. It was [Sandars 1977] who first suggested that since the operator is a scalar this could be done by including the weak Hamiltonian in the Hartree Fock equation at the lowest order by considering all the orbitals in the HF potential to be parity mixed ones (i.e. each can be considered to be the nominal parity orbital with an admixture of opposite parity of order G_F). By taking angular projections of the resulting equation to project out the required parity equation or by considering terms of the same order of G_F, the equations for the parity non-conserving parts of the orbitals can be obtained.

Since this method shall be used to derive all the PNC equations in this thesis we shall go into it in some detail here in order to derive the PNC counterpart to the HF equations.

We shall start with the HF equation:

$$(\epsilon_a - h_0 - V_{hf}) \,|a\rangle = 0 \qquad (3.29)$$

where

$$V_{hf} \,|a\rangle = \sum_b \langle b|g_{12} \,|b\rangle|a\rangle \qquad (3.30)$$

and $h_0 \equiv c\ \underline{\alpha}.\underline{p} + c^2\,(\beta - I) + V_{nuc}(r)$.

If we now add the weak Hamiltonian and allow all the orbitals to be parity mixed ones (and there is no restriction on this from the original derivation of the HF equations) then we can write each orbital as $|a_0 + a_1\rangle$ where $|a_1\rangle$ ($\equiv |a^{pnc}\rangle$) is the opposite parity admixture. Doing this for each orbital gives:

$$(\epsilon_a + \delta\epsilon_a - h_0 - h^{pnc})\,|a_0+a_1\rangle = \sum_b \langle b_0+b_1|g_{12} \,|b_0+b_1\rangle|a_0+a_1\rangle \qquad (3.31)$$

Here $\delta\epsilon_a$ is the order G_F shift to the energy. Taking the lowest order terms gives equation (3.29) once more. To first order in G_F we obtain:

$$(\epsilon_a - h_0)|a_1\rangle + (\delta\epsilon_a - h^{pnc})|a_0\rangle = \sum_b \langle b_0| g_{12} |b_0\rangle|a_1\rangle + \sum_b \langle b_0| g_{12} |b_1\rangle|a_0\rangle + \sum_b \langle b_1| g_{12} |b_0\rangle|a_0\rangle \qquad (3.32)$$

The direct parts of the second and third terms cancel out exactly (remember $g_{12} \equiv r_{12}^{-1}(1-P_{12})$) because of the purely imaginary nature of the parity admixtures. That is:

$$\langle b_0|r_{12}^{-1}|b_1\rangle|a_0\rangle + \langle b_1|r_{12}^{-1}|b_0\rangle|a_0\rangle \equiv 0 \qquad (3.33)$$

This leaves us with:

$$(\epsilon_a - h_0 - V_{hf})|a_1\rangle = h^{pnc}|a_0\rangle + V_{hf}^{pnc}|a_0\rangle \qquad (3.34)$$

where

$$V_{hf}^{pnc}|a_0\rangle \equiv \sum_b - \langle b_1|r_{12}^{-1}|a_0\rangle|b_0\rangle - \langle b_0|r_{12}^{-1}|a_0\rangle|b_1\rangle \qquad (3.35)$$

and we have put $\delta\epsilon_a$ equal to zero because

$$\delta\epsilon_a = \langle a_0|h^{pnc}|a_0\rangle + \langle a_0|V_{hf}^{pnc}|a_0\rangle = 0 \qquad (3.36)$$

due to the opposite parities involved.

Equation (3.34) is called the parity non-conserving Hartree-Fock equation (PNC HF). It has to be solved self consistently since each PNC orbital interacts with all the others via the V_{hf}^{pnc} potential (3.35). This self consistent technique effectively sums certain MBPT diagrams to all orders and is a very practical way of including such diagrams in a calculation. We shall be making extensive use of similar methods in later sections.

Since the PNC HF equation is derived from the usual HF equation but with

parity mixed orbitals, we can use the standard HF orthogonality relationship to derive an orthogonality relationship to order G_F between the HF orbitals and parity admixtures :

$$\begin{aligned}
\langle \tilde{a} | \tilde{b} \rangle &= \delta_{ab} \\
\langle a_0 + a_1 | b_0 + b_1 \rangle &= \langle a_0 | b_0 \rangle + \langle a_1 | b_0 \rangle + \langle a_0 | b_1 \rangle \\
&= \delta_{ab} + \langle a_1 | b_0 \rangle + \langle a_0 | b_1 \rangle \\
\therefore \langle a_1 | b_0 \rangle + \langle a_0 | b_1 \rangle &= 0 \qquad (3.37)
\end{aligned}$$

The evaluation of these overlaps provides a good numerical check on the correctness of the solution.

This method of adding PNC to a parity conserving set of equations carries over just as well for the equations that we use later. Since each orbital in an equation has to be replaced by its PNC counterpart there will be many more terms in the PNC counter-part to an equation.

In figure 3.6 we have given the parity conserving and the PNC upper components of the caesium $6s_{\frac{1}{2}}$ wavefunction. The horizontal axis is a logarithmic scale representing the radial grid points (see chapter 5).

3.7 Conclusion

Starting from the HF equations one can systematically add the higher order correction terms using a formalism such as MBPT to obtain an increasingly physically accurate description of the atom. However the MBPT corrections are complicated and there are many of them to be included if one wants to have accurate *ab-initio* calculations. Certain equations such as the RPA equations effectively sum certain classes of MBPT terms to all orders by using iterative self-consistent equations. PNC effects can be included by inserting the weak interaction PNC Hamiltonian directly into the equation and expanding terms to first order in G_F.

Figure 3.6

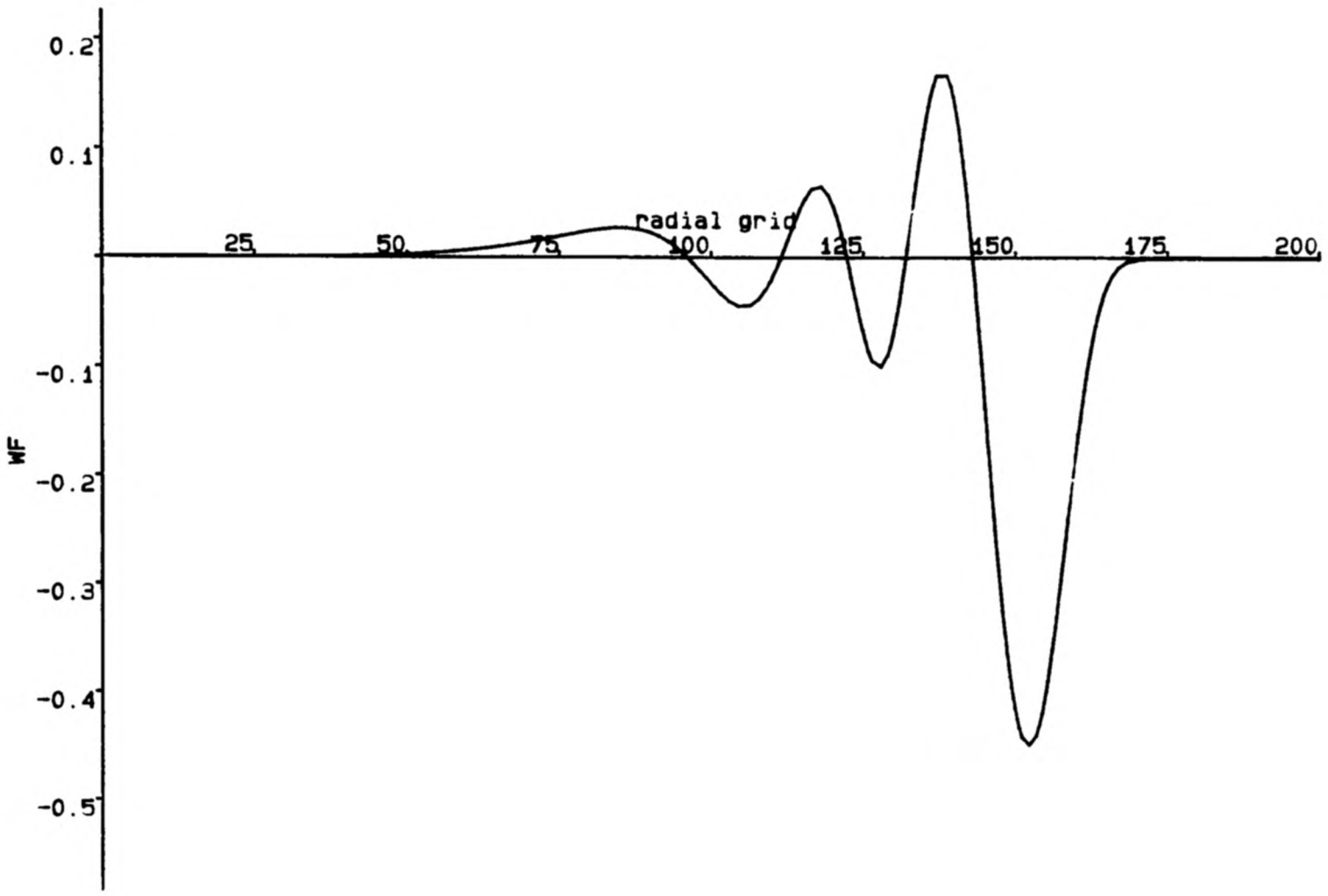

Caesium 6s HF upper component

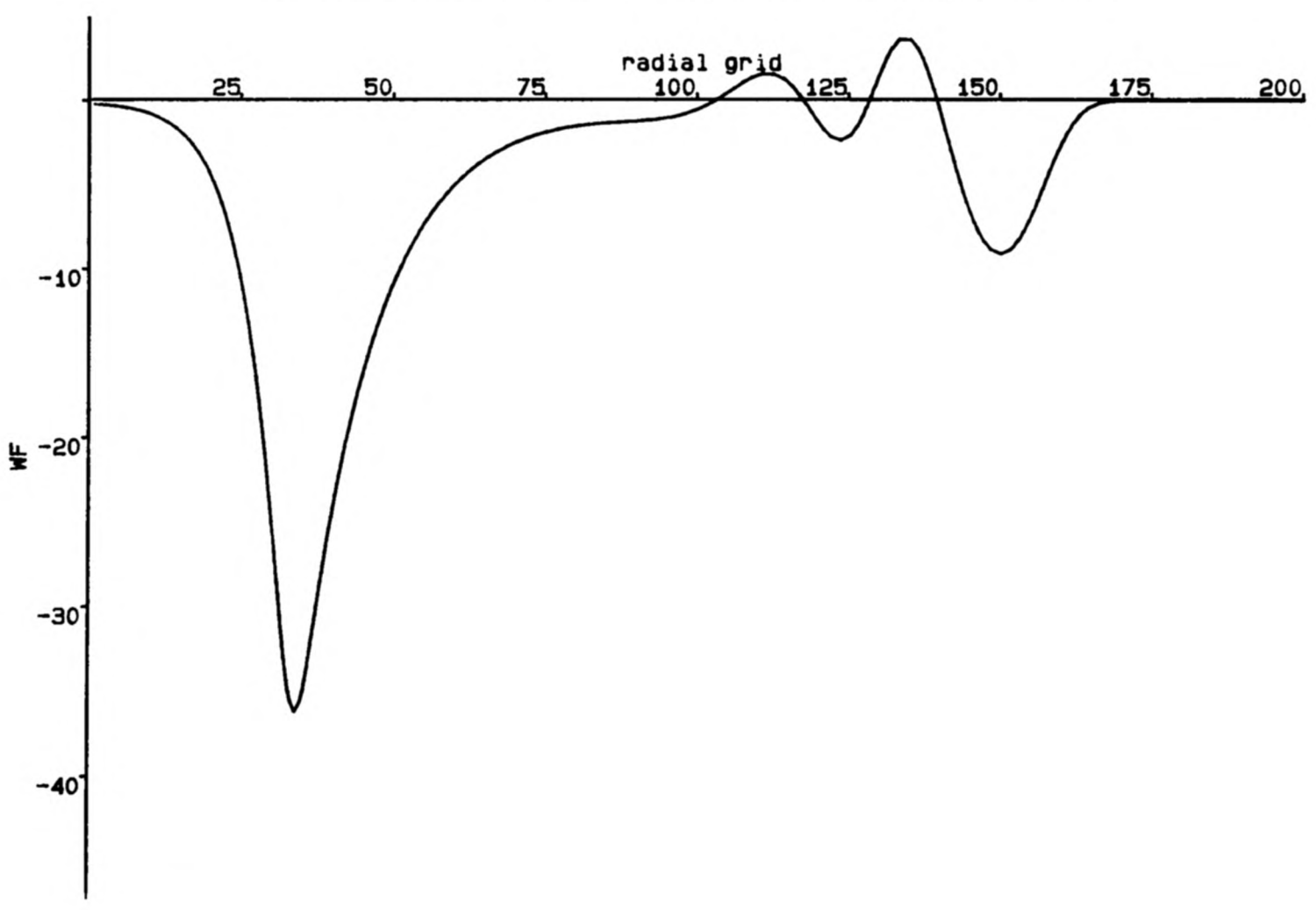

Caesium 6s PNC HF upper component

CHAPTER 4: The Equations of Motion Theory

4.1 Introduction

In this chapter we derive the Equations of Motion (EOM) from first principles. We shall first look at the more simple closed–shell case before going on to derive the open–shell EOM.

Many Body Perturbation Theory (MBPT) and EOM have differing approaches to the calculation of transition matrix elements. In the former case one starts with an approximate determinantal wavefunction, which is often the V_{N-1} HF determinant as this usually leads to less perturbation corrections. An operator is then defined which when acting on the approximate wavefunction gives the exact one. This operator is usually expanded as a series of correction terms of decreasing size; these correction terms are given in terms of matrix elements of the Coulomb interaction and energy denominators. It is also possible to expand the operator in order of complexity: single particle effects, two particle and so on.

The EOM approach is concerned with the direct calculation of transition matrix elements between a ground and an excited state rather than with finding the eigenfunctions. This is expressed formally by defining an excitation operator which when operating on the exact ground state gives the exact excited state. The EOM itself re–expresses the eigenvalue equation for the excited state involved in the transition in terms of the ground state and the excitation operator. Whilst the full EOM is exact it is no more soluble than the exact eigenvalue equations are and approximations have to be made. These approximations are in the degree of complexity of the ground state and excitation operator, rather than in the choice of correction terms to include as in a MBPT calculation.

4.1.1. Nomenclature and Approximations

There is always a great increase in the complexity of calculations when open shell systems are considered and the EOM formalism is no exception. We therefore begin by considering a closed shell system and derive what we shall call the Closed Shell EOM or EOM/CS for short.

Next we consider the open shell problem. The EOM are re-formulated for the open shell case. This involves a great increase in the complexity of the equations. In order to keep the problem simple we make several approximations which reduce the problem to a set of equations which for a single valence system are equivalent to the TDHF or MBPT RPA equations. We call our open shell EOM with these approximations the RPA EOM (usually written EOM/RPA).

Finally, in chapter eight we shall reconsider the approximations that lead to the EOM/RPA equations. We shall re-derive the equations with fewer approximations that treat the problem more rigorously. We shall call these equations the Full Open Shell EOM or EOM/FOS.

In all three cases (i.e. EOM/CS, EOM/RPA AND EOM/FOS) we shall derive the corresponding PNC equations. We shall usually refer to these by by prefixing PNC so we obtain PNC EOM/CS, PNC EOM/RPA and PNC EOM/FOS.

4.2 Derivation of the Equations

We begin by defining an excitation operator U such that it gives the required excited state when operating on the ground state.

$$U \mid 0 > = \mid 1 > \tag{4.1}$$

We also impose the constraint

$$U^{\dagger} \mid 0 > = 0 \tag{4.2}$$

Since U, when operating on a zero angular momentum state, gives an excited state which may have a different angular momentum, U is a tensor of rank equal to the excited state angular momentum and with component equal to the excited state magnetic quantum number.

We next define a symmetrised double commutator:

$$\begin{aligned} [A,B,C] &\equiv \tfrac{1}{2}\,[\,[A,B],C] + \tfrac{1}{2}\,[A,[B,C]] \\ &= ABC - \tfrac{1}{2}BAC - \tfrac{1}{2}CAB - \tfrac{1}{2}ACB - \tfrac{1}{2}BCA + CBA \end{aligned} \tag{4.3}$$

The ground and excited states are solutions of :

$$H \mid 0 > = E_0 \mid 0 >$$
$$H \mid 1 > = E_1 \mid 1 > \qquad (4.4)$$

where H is the Hamiltonian given in (3.1). Using these definitions it is then possible to re-express the fundamental equation in (4.4) for the excited state in terms of the excitation operator and the ground state.

$$<0| [P^\dagger, H , U] |0> = \omega <0|[P^\dagger, U]|0> \qquad (4.5)$$

where $\omega = E_1 - E_0$ and P is an arbitrary projection operator. Equation (4.5) is the Closed Shell Equation of Motion. P is covers the same space as U so that as many equations are obtained as there are unknowns to be determined in U.

The normalisation condition is that $<1|1> = 1$ which can be expressed as

$$<0| [U^\dagger , U] |0> = 1 \qquad (4.6)$$

where we have used the constraint of equation (4.2) to allow the inclusion of a commutator.

We shall be calculating transition matrix elements between the excited and ground states. Again using (4.2) this can be expressed as

$$<1| T |0> = <0| [U^\dagger , T] |0> \qquad (4.7)$$

where T is the transition operator.

4.2.1 Approximations

The EOM (4.5) is exact but not soluble as it stands and approximations have to be made. These approximations are in levels of complexity rather than in orders of Coulomb interaction. There are two main approximations:

1. The ground state $|0>$ is a single particle determinant which can be given in terms of creation and annihilation operators.

$$|0> = a^\dagger_a a^\dagger_b a^\dagger_c \ldots . |vacuum> \qquad (4.8)$$

Initially we shall use a HF ground state for closed shell systems. This means that correlation effects are being left out and the ground state is not an

exact eigenfunction of the Hamiltonian H. For a more accurate calculation a more sophisticated $|0>$ should be used.

2. The excitation operator is expanded in levels of complexity, i.e. in single particle effects, two particle effects and so on. We shall make the approximation of only including one particle terms. The most general form of our excitation operator is therefore going to be

$$U = \sum_{r,a} (a^{\dagger}_r \, a_a \, Y_{ra} - a^{\dagger}_a \, a_r \, Z_{ra}) \qquad (4.9)$$

where we have used creation and annihilation operators to give a second quantised formulation. In equations (4.8) and (4.9) and in all subsequent ones r, s, t etc. represent excited (unoccupied) states, whereas a, b, c etc. represent core (occupied) states.

The inclusion of the first term is straight forward and is equivalent to the Tamm–Dancoff approximation (see [G. Brown]). The second term produces negative excitations which include some two particle effects (see later). It should also be noted that equation (4.2) does not hold exactly for the excitation operator given in (4.9) acting on the single determinant $|0>$ of (4.8). This will also be discussed later.

4.2.2 EOM Diagrams

In order to derive the required equations to solve for U it is necessary to use a creation and annihilation operator formalism where the terms are expressed in terms of operators which create or destroy single particle states. These operators are most easily manipulated by diagrammatic techniques.

For example:

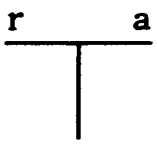

$$\equiv \sum_{r,a} a^{\dagger}_r \, a_a \, Y_{r,a} \qquad (4.10)$$

where the left hand operator at any junction is a creation operator and the right hand one is an annihilation one. There is usually an implicit summation over all orbitals. There is an amplitude coefficient (in this case $Y_{r,a}$) associated with the vertex. The

negative excitation part of U would be given by:

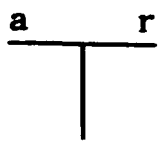

$$\equiv \sum_{r,a} - a^{\dagger}_{a}\, a_{r}\, Z_{r,a} \qquad (4.11)$$

Similarly the projection operator $P^{\dagger}$ has two parts (so that it occupies the same space as U) given by:

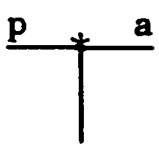

$$\equiv \quad a^{\dagger}_{p}\, a_{a}\, P^{-}_{p,a}$$

and (4.12)

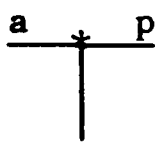

$$\equiv \quad a^{\dagger}_{a}\, a_{p}\, P^{+}_{a,p}$$

where P^{+} and P^{-} are arbitrary coefficients.

We shall also need to express the Hamiltonian in terms of creation and annihilation operators. The operator is split into two parts:

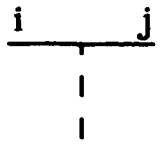

$$\equiv \sum_{i,j} a^{\dagger}_{i}\, a_{j} \langle i|h_{0}|j\rangle \qquad (4.13)$$

where $h_0 = c\ \underline{\alpha}.\underline{p} + c^2\ (\beta - 1) + V_{nuc}(r)$ is part of the Dirac operator ($V_{nuc}(r)$ being the nuclear potential) and

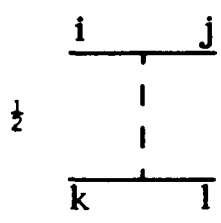

$$\equiv \tfrac{1}{2} \sum_{ijkl} a^{\dagger}_{i}\, a^{\dagger}_{k}\, a_{l}\, a_{j} \langle ik|r_{12}^{-1}|jl\rangle \qquad (4.14)$$

which represents the Coulomb interaction term. Thus the Hamiltonian can be expressed diagrammatically as:

$H_0 =$ 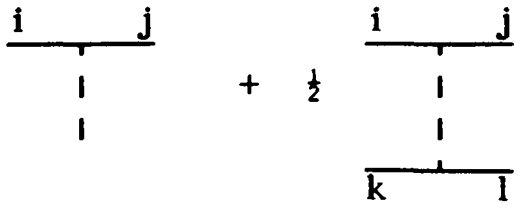 (4.15)

4.2.3. Commutators in Diagram Form

Consider a commutator of the form $[\ a^{\dagger}_i\ a_j\ ,\ a^{\dagger}_k\ a_l\ ]$. Using the anti-commutation relationships of Appendix 1 this can easily be shown to be given by:

$$[\ a^{\dagger}_i\ a_j\ ,\ a^{\dagger}_k\ a_l\ ] = a^{\dagger}_i\ a_l\ \delta_{jk} - a^{\dagger}_k\ a_j\ \delta_{il} \qquad (4.16)$$

so that if we had a commutator involving two excitation amplitudes, for example, we would obtain

$$[\ a^{\dagger}_i\ a_j\ Y_{ij}\ ,\ a^{\dagger}_k\ a_l\ P_{kl}\ ] = a^{\dagger}_i\ a_l\ Y_{ij}\ P_{jl} - a^{\dagger}_k\ a_j\ P_{ki}\ Y_{ij} \qquad (4.17)$$

The advantage of using diagrams becomes apparent when we express (4.17) in diagrammatic form:

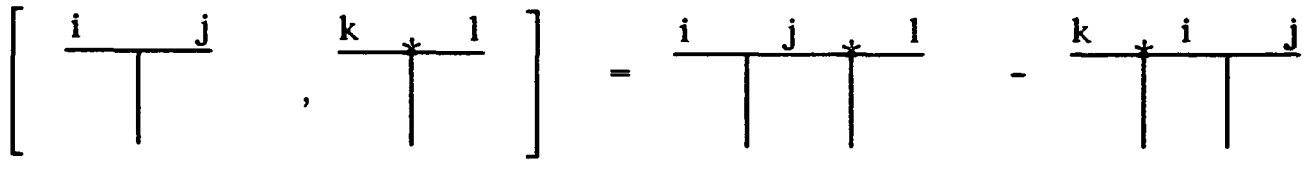

(4.18)

Similarly, for a commutator involving six operators:

$$[\ a^{\dagger}_i\ a^{\dagger}_j\ a_l\ a_k\ ,\ a^{\dagger}_r\ a_a\ ] = a^{\dagger}_i\ a^{\dagger}_j\ a_l\ a_a\ \delta_{kr} + a^{\dagger}_i\ a^{\dagger}_j\ a_a\ a_k\ \delta_{lr} - a^{\dagger}_r\ a^{\dagger}_j\ a_l\ a_k\ \delta_{ia} - a^{\dagger}_i\ a^{\dagger}_r\ a_l\ a_k\ \delta_{ja} \qquad (4.19)$$

so that if we had a commutator between a Coulomb matrix element and an excitation amplitude (which would involve a commutator such as in (4.19)) this could be represented diagrammatically by:

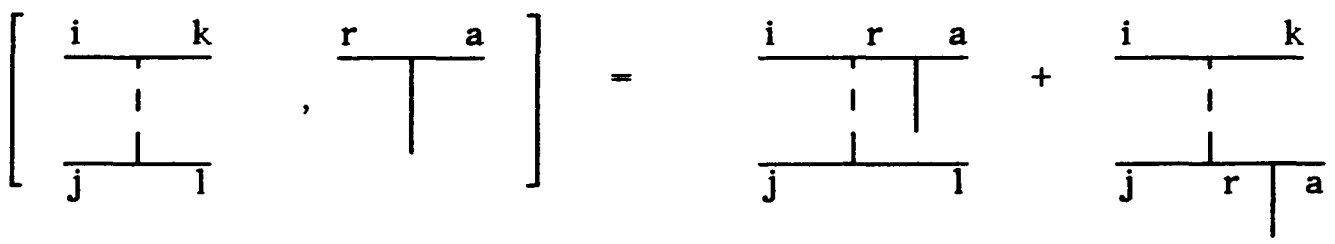

(4.20)

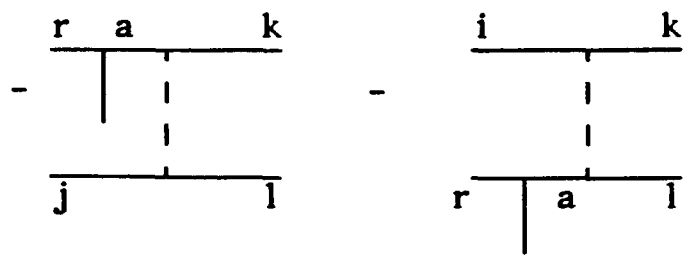

Thus highly complex creation and annihilation operator commutators can be quickly evaluated by this diagrammatic technique.

4.2.4. The Equations of Motion Diagrams

Using our expressions for U, H and P (equations (4.9), (4.15) and (4.10) to (4.12)) with the representation of the ground state by (4.8) we can now evaluate all the commutators in equation (4.5) using the diagram techniques mentioned above. After some simplification we obtain the single excitation EOM commutator diagrams given in table 4.1

It is important to remember that there are implied ground state bras and kets around these diagrams (i.e. $\langle 0|$ and $|0\rangle$ around each side of the equation).

4.2.5. Evaluating the Diagrams

Each vertex in table 4.1 has creation and annihilation operators associated with it as given earlier. Remembering that a line between two vertices implies a Kronecker delta for the orbitals involved and that all creations and annihilations should 'match up' at the end so that one starts and finishes in the ground state, the vertices can then have orbitals assigned to them. It is now that the function of the projection operator becomes more apparent: each projection operator vertex will have an excited orbital *p* and a core orbital *a* associated with it; the appropriate equations for each core orbital can thus be chosen or projected out by selecting the appropriate projection operator for that orbital *a* (the operator has no constraints on it other than it occupies the same space as the excitation operator).

We have not yet said anything specific about the nature of our closed shell ground state other than it is represented by a single particle determinant. In discussing the particle states we shall use the following notation for designating orbitals:

letter	orbital type
a,b,c...	core
p,q,r...	excited
i,j,k,l	any

(4.22)

Table 4.1: Single Excitation EOM in Terms of Commutator Diagrams

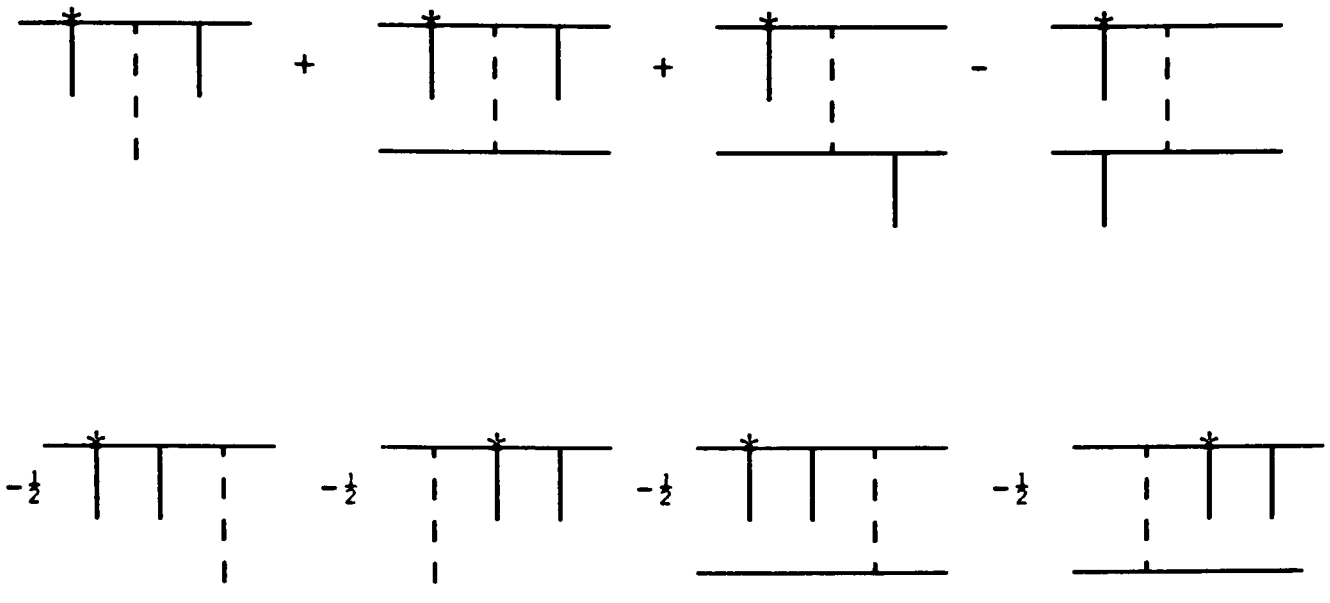

+ all left/right reflections of the above diagrams

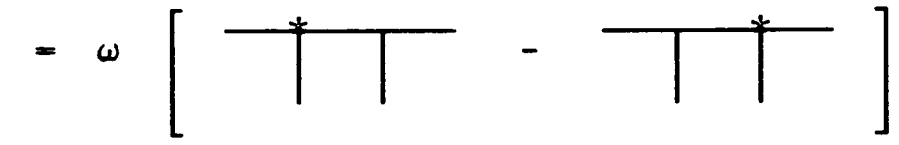

For the sake of brevity the direct and exchange parts to the diagram will be denoted using a '/' so that two diagrams are actually represented: one with the orbital before the '/' on each 'leg' of the diagram and one with the orbital after it. It should be noted that there is an implicit minus sign associated with exchange diagrams (i.e. with diagrams where an orbital appears on the top leg on the left and on the bottom leg on the right). This is because of the commutation relationships for the creation and annihilation operators. Using this notation we obtain the diagrams for both the left and right hand reflections given in table 4.2.

Evaluating these diagrams one by one we obtain the contributions given in table 4.3. Table 4.4 gives the contributions for the reflected diagrams.

4.2.6. The Closed Shell EOM

It should be noted that in the above equation no assumption has been made about the nature of the single-particle states. As mentioned earlier we use a HF ground state for our closed shell systems. We can then use the fact that

$$(h_0 + V_{hf,core}) \, |b\rangle = \epsilon_b \, |b\rangle \tag{4.23}$$

in equation 2 in table 4.3. This greatly simplifies the equations by forcing terms such as equation 2 to be diagonal. If we now define negative and positive excitations by

$$|a^+\rangle \equiv \sum_r |r\rangle \, Y_{ra} \tag{4.24}$$

$$|a^-\rangle \equiv \sum_r |r\rangle \, Z^*_{ra} \tag{4.25}$$

then using equations (4.23) to (4.25) in the equations in table 4.3 we obtain

$$P^+_{ap} \langle p| \, (\epsilon_a + \omega - h_0 - V_{hf,core}) \, |a^+\rangle = P^+_{ap} \langle p|V^+|a\rangle \tag{4.26}$$

where

$$V^+|a\rangle \equiv \sum_{b,b^\pm} \left[\langle b|r_{12}^{-1}(1-P_{12})|b^+\rangle|a\rangle + \langle b^-|r_{12}^{-1}(1-P_{12})|b\rangle|a\rangle \right] \tag{4.27}$$

Table 4.2 Assignment of Particle States to Closed Shell EOM Diagrams

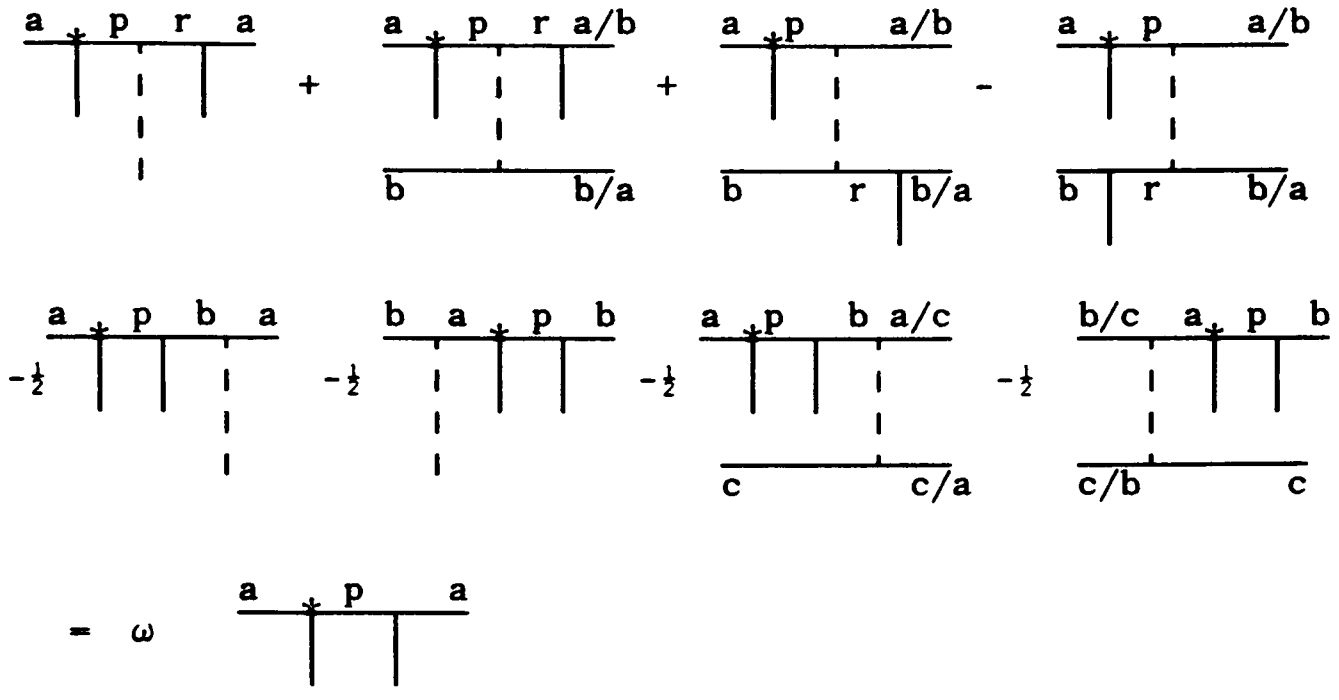

Reflected Diagrams

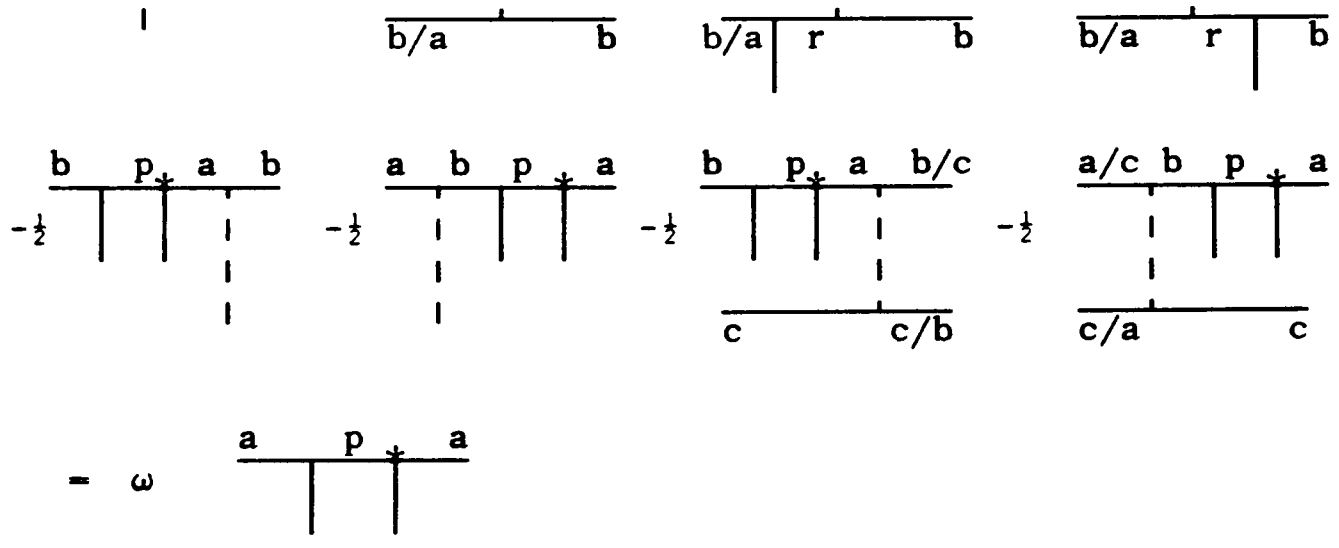

Table 4.3. Contributions from the Diagrams for the Positive Excitations

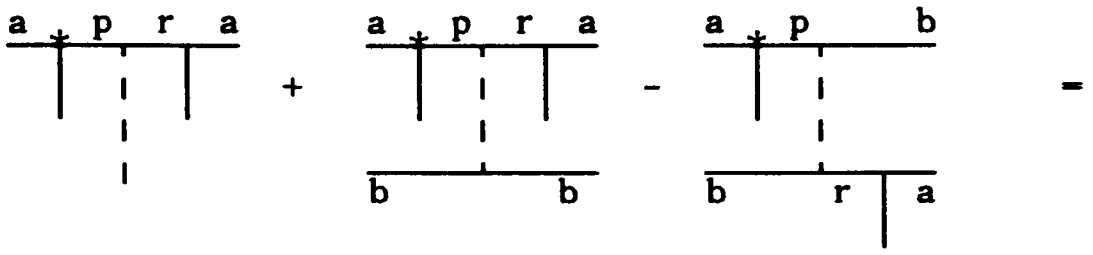

$$= P^{+}_{ap} \sum_{r} \langle p|h_0 + V_{hf,core}|r\rangle Y_{ra} \qquad (1)$$

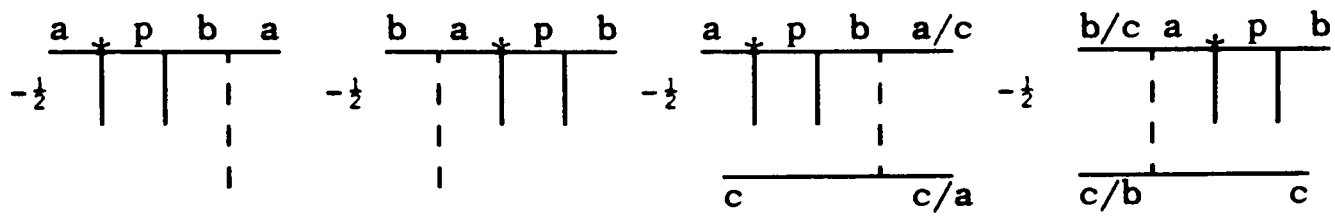

$$= P^{+}_{ap} \sum_{r,b} \langle p|r\rangle\langle b|- h_0 - V_{hf,core}|a\rangle Y_{rb} \qquad (2)$$

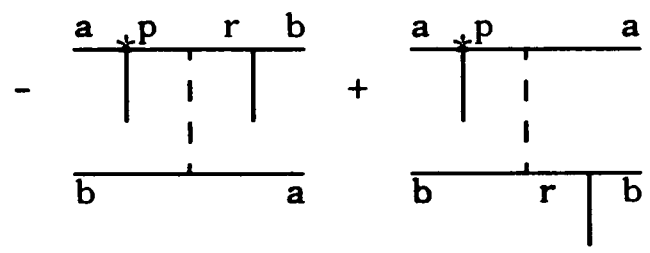

$$= P^{+}_{ap} \sum_{r,b} \langle pb|r_{12}^{-1}\ (1-P_{12})|ar\rangle Y_{rb} \qquad (3)$$

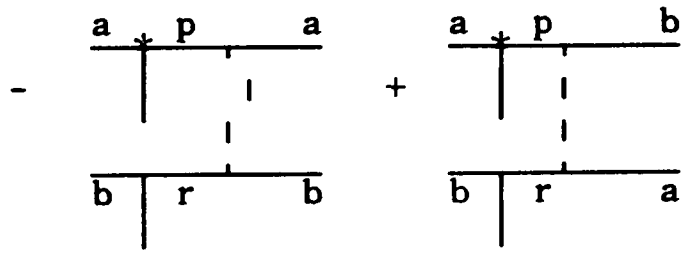

$$= P^{+}_{ap} \sum_{r,b} - \langle pr|r_{12}^{-1}\ (1-P_{12})|ab\rangle\ (-Z_{br}) \qquad (4)$$

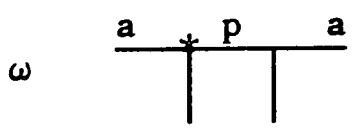

$$= P^{+}_{ap} \sum_{r} \omega \langle p|r\rangle Y_{ra} \qquad (5)$$

where

$$V_{hf,core}\ |x\rangle \equiv \sum_{b} \langle b|r_{12}^{-1}\ (1-P_{12})|b\rangle|x\rangle$$

Table 4.4. Contributions from the Diagrams for the Negative Excitations

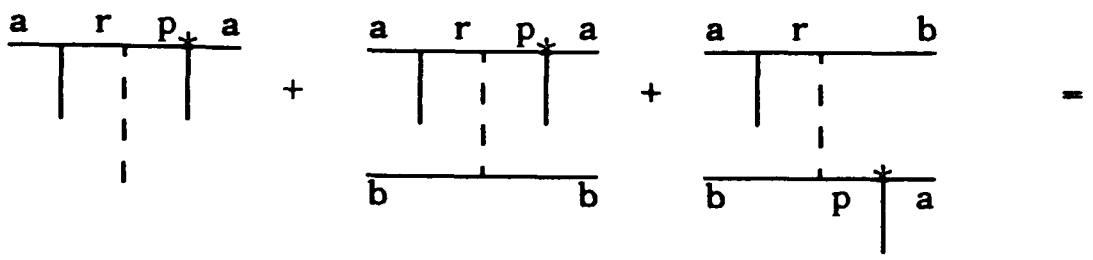

$$= \sum_{r} (-Z_{ra}) \langle r|h_0 + V_{hf,core}|p\rangle P^{-}_{ap} \qquad (1)$$

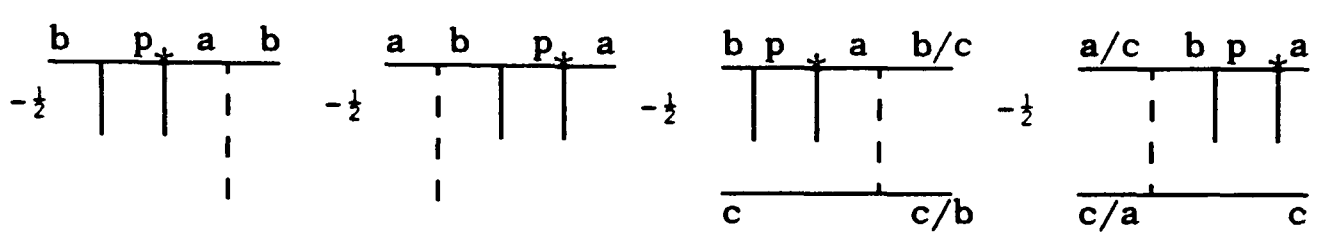

$$= \sum_{r,b} (-Z_{rb}) \langle r|p\rangle\langle a|- h_0 - V_{hf,core}|b\rangle P^{-}_{ap} \qquad (2)$$

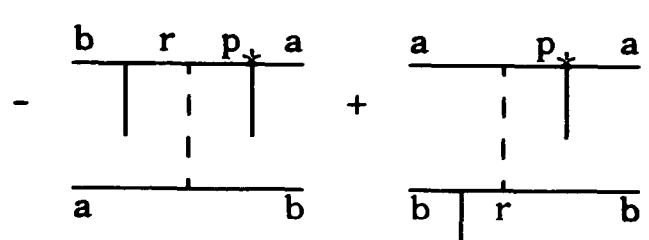

$$= \sum_{r,b} (-Z_{rb}) \langle ra|r_{12}^{-1} (1-P_{12})|bp\rangle P^{-}_{ap} \qquad (3)$$

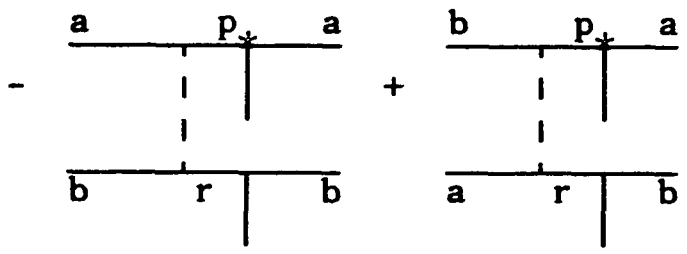

$$= \sum_{r,b} -Y_{br} \langle ab|r_{12}^{-1} (1-P_{12})|pr\rangle P^{-}_{ap} \qquad (4)$$

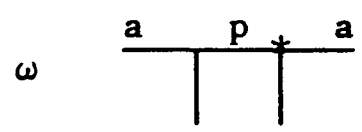

$$= \sum_{r} (-Z_{ra}) \omega \langle r|p\rangle P^{-}_{ap} \qquad (5)$$

where

$$V_{hf,core}|x\rangle \equiv \sum_{b} \langle b|r_{12}^{-1} (1-P_{12})|b\rangle|x\rangle$$

For the reflected diagrams we take the hermitian conjugate of the equations in table 4.4 and multiply by minus one to obtain an equation similar in form to (4.27):

$$P^{-\dagger}_{ap} \langle p| \left(\epsilon_a - \omega - h_0 - V_{hf,core} \right) |a^-\rangle = P^{-\dagger}_{ap} \langle p|V^-|a\rangle \tag{4.28}$$

where

$$V^-|a\rangle \equiv \sum_{b,b^\pm} \left[\langle b|r_{12}^{-1} (1-P_{12})|b^-\rangle|a\rangle + \langle b^+|r_{12}^{-1} (1-P_{12})|b\rangle|a\rangle \right] \tag{4.29}$$

We have said nothing about the projection operator yet. It is an arbitrary operator (apart from covering the same space as U) that enables us to pick out the equations for each orbital excitation. The coefficients P^+_{ap} and P^-_{ap} are arbitrary coefficients. The orbital p in the equations above is an excited state. If we define the coefficients as an overlap with an arbitrary function η_a:

$$P^+_{ap} = P^{-\dagger}_{ap} = \langle \eta_a | p \rangle \tag{4.30}$$

and we put this definition into equations (4.26) and (4.28) above we can then sum over the excited states p. We can then use the closure relationship to write

$$\sum_p P_{ap}\langle p| = \sum_p \langle \eta_a|p\rangle\langle p| = \langle \eta_a|(1 - \sum_b |b\rangle\langle b|) \tag{4.31}$$

The sum over the core orbitals b will have no effect on the left-hand side of equations (4.26) and (4.28) because of our definitions (4.24) and (4.25). However, it adds an extra orthogonality term to the right-hand side of the form

$$-\sum_b |b\rangle\langle b| V^\pm |a\rangle \tag{4.32}$$

Since η_a is arbitrary the equations must hold for all η_a and we can simply write the Closed Shell EOM as

$$\left(\epsilon_a \pm \omega - h_0 - V_{hf,core} \right) |a^\pm\rangle = V^\pm|a\rangle - \sum_b |b\rangle\langle b| V^\pm |a\rangle \tag{4.33}$$

This is the EOM/CS. It of the same form as the closed shell TDHF or

MBPT/RPA equations. The set of equations for all the core excitations form a set of coupled equations to be solved self–consistently.

4.2.7 Evaluation of Normalisation and Matrix Elements

The normalisation of the equations is defined by the relationship:

$$\langle 0 | [\ U^{\dagger}\ ,\ U\ ] | 0 \rangle = 1 \qquad (4.34)$$

This is represented diagrammatically by the commutator of the excitation operator and its hermitian conjugate.

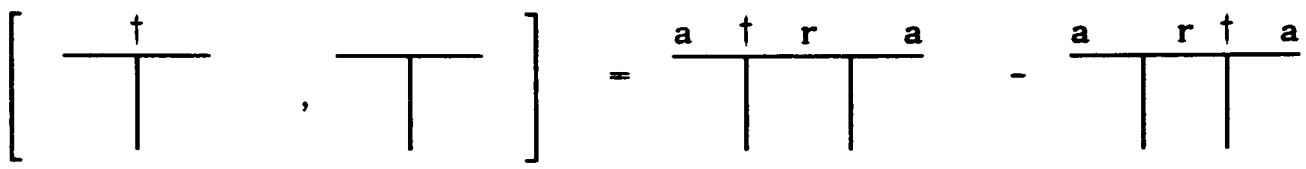

(4.35)

where the † in the diagram refers to the hermitian conjugate of the excitation. These diagrams give

$$\sum_{+} \left(\langle a^{+} | a^{+} \rangle - \langle a^{-} | a^{-} \rangle \right) = 1 \qquad (4.36)$$
$$a^{-}$$

The minus sign for the negative excitations might at first appear a little odd as a contribution to a normalisation. But, as is discussed later, the negative excitations are actually modelling some two particle effects in the ground state, unlike the positive excitations which are generating the excited state, so that one would not necessarily expect the negative excitation contributions to the normalisation of the excited state to be the same.

The matrix element of a transition operator T between the ground and excited state can be calculated using the relationship:

$$\langle 1 | T | 0 \rangle = \langle 0 | \ [\ (U)^{\dagger}\ ,\ T\ ]\ | 0 \rangle \qquad (4.37)$$

which gives, using the diagrams, a sum over single particle matrix elements:

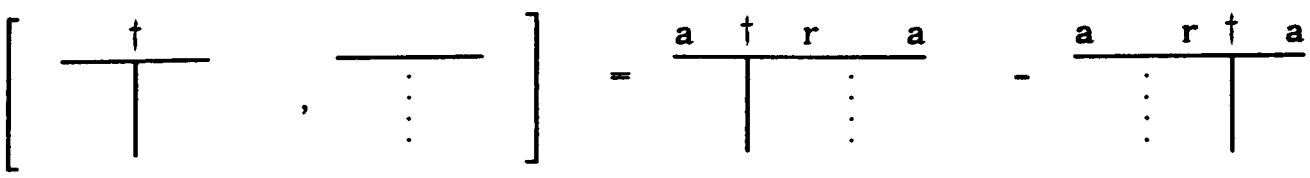

(4.38)

which, when evaluated gives

$$\langle 1|T|0\rangle = \sum_{a^{\pm}} (\langle a^{+}|T|a\rangle + \langle a|T|a^{-}\rangle) \qquad (4.39)$$

We shall discuss the contributions of the negative excitations to the transition matrix element in a later section.

4.2.8. Angular Reductions

So far we have derived a whole series of equations for the excitations of each core orbital for each of the magnetic quantum numbers. As might be guessed the number of equations can be considerably reduced by angular summation techniques. We shall now define reduced excitations by the relationship

$$Y_{r,a} = \overline{Y}_{r,a} \qquad (4.40)$$

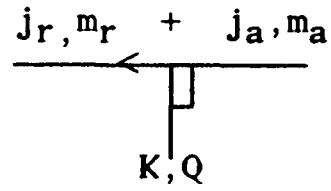

$$Z_{ar} = \overline{Z}_{a,r} \qquad (4.41)$$

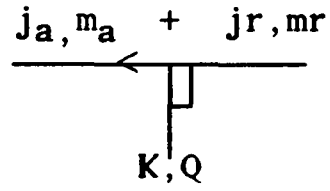

where the lines above the $Y_{r,a}$ and the $Z_{a,r}$ on the right-hand side denote reduced coefficients that do not depend on magnetic quantum numbers. The angular diagrams are as defined in [Lindgren and Morrison]. The K and Q are the rank and component of the tensor U and equal the angular momentum and magnetic quantum number of the excited state. We shall similarly reduce the projection operators by defining:

$$P^{-}{}_{r,a} = \overline{P}^{-}{}_{r,a} \qquad (4.42)$$

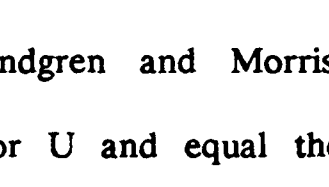

$$P^{+}{}_{r,a} = \overline{P}^{+}{}_{r,a} \qquad (4.43)$$

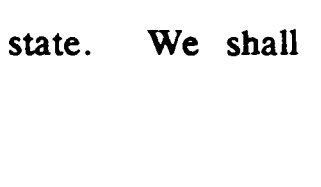

We are now almost in a position to derive the radial equations but we still need an explicit form of the reduced projection operator.

4.2.9. The Projection Operator

In equation (4.30) we have an arbitrary function η_a. It is convenient to define this as a projection operator that projects out a specified angular momentum κ at a specified radial distance r and either the upper or lower component of the Dirac spinor. We shall take the reduced P^+_{ap} to be given by

$$\bar{P}^+_{ap} = < \delta_a{}^i{}_\kappa \ (r) \ | \ p > \tag{4.44}$$

where

$$< \delta_a{}^1{}_\kappa \ (r) \ | \ p > = \int \frac{1}{r'} \begin{bmatrix} \delta(r-r') \\ 0 \end{bmatrix}^\dagger R_p(r') \ r'^2 \ dr'$$

$$< \delta_a{}^2{}_\kappa \ (r) \ | \ p > = \int \frac{1}{r'} \begin{bmatrix} 0 \\ \delta(r-r') \end{bmatrix}^\dagger R_p(r') \ r'^2 \ dr' \tag{4.45}$$

where $R_p(r')$ is the radial part of the Dirac spinor. Thus the projection operator projects out angular factor κ at radial distance r.

We now substitute our definitions for our reduced excitations and projections into our equations (4.26), (4.28), (4.36) and (4.39). The Coulomb matrix elements have the standard associated angular factors (see e.g. [Case Studies]) and we can now sum over the magnetic quantum numbers to obtain radial equations for the reduced excitations. The advantage of our definitions of the reduced angular factors is that the full angular momentum diagram is topologically equivalent to the EOM one: the 'stems' of the projection and excitation operators corresponding to the stems of the angular diagrams (4.40) to (4.43). The projection operator has its 3J symbol associated with it so that in diagrams such as equation 1 in table 4.3 the sum over the magnetic states for both the 3J symbols of the projection operator and the excitation has a very simple angular reduction. Its effect is to 'cancel out' the excitation 3J symbol.

4.2.10. Example of Derivation of Radial Contribution

To demonstrate the angular summation we shall derive the exact expression for one of the diagrams. We shall evaluate the diagram:

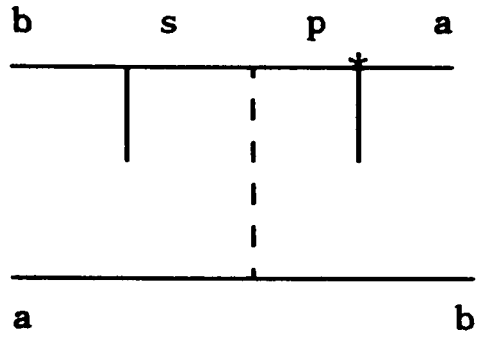

(4.46)

There are three parts to the process of calculating a diagram: the diagram phase factor, its angular part and its radial part.

Phase

Every diagram has a phase (i.e. a +1 or −1) associated with it which comes from factors other than angular considerations. There are five different contributions to the phase of a diagram:

1. Direct or exchange diagrams:

   This is purely determined by the properties of the creation and annihilation operators. The same particle states must occur at either end of the diagram; if the two matching states are both at the top or bottom (a direct diagram) the phase contribution is +1, if one at the top and one at the bottom (an exchange diagram) then the phase is −1. The above diagram is an exchange type because the *a*'s and *b*'s occur at the top and bottom on each side.

2. EOM commutator diagram factor:

   This arises from the evalutation of the commutator diagrams in table 4.1. There are factors of $\frac{1}{2}$ and ω to be inserted and signs of ±1. The above diagram has a factor of +1.

3. Negative excitations:

   From our definition of U in equation (4.9) there is a minus sign associated with the negative excitations (the terms with the Z_{ar} coefficients). The above diagram contains a negative excitation so the factor is −1.

4. Re-arrangement:

   In the EOM/CS (equation (4.33)) we arranged the terms in a convenient form. There is a phase factor from this re-arrangement. It results in a minus sign for all terms except ones with ω in or ones that contribute to $V^{\pm}$. This diagram is part of V^{-} so the factor is +1.

5. Equation being solved for:

   The negative excitation equations were multiplied by a factor of −1 and the hermitian conjugate taken. There is therefore a −1 phase factor when solving for negative excitations. Since this diagram is for a negative excitation there is a −1 factor.

In evaluating the overall factor we multiply the five component factors to get

$$-1 \times +1 \times -1 \times +1 \times -1 = -1 \qquad (4.47)$$

so the overall phase factor is −1.

Angular Summation

The Coulomb interaction will have two 3J symbols and two reduced C^k tensor matrix elements associated with it. Each excitation and projection operator has a 3J symbol in its definition. Using the angular diagrammatic techniques of [Lindgren and Morrison] we obtain an angular diagram that is topologically identical to the EOM commutator diagram we are solving. The signs at the vertices and the phase arrows have to be added. The angular diagram for the diagram we are solving is given by

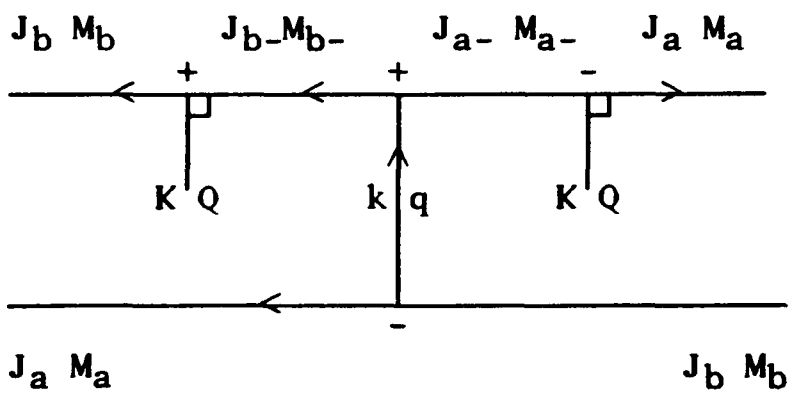

(4.48)

We can now sum over the M quantum numbers using the angular momentum diagram techniques of [Lindgren and Morrison]. We obtain

$$(-1)^{K + J_b + J_{b-}} \begin{Bmatrix} J_{a-} & J_{b-} & k \\ J_b & J_a & K \end{Bmatrix} X^k(K_{b-}, K_a, K_{a-}, K_b) \qquad (4.49)$$

where we have included the X^k function which consists of the two reduced C^k matrix elements and a phase of $(-1)^k$ (see e.g. [Case Studies]).

Radial Part

This can usually be written down by inspection. It must be remembered that the negative excitation equations have to have their hermitian conjugate taken. The projection operator in equation (4.44) turns the Slater integral into the product of a radial wavefunction and a $Z^k(ba;r)$ function (which is $1/r\ Y^k(ba;r)$, where $Y^k(ab;r)$ is the usual Hartree function; see e.g. [Case Studies]).

In our example above we have to take the hermitian conjugate (which amounts to a mirror reflection of the radial parts). Using equation (4.25) we can write the negative excitation vertex as

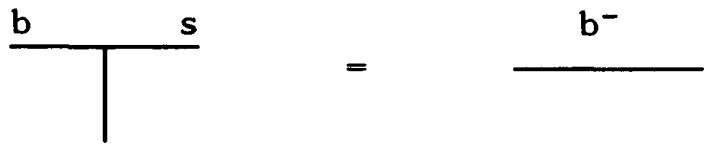

We can also use (4.30) and (4.44) to write

The radial diagram we end up with after reflecting it is

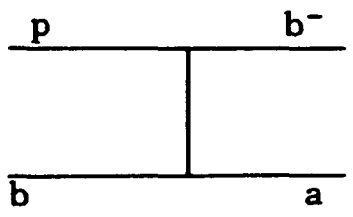

$$<\delta\,|\,p> \qquad (4.50)$$

The left-hand part is the Slater integral given by

$$\int_0^\infty R^\dagger(p;r_1)\; R^\dagger(b;r_2)\; \frac{r_<^{\,k}}{r_>^{\,k+1}}\; R(b^-;r_1)\; R(a;r_2)\; r_1^{\,2}\, dr_1\; r_2^{\,2}\, dr_2 \qquad (4.51)$$

The R's are the radial parts of the Dirac two component spinors. The final summation over the excited state p together with the $<\delta|p>$ factor as in equation (4.31) will effectively replace the $R^\dagger(p;r_1)$ by the upper or lower component of the delta projection operator as given in equation (4.45). There will also be the orthogonalisation term of (4.32). Thus the upper or lower component projector picks out either the upper or lower component of the radial equation. The final radial function can be written as

$$Z^k(ba;r)\; r\; R(b^-;r) \qquad (4.52)$$

This is the radial part of the diagram.

4.2.11. Final Expression for the Diagram

Collecting together the component parts for the diagram we obtain

$$-1 \times (-1)^{K + J_b + J_{b-}} \begin{Bmatrix} J_{a-} & J_{b-} & k \\ J_b & J_a & K \end{Bmatrix} Z^k(ba;r)\; r\; R(b^-;r)\; X^k(K_{b-},K_a,K_{a-},K_b) \qquad (4.53)$$

This term appears in the negative excitation equation for orbital a. The formal expression that it corresponds to is

$$<b|\; r_{12}^{-1}|a>\; |b^-> \qquad (4.54)$$

which appears in (4.29) in $V^-|a>$.

4.2.12. Normalisation and Transition Matrix Element Angular Factors

In summing over the angular factors for the normalisation and transition matrix elements we use the same techniques as for the other diagrams. In the normalisation diagrams (4.35) there are 3J symbols associated with the excitations and their hermitian counterparts. The angular summations give a factor of one so the radial normalisation condition is

$$\sum_{a^{\pm}} \int_0^{\infty} R^{\dagger}(a^{+};r)\, R(a^{+};r)\, r^2\, dr - \int_0^{\infty} R^{\dagger}(a^{-};r)\, R(a^{-};r)\, r^2\, dr = 1 \qquad (4.55)$$

The angular summation for the transition matrix element is similar. The result is

$$\langle J_1 M_1 | T^{\lambda}{}_{\mu} | 00 \rangle = \sum_{a^{+}} \delta(K,\lambda)\ \delta(Q,\mu)\ [K]^{-\frac{1}{2}} \left[\langle a^{+} || T^{\lambda} || a \rangle + \langle a || T^{\lambda} || a^{-} \rangle \right] \qquad (4.56)$$

We usually require a reduced transition matrix element. This is given by

$$\langle J_1 M_1 | T^{\lambda}{}_{\mu} | 00 \rangle = -[J_1]^{-\frac{1}{2}}\ \delta(J_1,\lambda)\ \delta(M_1,\mu)\ \langle J_1 ||\ T^{\lambda}\ || 0 \rangle \qquad (4.57)$$

Thus we obtain

$$\langle J_1 || T^{\lambda}{}_{\mu} || 0 \rangle = \sum_{a^{+}} -\ \delta(K,\lambda)\ [J_1]^{+\frac{1}{2}} [K]^{-\frac{1}{2}} \left[\langle a^{+} || T^{\lambda} || a \rangle + \langle a || T^{\lambda} || a^{-} \rangle \right] \qquad (4.58)$$

4.2.13. Summary for Closed Shell Equations

Starting with the EOM and making a single excitation approximation for the excitation operator and using a HF ground state determinant we end up with equation (4.33) which is the Closed Shell EOM for the positive and negative excitations of the core orbitals. These equations are equivalent to the standard Time Dependent HF (TDHF) equations for closed shell systems or alternatively, may be derived from MBPT using the RPA approximation. In the MBPT picture, the resonant transition dipole induces polarisation in the other core orbitals which in a self-consistent way produces a modified transition dipole for the atom as a whole. In this way all the

RPA 'bubble diagrams' (see chapter three) are included in the equations by iterating them till they are self consistent.

The positive excitations for a given core orbital are sums over excited state orbitals that the core orbital can go to; negative excitations on the other hand are sums over excited states that can be de-excited into the core state. Due to the ω term on the left-hand side of the equation there is a resonance for positive excitations when the excitation energy equals omega. Thus the resonant excitation is represented by a large contribution to one of the positive core excitations. This resonance was dealt with numerically by techniques which will be described later.

It is fairly easy to see what the positive excitations represent. However it is not so clear as to the physics represented by the negative excitations. If we consider the ground state $|\alpha\rangle$ then the excited state is represented by single particle excitations from this ground state which we can write as $|\alpha^r{}_a\rangle$. The resonant single particle excitation is included in this and will be the dominant term. We are interested in single particle matrix elements between the ground and excited states so we require matrix elements between the two determinantal states that differ by only one particle. $|\alpha^r{}_a\rangle$ differs by a single particle excitation from $|\alpha\rangle$. Taking matrix elements between the excited and ground states we obtain

$$\langle\alpha^r{}_a|T|\alpha\rangle = \langle r|T|a\rangle \qquad (4.59)$$

This matrix element is of the form of the positive excitation contributions to the total matrix element. Now we can also have matrix elements between the excited state and and a state differing by a single excitation from it, e.g. a state such as $|\alpha^r{}_a{}^s{}_b\rangle$. Matrix elements between the excited state and this state will be given by

$$\langle\alpha^r{}_a|T|\alpha^r{}_a{}^s{}_b\rangle = \langle b|T|s\rangle \qquad (4.60)$$

This matrix element is in the form of a negative excitation. Thus the negative excitations represent single excitations from the excited state. They are modelling some two particle effects in the ground state. However they are not true two particle excitations of the ground state because they can only differ from the excited state by a single excitation: they are correlated to the excited state.

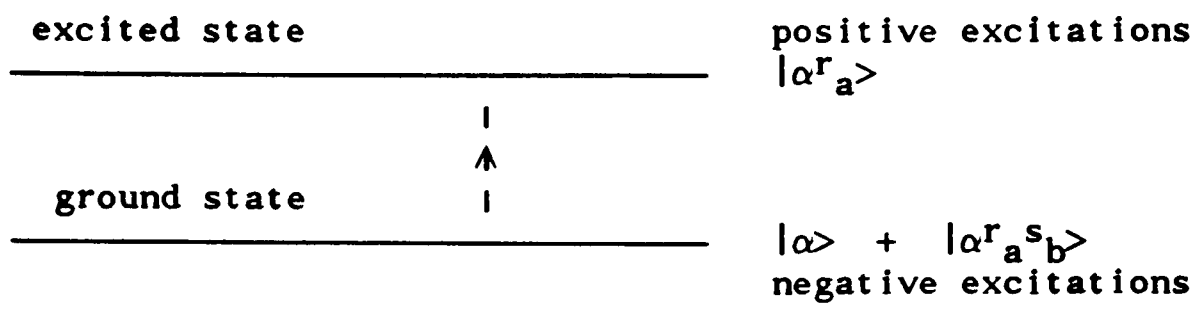

To understand why in the expression for the normalisation the negative excitations have a minus contribution (see (4.36)) consider the ground and excited states:

$$|0_{exact}\rangle = |0_{HF}\rangle + |\alpha(a^-)\rangle$$
$$|1\rangle = |\alpha(a^+)\rangle \qquad (4.61)$$

Where $|\alpha(a^-)\rangle \equiv |\alpha^r_a s_b\rangle$ and $|\alpha(a^+)\rangle \equiv |\alpha^r_a s_b\rangle$. The normalisation condition for each state gives

$$\langle 0_{HF}|0_{HF}\rangle + \langle\alpha(a^-)|\alpha(a^-)\rangle = \langle\alpha(a^+)|\alpha(a^+)\rangle = 1 \qquad (4.62)$$

$$\rightarrow \quad \langle 0_{HF}|0_{HF}\rangle = \langle\alpha(a^+)|\alpha(a^+)\rangle - \langle\alpha(a^-)|\alpha(a^-)\rangle \neq 1 \qquad (4.63)$$

In our calculation we used an intermediate normalisation given by

$$\langle 0_{HF}|0_{HF}\rangle = 1 \qquad (4.64)$$

Renormalising equation (4.63) we obtain

$$\langle\alpha'(a^+)|\alpha'(a^+)\rangle - \langle\alpha'(a^-)|\alpha'(a^-)\rangle = 1 \qquad (4.65)$$

where the primed excitations indicate renormalisation. So the negative excitations, because they are modelling some two particle effects in the ground state, have a negative contribution to the normalisation condition.

Despite the fact that the equations so far derived have no new physics in them, they have several points of interest:

1. the method of derivation of the equations is simpler than summing certain MBPT diagrams to all orders with the 'feed back' of the 'bubble diagrams' being automatically derived.
2. the approximations that have been made are in the complexity of the ground state and the excitation operator rather than in the order of the Coulomb matrix element.
3. by including negative excitations in the excitation operator certain ground state two

particle effects are modelled.

4. the method can easily be extended to open shell problems as we shall now discuss.

4.3 Extension to Open Shell Systems

All the systems of interest for parity violating effects have at least one valence electron (except lead) so it is necessary to extend our method to include such systems. For closed shell atoms an orbital is either a core or an excited orbital and a core orbital can only be excited into an excited orbital. In the open shell case, however, there is a third type of orbital, namely the valence orbital which can have excitations both to and from it. This means that there will be many more creation and annihilation operator diagrams than for the closed shell diagrams. One also has to be careful about Exclusion Principle violating diagrams and the fact that some of the valence shell is occupied and cannot be excited to. Another problem that has to be tackled is to ensure that both the ground and excited states are eigenstates of angular momentum. The state produced by the excitation operator acting on the ground state will now not necessarily be an exact angular momentum eigenstate because U^K_Q is now acting on a non-zero angular momentum state.

We shall approach this last problem by starting with the ground state of angular momentum j_0 and magnetic quantum number m_0. The excitation operator is a tensor of rank K, component Q, denoted by U^K_Q. In order to produce an exact angular momentum eigenstate we need to consider a linear combination of excitation operators with different Q's acting on ground states with different m_0's.

$$|j_1,m_1\rangle \equiv \sum_{Q,m_0} U^K_Q \, |j_0,m_0\rangle\langle KQ, j_0m_0|j_1m_1\rangle \qquad (4.66)$$

The linear combination coefficients $\langle KQ,j_0m_0|j_1m_1\rangle$ are Clebsch-Gordan coefficients. The tensor rank K is not fixed by this definition but we shall in practice assume that only excitations of rank one are important. Of the core excitations, only those of rank one actually contribute directly to the matrix element and it is assumed that the contributions of other ranks to the rank one excitations are small. The role

of the rank of the excitation operator will be discussed more fully in chapter eight. The requirement equivalent to (4.2) in the closed shell case is similar:

$$(U^K_Q)^\dagger \; |j_0, m_0\rangle = 0 \tag{4.67}$$

We require, as before, a projection operator P which when operating on the ground state will also produce the excited state angular momentum but which we shall define in terms of its tensor adjoint

$$\langle j_1, m_1| = \sum_{Q', m_0'} \langle j_1 m_1 | KQ', j_0 m_0' \rangle \langle j_0 m_0' | \; (P^K_{Q'})^\dagger \tag{4.68}$$

The extension of the closed shell EOM (4.5) using the new definitions of the excitation operator leads to the open shell equation of motion.

$$\sum_{\substack{Q,Q' \\ m_0,m_0'}} \langle j_1 m_1 | KQ', j_0 m_0' \rangle\langle j_0 m_0' | \; [\; (P^K_{Q'})^\dagger, H, \; U^K_Q \;] \; |j_0 m_0\rangle\langle KQ, j_0 m_0 | j_1 m_1\rangle$$

$$= \tag{4.69}$$

$$\omega \sum_{\substack{Q,Q' \\ m_0,m_0'}} \langle j_1 m_1 | KQ', j_0 m_0' \rangle\langle j_0 m_0' | \; [\; (P^K_{Q'})^\dagger, \; U^K_Q \;] \; |j_0 m_0\rangle\langle KQ, j_0 m_0 | j_1 m_1\rangle$$

This method is based on that first used by [Rowe] who first formulated the open shell EOM. The main difference between the open shell and the closed shell EOM is the presence of the Clebsch–Gordan coefficients and the summation over the magnetic quantum numbers.

4.3.1. Open Shell Normalisation and Transition Matrix Elements

In analogy with the closed shell case we require

$$\langle j_1 m_1 | j_1 m_1 \rangle = 1 \tag{4.70}$$

Using definitions (4.66) and (4.67) we can write this as

$$\sum_{\substack{Q,Q' \\ m_0,m_0'}} \langle j_1 m_1 | KQ', j_0 m_0' \rangle\langle j_0 m_0' | \; [\; (U^K_{Q'})^\dagger \; , \; U^K_Q \;] \; |j_0 m_0\rangle\langle KQ, j_0 m_0 | j_1 m_1\rangle$$

$$= \; 1 \tag{4.71}$$

This is the Open Shell EOM normalisation condition.

In evaluating the transition matrix element we usually require the reduced matrix element rather than one dependent on all the magnetic quantum numbers. Using the Wigner-Eckart theorem (see [Lindgren and Morrison]) we can express the reduced matrix element in terms of a sum of unreduced ones.

$$\langle j_1 || T^\lambda || j_0 \rangle = [J_1]^{\frac{1}{2}} (-1)^{J_1 - J_0 + \lambda} \sum_{m_0, \mu} \langle j_1 m_1 | T^\lambda{}_\mu | j_0 m_0 \rangle \langle \lambda \mu, j_0 m_0 | j_1 m_1 \rangle \tag{4.72}$$

Using (4.66) and (4.67) we can then express this as

$$\langle j_1 || T^\lambda || j_0 \rangle = [J_1]^{\frac{1}{2}} (-1)^{J_1 - J_0 + \lambda} \sum_{\substack{m_0, m_0' \\ Q', \mu}} \langle j_1 m_1 | KQ', j_0 m_0' \rangle \langle j_0 m_0' | [(U^K_{Q'})^\dagger , T^\lambda_\mu] | j_0 m_0 \rangle \langle \lambda \mu, j_0 m_0 | j_1 m_1 \rangle \tag{4.73}$$

This is the Open Shell EOM expression for the reduced transition matrix element.

4.3.2. Open Shell Notation

Now that we have three types of single particle states: core, excited and valence, we need a notation to distinguish between them. We shall use

letter	orbital type	(4.74)
a,b,c...	core	
p,q,r...	excited (including valence)	
x,y,z	excited (excluding valence)	
v,n	valence	
i,j,k,l	any	

4.3.3. Open Shell Approximations

1. We shall make the same single particle approximation for the excitation operator as we did for the closed shell case except that now we must include excitations and de-excitations to and from the partially occupied valence shells as well

$$U^K_Q = \sum_{r,a} a^\dagger_r a_a Y_{ra} - a^\dagger_a a_r Z_{ra} + \sum_{x,n} a^\dagger_x a_n Y_{xn} - a^\dagger_n a_x Z_{nx} \tag{4.75}$$

2. There are again several choices for the ground state. We shall use a V_{N-1} HF ground state. In MBPT it does not matter what approximate wavefunction is started with, the correct solution is approached by adding correction terms in the perturbation series. With the EOM, however, there is an approximation in the complexity of U and the ground state and choosing an inaccurate ground state can lead to a less correct answer. The correspondence between a certain approximation in the ground state in the EOM and the equivalent order of MBPT diagram is not obvious.

The advantage of using a V_{N-1} HF ground state to start with is that it makes the equations simpler and a subset of the EOM diagrams obtained lead to the same equations as the RPA in MBPT. Thus we can check our method against RPA calculations done by others. However, in our initial derivation of the equations we shall, as before, make no assumptions about the nature of the ground state other than it is represented by a single particle determinant.

4.3.4. The Open Shell Diagrams

The ground state can be expressed in terms of creation and annihilation operators by

$$|j_0 m_0\rangle = a^\dagger_v \, |core\rangle \qquad (4.76)$$

so that in evaluating the commutators in equation (4.69) we must now include diagrams with a valence orbital on one of the outer 'legs'. Since we are only considering single valence elements there can be no diagrams with two outer valence legs. In addition we now have valence excitations as part of our excitation operator so that there will be diagrams with valence orbitals specified inside the diagram (as opposed to on the ends). Topologically the commutator diagrams are the same as for the closed shell case (i.e. the diagrams given in equation Table 4.1).

4.3.5. The RPA EOM Approximations

As with MBPT the number of diagrams to calculate increases greatly when open shell atoms are considered. The full list of diagrams is given in chapter eight. For the moment though we are going to make certain approximations, both in which diagrams we shall include in our equations and in the nature of the valence contributions to the excitation operator. These approximations lead to the EOM/RPA.

1. In the expression for the excitation operator (4.75) we are going to assume that the only important valence excitation term is the resonant one. Thus we are going to neglect all negative valence excitations and all positive ones apart from the single-particle resonant contribution. We can thus write the excitation operator as

$$U^K_Q = \sum_{r,a} \left(a^\dagger_r a_a Y_{ra} - a^\dagger_a a_r Z_{ra} \right) + a^\dagger_{v2} a_{v1} Y_{v2,v1} \qquad (4.77)$$

where v_1 going to v_2 is the single particle resonant transition with amplitude given by $Y_{v1,v2}$.

2. Having made approximation 1 this means that all the EOM commutator diagrams associated with negative valence excitations are to be neglected. In addition we shall neglect all other diagrams that explicitly involve valence states except four. Thus we shall only consider the closed shell diagrams (which of course will still be there) and the following four valence diagrams

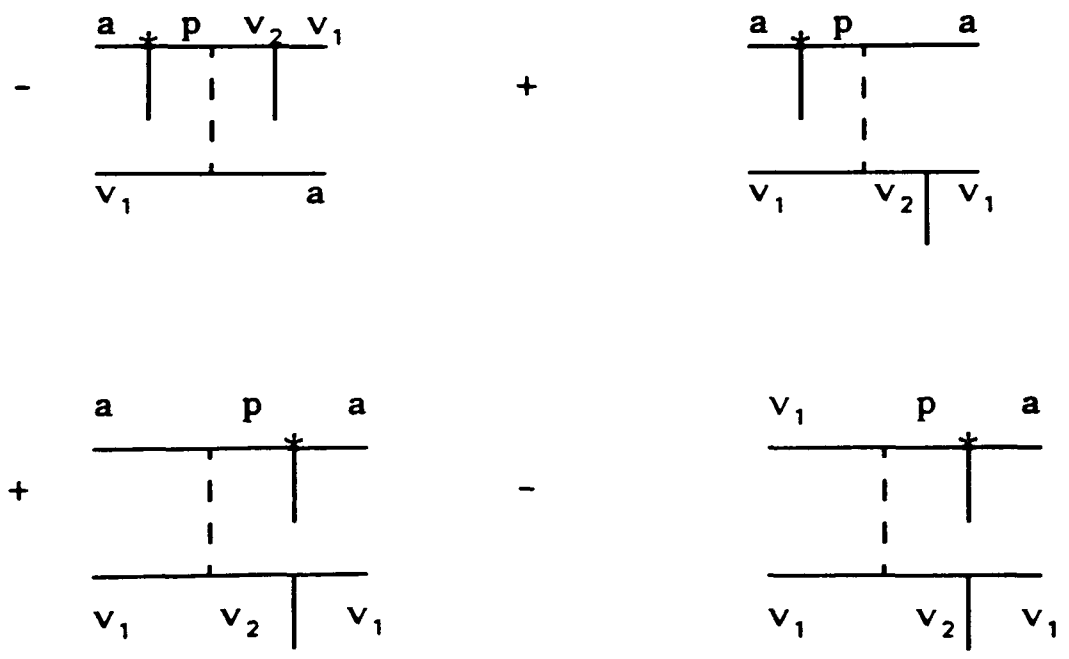

(4.78)

The upper two diagrams contribute to the positive core excitation equations giving

$$P^{+}_{ap} \; \langle pv_1 | \; r_{12}^{-1} \; (1-P_{12}) \; | av_2 \rangle \; Y_{v2,v1} \qquad (4.79)$$

The lower two diagrams contribute to the negative core excitation equations giving (after reflection)

$$P^{-}_{ap} \; \langle pv_2 | \; r_{12}^{-1} \; (1-P_{12}) \; | av_1 \rangle \; Y_{v2,v1} \qquad (4.80)$$

3. We shall approximate the transition frequency ω by the difference between the single particle state eigenvalues. Thus we put $\omega = \epsilon_{v2} - \epsilon_{v1}$.
4. We shall define the valence excitation in a similar manner to the core ones:

$$|v^{+}\rangle \equiv |v_2\rangle \; Y_{v2,v1} \qquad (4.81)$$

4.3.6. Open Shell Normalisation and Transition Matrix Elements

The full list of additional terms that are added to the normalisation are given in chapter eight. For the EOM/RPA we shall only include one additional contribution to the normalisation.

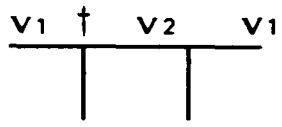

which, when evaluated gives $\langle v^{+}|v^{+}\rangle$ so that the expression for the normalisation now reads

$$\langle v^{+}|v^{+}\rangle \; + \; \sum_{a^{\pm}} \left[\langle a^{+}|a^{+}\rangle \; - \langle a^{-}|a^{-}\rangle \right] \; = \; 1 \qquad (4.82)$$

The full correction terms to the transition matrix element are also given in chapter eight. For the EOM/RPA we shall only consider the term given by

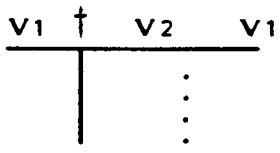

(4.83)

which, when evaluated gives $\langle v^{+}|T|v_1\rangle$. We now obtain for the transition matrix element:

$$\langle 1|T|0\rangle \; = \; \langle v^{+}|T|v_1\rangle \; + \; \sum_{a^{\pm}} \left[\langle a^{+}|T|a\rangle + \; \langle a^{-}|T|a\rangle \right] \qquad (4.84)$$

4.3.7. The RPA EOM

Making the EOM/RPA approximations given above we obtain a set of equations. We can treat the projection operator as we did for the EOM/CS (see equations (4.30) and (4.31)) and we obtain

$$(\epsilon_a \pm \omega - h_0 - V_{hf,core}) \, |a^{\pm}\rangle = V^{\pm}|a\rangle - \sum_b |b\rangle\langle b|V^{\pm}|a\rangle \tag{4.85}$$

$V^{\pm}$ is now defined by:

$$\begin{aligned} V^{\pm}|a\rangle \equiv & \sum_{b,b^{\pm}} \left[\langle b|r_{12}^{-1} (1-P_{12})|b^{\pm}\rangle|a\rangle + \langle b^{\mp}|r_{12}^{-1} (1-P_{12})|b\rangle|a\rangle \right] \\ & + \langle v_1|r_{12}^{-1} (1-P_{12})|v^{+}\rangle|a\rangle \qquad \text{for } V^{+} \\ & + \langle v^{+}|r_{12}^{-1} (1-P_{12})|v_1\rangle|a\rangle \qquad \text{for } V^{-} \end{aligned} \tag{4.86}$$

with the transition matrix element given by

$$\langle 1|T|0\rangle = \langle v^{+}|T|v_1\rangle + \sum_{a^{\pm}} (\langle a^{+}|T|a\rangle + \langle a^{-}|T|a\rangle) \tag{4.87}$$

with the normalisation condition

$$\langle v^{+}|v^{+}\rangle + \sum_{a^{\pm}} (\langle a^{+}|a^{+}\rangle - \langle a^{-}|a^{-}\rangle) = 1 \tag{4.88}$$

These are the EOM/RPA.

4.3.8. Angular Reductions for the EOM/RPA

Similarly to the closed shell case we define the valence excitation and its angular reduction by

$Y_{v1,v2} =$

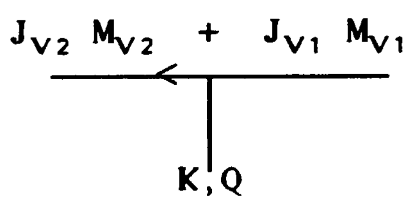

$\bar{Y}_{v1,v2} \; [J_1]^{\frac{1}{2}}$ (4.89)

Note the difference between this definition and the core excitations: there is a factor of $(2J_1+1)^{\frac{1}{2}}$ instead of $(2K+1)^{\frac{1}{2}}$. The reason for this is that it gives more convenient

angular factors when we come to evaluate the matrix elements.

The rules for deriving the actual radial equation are the same as for the EOM/CS. There is a phase factor, an angular summation and the radial part. The phase evaluation is identical to the EOM/CS. In the angular summation however there are now the two Clebsch–Gordan coefficients to be included. Using the same angular diagrammatic technique as before we write these two coefficients as

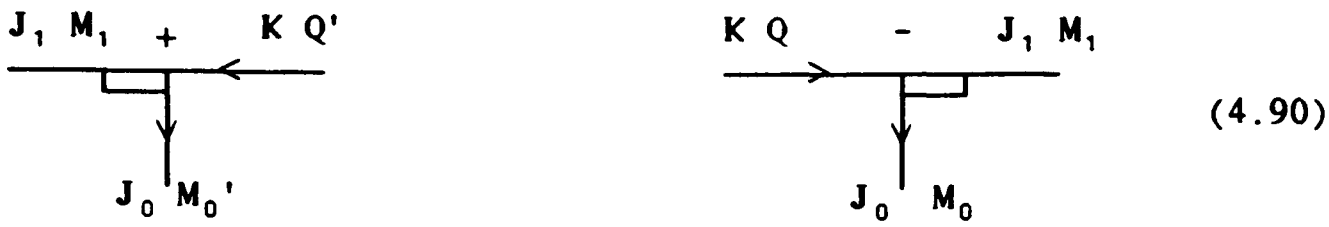

(4.90)

We must now include these diagrams in our total angular momentum diagram. It must also be remembered that Q, Q', M_0 and M_0' have to be summed over. Using a theorem first given by [Jucys, Levinson and Vanagas] it is possible to show that for all the core diagrams these two Clebsch–Gordan coefficients factorise off to give a multiplicative factor of unity. Thus we can use the same expressions for the diagrams with only core assignments that we evaluated for the EOM/CS. For diagrams that contain valence states we have to include the two factors though. For the EOM/RPA it is only the four extra commutator diagrams, one normalisation diagram and one transition matrix element diagram that have to be evaluated to obtain the radial EOM/RPA equations from the EOM/CS ones.

Radial Part

The evaluation of the radial contributions from a diagram follows the same method as for the EOM/CS. Though we have replaced the valence excitation by the single particle state v_2 the choice of normalisation is up to us since the EOM/RPA are linear in the excitations and any multiplicative factors will be cancelled out by the normalisation factor. For convenience we shall choose a factor such that the overlap of the valence excitation with the local RSCF excited state wavefunction is unity. The reason for this is to make the equations more convenient when modifying them to give the Full Open Shell EOM. For details see chapter eight.

4.3.9. Properties of the EOM

There are several important properties of both the EOM/CS and the EOM/RPA which are worth noting

1. Although the core excitations have been defined to be orthogonal to all the core orbitals this is not a necessary requisite and the orthogonality terms need only be included for the orbital being excited. The reason for this is that all the contributions to the final matrix element from admixtures between core orbitals will exactly cancel (see [Botham]).

2. It appears from (4.85) that the excitation $|a^+\rangle$ which is a correction to core orbital $|a\rangle$ can interact with that same core orbital in the HF potential. This is not actually so because the feedback terms on the right-hand side of the equation that involves $|a^+\rangle$ exactly cancel this self-interaction term. This means that the core excitations interact with N-2 electrons as did the core orbitals in the V_{N-1} HF equation. The correction term for this is included in the full set of diagrams and we shall evaluate it in chapter eight.

3. The length and velocity gauges are equivalent for the EOM/CS and the EOM/RPA (see Appendix 3).

4.4. Parity Non-Conserving Equations

Having derived the parity conserving EOM/CS and EOM/RPA we now derive their PNC counterparts. As mentioned in chapter three the method is fairly straightforward.

Let us start with a ground state made up of parity mixed single particle states that are solutions to the parity mixed HF equation

$$(\epsilon_a - h_0 - h_{pnc} - \tilde{V}_{hf,core})|\tilde{a}> = 0 \qquad (4.91)$$

where the tilde denotes parity mixed orbitals including all the orbitals contributing to the HF potential. If in our full Hamiltonian the part h_0 in (4.13) now has h_{pnc} included in it then we can follow through with our derivation as before except now we are using parity mixed orbitals. We obtain

$$P^{\pm}_{ap}<\tilde{p}|(\epsilon_a \pm \omega - h_0 - h_{pnc} - \tilde{V}_{hf,core})|\tilde{a}^{\pm}> = P^{\pm}_{ap}<\tilde{p}|\tilde{V}^{\pm}|\tilde{a}> \qquad (4.91)$$

where the tildes over the various potential terms denote that all the contributing orbitals and excitations in the potential are parity mixed. We have not yet specified the form of the projection operator. We shall write it as

$$P^{\pm}_{ap} = < \eta_a \mid \tilde{p} > \qquad (4.92)$$

We can use the parity mixed version of the closure relationship (since the eigenfunctions of equation (4.91) form a complete set. This gives

$$<\eta_a|(\epsilon_a \pm \omega - h_0 - h_{pnc} - \tilde{V}_{hf,core})|\tilde{a}^{\pm}> = <\eta_a|\tilde{V}^{\pm}|\tilde{a}> \qquad (4.93)$$

$$- \sum_{\tilde{b}} <\eta_a|\tilde{b}><\tilde{b}|\tilde{V}^{\pm}|\tilde{a}>$$

where we have not yet specified η_a.

We can now expand (4.93) in powers of G_F. The zeroth order terms correspond to the appropriate parity conserving EOM (EOM/CS or EOM/RPA according to which PNC equation is being derived). The first order terms give the PNC EOM:

$$(\epsilon_a \pm \omega - h_0 - V_{hf,core}) |a^{\pm pnc}\rangle = V^{\pm}|a^{pnc}\rangle + V^{\pm pnc}|a\rangle$$

$$+ h^{pnc}|a^{\pm}\rangle + V^{pnc}_{hf,core}|a^{\pm}\rangle$$

$$- \sum_b |b\rangle\langle b| (V^{\pm}|a^{pnc}\rangle + V^{\pm pnc}|a\rangle)$$

$$- \sum_b |b^{pnc}\rangle\langle b|V^{\pm}|a\rangle + |b\rangle\langle b^{pnc}|V^{\pm}|a\rangle$$

(4.94)

where we have removed the η_a since it is arbitrary. These are the PNC EOM equations where the appropriate $V^{\pm}$ is used according to whether the PNC EOM/CS or PNC EOM/RPA are required.

<u>$V^{\pm\ pnc}$ for PNC EOM/CS</u>

$$V^{\pm pnc}|a\rangle \equiv \sum_{b,b^{\pm}} \langle b^{pnc}|g_{12}|b^{\pm}\rangle|a\rangle + \langle b|g_{12}|b^{\pm pnc}\rangle|a\rangle$$

$$+ \langle b^{\mp pnc}|g_{12}|b\rangle|a\rangle + \langle b^{\mp}|g_{12}|b^{pnc}\rangle|a\rangle$$

(4.95)

For the PNC EOM/RPA there are two extra terms to add to $V^{\pm pnc}$

<u>Extra Terms for $V^{+pnc}|a\rangle$ in PNC EOM/RPA</u>

$$+ \langle v_1{}^{pnc}|g_{12}|v^{+}\rangle|a\rangle + \langle v_1|g_{12}|v^{+pnc}\rangle|a\rangle$$

(4.96)

<u>Extra Terms for $V^{-pnc}\ |a\rangle$ in PNC EOM/RPA</u>

$$+ \langle v^{+pnc}|g_{12}|v_1\rangle|a\rangle + \langle v^{+}|g_{12}|v_1{}^{pnc}\rangle|a\rangle$$

(4.97)

4.4.1. PNC Normalisation and Transition Matrix Elements

Replacing the orbitals and excitations in the parity conserving expression for the normalisation with parity mixed ones and expanding in orders of G_F as above we obtain the parity conserving expression for the zero order G_F. For the first order terms the PNC contributions cancel as they did for the PNC HF in chapter three due

to the imaginary nature of the PNC functions. Thus the PNC matrix element is normalised by the parity conserving normalisation condition.

For the PNC transition matrix element we obtain

$$\langle 1|T|0\rangle = \sum_{a^{\pm}} \langle a^{+pnc}|T|a\rangle + \langle a^{+}|T|a^{pnc}\rangle$$

$$+ \langle a^{pnc}|T|a^{-}\rangle + \langle a|T|a^{-pnc}\rangle \qquad (4.98)$$

for the PNC EOM/CS with an extra contribution for the PNC EOM/RPA.

$$+ \langle v^{+pnc}|T|v_1\rangle + \langle v^{+}|T|v_1{}^{pnc}\rangle \qquad (4.99)$$

4.4.2 PNC Angular Summations and Radial Equations

The derivation of the radial equations is fairly straightforward. The expressions are the same as for the corresponding parity conserving case except that a PNC function has the opposite parity to its parity conserving counterpart. Thus in all the angular expressions that were derived the J's are the same for the PNC components but the L's are given by $L_{pnc} = 2J - L$. We can therefore immediately write down the angular parts of the radial equations. The commutator phases will be identical to the parity conserving equations.

When deriving the radial contribution it must be remembered that since the PNC functions are purely imaginary there is a factor of -1 for the radial parts that are hermitian conjugated. The radial projection operator we write as before except that the angular factors κ of the PNC excitation that it projects out will be the opposite parity to the κ of the corresponding parity conserving excitations.

4.5. Conclusion

The EOM, if no approximations are made, are equivalent to solving the 'exact' Dirac atomic Hamiltonian for the ground and excited states. They are solved for an excitation operator which when operating on the ground state gives the excited state. To obtain the 'exact' answer we would require the exact ground state eigenfunction of the Hamiltonian and the exact excitation operator; in practice approximations are made in both cases. The approximations that are made for the EOM/CS are using a V_{N-1}

HF ground state and only considering single particle excitations. For open shell systems we have the Open Shell EOM which includes angular momentum coupling. If we approximate the valence contributions to the excitation operator by the positive single particle resonant excitation only and if in addition we only take a sub–set of the commutator valence diagrams obtained, with ω equalling the HF transition difference, then we obtain the EOM/RPA which are identical to the standard open shell MBPT/RPA equations apart from a normalisation factor.

If we include the spin independent weak force interaction in the Hamiltonian we obtain the PNC EOM/CS for closed shell systems and the PNC EOM/RPA for single valence systems.

CHAPTER 5: Method of Solution of Equations

5.1 Introduction

So far we have described the main equations that we are going to use in this thesis, though we shall be adding modifications in a later chapter to improve them. We next describe how we solve these equations. If, for example, we have an equation such as the Hartree–Fock equation

$$\left[\epsilon_a - h_0 - V_{hf}\right]|a\rangle = 0 \tag{5.1}$$

how do we actually arrive at a numerical solution? In order to investigate this it is first necessary to examine the nature of the Dirac operator h_0.

$$\begin{aligned} h_0 &= h_D + V_{nuc}(r) \\ h_D &= c\,\underline{\alpha}.\underline{p} + c^2\,(\beta - I) \end{aligned} \tag{5.2}$$

It is important to remember that the relativistic wavefunctions are represented by four component spinors corresponding to the positive and negative energy solutions each with two spin components. We shall be assuming that all our wavefunctions can be written as a product of a radial part and an angular part, namely:

$$|a\rangle = \frac{1}{r}\begin{bmatrix} P_a(r)\chi_{\kappa a} \\ iQ_a(r)\chi_{-\kappa a} \end{bmatrix} \tag{5.3}$$

We have conveniently taken out a factor of 1/r and defined the lower component to have a phase factor of i. $\chi_{\kappa a}$ is a vector–coupled combination of an angular part and a spin part to the wave function and is equivalent to

$$\begin{aligned} \chi_{\kappa a} &= |(ls)jm\rangle \\ \chi_{-\kappa a} &= |(l's)jm\rangle \end{aligned} \tag{5.4}$$

with κ given by the definition

$$(\underline{\sigma}.\underline{l} + 1)\chi_\kappa = -\kappa\ \chi_\kappa \tag{5.5}$$

so that each j value has a particular $|\kappa|$ associated with it; the two l values for that j have κ's of opposite sign with the lower l having the negative κ. For example $s_{\frac{1}{2}}$

has κ=−1, and $p_{\frac{1}{2}}$ has κ=+1. In (5.4), $l' = 2j - l$ has the opposite parity to l. We use the representation corresponding to ls j−j coupling. Another convention that is used elsewhere is sl coupled to j which will result in different phases for some of the angular factors.

It can be shown (e.q. [Case Studies]) that when h_0 acts on a wave function such as is given in (5.3) the result is

$$\left[c\ \underline{\alpha}.\underline{p} + c^2\ (\beta-I) + V_{nuc}(r)\right] \frac{1}{r} \begin{bmatrix} P_a(r)\chi_{\kappa a} \\ iQ_a(r)\chi_{-\kappa a} \end{bmatrix} = \tag{5.6}$$

$$\frac{1}{r} \begin{bmatrix} -c\left[\frac{d}{dr} - \frac{\kappa_a}{r}\right] Q_a(r)\ \chi_{\kappa a} + V_{nuc}(r)P_a(r)\chi_{\kappa a} \\ +i\ c\left[\frac{d}{dr} + \frac{\kappa_a}{r}\right] P_a(r)\chi_{-\kappa a} + \left[V_{nuc}(r) - 2c^2\right]\ iQ_a(r)\chi_{-\kappa a} \end{bmatrix}$$

A difficulty with the HF equation (5.1) is that the V_{hf} potential term is non−local which makes finding numerical solutions to the equation as it stands less straightforward. The way around this is to rearrange the equation so that we have a local potential on the left−hand side of the equation.

$$\left[\epsilon_a - c\ \underline{\alpha}.\underline{p} + c^2\ (\beta-I) - V_{eff}(r)\right]|a\rangle = \left[V_{hf} + V_{nuc}(r) - V_{eff}(r)\right]|a\rangle \tag{5.7}$$

The potential $V_{eff}(r) = -Z_{eff}(r)/r$ where $Z_{eff}(r)$ is a (positive) effective charge. Using (5.6) we can write the resulting equations as two coupled first order differential equations. We remove the angular factors by multiplying from the left by the appropriate angular momentum and integrating over the angular space. We are then left with

$$\left[V_{eff}(r) - \epsilon_a\right] P_a(r) \qquad - c\left[\frac{d}{dr} - \frac{\kappa_a}{r}\right] Q_a(r) = - R_{La}(r)$$

(5.8)

$$\left[V_{eff}(r) - 2c^2 - \epsilon_a\right] Q_a(r) + c\left[\frac{d}{dr} + \frac{\kappa_a}{r}\right] P_a(r) = - R_{Sa}(r)$$

where we have written the right-hand side of equation (5.7) as

$$|RHS\ \chi_{\kappa a}\rangle = \frac{1}{r}\begin{bmatrix} R_{La}(r)\chi_{\kappa a} \\ iR_{Sa}(r)\chi_{-\kappa a} \end{bmatrix} \tag{5.9}$$

Many of the equations that we solve in this thesis are of the form of (5.1) but with a non-zero right-hand side. We can use $V_{eff}(r)$ in the same manner as before except that there will be additional terms on the right-hand side of the equation.

5.2 Boundary Conditions

5.2.1 Nuclear Boundary Conditions

The V_{eff} term deep within the nucleus will just be given by the nuclear potential contribution; the electronic part of the potential will be negligible. In most of our calculations we have used a Fermi nuclear charge distribution given by

$$\rho(r) = \frac{\rho_0}{1 + \exp[(r-c)/a]} \tag{5.10}$$

ρ_0 is found by the condition that the integral of the charge over all volume must equal Z, the charge of the nucleus. c and a are experimentally determined nuclear parameters which define the shape of the nucleus. The nuclear potential energy is found from this by numerical integration

$$V_{nuc}(r) = - \frac{1}{r}\int_0^r 4\ \pi\ \rho(x)x^2dx \quad - \int_r^\infty 4\ \pi\ x\ \rho(x)\ dx \tag{5.11}$$

5.2.2 Homogeneous Solution

To determine the starting values for the large and small components of the wave function in the nucleus we shall use power series expansions of P_a and Q_a (see [Rose]).

$$P_a = \sum_{n=0}^{\infty} p_n \, r^{n+s}$$
$$Q_a = \sum_{n=0}^{\infty} q_n \, r^{n+s} \qquad (5.12)$$

where s must be positive but not necessarily integer and n is a positive integer.

Substituting these into (5.8) with the right-hand side of the equation equal to zero for the homogeneous solution, we obtain by comparing coefficients

$$s = +\kappa \quad \text{and} \quad p_0 = 0 \qquad (i.e.\ \kappa>0)$$
$$s = -\kappa \quad \text{and} \quad q_0 = 0 \qquad (i.e.\ \kappa<0) \qquad (5.13)$$

The leading terms for the solutions for P and Q are given by

$\kappa>0$

$$P_a = p_1 \, r^{\kappa+1} + \ldots$$
$$Q_a = q_0 \, r^{\kappa} + \ldots$$

with

$$p_1 = \frac{(\epsilon_a + 2c^2 - V_0)}{c\,(2\kappa+1)} \, q_0 \qquad (5.14)$$

$\kappa<0$

$$P_a = p_0 \, r^{-\kappa} + \ldots$$
$$Q_a = q_1 \, r^{-\kappa+1} + \ldots$$

with

$$q_1 = \frac{(\epsilon_a - V_0)}{c\,(2\kappa-1)} \, p_0 \qquad (5.15)$$

where V_0 is the nuclear potential V_{nuc} at the origin.

5.2.3 Inhomogeneous Solution

With the right-hand side of the equation present we can again use a series expansion for the solution. Note that 's' does not now necessarily equal $\pm\kappa$ as before. In addition we expand the right-hand side large and small components as

$$R_{La} = \sum_{n=0}^{\infty} X_n \, r^{n+F}$$

$$R_{Sa} = \sum_{n=0}^{\infty} Y_n \, r^{n+G} \qquad (5.16)$$

where F and G can be found by differentiating the function R_a near the origin so that it can be assumed that its 'r' dependence is from the leading term only.

$$F = \frac{r}{R_{La}} \times \frac{d\,R_{La}}{dr}$$

$$G = \frac{r}{R_{Sa}} \times \frac{d\,R_{Sa}}{dr} \qquad (5.17)$$

It is assumed that $F = G \pm 1$. If this is not true, or if any of the other criteria stated here are not satisfied then the starting values of the inhomogeneous solution are set to zero.

We obtain, by comparing coefficients

$$s = G \quad \text{and} \quad p_0 = 0$$

$$s = F \quad \text{and} \quad q_0 = 0 \qquad (5.18)$$

The leading terms for the solutions for P and Q are now given by

<u>s=G</u>

$$P_a = p_1 \, r^{G+1} + \ldots$$

$$Q_a = q_0 \, r^{G} + \ldots$$

with

$$p_1 = \frac{-Y_0 + (\epsilon_a + 2c^2 - V_0)}{c\,(F + G + 1)}\, q_0 \qquad (5.19)$$

<u>s=F</u>

$$P_a = p_0 \, r^{F} + \ldots$$

$$Q_a = q_1 \, r^{G+1} + \ldots$$

with

$$q_1 = \frac{-X_0 + (\epsilon_a - V_0)}{c\,(G - F + 1)}\, p_0 \qquad (5.20)$$

5.2.4 Boundary Conditions As r→∞

As $r \to \infty$ the effective potential $V_{eff}(r) \to 0$ and the term $\kappa/r \to 0$ in equation (5.8). Putting these terms to zero in the homogeneous equation and solving the resulting second order differential equations in P and Q we obtain the large r limits of the large and small components of the wave function.

$$P_a = A\, e^{-\beta r}$$
$$Q_a = \epsilon_a\, \alpha\, (1/\beta)\, e^{-\beta r} \qquad (5.24)$$

where $\beta = + \sqrt{[\, -\epsilon_a (\, 2 + \epsilon_a\, \alpha^2\,)\,]}$

The inhomogeneous solutions are set to zero at infinity.

5.2.5 Solving The Differential Equations

The method used to solve the coupled first order differential equations (5.8) is to represent all wave functions and potentials etc. on a radial grid of points. Functions such as integration and differentiation can then be performed by using various standard numerical algorithms. Since near the nucleus there is more important 'physics per unit length' (i.e. it is more important to have a more accurate wavefunction and therefore smaller grid step size) we use an exponential grid to define our points

$$r(I) = \exp(-A_{min} + (I-1)\, A_{delta}) \qquad (5.25)$$

where r(I) is the radial distance from the origin of the I'th point on the grid. The innermost point is therefore given by $\exp(-A_{min})$ and each successive point is given by the previous one multiplied by a factor of $\exp(A_{delta})$. Since, in order to perform our various numerical algorithms, we require a linear grid of points we make a transformation which gives us back a linear grid from the exponential one

$$x(I) = \ln\,(r(I)) = -A_{min} + (I-1)\, A_{delta} \qquad (5.26)$$

Inserting this transformation into the coupled equations (5.8) gives us a transformed set of coupled equations

$$r\left[V_{eff}(r) - \epsilon_a\right]P_a(r) \qquad + c\,\kappa_a\,Q_a(r) + r\,R_{La}(r) = c\,\frac{d\,Q_a(r)}{d\,x}$$

(5.27)

$$r\left[-V_{eff}(r) + 2c^2 + \epsilon_a\right]Q_a(r) - c\,\kappa_a\,P_a(r) - r\,R_{Sa}(r) = c\,\frac{d\,P_a(r)}{d\,x}$$

Having determined the starting values for our solution to equations we evaluate the succeeding points on our grid using the Runge-Kutta method employed to fourth order (see Appendix 6).

5.2.6 Matching Outwards And Inwards Integrations

We start with our nuclear boundary conditions and work outwards evaluating each successive point from the previous one for both the homogeneous and the inhomogenous equations up until the classical turning point. This is the point where the form of the solution changes: beyond the turning point the solution is exponentially decaying; before the turning point it is first exponentially increasing and then oscillating with n-l-1 nodes. We then also integrate inwards from infinity starting with the boundary conditions given in equation (5.24). The condition for the outward and inward integrations to match up is that, at the turning point, the wave function and its first derivative should be equal. This is equivalent to the two grid points on either side of the turning point matching up. In order to achieve this, the solution is taken to be the inhomogeneous souluion plus an admixture of the homogeneous solution such that the total wave function fulfills the boundary conditions. If the turning point is between grid point M and M+1 then we have

$$\begin{aligned}
\alpha\,P_{out,hom}(M) \quad &+ P_{out,inhom}(M) \quad = \beta\,P_{in,hom}(M) \quad + P_{in,inhom}(M) \\
\alpha\,P_{out,hom}(M+1) &+ P_{out,inhom}(M+1) = \beta\,P_{in,hom}(M+1) + P_{in,inhom}(M+1)
\end{aligned}$$

(5.28)

where α and β are parameters to be determined from these two equations. The corresponding condition for the lower component Q will automatically be satisfied if equations (5.28) are satisfied. The final solution is then given by

$$
\begin{aligned}
P(r) &= \alpha\, P_{out,hom}(r) + P_{out,inhom}(r) && r \leq r(M) \\
&= \beta\, P_{in,hom}(r) + P_{in,inhom}(r) && r \geq r(M+1) \\
Q(r) &= \alpha\, Q_{out,hom}(r) + Q_{out,inhom}(r) && r \leq r(M) \\
&= \beta\, Q_{in,hom}(r) + Q_{in,inhom}(r) && r \geq r(M+1)
\end{aligned}
\qquad (5.29)
$$

5.3 Practicalities in Solving the Radial Equations

5.3.1 Numerical Accuracy

The numerical solving methods used are obviously only approximate and the answers will have an error that depends on the grid step size. For the order of Runge–Kutta method that we use the error should depend on h^4 where h is the step size A_{delta} in equation (5.25). A good estimate of the numerical errors and an improved answer can be obtained by repeating the calculation for several step sizes and then extrapolating to a zero step size solution. We solved the equations for three step sizes: 0.12, 0.105 and 0.09 with A_{min} = 12 in each case (see (5.25)) and then fitted the solutions to the equation

$$
Ans(h) = Ans_0 + \alpha\, h^n \qquad (5.30)
$$

where Ans(h) is the numerical answer for step size h and α, Ans_0 and n are parameters to be fitted to the answers. This method provides a good check that the dependence of the solution is h^4 or higher. If n is much less than 4 then perhaps more grid sizes should be tried and a different form of fitting used. Using the method described above, the extrapolated answer is immediately given by Ans_0.

5.3.2 Hartree–Fock Solution

In solving the HF equations one has a fairly good approximation to the solution already with the RSCF local central potential wavefunctions (see chapter 3). It is far easier to express the HF wavefunction as a correction to this local wavefunction rather than to solve for the former *ab initio*. One might otherwise also have numerical problems with resonances in the homogeneous solution. That is, if the HF eigenvalue is close to the RSCF one then the left–hand side of the equation is nearly identical to the RSCF eigenvalue equation and the solution can have an arbitrarily large admixture of the RSCF one. If we make the substitution

$$|a_{hf}\rangle = [\ |a_{loc}\rangle + |\delta a\rangle\ ] \ / \ \sqrt{\langle a_{hf}|a_{hf}\rangle} \tag{5.31}$$

in equation (5.7), where $|\delta a\rangle$ is orthogonal to $|a_{loc}\rangle$, then, using the fact that $|a_{loc}\rangle$ is an eigenfunction of the Hamiltonian $h_D + V_{eff}(r)$ with eigenvalue $\epsilon_{a,loc}$ we obtain

$$\left[\ \epsilon_a - h_D - V_{eff}(r)\ \right]|\delta a\rangle \quad =$$

$$\left[\ V_{hf} + V_{nuc}(r) - V_{eff}(r)\right]\ |a\rangle \ / \ \langle a_{hf}|a_{hf}\rangle \quad - \delta\epsilon_a\ |a_{loc}\rangle \tag{5.32}$$

where

$$\epsilon_a \quad = \quad \epsilon_{a,loc} + \delta\epsilon_a \tag{5.33}$$

$$\delta\epsilon_a \quad = \quad \langle a_{loc}|\ \left[\ V_{hf} + V_{nuc}(r) - V_{eff}(r)\right]\ |a\rangle \ / \ \langle a_{hf}|a_{hf}\rangle \tag{5.34}$$

5.3.3 Homogeneous Equation Resonances

As mentioned above one frequently encounters numerical problems in solving the radial equations due to large admixtures of the homogeneous solution in the inhomogeneous one. This will only occur if there is a local wave function with a very close eigenvalue to the one in the equation which also has the same κ value as the function being solved for. This clearly is the case when solving for the HF orbitals but it also occurs when solving for other functions as well. There are two possible solutions to this problem:

1. The function being solved for can be written as an admixture of the local function and an orthogonal part

$$|x\rangle = \lambda\ |a_{loc}\rangle + |\delta x\rangle \qquad \text{with} \quad \langle a_{loc}|\delta x\rangle = 0 \tag{5.35}$$

where we are solving an equation of the type

$$\left[\ \epsilon_a - h_D - V_{eff}(r)\ \right]\ |x\rangle \quad = \quad |rhs\rangle \tag{5.36}$$

λ is then given by

$$\lambda = \langle a_{loc}|rhs\rangle \ / \ (\epsilon_a - \epsilon_{loc}) \tag{5.37}$$

and one solves the equation

$$\left[\epsilon_a - h_D - V_{eff} \right] |\delta x\rangle = |rhs\rangle - |a_{loc}\rangle\langle a_{loc}|rhs\rangle \qquad (5.38)$$

and then reconstructs $|x\rangle$ from equation (5.35). One should more strictly split up the $|rhs\rangle$ term into those proportional to λ and those independent of λ so that one gets

$$\lambda = \langle a_{loc}|rhs(\text{no } \lambda)\rangle \; / \; [\; \epsilon_a - \epsilon_{loc} - \langle a_{loc}|rhs(\lambda)\rangle \;] \qquad (5.39)$$

but the two methods will usually converge to the same value of λ when iterated.

2. One can simply shift both sides of the equation by the same amount so that the left-hand side is more 'off resonance' and there is numerical stability.

$$\left[\epsilon_a + \delta\epsilon - h_D - V_{eff} \right] |x\rangle = |rhs\rangle + \delta\epsilon|x\rangle \qquad (5.40)$$

Thus the homogeneous equation eigenvalue is shifted by $\delta\epsilon$ so as to remove the resonance.

There are other numerical pitfalls and problems that were encountered and indeed a lot of work goes on behind the statement *we solved this equation numerically and obtained...* Techniques of interest will be mentioned where appropriate

5.4. The Radial Equations

In chapters 3 and 4 we derived the equations that we are going to use for our calculations. In this chapter we have seen how to solve the radial equations for any given right-hand side to the basic equation. To derive the radial equations angular summation techniques are used; these are fully described in [Lindgren and Morrison]. The forms of the radial equations are given in Appendix two. The exact angular expressions take up too much space to be presented in full but are contained in the micro-fiche at the end of the thesis.

There is a hierarchical structure to solving the equations: since all the calculations use HF orbitals, these have to be solved for first. The parity conserving EOM calculations can then be done, as well as the hyperfine dipole interaction constant.

For the PNC calculations first the PNC HF has to be solved which uses the HF solutions. Finally the PNC EOM are solved; this requires the HF, EOM and PNC HF solutions.

5.5 Conclusion

In this chapter we have discussed how the equations derived in the previous chapters are solved in practice. The equations are in the form of coupled first order differential equations; the boundary conditions are evaluated using power series expansions and the fourth order Runge-Kutta technique is employed to solve them. The outward and inward integrations are matched by mixing in the appropriate amounts of the homogeneous solution to the inhomogeneous one.

CHAPTER 6: Results Of Calculations

6.1 Introduction

In this chapter we give the numerical solutions to the various equations that we have described in the previous chapters. We have performed the calculations for two elements: caesium and thallium.

In all the calculations there is a hierarchy of equations to solve: we begin with the HF equations and calculate the eigenvalues, some E1 transition matrix elements and the hyperfine dipole interaction constants. Having calculated the HF wavefunctions we can use them in RPA type calculations to obtain the EOM/RPA E1 transition matrix elements and the RPA hyperfine values. To calculate PNC transitions we start off with the HF wavefunctions and perform a PNC HF calculation. Using the PNC HF wavefunctions and the EOM/RPA excitations we finally perform a PNC EOM/RPA calculation.

We solved the numerical equations, using the techniques outlined in chapter five, on a Vax Cluster system. In all cases we extrapolated the results to zero grid size. We used a Fermi nuclear charge distribution of the form of equation (5.10). The nuclear parameters that we used were

$$\begin{aligned} &\text{Cs} : c = 5.674 \text{ fm} \qquad a = 0.52339 \text{ fm} \\ &\text{Tl} : c = 6.617 \text{ fm} \qquad a = 0.52339 \text{ fm} \end{aligned} \tag{6.1}$$

The units used are in all cases atomic units (see appendix 5)

6.2 The Hartree-Fock Equations

The eigenvalues are given in tables 6.1 to 6.4 for all the core orbitals of caesium and thallium and the s and p excited and valence states up to $8s_{\frac{1}{2}}$. The quoted experimental energies for the valence and excited state orbitals are known with precision since they are easily measurable in transitions. The core states on the other hand can only be determined by X-ray measurements which cannot be done to the same degree of accuracy.

The quoted electric dipole values are reduced matrix elements. To get the full

matrix element the reduced one is multiplied by the appropriate angular factor as given by the Wigner–Eckart Theorem to be

$$(-1)^{j_2-m_2} \begin{pmatrix} j_2 & 1 & j_1 \\ -m_2 & q & m_1 \end{pmatrix} \qquad (6.2)$$

It should be noted that there is no length–velocity equivalence for the Hartree–Fock equations due to the presence of the non–local exchange terms in the HF potential (see Appendix 3). Several authors have discussed the problem of which gauge is the most reliable (e.g. [Yang]) and the general consensus is that the length gauge is more so.

6.2.1 Discussion of Results

It can be seen that the Hartree–Fock equations, as an *ab initio* theoretical calculation, provide a reasonable physical description of the atom. However the errors in the eigenvalues of the excited states vary between 11% (Cs $6s_{\frac{1}{2}}$ and Tl $6p_{\frac{1}{2}}$) and 4% (Cs and Tl $8s_{\frac{1}{2}}$) and the binding energy is underestimated (in magnitude). The core states energies are all overestimated by between 0.6% (Cs and Tl $1s_{\frac{1}{2}}$) and greater than 100% (Cs $5p_{3/2}$ and Tl 5d's and $6s_{\frac{1}{2}}$).

The main atomic effects not included in the V_{N-1} HF equations that account for the discrepancies between the HF eigenvalues and experiment are:

1. The V_{N-1} HF potential contains no valence orbital contribution so that the core orbitals do not interact with the valence orbital. Allowing the core to 'see' the valence electron would mean that the core electrons were screened from the nucleus slightly more due to the penetration of the core by the valence electron. They would therefore be less bound.

2. An electron external to the core, such as a valence electron, will polarise the core slightly. This can then interact back on the polarising electron. The interaction of the polarised core on the excited states leads to the excited states being more bound.

3. The detailed movements of the electrons are not independent: they are rather correlated to the movements of the other electrons

4. There are also more complex effects that will be combinations of 2 and 3 together.

One would expect the outer excited states to be more accurate because the atom looks more like the nuclear charge Z shielded by the Z−1 core electrons and there is less penetration of the core and less correlation and polarisation because the electron is further out from the nucleus. The very large errors in the outermost core states are due to the fact that we have used a V_{N-1} HF potential so that the core electrons do not 'see' the valence electron. This effect would be most severe for the outer core orbitals that are close to the valence electron.

The errors in the E1 reduced transition matrix elements are of the order of 17% in Cs and 20% for Tl $6p_{3/2}$ and 11% for Tl $6p_{\frac{1}{2}}$. In all cases the matrix elements are over−estimated in magnitude. In calculating transition matrix elements one of the major effects not accounted for is the valence transition dipole inducing polarisation of the core which, in a self−consistent way, produces a modified transition dipole for the atom as a whole. This effect is taken account of in the EOM/RPA calculations.

In conclusion, the HF equations can therefore give the basic atomic structure to an error of about 10% to 20%.

Table 6.1

The Hartree-Fock Core Eigenvalues For Caesium

Orbital	HF eigenvalues	Experiment [a]	< r >
$1s_{1/2}$	-1330.1	-1322	0.026
$2s_{1/2}$	-212.56	-210	0.112
$2p_{1/2}$	-199.43	-197	0.094
$2p_{3/2}$	-186.44	-184	0.1000
$3s_{1/2}$	-45.969	-44.7	0.297
$3p_{1/2}$	-40.447	-39.1	0.287
$3p_{3/2}$	-37.895	-36.7	0.299
$3d_{3/2}$	-28.310	-27.2	0.271
$3d_{5/2}$	-27.776	-26.7	0.274
$4s_{1/2}$	-9.5121	-8.48	0.695
$4p_{1/2}$	-7.4455	-6.33	0.722
$4p_{3/2}$	-6.9210	-5.93	0.747
$4d_{3/2}$	-3.4856	-2.90	0.831
$4d_{5/2}$	-3.3972	-2.81	0.841
$5s_{1/2}$	-1.4897	-0.83	1.77
$5p_{1/2}$	-0.90779	-0.48	2.02
$5p_{3/2}$	-0.84039	-0.41	2.11

Table 6.2

The Hartree-Fock Valence and Excited State Eigenvalues for Caesium

Orbital	HF eigenvalues	Experiment [b]	< r >
$6s_{1/2}$	-0.12737	-0.14310	6.12
$6p_{1/2}$	-0.08562	-0.09217	8.14
$6p_{3/2}$	-0.08379	-0.08964	8.35
$7s_{1/2}$	-0.05519	-0.05865	13.76
$7p_{1/2}$	-0.04202	-0.04393	17.13
$7p_{3/2}$	-0.04137	-0.04310	17.42
$8s_{1/2}$	-0.03095	-0.03230	24.37

a: [Bearden and Burr]
b: [C.E. Moore]

Table 6.3

The Hartree-Fock Core Eigenvalues For Thallium

Orbital	HF eigenvalues	Experiment [a]	< r >
$1s_{1/2}$	-3164.4	-3145	0.016
$2s_{1/2}$	-569.11	-564	0.068
$2p_{1/2}$	-545.22	-540	0.056
$2p_{3/2}$	-469.19	-465	0.065
$3s_{1/2}$	-138.63	-136	0.177
$3p_{1/2}$	-127.92	-126	0.167
$3p_{3/2}$	-110.80	-109	0.183
$3d_{3/2}$	-93.351	-91.4	0.160
$3d_{5/2}$	-89.729	-87.8	0.164
$4s_{1/2}$	-32.556	-31.1	0.391
$4p_{1/2}$	-27.907	-26.5	0.394
$4p_{3/2}$	-23.693	-22.4	0.426
$4d_{3/2}$	-16.110	-14.9	0.432
$4d_{5/2}$	-15.314	-14.2	0.443
$4f_{5/2}$	-5.4581	-4.51	0.462
$4f_{7/2}$	-5.2824	-4.36	0.469
$5s_{1/2}$	-5.8851	-5.01	0.889
$5p_{1/2}$	-4.2506	-3.66	0.955
$5p_{3/2}$	-3.4843	-2.77	1.04
$5d_{3/2}$	-1.1611	-0.563	1.33
$5d_{5/2}$	-1.0736	-0.482	1.39
$6s_{1/2}$	-0.68941	----	2.47

Table 6.4

The Hartree-Fock Valence and Excited State Eigenvalues for Thallium

Orbital	HF eigenvalues	Experiment [b]	< r >
$6p_{1/2}$	-0.19968	-0.22446	3.59
$6p_{3/2}$	-0.16693	-0.18896	4.12
$7s_{1/2}$	-0.09618	-0.10382	8.11
$7p_{1/2}$	-0.06505	-0.06882	10.9
$7p_{3/2}$	-0.06086	-0.06426	11.7
$8s_{1/2}$	-0.04574	-0.04792	16.6

a: [Bearden and Burr]
b: [C.E. Moore]

Table 6.5.

HF Reduced Electric Dipole Transition Matrix Elements

Caesium

Transition	(length gauge)	(velocity gauge)	Expt.[a]
$6s_{1/2} \rightarrow 6p_{1/2}$	-5.28	-5.04	-4.52(0.01)
$6s_{1/2} \rightarrow 6p_{3/2}$	+7.43	+7.07	+6.36(0.01)

Thallium

Transition	(length gauge)	(velocity gauge)	Expt.[b]
$6p_{1/2} \rightarrow 7s_{1/2}$	+2.05	1.64	+1.84 (0.06)
$6p_{3/2} \rightarrow 7s_{1/2}$	+3.97	3.19	+3.29 (0.09)

a: [Shabanova *et al.*]
b: quoted in [Johnson 1986]

6.3 The EOM/RPA Transition Matrix Elements

The EOM/RPA transition matrix elements were calculated for the same transitions as before. The only difference between the EOM/RPA calculation and the MBPT/RPA ones is that the EOM matrix element is normalised (see chapter 4) and there is no renormalisation in the MBPT/RPA calculations. The reason for this is that if MBPT is carried out to all orders then all the 'unlinked diagrams' (see [Lindgren and Morrison]) cancel out exactly with the normalisation term. If a subset of the full MBPT corrections is used then this cancellation is only approximate. The normalisation does not change the answer to the quoted degree of accuracy.

6.4 Discussion of EOM/RPA Results

The errors in the transition matrix elements are now at the 10% level when comparing with the experimental answers (except for the Tl $6p_{\frac{1}{2}} \rightarrow 7s_{\frac{1}{2}}$ transition which has an error of only 4%). The main additional physical effect which has been included is the interaction between the valence and the core electrons which modifies the transition probability. The core is not allowed to interact directly back on the valence electron but the polarisation of the core leads to a modification of the atomic transition matrix element. The physical effects that have not been included are correlation effects that involve interactions such as the polarised core acting back on the valence orbital. We shall discuss a method of calculating these in chapter seven.

The contributions to the total matrix element from each core excitation are given in tables 6.7 and 6.8. We have only given the contributions for the n=4 and n=5 shells for caesium and the n=5 and n=6 shells for thallium. As can be seen from the table in the length gauge the outermost core orbital excitations give the largest contribution with the inner shells contributing a great deal less. Extending the calculation to include all the shells makes no noticeable difference to the answers for the length gauge transition matrix element. There are more contributions to the velocity gauge from the inner orbitals so that one has to calculate the inner orbital excitations as well in order to arrive at the same answer as the length gauge calculation. As can be seen from the table, there are also generally more cancelling terms in the velocity gauge calculation. This is why the length gauge is considered to

be more reliable. The degree to which we obtain the same answers for each gauge gives an indication of the numerical accuracy of the calculation. For the parity conserving E1 transition matrix elements we obtained agreement to four significant figures.

Table 6.6.

Reduced EOM/RPA E1 Transition Matrix Elements

Caesium

Transition	reduced E1 matrix element (length)	(velocity)	Expt [a]
$6p_{\frac{1}{2}} \rightarrow 6s_{\frac{1}{2}}$	-4.97	-4.97	-4.52 (0.01)
$6p_{3/2} \rightarrow 6p_{\frac{1}{2}}$	+7.01	+7.01	+6.36 (0.01)

Thallium

Transition	reduced E1 matrix element (length)	(velocity)	Expt [b]
$7s_{\frac{1}{2}} \rightarrow 6p_{\frac{1}{2}}$	+1.91	+1.91	+1.84 (0.06)
$7s_{\frac{1}{2}} \rightarrow 6p_{3/2}$	+3.61	+3.61	+3.29 (0.09)

a: [Shabanova *et al.*]
b: quoted in [W. Johnson 1986]

Table 6.7.

Contribution of Excitations to the E1 Matrix Element

Caesium $6s_{\frac{1}{2}} \rightarrow 6p_{\frac{1}{2}}$ Transition

excitation	contribution length	contribution velocity
$6s_{\frac{1}{2}} \rightarrow 7p_{\frac{1}{2}}$	-5.278	-5.036
$5p_{3/2} \rightarrow d_{5/2}^{+}$	+0.070	-0.897
$5p_{3/2} \rightarrow d_{5/2}^{-}$	+0.095	+1.197
$5p_{3/2} \rightarrow d_{3/2}^{+}$	+0.003	+0.053
$5p_{3/2} \rightarrow d_{3/2}^{-}$	+0.011	-0.135
$5p_{3/2} \rightarrow s_{1/2}^{+}$	+0.012	+0.201
$5p_{3/2} \rightarrow s_{1/2}^{-}$	+0.018	-0.258
$5p_{1/2} \rightarrow d_{3/2}^{+}$	+0.031	+0.449
$5p_{1/2} \rightarrow d_{3/2}^{-}$	+0.036	-0.503
$5p_{1/2} \rightarrow s_{1/2}^{+}$	+0.009	+0.129
$5p_{1/2} \rightarrow s_{1/2}^{-}$	+0.011	-0.188
$5s_{1/2} \rightarrow p_{3/2}^{+}$	+0.000	+0.011
$5s_{1/2} \rightarrow p_{3/2}^{-}$	+0.000	-0.017
$5s_{1/2} \rightarrow p_{1/2}^{+}$	+0.000	+0.026
$5s_{1/2} \rightarrow p_{1/2}^{-}$	+0.000	-0.008
$4d_{5/2} \rightarrow f_{7/2}^{+}$	+0.002	+0.139
$4d_{5/2} \rightarrow f_{7/2}^{-}$	+0.001	-0.110

Caesium $6s_{\frac{1}{2}} \rightarrow 6p_{3/2}$ Transition

excitation	contribution length	contribution velocity
$6s_{\frac{1}{2}} \rightarrow 7p_{3/2}$	+7.428	+7.066
$5p_{3/2} \rightarrow d_{5/2}^{+}$	-0.102	-1.276
$5p_{3/2} \rightarrow d_{5/2}^{-}$	-0.105	+1.267
$5p_{3/2} \rightarrow d_{3/2}^{+}$	-0.016	-0.189
$5p_{3/2} \rightarrow d_{3/2}^{-}$	-0.010	+0.123
$5p_{3/2} \rightarrow s_{1/2}^{+}$	-0.026	-0.352
$5p_{3/2} \rightarrow s_{1/2}^{-}$	-0.034	+0.469
$5p_{1/2} \rightarrow d_{3/2}^{+}$	-0.052	-0.702
$5p_{1/2} \rightarrow d_{3/2}^{-}$	-0.044	+0.592
$5p_{1/2} \rightarrow s_{1/2}^{+}$	-0.006	-0.112
$5p_{1/2} \rightarrow s_{1/2}^{-}$	-0.008	+0.128
$5s_{1/2} \rightarrow p_{3/2}^{+}$	-0.000	-0.024
$5s_{1/2} \rightarrow p_{3/2}^{-}$	-0.000	+0.015
$5s_{1/2} \rightarrow p_{1/2}^{+}$	-0.000	-0.015
$5s_{1/2} \rightarrow p_{1/2}^{-}$	-0.000	+0.022
$4d_{5/2} \rightarrow f_{7/2}^{+}$	-0.002	-0.142
$4d_{5/2} \rightarrow f_{7/2}^{-}$	-0.002	+0.163

Table 6.8.

Contribution of Excitations to the E1 Matrix Element

Thallium $6p_{\frac{1}{2}} \rightarrow 7s_{\frac{1}{2}}$ Transition

excitation	contribution length	contribution velocity
$6p_{\frac{1}{2}} \rightarrow 7s_{\frac{1}{2}}$	2.050	1.640
$6s_{\frac{1}{2}} \rightarrow p_{3/2}^{-}$	+0.027	-0.088
$6s_{\frac{1}{2}} \rightarrow p_{3/2}^{+}$	-0.118	-0.385
$6s_{\frac{1}{2}} \rightarrow p_{\frac{1}{2}}^{-}$	-0.186	+0.432
$6s_{\frac{1}{2}} \rightarrow p_{\frac{1}{2}}^{+}$	+0.123	+0.286
$5d_{5/2} \rightarrow f_{7/2}^{-}$	+0.145	-0.229
$5d_{5/2} \rightarrow f_{7/2}^{+}$	-0.002	+0.008
$5d_{5/2} \rightarrow f_{5/2}^{-}$	-0.003	+0.004
$5d_{5/2} \rightarrow f_{5/2}^{+}$	+0.003	+0.005
$5d_{5/2} \rightarrow p_{3/2}^{-}$	-0.016	+0.101
$5d_{5/2} \rightarrow p_{3/2}^{+}$	+0.013	+0.103
$5d_{3/2} \rightarrow f_{5/2}^{-}$	-0.004	+0.023
$5d_{3/2} \rightarrow f_{5/2}^{+}$	+0.011	+0.184
$5d_{3/2} \rightarrow p_{3/2}^{-}$	+0.005	-0.038
$5d_{3/2} \rightarrow p^{3/2+}$	-0.007	-0.057
$5d_{3/2} \rightarrow p_{\frac{1}{2}}^{-}$	+0.008	-0.061
$5d_{3/2} \rightarrow p_{\frac{1}{2}}^{+}$	-0.013	-0.093
$5p_{3/2} \rightarrow d_{5/2}^{-}$	+0.000	-0.002
$5p_{3/2} \rightarrow d_{5/2}^{+}$	+0.000	+0.011

Thallium $6p_{3/2} \rightarrow 7s_{\frac{1}{2}}$ Transition

excitation	contribution length	contribution velocity
$6p_{3/2} \rightarrow 7s_{\frac{1}{2}}$	+3.967	+3.187
$6s_{\frac{1}{2}} \rightarrow p_{3/2}^{-}$	-0.213	-0.886
$6s_{\frac{1}{2}} \rightarrow p_{3/2}^{+}$	-0.039	-0.161
$6s_{\frac{1}{2}} \rightarrow p_{\frac{1}{2}}^{-}$	+0.004	-0.011
$6s_{\frac{1}{2}} \rightarrow p_{\frac{1}{2}}^{+}$	-0.114	-0.398
$5d_{5/2} \rightarrow f_{7/2}^{-}$	+0.001	-0.073
$5d_{5/2} \rightarrow f_{7/2}^{+}$	+0.013	+0.034
$5d_{5/2} \rightarrow f_{5/2}^{-}$	+0.002	-0.004
$5d_{5/2} \rightarrow f_{5/2}^{+}$	-0.001	-0.018
$5d_{5/2} \rightarrow p_{3/2}^{-}$	+0.001	-0.039
$5d_{5/2} \rightarrow p_{3/2}^{+}$	-0.014	-0.143
$5d_{3/2} \rightarrow f_{5/2}^{-}$	+0.007	-0.206
$5d_{3/2} \rightarrow f_{5/2}^{+}$	+0.003	+0.111
$5d_{3/2} \rightarrow p_{3/2}^{-}$	-0.003	+0.037
$5d_{3/2} \rightarrow p^{3/2+}$	+0.002	-0.002
$5d_{3/2} \rightarrow p_{\frac{1}{2}}^{-}$	-0.007	+0.053
$5d_{3/2} \rightarrow p_{\frac{1}{2}}^{+}$	+0.003	+0.045
$5p_{3/2} \rightarrow d_{5/2}^{-}$	+0.000	-0.028
$5p_{3/2} \rightarrow d_{5/2}^{+}$	+0.000	+0.009

6.5 Hyperfine Dipole Interaction Constant

The structure of these equations are similar in form to the RPA and EOM equations in that they involve a basic perturbation and its 'feed-back' effect on the core orbitals. However as the hyperfine interaction involves the wavefunction at the nucleus it provides an important indication of how accurate the wavefunctions are in the inner regions of the atom. This may be relevant to PNC phenomena since the PNC interaction occurs principally at the nucleus.

As mentioned in chapter three the calculation can be approached from two angles: either the perturbation of the core orbitals by the valence electron can be calculated and then the effect this has on the hyperfine matrix element determined or the hyperfine interaction itself can be treated as the perturbation and the effect this has on the interaction between the core and valence orbitals determined. These two methods, when taken to all orders as in the RPA equations, are numerically equivalent. We did the calculation both ways as a numerical check. This was extremely useful because the finite grid size errors changed the answers in the opposite directions to each other as the step size was decreased but when the results were extrapolated to zero grid step size the answers agreed exactly. The results are given in table 6.9. In tables 6.10 and 6.11 we have given the excitation contributions for grid step size 0.09.

The physical effects not included in the calculation are correlation interactions similar to those described for the transition matrix element calculation above.

6.6 Discussion of Hyperfine Results

The V_{N-1} HF result is too low by 37% for Cs $6s_{\frac{1}{2}}$ and 28% for $7s_{\frac{1}{2}}$. In thallium the errors are between 17% and 8%. The addition of the RPA corrections reduces the errors for Cs to between 25% ($6s_{\frac{1}{2}}$) and 13% ($7s_{\frac{1}{2}}$) and for thallium 3% ($6p_{\frac{1}{2}}$) and 5% ($7p_{\frac{1}{2}}$). Thus there are still quite large errors.

It should be noted that, unlike the transition matrix element calculations, the core excitation contributions are significant even for the innermost orbital. The correct answer is only obtained if all the core excitations are included. The contributions also vary greatly with their angular momentum because (non-relativistically) only the $s_{\frac{1}{2}}$

Table 6.9.

Hyperfine Dipole Interaction Constant (in MHz)

Caesium $g_I = 0.7377208$

Orbital		HF value	+RPA	Answer	Expt [a]
Cs	$6s_{\frac{1}{2}}$	1433.6	+294.4	1728.0	2298.2
	$6p_{\frac{1}{2}}$	161.0	+ 40.6	201.6	291.9 (0.1)
	$6p_{3/2}$	23.9	+ 18.8	42.7	50.34 (0.06)
	$7s_{\frac{1}{2}}$	393.9	+ 80.1	474.0	546.3 (3.0)
	$7s_{\frac{1}{2}}$	57.64	+ 14.00	71.64	94.34 (0.02)

Thallium $g_I = 3.2764268$

Orbital		HF value	+RPA	Answer	Expt [b]
Tl	$6p_{\frac{1}{2}}$	17655.6	+ 4315.4	21971.0	21310.8
	$6p_{3/2}$	-1302.1	- 777.9	-2080.0	265.0
	$7s_{\frac{1}{2}}$	7765.2	+ 3148.6	10913.8	12500
	$7p_{\frac{1}{2}}$	1968.2	+ 61.21	2029.4	2130 (60)

a: quoted in [Johnson 1986] and [Dzuba 1984]
b: quoted in [Dzuba 1987_a]

Table 6.10.

Core Orbital Excitation Contributions to Ahyp

Caesium (h=0.09)

excitation	contribution
$1s_{\frac{1}{2}} \rightarrow s_{\frac{1}{2}}$	14.36
$2s_{\frac{1}{2}} \rightarrow s_{\frac{1}{2}}$	15.96
$2p_{\frac{1}{2}} \rightarrow p_{\frac{1}{2}}$	-0.04
$2p_{\frac{1}{2}} \rightarrow p_{3/2}$	-0.02
$2p_{3/2} \rightarrow p_{\frac{1}{2}}$	-0.01
$2p_{3/2} \rightarrow p_{3/2}$	0.09
$3s_{\frac{1}{2}} \rightarrow s_{\frac{1}{2}}$	25.08
$3p_{\frac{1}{2}} \rightarrow p_{\frac{1}{2}}$	-0.20
$3p_{3/2} \rightarrow p_{3/2}$	-0.06
$3d_{3/2} \rightarrow d_{3/2}$	-0.07
$3d_{3/2} \rightarrow d_{5/2}$	-0.02
$3d_{5/2} \rightarrow d_{3/2}$	-0.02
$3d_{5/2} \rightarrow d_{5/2}$	-0.10
$4s_{\frac{1}{2}} \rightarrow s_{\frac{1}{2}}$	55.29
$4p_{\frac{1}{2}} \rightarrow p_{\frac{1}{2}}$	0.13
$4p_{\frac{1}{2}} \rightarrow p_{3/2}$	0.14
$4p_{3/2} \rightarrow p_{\frac{1}{2}}$	0.27
$4p_{3/2} \rightarrow p_{3/2}$	-1.09
$4d_{3/2} \rightarrow d_{3/2}$	1.13
$4d_{3/2} \rightarrow d_{5/2}$	0.39
$4d_{5/2} \rightarrow d_{3/2}$	0.42
$4d_{5/2} \rightarrow d_{5/2}$	-1.53
$5s_{\frac{1}{2}} \rightarrow s_{\frac{1}{2}}$	226.73
$5p_{\frac{1}{2}} \rightarrow p_{\frac{1}{2}}$	12.49
$5p_{\frac{1}{2}} \rightarrow p_{3/2}$	-4.05
$5p_{3/2} \rightarrow p_{\frac{1}{2}}$	-7.54
$5p_{3/2} \rightarrow p_{3/2}$	-43.50
HF $6s_{\frac{1}{2}}$	1434.76
Total	1729.40

Table 6.11.

Core Orbital Excitation Cotributions to Ahyp

Thallium (h=0.09)

excitation	contribution
$1s_{\frac{1}{2}} \rightarrow s_{\frac{1}{2}}$	47.00
$1s_{\frac{1}{2}} \rightarrow d_{3/2}$	14.36
$2s_{\frac{1}{2}} \rightarrow s_{\frac{1}{2}}$	8.64
$2p_{\frac{1}{2}} \rightarrow p_{\frac{1}{2}}$	155.34
$2p_{3/2} \rightarrow p_{3/2}$	-0.77
$2p_{3/2} \rightarrow f_{5/2}$	1.95
$3s_{\frac{1}{2}} \rightarrow s_{\frac{1}{2}}$	-21.66
$3s_{\frac{1}{2}} \rightarrow d_{3/2}$	-0.61
$3p_{\frac{1}{2}} \rightarrow p_{\frac{1}{2}}$	215.61
$3p_{3/2} \rightarrow p_{3/2}$	-0.37
$3p_{3/2} \rightarrow f_{5/2}$	0.64
$3d_{3/2} \rightarrow s_{\frac{1}{2}}$	0.11
$3d_{3/2} \rightarrow d_{3/2}$	-0.87
$3d_{5/2} \rightarrow d_{5/2}$	0.23
$3d_{5/2} \rightarrow g_{7/2}$	0.66
$4s_{\frac{1}{2}} \rightarrow s_{\frac{1}{2}}$	-84.15
$4s_{\frac{1}{2}} \rightarrow d_{3/2}$	0.43
$4p_{\frac{1}{2}} \rightarrow p_{\frac{1}{2}}$	398.79
$4p_{3/2} \rightarrow p_{3/2}$	1.68
$4p_{3/2} \rightarrow f_{5/2}$	0.31
$4d_{3/2} \rightarrow s_{\frac{1}{2}}$	0.57
$4d_{3/2} \rightarrow d_{3/2}$	-22.07
$4d_{5/2} \rightarrow d_{5/2}$	4.13
$4d_{5/2} \rightarrow g_{7/2}$	0.52
$4f_{5/2} \rightarrow p_{3/2}$	0.28
$4f_{5/2} \rightarrow f_{5/2}$	-11.13
$4f_{7/2} \rightarrow f_{7/2}$	3.63
$4f_{7/2} \rightarrow h_{9/2}$	0.47
$5s_{\frac{1}{2}} \rightarrow s_{\frac{1}{2}}$	-302.27
$5s_{\frac{1}{2}} \rightarrow d_{3/2}$	9.97
$5p_{\frac{1}{2}} \rightarrow p_{\frac{1}{2}}$	1400.06
$5p_{3/2} \rightarrow p_{3/2}$	-0.37
$5p_{3/2} \rightarrow f_{5/2}$	29.12
$5d_{3/2} \rightarrow s_{\frac{1}{2}}$	54.01
$5d_{3/2} \rightarrow d_{3/2}$	-769.96
$5d_{5/2} \rightarrow d_{5/2}$	88.33
$5d_{5/2} \rightarrow g_{7/2}$	-13.59
$6s_{\frac{1}{2}} \rightarrow s_{\frac{1}{2}}$	2849.56
$6s_{\frac{1}{2}} \rightarrow d_{3/2}$	267.93
HF $6p_{\frac{1}{2}}$	17663.83
Total	21985.58

orbitals have any significant amplitude at the nucleus.

6.7 PNC HF Results

The quoted matrix elements are for transitions between the parity-mixed states concerned. As described in chapter 3 we have only calculated them to first order in G_F which is perfectly acceptable in view of the size of G_F. Length/velocity equivalence does not hold for the PNC HF equations but the orthonormalisation condition for the orbitals means that there is the additional numerical check that

$$\langle a | b^{pnc} \rangle + \langle a^{pnc} | b \rangle = 0 \qquad (6.4)$$

We evaluated all the orbital overlaps of this kind to ensure that this condition was satisfied. It was noticed that this condition was met to more significant figures the smaller the step size and hence the greater the numerical accuracy was. By extrapolating the overlaps, the condition was found to hold exactly as $h \to 0$.

The PNC HF equations required a large number of iterations to converge and the PNC matrix element was quite sensitive to the convergence.

There are no experimental results with which to compare the PNC transitions (unless we assume a value for Q_W) so we cannot attach a figure for their errors. There have been numerous different calculations of the Cs and Tl PNC HF E1 matrix elements by different groups which we shall compare later.

6.8 The PNC EOM/RPA Results

We calculated the PNC EOM/RPA results for the same transitions as in the PNC HF case. Length and velocity gauges should agree again so we have a good numerical yardstick to go by. We started off by solving for excitations of the outermost core orbitals and gradually extended this to deeper within the core. It was found that the length gauge answer did not change much as this was done whereas the velocity gauge was far more dependent on the inner orbital excitations. We have given the outer core excitation contributions to the PNC E1 transition matrix element in table 6.14. For each excitation there are two contributions: one with the PNC excitation and Parity conserving HF orbital and one the other way round. We have

Table 6.12. PNC HF E1 Transition Matrix Elements

Caesium

Transition	length	velocity
	$(-iea_0Q_W/N)\times10^{-11}$	
$6s_{\frac{1}{2}} \rightarrow 7s_{\frac{1}{2}}$	0.927	0.830

Thallium

Transition	length	velocity
	$(-iea_0Q_W/N)\times10^{-11}$	
$6p_{\frac{1}{2}} \rightarrow 7p_{\frac{1}{2}}$	-10.00	-7.53
$6p_{\frac{1}{2}} \rightarrow 6p_{3/2}$	-39.75	-38.71

Table 6.13 PNC EOM/RPA E1 Transition Matrix Elements

Caesium

Transition	length	velocity
	$(-iea_0Q_W/N)\times10^{-11}$	
$6s_{\frac{1}{2}} \rightarrow 7s_{\frac{1}{2}}$	0.891	0.891

Thallium

Transition	length	velocity
	$(-iea_0Q_W/N)\times10^{-11}$	
$6p_{\frac{1}{2}} \rightarrow 7p_{\frac{1}{2}}$	-9.66	-9.66
$6p_{\frac{1}{2}} \rightarrow 6p_{3/2}$	-30.38	-30.38

Table 6.14.

Core Excitation Contributions to PNC EOM/RPA E1 Transition Matrix Element

Caesium (units $(-iea_0Q_W/N)\times10^{-11}$)

excitation	contribution (length)	(velocity)
$6s_{\frac{1}{2}} \rightarrow p_{\frac{1}{2}}$	0.927	+0.829
$5p_{3/2} \rightarrow d_{5/2}^-$	-0.019	0.127
$5p_{3/2} \rightarrow d_{5/2}^+$	0.000	-0.003
$5p_{3/2} \rightarrow d_{3/2}^-$	0.004	-0.025
$5p_{3/2} \rightarrow d_{3/2}^-$	-0.007	-0.050
$5p_{3/2} \rightarrow s_{\frac{1}{2}}^-$	-0.001	0.002
$5p_{3/2} \rightarrow s_{\frac{1}{2}}^+$	-0.004	-0.035
$5p_{\frac{1}{2}} \rightarrow d_{3/2}^-$	-0.002	0.022
$5p_{\frac{1}{2}} \rightarrow d_{3/2}^+$	-0.007	-0.054
$5p_{\frac{1}{2}} \rightarrow s_{\frac{1}{2}}^-$	-0.002	0.022
$5p_{\frac{1}{2}} \rightarrow s_{\frac{1}{2}}^+$	+0.001	0.010
$5s_{\frac{1}{2}} \rightarrow p_{3/2}^-$	0.000	0.003
$5s_{\frac{1}{2}} \rightarrow p_{3/2}^+$	0.000	0.002
$5s_{\frac{1}{2}} \rightarrow p_{\frac{1}{2}}^-$	-0.001	0.011
$5s_{\frac{1}{2}} \rightarrow p_{\frac{1}{2}}+$	+0.001	0.011

Thallium (units $(-iea_0Q_W/N)\times10^{-11}$)

excitation	contribution (length)	(velocity)
$6p_{\frac{1}{2}} \rightarrow s_{\frac{1}{2}}$	-10.00	-7.53
$6s_{\frac{1}{2}} \rightarrow p_{3/2}^-$	+0.91	-1.14
$6s_{\frac{1}{2}} \rightarrow p_{3/2}^+$	-1.74	+1.43
$6s_{\frac{1}{2}} \rightarrow p_{\frac{1}{2}}^-$	+0.21	-0.35
$6s_{\frac{1}{2}} \rightarrow p_{\frac{1}{2}}+$	+0.72	+1.31
$5d_{5/2} \rightarrow f_{7/2}^-$	+0.09	-0.82
$5d_{5/2} \rightarrow f_{7/2}^+$	-0.06	+0.53
$5d_{5/2} \rightarrow f_{5/2}^-$	-0.02	+0.15
$5d_{5/2} \rightarrow f_{5/2}^+$	+0.03	+0.25
$5d_{5/2} \rightarrow p_{3/2}^-$	-0.07	+0.33
$5d_{5/2} \rightarrow p_{3/2}^+$	+0.19	+0.91
$5d_{3/2} \rightarrow f_{5/2}^-$	+0.02	+0.21
$5d_{3/2} \rightarrow f_{5/2}^+$	+0.07	+0.68
$5d_{3/2} \rightarrow p_{3/2}^-$	+0.05	-0.27
$5d_{3/2} \rightarrow p_{3/2}^+$	-0.06	-0.32
$5d_{3/2} \rightarrow p_{\frac{1}{2}}^-$	+0.01	+0.03
$5d_{3/2} \rightarrow p_{\frac{1}{2}}^+$	+0.03	+0.23

merely quoted the sum in the table. The velocity gauge has many small contributions and cancellations. When solving for all the core excitations, we obtained length/velocity agreement to three significant figures but no more, even though grid extrapolation has been done. This sets a limit on the numerical accuracy of the calculation, though the length gauge answer is likely to be more reliable. We can still be confident in quoting the answer to three significant figures.

It is interesting to note that in thallium there is a far greater percentage change between the PNC HF and the PNC EOM/RPA transition matrix elements for the $6p_{\frac{1}{2}}$ $\rightarrow$ $6p_{3/2}$ transition than for the $6p_{\frac{1}{2}} \rightarrow 7p_{\frac{1}{2}}$ one. This indicates that shielding effects are more important for the former transition.

6.9 Comparison with Other Calculations

In table 6.15 we give a summary of our results and the equivalent calculations by two other groups. Dzuba's group (DZ) have done the most extensive MBPT calculations for theses quantities to date (see chapter seven). However they make several approximations in their methods which makes comparison difficult at times. Johnson group (WJ) are more rigorous in their approach. We have deliberately used the same nuclear charge distributions as was used in their calculations to make comparisons easier. DZ uses different parameters in his Fermi distribution.

Our E1 transition matrix elements agree exactly with WJ's and nearly exactly with DZ's. For the hyperfine constants we disagree with WJ's Cs $6s_{\frac{1}{2}}$ value by 0.2% whereas for the Cs $8s_{\frac{1}{2}}$ value agreement is almost exact. DZ's values are in reasonable agreement though his Cs $6s_{\frac{1}{2}}$ and Tl $6p_{\frac{1}{2}}$ values are somewhat lower than WJ's or ours. This is because he only considers core excitations that are diagonal in l (see chapter seven). The same calculation has been done by [Heully and A.M. Martensson-Pendrill] (AMP) who obtained 1722 for the Cs $6s_{\frac{1}{2}}$ value. However, in communication with AMP she has revealed that in her more accurate recent calculations she obtains 1733.

For the PNC phenomena the discrepancies are partly due to the different nuclear charge distributions used by DZ and WJ. Our distribution is the same as WJ's so the fact that we disagree by 0.5% for the Tl PNC $6p_{\frac{1}{2}} \rightarrow 7p_{\frac{1}{2}}$ transition is a little

Table 6.15.

Comparison of RPA Calculations of Various Groups

Parity Conserving RPA

Transition	Dzuba [1987_b]	Johnson [1986]	ours
Cs $6s_{\frac{1}{2}} \rightarrow 6p_{\frac{1}{2}}$	4.96	4.97	4.97
Cs $6s_{\frac{1}{2}} \rightarrow 6p_{3/2}$	---	7.01	7.01
Tl $6p_{\frac{1}{2}} \rightarrow 7s_{\frac{1}{2}}$	1.89	1.91	1.91
Tl $6p_{3/2} \rightarrow 7s_{\frac{1}{2}}$	3.61	3.61	3.61

PNC RPA

Transition	Dzuba [1987_b]	Johnson [1986]	ours
Cs $6s_{\frac{1}{2}} \rightarrow 7s_{\frac{1}{2}}$	0.887	0.890	0.891
Tl $6p_{\frac{1}{2}} \rightarrow 7p_{\frac{1}{2}}$	9.65	9.71	9.66
Tl $6p_{\frac{1}{2}} \rightarrow 6p_{3/2}$	30.34	----	30.38

Hyperfine RPA

Hyperfine constant	Dzuba [1987_a,1985]	Johnson [1986]	ours
Cs $6s_{\frac{1}{2}}$	1703	1724	1728
Cs $6p_{\frac{1}{2}}$	200.0	---	201.6
Cs $6p_{3/2}$	42.8	---	42.7
Cs $7s_{\frac{1}{2}}$	467.4	474.0	473.9
Cs $7p_{\frac{1}{2}}$	71.1	---	71.6
Tl $6p_{\frac{1}{2}}$	21199	21971	21971
Tl $6p_{3/2}$	-1919	---	-2080
Tl $7s_{\frac{1}{2}}$	10404	---	10914
Tl $7p_{\frac{1}{2}}$	1979	2029	2029

worrying. This is probably due to numerical errors (in a PNC there are a lot of cancellations of contributions which tend to lead to numerical errors). We have extrapolated to a zero grid size to try and minimise this; WJ does not extrapolate but uses a very small grid size. The difference is of the same order of magnitude as the difference between AMP's and WJ's hyperfine calculations.

6.10. Conclusions

We have set up and performed the basic hierarchy of equations as described earlier in this thesis and checked their results against similar calculations by other groups where possible. All the calculations seem to be correct.

Using RPA type equations gave transition matrix elements to an error of 10% with experiment in general and the hyperfine dipole interaction constant to 30% to 40%. There is no necessary reason why the PNC E1 matrix element should have the same size errors with the physical value as for the other calculations, but there is little else to go on. This will be discussed in more detail in chapter seven.

CHAPTER 7: The Semi-Empirical Approach to Correlation

7.1 Introduction

So far we have derived a set of *ab initio* equations that can be solved which give a reasonable physical answer. However, the level of accuracy that we obtain for the physical values that are known experimentally is not good enough for any PNC calculation using those equations to be of much value. The next stage is to provide a more accurate description of the atom and to include as much of the relevant physics as we can. As described in chapter three, starting with any given Hamiltonian we can, in theory, systematically work out perturbation corrections to any desired order and thus obtain an increasingly accurate description of the atom. As we have described, certain one particle effects can be included to all orders by using a self consistent set of equations. The question that arises is how accurately does this represent the actual physical situation? If it is not sufficiently accurate then what corrections do we have to apply to obtain a better one? The results of the equations so far given were presented in chapter six. We can see that while the methods give reasonble *ab initio* answers they are in general only accurate to 10% in the E1 parity conserving matrix elements and about 25% in the hyperfine dipole value and we cannot easily claim a higher accuracy for the PNC E1 matrix element. The straightforward approach would be to look at the next order of perturbation theory. It has been shown by several authors (e.g. [Johnson 1987], [Dzuba 1985,1987$_{a,b}$]) that of the second order diagrams not included in the RPA equations the most significant are the lowest order Brueckner orbital corrections (for example see figure 7.1). A Brueckner orbital (BO) is defined to have no single-particle perturbation corrections to it to any order (this is to be compared with HF orbitals which have no single-particle corrections to them to lowest order only). The lowest order valence contributions to the BO corrections are the ones given in the figure. It should be noted that these diagrams are correlation diagrams with two simultaneously excited states. The actual matrix elements represented by the diagrams are given by:

Figure 7.1 Valence 'Brueckner Orbital' Corrections

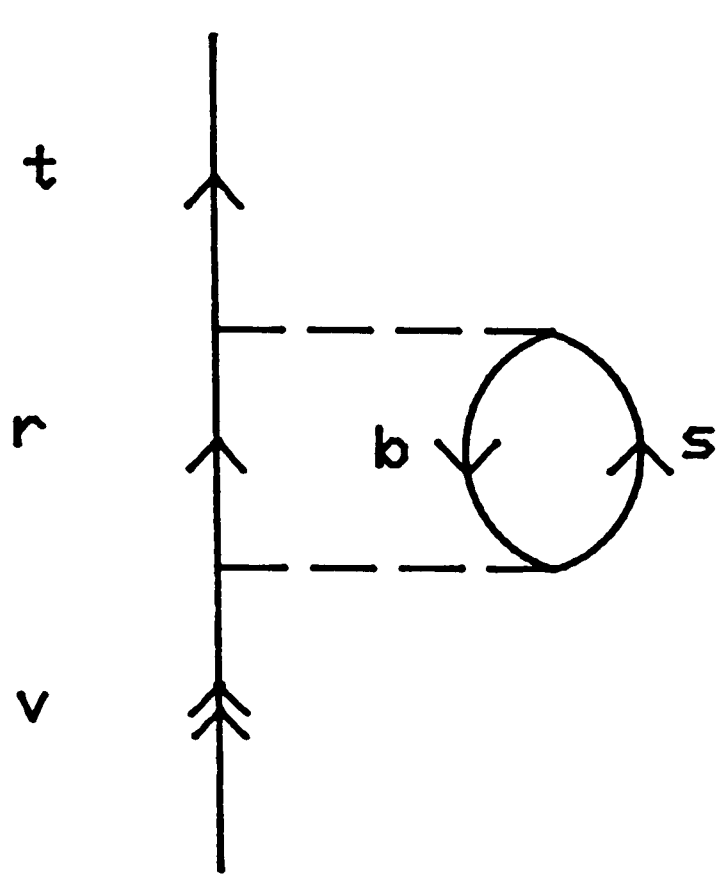

a

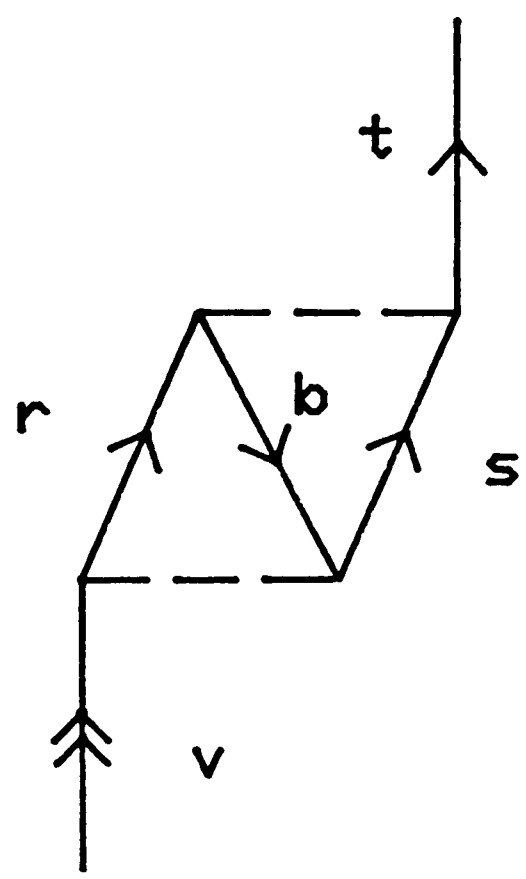

b

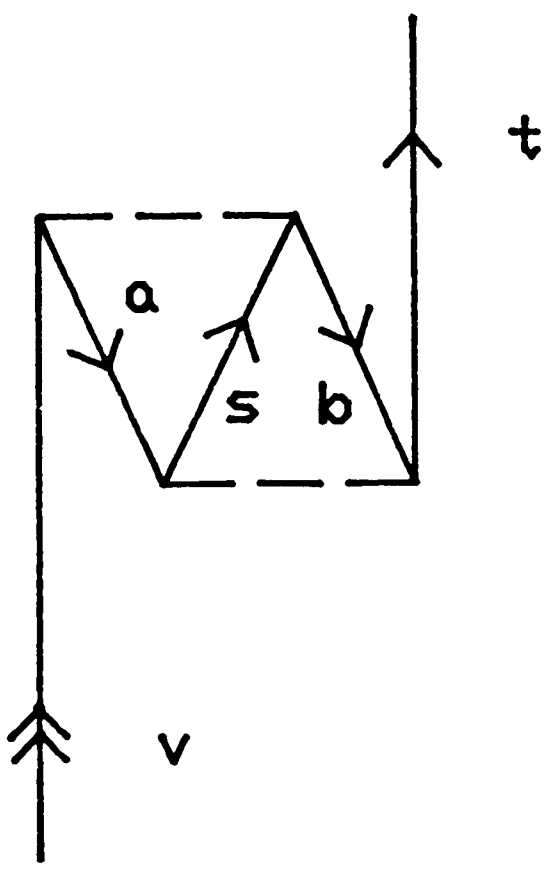

c

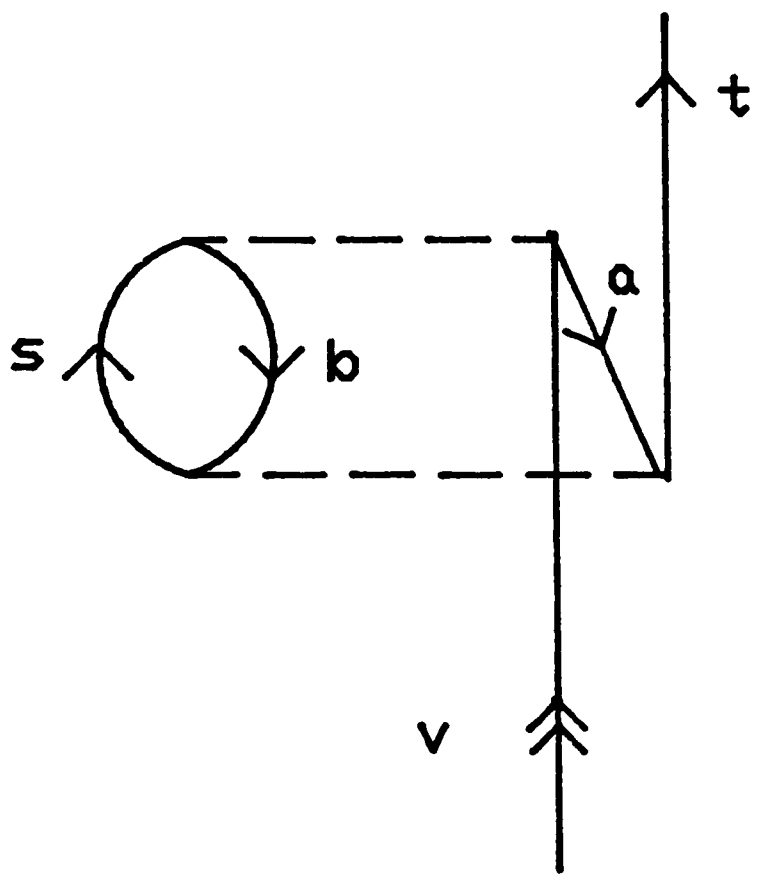

d

$$\text{a:} \quad a^{\dagger}_t \, a_v \quad \frac{\langle tb|r_{12}^{-1}|rs\rangle\langle rs|r_{12}^{-1}|vb\rangle}{(\epsilon_v - \epsilon_t)\,(\epsilon_v + \epsilon_b - \epsilon_r - \epsilon_s)}$$

$$\text{b:} \quad a^{\dagger}_t \, a_v \quad \frac{\langle tb|r_{12}^{-1}|sr\rangle\langle rs|r_{12}^{-1}|vb\rangle}{(\epsilon_v - \epsilon_t)\,(\epsilon_v + \epsilon_b - \epsilon_r - \epsilon_s)} \qquad (7.1)$$

$$\text{c:} \quad a^{\dagger}_t \, a_v \quad \frac{\langle st|r_{12}^{-1}|ab\rangle\langle ab|r_{12}^{-1}|vs\rangle}{(\epsilon_v - \epsilon_t)\,(\epsilon_a + \epsilon_b - \epsilon_t - \epsilon_s)}$$

$$\text{d:} \quad a^{\dagger}_t \, a_v \quad \frac{\langle st|r_{12}^{-1}|ba\rangle\langle ab|r_{12}^{-1}|vs\rangle}{(\epsilon_v - \epsilon_t)\,(\epsilon_a + \epsilon_b - \epsilon_t - \epsilon_s)}$$

Consider diagram *a* for the moment. If we define a pair function by

$$|\eta_{vb}\rangle \equiv \sum_{rs} \frac{|rs\rangle\langle rs|r_{12}^{-1}|vb\rangle}{(\epsilon_v + \epsilon_b - \epsilon_r - \epsilon_s)} \qquad (7.2)$$

It satisfies the pair equation

$$(\epsilon_v + \epsilon_b - H_0^{HF}(1) - H_0^{HF}(2))\,|\eta_{vb}\rangle = \sum_{rs} |rs\rangle\langle rs|r_{12}^{-1}|vb\rangle \qquad (7.3)$$

where H_0^{HF} is the HF Hamiltonian. If we then substitute this into the expression for diagram *a*, after summing over the orbital states we obtain a single-particle function satisfying the equation

$$\left[\, \epsilon_v - H_0^{HF}(1) \,\right] |\eta_v(1)\rangle = \sum_{b} \frac{|t\rangle\langle tb|r_{12}^{-1}|\eta_{vb}\rangle}{(\epsilon_v - \epsilon_t)} \qquad (7.4)$$

The difficulty in evaluating this expression is the double sum over the excited states in equation (7.3). Most groups ([Dzuba 1985, $1987_{a,b}$], [Johnson 1987]) do the sum explicitly, truncating it at certain maximum angular momenta and using approximate methods for evaluating the higher orbital and continuum contributions. It is possible to use differential equation methods to do the sums but the numerical computation involved is complicated.

7.2 The Semi-Empirical Approach

7.2.1 Introduction

As mentioned above there is a great deal of complexity involved in calculating the lowest order BO corrections. The alternative approach which we shall adopt is that of using a local potential to model the main correlation effects described above. Classically, in single-valence systems the valence electron interacts with the closed spherically symmetric core of electrons and polarises it slightly by its Coulomb interaction. This polarisation is calculated by RPA type equations. The polarised core produces a slight dipolar field which the valence orbital interacts with and it is this interaction which is represented by the BO corrections. If one assumes that the strength of the induced dipole is proportional to the polarising field then the dipole strength depends on $1/r^2$ where r is the distance of the valence electron from the core. Thus the potential affecting the valence electron depends on r^{-4}. As the valence electron penetrates the core the effect should diminish. We are going to use a local potential to model this effect so that instead of the expressions in (7.1) we write

$$a^\dagger_t \, a_v \, < t \mid \delta V(r) \mid v > \qquad (7.5)$$

where $\delta V(r)$ is a suitable local potential.

One could argue from looking at the terms in figure 7.1 and the expressions in equation (7.1) that the potential should not produce excitations to other core orbitals. This can easily be achieved by orthogonalising the potential to the core.

$$\delta V(r)|v> - \sum_b |b><b|\delta V(r)|v> \qquad (7.6)$$

where the *b*'s are core orbitals so that we are effectively summing over the excited states *t* in (7.5) above. The trouble with this is that one then has to apply any additional perturbations, such as the hyperfine interaction or the electric field or PNC (or both of the last two for PNC EOM) to the orbitals in the orthogonalisation terms as well. This produces many more terms in the higher order calculations.

An additional problem with this is that the potential in equation (7.6) is not hermitian and so if the potential is simply added to the HF equation it will produce eigenfunctions that are no longer orthogonal to each other and orthonormality is necessary in the derivation of the EOM and hyperfine calculations. One solution to this would be to surround the potential by projection operators so that it only acts on the excited state orbitals.

$$\left(1 - \sum_{b} |b\rangle\langle b| \right) \delta V(r) \left(1 - \sum_{b'} |b'\rangle\langle b'| \right) \qquad (7.7)$$

This might be reasonable from a physical point of view also: the polarisation affect should not have much affect on the core orbitals themselves. But again we would be adding greatly to the complexity of the higher order equations if we were to include such a projected potential rigorously in all the equations. We therefore simply used a single local potential acting on all the orbitals as in (7.6) but without orthogonalising to the core.

7.2.2 Inclusion of the Semi-Empirical Potential in the HF Equations

The basic approach is to take a parameterised local polarisation potential and to adjust the parameters to obtain a good fit to experiment for the eigenvalues of the valence orbitals. We therefore solved the modified HF equations:

$$(\epsilon_a - h_0 - V_{hf}) \, |a\rangle = V_{semp}(r) |a\rangle \qquad (7.8)$$

where $V_{semp}(r)$ is our parameterised local potential. We started with V_{N-1} HF eigenfunctions and solved equation (7.8) until self-consistency was reached. The lowest order eigenvalue corrections to the unperturbed HF orbitals due to the local potential can be easily found by taking the diagonal matrix elements with the unmodified HF orbitals. The optimum parameters to give the best fit to lowest order can easily be found this way. It should be remembered, however, that since V_{hf} is a function of all the core orbitals the corrections to each orbital 'feed back' to all the others in a non-trivial way so there is no obvious way to predict the outcome for a given set of parameters when iterating (7.8) to self-consistency. We used as a measure of the quality of the fit a residue function defined as the weighted sum of the squares of the

errors in the eigenvalues to be fitted. The weightings were the reciprocals of the experimental energies squared so that the residue is a dimensionless quantity. We also weighted the orbitals so that the two components of the fine structure levels each had half the weighting of non-fine structure split orbitals. Thus the residue is defined as:

$$R = \sum_i C_i \frac{(\epsilon_i - \epsilon_{expt,i})^2}{(\epsilon_{expt,i})^2} \qquad (7.9)$$

The sum is over the orbitals to be fitted and the coefficients C_i equal 1 for $s_{\frac{1}{2}}$ orbitals and 0.5 for all others. We chose to fit all valence and excited state $s_{\frac{1}{2}}$ and $p_{\frac{1}{2}}$ levels up to $8s_{\frac{1}{2}}$. We simply started with some approximately fitted wavefunctions and iterated the equation for different parameters and so found the optimum parameters by 'brute force'. Some investigation was made into using quadratic fitting programs to predict the next best choice of parameters for a given choice but it was found that the residual surface was quite flat bottomed and not suited to this type of fitting. The surface was however smoothly varying with the parameters and it was not too difficult to find the parameters to minimise the residue.

7.2.3. Inclusion of the Semi-Empirical Potential in the Other Equations

Since we initially opted for a purely local potential with no projection operators its addition to the other equations is straightforward: it is simply added to the right-hand side of the equation acting on whatever is being solved for. The modified EOM excitation equations can be written as

$$(\epsilon_i \pm \omega - h_0 - V_{hf,core})\,|i^{\pm}\rangle = V^{\pm}(i)|i\rangle + V_{semp}(r)|i^{\pm}\rangle - \sum_b |b\rangle\langle b|V^{\pm}(i)|i\rangle \qquad (7.10)$$

where we have used a similar notation to chapter four. Since $V_{semp}(r)$ is a scalar potential the actual inclusion in the radial equations is straightforward.

Similarly for the hyperfine equations (see Appendix 2) we simply add on the term:

$$V_{semp}(r)\,|a^{+}_{hyp}\rangle \qquad (7.11)$$

The great simplicity of this approach can now be appreciated. The existing programs are easily modified to include the extra term on the right-hand side of the equation. Because the $V_{semp}(r)$ term is scalar, it will commute with the dipole operator and thus the length/velocity equivalence of the dipole transition matrix element will be maintained (see Appendix 3). The inclusion of V_{semp} in the PNC equations is done in a similar manner. We now solve the modified PNC HF equations:

$$(\epsilon_a - h_0 - V_{hf})\ |a^{pnc}\rangle = h^{pnc}|a\rangle + V_{semp}(r)|a^{pnc}\rangle + V_{hf}{}^{pnc}|a\rangle \qquad (7.12)$$

Similarly for the PNC EOM/RPA equations we simply add to the right-hand side the term

$$V_{semp}(r)\ |a^{\pm pnc}\rangle \qquad (7.13)$$

We will discuss exactly what MBPT terms the semi-empirical potential is modelling in a later section when we discuss the results.

7.2.4. The Semi-Empirical Potentials Used

As mentioned above we required the semi-empirical potentials to go as r^{-4} for large r and to go to zero below some cut-off radius. We tried two basic types of potential of the form that have been used before in other semi-empirical work. The first one was originally used by [Norcross] and which has since been used by several groups (e.g. [Parpia *et al.*]) in semi-empirical calculations. It is of the form

type A:

$$V_{semp}(r) = \frac{P_1}{r^4}\ [\ 1.0 - \exp(\ -(\ r/P_2\ )^n\ )\ ] \qquad (7.14)$$

where the condition on *n* is that it must be greater than 4 for the potential to remain finite at the origin. We tried with n equals 6 and 8. P_2 controls the cut-off of the potential: when $r > P_2$ the exponential term is very small and the potential approximates to P_1/r^4; when $r < P_2$ the exponential tend to 1.0 and the potential to zero. The lowest term in the power expansion of the potential is of order n-4.

Figure 7.2: Semi-Empirical Potentials

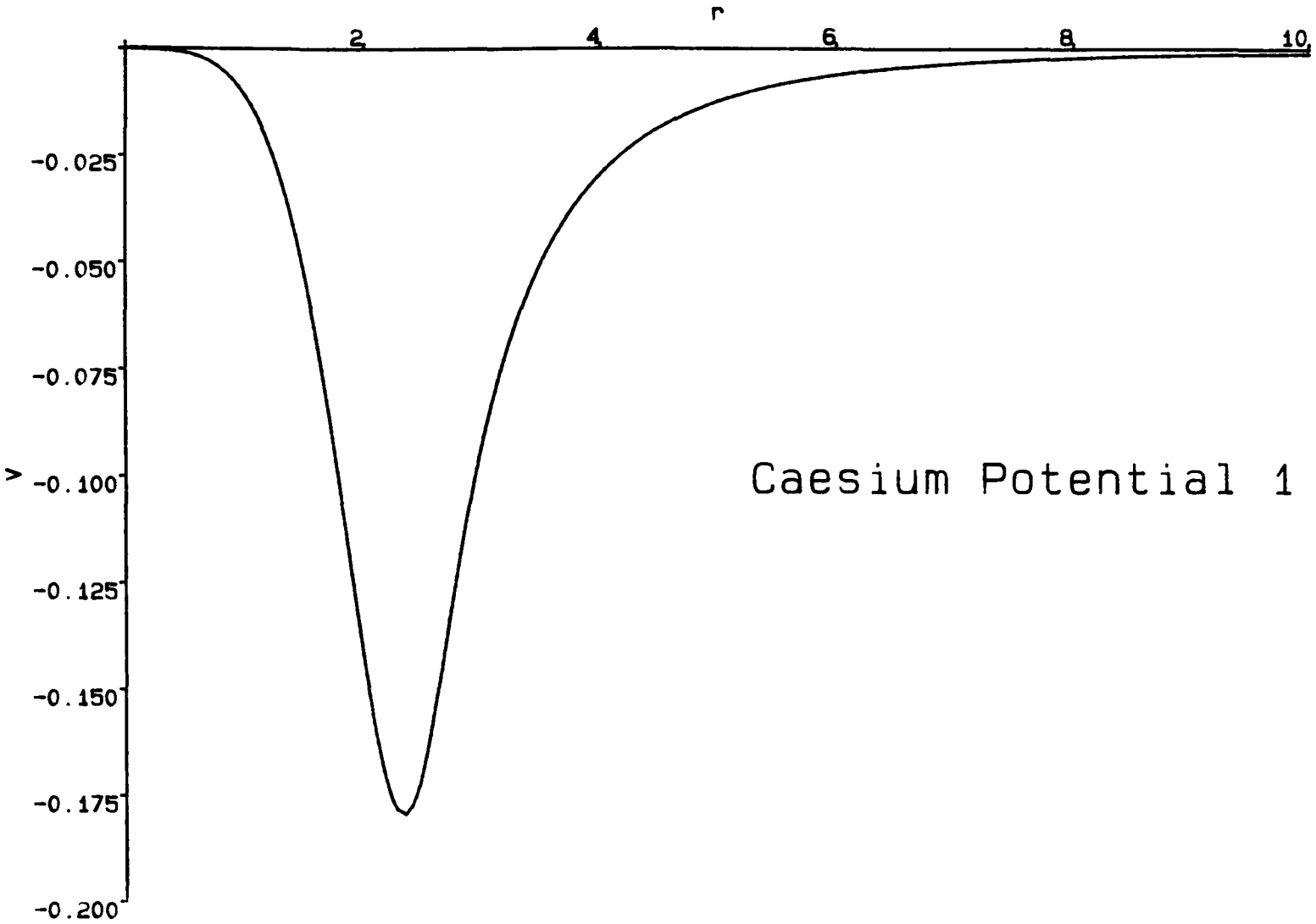

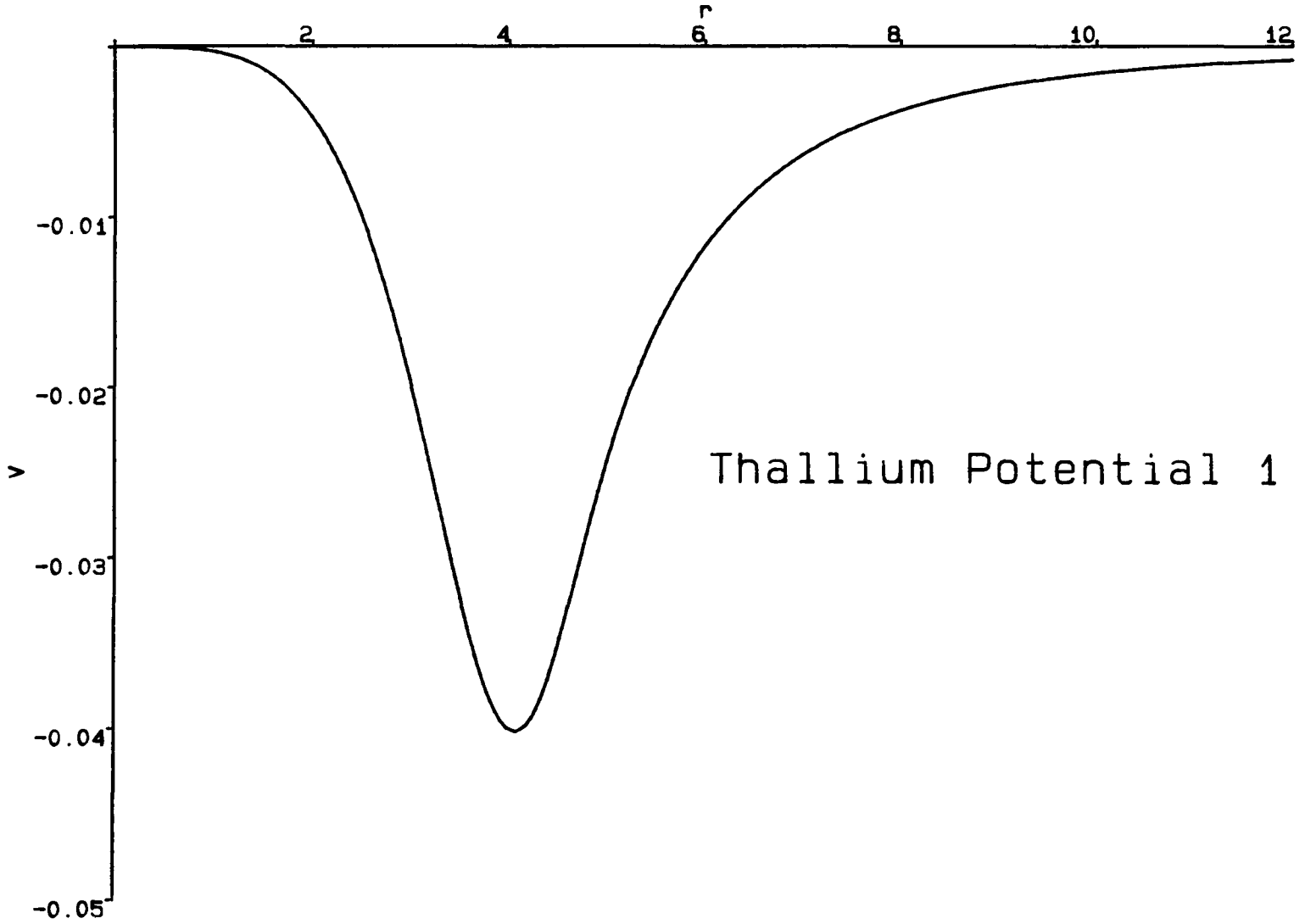

Table 7.1.

Optimised Parameters for the Semi–Empirical Potentials Used

Caesium

NUMBER	type	P_1	P_2	n	n_2	n_3	a	Residue
1	A	-7.469	2.270	8	-	-	-	0.360×10^{-5}
2	A	-7.523	2.484	6	-	-	-	0.143×10^{-5}
3	B	-8.22	2.49	3	7	1	-	0.368×10^{-5}
4	B	-10.31	2.23	2	3	2	-	0.124×10^{-3}
5	B	-9.41	2.43	2	6	1		0.663×10^{-4}
6	C	-10.65	2.51	3	7	1	2.0	0.105×10^{-4}
7	C	-13.58	2.43	3	7	1	1.0	0.233×10^{-4}

Thallium

NUMBER	type	P_1	P_2	n	n_2	n_3	a	Residue
1	A	-15.28	3.94	8	-	-	-	0.194×10^{-3}
2	A	-15.84	4.20	6	-	-	-	0.102×10^{-3}
3	B	-17.08	4.00	3	7	1	-	0.923×10^{-4}
4	B	-24.08	3.89	2	3	2	-	0.358×10^{-4}
5	B	-20.51	4.04	2	6	1		0.356×10^{-4}
6	C	-19.79	3.87	3	7	1	2.0	0.852×10^{-4}
7	C	-22.93	3.72	3	7	1	1.0	0.776×10^{-4}

Thus the greater the value of *n* the faster the cut–off and the quicker it tends to zero for small r.

The second potential used was of the form

type B

$$V_{semp}(r) = \frac{P_1\, r^n}{(\, P_2^{n_2} + r^{n_2}\,)^{n_3}} \qquad (7.15)$$

Again, P_2 is the cut–off parameter and P_1 the overall scaling parameter. For $r \gg P_2$ V_{semp} goes as r to the power of $(n - n_2\, n_3)$ which we require to equal −4. For $r \ll P_2$ the power is r^n. We made several choices for the parameters and fitted P_1 and P_2 in the usual way.

Both these types of potential have similar shapes so in order to test how dependent the answers were on the type of potential we also tried multiplying one of them by an additional factor which changes the sign of the function at some point near the origin. We tried a potential of the form

type C

$$V_{semp}(r) = \frac{(\,\alpha r - 1\,)\, P_1\, r^n}{(\,\alpha r + 1\,)(\, P_2^{n_2} + r^{n_2}\,)^{n_3}} \qquad (7.16)$$

For values of $\alpha r \gg 1$ the function is of the same form as type B. When $\alpha r \ll 1$ the potential changes sign, the actual change occurring at $\alpha r = 1$. The potential is thus similar to our other one as regards its dependence on r at large distances but has a different form at small r.

7.3 Results

We tried seven different combinations of parameters which we have labelled as potentials 1 to 7 in the tables 7.1a and b. In all the tables *a* refers to caesium and *b* to thallium. The potential type refers to the three types of potential as given in (7.14), (7.15) and (7.16). The optimised parameters are given where applicable. We have given plots of potential 1 for caesium and thallium in figure 7.2.

Table 7.2a

Caesium Unmodified HF and Experimental Eigenvalues

Orbital	HF	Expt.
$6s_{1/2}$	-0.12737	-0.14310
$6p_{1/2}$	-0.08562	-0.09217
$6p_{3/2}$	-0.08379	-0.08964
$7s_{1/2}$	-0.05519	-0.05865
$7p_{1/2}$	-0.04202	-0.04393
$7p_{3/2}$	-0.04137	-0.04310
$8s_{1/2}$	-0.03095	-0.03232

Table 7.3a

Caesium Excited State Eigenvalues for The Semi-Empirical Potentials

Orbital	Potential Type			
	1	2	3	4
$6s_{1/2}$	-0.14305	-0.14311	-0.14314	-0.14244
$6p_{1/2}$	-0.09205	-0.09209	-0.09221	-0.09284
$6p_{3/2}$	-0.08975	-0.08972	-0.08981	-0.09049
$7s_{1/2}$	-0.05869	-0.05866	-0.05860	-0.05844
$7p_{1/2}$	-0.04387	-0.04389	-0.04389	-0.04403
$7p_{3/2}$	-0.04312	-0.04311	-0.04311	-0.04328
$8s_{1/2}$	-0.03232	-0.03231	-0.03227	-0.03220

Orbital	Potential Type		
	5	6	7
$6s_{1/2}$	-0.14271	-0.14308	-0.14297
$6p_{1/2}$	-0.09265	-0.09232	-0.09247
$6p_{3/2}$	-0.09028	-0.08990	-0.09004
$7s_{1/2}$	-0.05848	-0.05856	-0.05854
$7p_{1/2}$	-0.04399	-0.04390	-0.04391
$7p_{3/2}$	-0.04322	-0.04311	-0.04313
$8s_{1/2}$	-0.03222	-0.03225	-0.03224

Table 7.4a

The Modified Hartree-Fock Core Eigenvalues For Caesium

Orbital	HF	+ V_{semp}	Expt
$1s_{1/2}$	-1330.1	-1330.2	-1322
$2s_{1/2}$	-212.56	-212.6	-210
$2p_{1/2}$	-199.43	-199.5	-197
$2p_{3/2}$	-186.44	-186.5	-184
$3s_{1/2}$	-45.969	-46.020	-44.7
$3p_{1/2}$	-40.447	-40.499	-39.1
$3p_{3/2}$	-37.895	-37.946	-36.7
$3d_{3/2}$	-28.310	-28.362	-27.2
$3d_{5/2}$	-27.776	-27.828	-26.7
$4s_{1/2}$	-9.5121	-9.5528	-8.48
$4p_{1/2}$	-7.4455	-7.4867	-6.33
$4p_{3/2}$	-6.9210	-6.9622	-5.93
$4d_{3/2}$	-3.4856	-3.5286	-2.90
$4d_{5/2}$	-3.3972	-3.4405	-2.81
$5s_{1/2}$	-1.4897	-1.5834	-0.83
$5p_{1/2}$	-0.90779	-1.0128	-0.48
$5p_{3/2}$	-0.84039	-0.9485	-0.41

Table 7.2b

Thallium Unmodified HF and Experimental Eigenvalues

Orbital	HF	Expt.
$6p_{1/2}$	-0.19968	-0.22446
$6p_{3/2}$	-0.16693	-0.18896
$7s_{1/2}$	-0.09618	-0.10382
$7p_{1/2}$	-0.06505	-0.06882
$7p_{3/2}$	-0.06086	-0.06426
$8s_{1/2}$	-0.04574	-0.04792

Table 7.3b

Thallium Excited State Eigenvalues for The Semi-Empirical Potentials

Orbital	Potential Type			
	1	2	3	4
$6p_{1/2}$	-0.22294	-0.22326	-0.22311	-0.22376
$6p_{3/2}$	-0.19083	-0.19030	-0.19033	-0.18947
$7s_{1/2}$	-0.10416	-0.10418	-0.10415	-0.10384
$7p_{1/2}$	-0.06802	-0.06832	-0.06839	-0.06899
$7p_{3/2}$	-0.06368	-0.06387	-0.06397	-0.06447
$8s_{1/2}$	-0.04783	-0.04780	-0.04778	-0.04771

Orbital	Potential Type		
	5	6	7
$6p_{1/2}$	-0.22361	-0.22307	-0.22306
$6p_{3/2}$	-0.18977	-0.19034	-0.19037
$7s_{1/2}$	-0.10396	-0.10412	-0.10406
$7p_{1/2}$	-0.06881	-0.06843	-0.06848
$7p_{3/2}$	-0.06431	-0.06402	-0.06408
$8s_{1/2}$	-0.04772	-0.04778	-0.04778

Table 7.4b

The Modified Hartree-Fock Core Eigenvalues For Thallium

Orbital	HF	+ $V_{semp}(r)$	Expt
$1s_{1/2}$	-3164.4	-3164.5	-3145
$2s_{1/2}$	-569.11	-569.12	-564
$2p_{1/2}$	-545.22	-545.23	-540
$2p_{3/2}$	-469.19	-469.20	-465
$3s_{1/2}$	-138.63	-138.64	-136
$3p_{1/2}$	-127.92	-127.93	-126
$3p_{3/2}$	-110.80	-110.81	-109
$3d_{3/2}$	-93.351	-93.364	-91.4
$3d_{5/2}$	-89.729	-89.742	-87.8
$4s_{1/2}$	-32.556	-32.569	-31.1
$4p_{1/2}$	-27.907	-27.920	-26.5
$4p_{3/2}$	-23.693	-23.706	-22.4
$4d_{3/2}$	-16.110	-16.122	-14.9
$4d_{5/2}$	-15.314	-15.327	-14.2
$4f_{5/2}$	-5.4581	-5.4705	-4.51
$4f_{7/2}$	-5.2824	-5.2948	-4.36
$5s_{1/2}$	-5.8851	-5.8962	-5.01
$5p_{1/2}$	-4.2506	-4.2618	-3.66
$5p_{3/2}$	-3.4843	-3.4953	-2.77
$5d_{3/2}$	-1.1611	-1.1720	-0.563
$5d_{5/2}$	-1.0736	-1.0844	-0.482
$6s_{1/2}$	-0.68941	-7.0515	---

In tables 7.2a. and b we give the unmodified HF and the experimental results for comparison with table 7.3, which contains the optimised fits for the valence and excited state eigenvalues for the seven potentials.

Table 7.4 gives the modified core HF eigenvalues for potential number 1. The results are similar for the other potentials as well. The experimental results are also quoted for comparison.

Table 7.5 gives the E1 transition matrix elements for the length gauge. For the modified EOM/RPA calculations we obtained length/velocity agreement to the same accuracy as for the unmodified calculations (i.e. four significant figures).

The unmodified, experimental and modified hyperfine dipole interaction constants have been given in table 7.6.

7.4. Discussion of the Semi-Empirical Results

We have summarised the results of the calculation in tables 7.7. We have rearranged the potentials in diminishing order of residues with the unmodified HF results at the top and the experimental results at the bottom. Several observations can immediately be made:

Caesium

1. From table 7.5a. it can be seen that the effect of the shielding is to reduce the magnitude of the transition matrix element by about 6% or 7%. Without the shielding the magnitude of the matrix element is over-estimated, inclusion of the shielding gives very good agreement with experiment.
2. From table 7.7a it can be seen that the transition matrix elements change by the same proportion for both transitions so that the fractional errors are about the same in each one. As the residues decrease the transition matrix elements decrease from above the experimental value to slightly below it. Potentials 7, 6 and 3 match the $6p_{\frac{1}{2}}$ transition error range; potentials 6 and 3 match the $6p_{3/2}$ range. The worst case error is 0.8% for the $6p_{\frac{1}{2}}$ transition and 1% for the $6p_{3/2}$ one.

Table 7.5a

Reduced E1 Transition Matrix Elements for Caesium (Length Gauge)

$6s_{\frac{1}{2}} \rightarrow 6p_{\frac{1}{2}}$ Transition

	Potential Type 1	2	3	4	5	6	7	unmodified value
HF + V_{semp}	-4.83	-4.83	-4.84	-4.88	-4.86	-4.85	-4.87	-5.28
EOM/RPA + V_{semp}	-4.50	-4.50	-4.51	-4.56	-4.55	-4.52	-4.53	-4.97
Expt.	-4.52 (0.01)							

$6s_{\frac{1}{2}} \rightarrow 6p_{3/2}$ Transition

	Potential Type 1	2	3	4	5	6	7	unmodified value
HF + V_{semp}	+6.78	+6.78	+6.80	+6.86	+6.84	+6.81	+6.84	+7.43
EOM/RPA + V_{semp}	+6.34	+6.34	+6.35	+6.43	+6.41	+6.36	+6.38	+7.01
Expt.	+6.36 (0.01)							

Table 7.6a

Caesium Hyperfine Dipole Interaction Constants (MHz)

g_I = 0.7377208

	Potential Type 1	2	3	4	5	6	7	unmodified value
$6s_{\frac{1}{2}}$ (Expt: = 2298 MHz)								
HF+V_{semp}	2091	2047	2021	1871	1915	1995	1970	1434
RPA+V_{semp}	2523	2468	2438	2251	2307	2408	2379	1728
$6p_{\frac{1}{2}}$ (Expt = 291.9 (0.1) MHz)								
HF+V_{semp}	212.2	217.1	219.1	213.0	215.6	220.4	219.9	161.0
RPA+V_{semp}	260.1	267.2	270.4	262.8	266.0	272.8	272.6	201.6
$7s_{\frac{1}{2}}$ (Expt = 546.2 (3.0) MHz)								
HF+V_{semp}	500.9	486.8	497.1	452.8	459.4	474.1	470.9	393.8
RPA+V_{semp}	602.3	585.1	576.2	543.3	551.7	570.5	566.9	473.9
$7p_{\frac{1}{2}}$ (Expt = 94.34 (0.2) MHz)								
HF+V_{semp}	67.77	71.09	71.26	68.77	69.61	71.45	71.19	57.64
RPA+V_{semp}	84.95	86.92	87.33	84.26	85.33	87.78	87.57	71.64

Table 7.7a

Summary of Modified Results for Caesium

Potential		Reduced E1 $6s_{\frac{1}{2}} \rightarrow$		Hyperfine A_{hyp} (MHz)			
no.	Residue	$6p_{\frac{1}{2}}$	$6p_{3/2}$	$6s_{\frac{1}{2}}$	$6p_{\frac{1}{2}}$	$7s_{\frac{1}{2}}$	$7p_{\frac{1}{2}}$
unmodified		4.97	7.01	1728	201.6	474.0	71.64
4	0.12×10^{-3}	4.56	6.43	2251	262.8	543.3	84.26
5	0.66×10^{-4}	4.55	6.41	2307	266.0	551.7	85.33
7	0.23×10^{-4}	4.53	6.38	2379	272.6	566.9	87.57
6	0.11×10^{-4}	4.52	6.36	2408	272.8	570.5	87.78
3	0.37×10^{-5}	4.51	6.35	2438	270.4	576.2	87.33
1	0.36×10^{-5}	4.50	6.34	2523	260.1	602.3	84.95
2	0.14×10^{-5}	4.50	6.34	2468	267.2	585.1	86.92
Expt.		4.52	6.36	2298	291.9	546.2	94.34
Expt. Errors		0.01	0.01	<0.1	0.01	3.0	0.02

3. From table 7.6a we find that the semi–empirical potential gives a significant proportion of the correlation correction for the hyperfine constants. The inclusion of the RPA terms increases the magnitude in all cases.

4. In table 7.7a we see that as the residues decrease the $6s_{\frac{1}{2}}$ and $7s_{\frac{1}{2}}$ hyperfine dipole interaction constants increases from just below the experimental value to about 10% above it. They thus match best for the potentials with the worst residues. The $p_{\frac{1}{2}}$ values peak for residues of the order of 0.1×10^{-4} i.e. for potentials 6 and 7. The peak values are 7% under the experimental values. The worst case $p_{\frac{1}{2}}$ values are 10% under–estimated. Apart from potentials 4 and 5 (which give poor fits of the transition matrix elements) the $s_{\frac{1}{2}}$ values are over–estimated.

5. If we were to take potential 6 as the 'best' one (as it matches the E1 transition matrix elements and gives the best $p_{\frac{1}{2}}$ hyperfine values with reasonable $s_{\frac{1}{2}}$ hyperfine values) then we have no error in the transition matrix elements, a 5% error in the $6s_{\frac{1}{2}}$ hyperfine constant, a 6.5% error in the $6p_{\frac{1}{2}}$ hyperfine value, a 4.4% error in the $7s_{\frac{1}{2}}$ value and a 7% error in the $7p_{\frac{1}{2}}$ value.

Thallium

1. The energy residues are in general an order of magnitude worse for the thallium calculations than for caesium. It is potentials 4 and 5 which give the best energy fits in Tl and 1 and 2 the worst whereas for Cs it is the other way round.

2. The parity conserving transition matrix elements behave similarly to Cs. From table 7.5b we find that the shielding reduces the magnitude by about 7% for the $6p_{\frac{1}{2}} \rightarrow 7s_{\frac{1}{2}}$ transition and 10% for the $6p_{3/2}$ one. In table 7.7b, the $6p_{3/2}$ values are all above the quoted experimental value; however the latter has a very large error range and all our answers fall within it. The percentage change in the $6p_{3/2}$ value across the range of the potentials is a less than for the $6p_{\frac{1}{2}}$ values.

3. From table 7.6b we find that the semi–empirical correction to the $6p_{\frac{1}{2}}$ hyperfine values from the HF are not of the same sign: potentials 4 and 5 actually give worse answers than the HF values. However these potentials give the best $7s_{\frac{1}{2}}$

Table 7.5b

Reduced E1 Transition Matrix Elements for Thallium (Length Gauge)

$6p_{\frac{1}{2}} \rightarrow 7s_{\frac{1}{2}}$ Transition

	Potential Type 1	2	3	4	5	6	7	unmodified value
HF + V_{semp}	2.02	2.00	2.00	1.95	1.96	2.00	1.99	2.05
EOM/RPA + V_{semp}	1.87	1.86	1.86	1.82	1.83	1.85	1.85	1.91
Expt.	1.84 (0.06)							

$6p_{3/2} \rightarrow 7s_{\frac{1}{2}}$ Transition

	Potential Type 1	2	3	4	5	6	7	unmodified value
HF + V_{semp}	3.74	3.73	3.73	3.69	3.70	3.73	3.72	3.97
EOM/RPA + V_{semp}	3.35	3.35	3.35	3.33	3.33	3.35	3.34	3.61
Expt.	3.29 (0.09)							

Table 7.6b

Thallium Hyperfine Dipole Interaction Constants (MHz)

g_I = 3.2764268

	Potential Type 1	2	3	4	5	6	7	unmodified value
$6p_{\frac{1}{2}}$ (Expt = 21310.8 MHz)								
HF+V_{semp}	17129	17571	17468	18241	18008	17439	17416	17656
RPA+V_{semp}	21444	21887	21775	22562	22323	21743	21717	21971
$7s_{\frac{1}{2}}$ (Expt = 12500 MHz)								
HF+V_{semp}	10358	10027	9994	9387	9561	9973	9940	7765
RPA+V_{semp}	14569	14060	14024	13109	13371	13997	13953	10914
$7p_{\frac{1}{2}}$ (Expt = 2130 (60) MHz)								
HF+V_{semp}	2130	2164	2154	2171	2165	2147	2139	1968
RPA+V_{semp}	2162	2200	2189	2206	2205	2182	2173	2029

Table 7.7b

Summary of Modified Results for Thallium

Potential		Reduced E1 $7s_{\frac{1}{2}} \leftarrow$		Hyperfine A_{hyp} (MHz)		
no.	Residue	$6p_{\frac{1}{2}}$	$6p_{3/2}$	$6p_{\frac{1}{2}}$	$7s_{\frac{1}{2}}$	$7p_{\frac{1}{2}}$
unmodified		1.91	3.61	21971	10913	2029
1	0.19×10^{-3}	1.87	3.35	21444	14569	2162
2	0.10×10^{-3}	1.86	3.35	21887	14060	2200
3	0.92×10^{-4}	1.86	3.35	21775	14024	2189
6	0.85×10^{-4}	1.85	3.35	21743	13997	2182
7	0.78×10^{-4}	1.85	3.34	21717	13953	2173
4	0.36×10^{-4}	1.82	3.33	22562	13109	2205
5	0.36×10^{-4}	1.83	3.33	22323	13371	2205
Expt.		1.84	3.29	21311	12500	2130
Expt. Errors		0.06	0.09			60

values. Potentials 3 and 6 give the best $p\frac{1}{2}$ values. When the RPA terms are included the magnitude increases in all cases. All the hyperfine constants in table 7.7b are overestimated in value. The worst case errors in the final answers are 6% for $6p\frac{1}{2}$, 17% for $7s\frac{1}{2}$ and 3.5% for $7p\frac{1}{2}$.

4. Choosing potential 6 again as the best reasonable fit gives less than 2% error in the parity conserving transition matrix elements (though there is a very large error in the experimental answers), and errors of 2% and 12% for the $p\frac{1}{2}$ and $s\frac{1}{2}$ hyperfine values respectively.

7.5. The Semi-Empirical PNC Results

The semi-empirical PNC calculations are presented in table 7.8. We have quoted the length gauge answers in each case. Length/velocity agreement was obtained, when expected, to three significant figures. The PNC HF + V_{semp} figures refer to the modified PNC HF calculations and the PNC EOM/RPA + V_{semp} to the modified PNC EOM/RPA ones.

7.6. Discussion of the Semi-Empirical PNC Results

Table 7.9 gives the summarised semi-empirical results with the semi-empirical PNC EOM/RPA results included. There are several things to notice:

Caesium

1. From table 7.8a we see that the effect of including the semi-empirical potential in the PNC HF equations is to increase the PNC E1 transition matrix element by between about 1% and 2%. The effect of including the shielding is to reduce it to below the unmodified PNC EOM/RPA value.
2. From table 7.9a we find relatively little change in the PNC matrix element for a large range of residues.
3. The PNC matrix element increases as the residues decrease though its change in value as the residues decrease by an order of magnitude (e.g. comparing potentials 6 and 2) is less than 1%.

Table 7.8a

PNC E1 Transition Matrix Elements for Caesium (Length Gauge)

$6s\frac{1}{2} \rightarrow 7s\frac{1}{2}$ Transition $(-iea_0Q_W/N)\times10^{-11}$

	Potential Type 1	2	3	4	5	6	7	unmodified value
PNC HF + V_{semp}	0.949	0.946	0.940	0.901	0.912	0.938	0.933	0.927
PNCEOM/RPA + V_{semp}	0.902	0.898	0.890	0.858	0.868	0.889	0.885	0.891

Table 7.9a

Summary of Modified Results for Caesium With PNC Results

Potential	Reduced E1 $6s_{\frac{1}{2}} \rightarrow$		Hyperfine A_{hyp} (MHz)				PNC E1
no. Residue	$6p_{\frac{1}{2}}$	$6p_{3/2}$	$6s_{\frac{1}{2}}$	$6p_{\frac{1}{2}}$	$7s_{\frac{1}{2}}$	$7p_{\frac{1}{2}}$	$6s_{\frac{1}{2}} \rightarrow 7s_{\frac{1}{2}}$
unmodified	4.97	7.01	1728	201.6	474.0	71.64	0.891
4 0.12×10^{-3}	4.56	6.43	2251	262.8	543.3	84.26	0.858
5 0.66×10^{-4}	4.55	6.41	2307	266.0	551.7	85.33	0.868
7 0.23×10^{-4}	4.53	6.38	2379	272.6	566.9	87.57	0.885
6 0.11×10^{-4}	4.52	6.36	2408	272.8	570.5	87.78	0.889
3 0.37×10^{-5}	4.51	6.35	2438	270.4	576.2	87.33	0.890
1 0.36×10^{-5}	4.50	6.34	2523	260.1	602.3	84.95	0.902
2 0.14×10^{-5}	4.50	6.34	2468	267.2	585.1	86.92	0.898
Expt.	4.52	6.36	2298	291.9	546.2	94.34	
Expt. Errors	0.01	0.01	<0.1	0.01	3.0	0.02	

Table 7.8b

PNC E1 Transition Matrix Elements for Thallium (Length Gauge)

$6p_{\frac{1}{2}} \rightarrow 7p_{\frac{1}{2}}$ Transition $(-iea_0 Q_W/N)\times 10^{-11}$

	Potential Type 1	2	3	4	5	6	7	unmodified value
PNC HF + V_{semp}	-8.98	-9.03	-9.02	-9.09	-9.07	-9.02	-9.01	-10.00
PNCEOM/RPA + V_{semp}	-7.80	-7.86	-7.85	-7.93	-7.91	-7.84	-7.84	-9.66

$6p_{\frac{1}{2}} \rightarrow 6p_{3/2}$ Transition $(-iea_0 Q_W/N)\times 10^{-11}$

	Potential Type 1	2	3	4	5	6	7	unmodified value
PNC HF + V_{semp}	-38.12	-38.05	-38.00	-37.81	-37.85	-37.97	-37.97	-39.75
PNCEOM/RPA + V_{semp}	-28.6	-28.5	-28.5	-28.4	-28.4	-28.4	-28.4	-30.38

Table 7.9b

Summary of Modified Results for Thallium With PNC Results

Potential		Reduced E1 $7s_{\frac{1}{2}} \leftarrow$		Hyperfine A_{hyp} (MHz)			PNC E1 $6p_{\frac{1}{2}} \rightarrow$	
no.	Residue	$6p_{\frac{1}{2}}$	$6p_{3/2}$	$6p_{\frac{1}{2}}$	$7s_{\frac{1}{2}}$	$7p_{\frac{1}{2}}$	$7p_{\frac{1}{2}}$	$6p_{3/2}$
unmodified		1.91	3.61	21971	10913	2029	9.66	30.38
1	0.19×10^{-3}	1.87	3.35	21444	14569	2162	7.80	28.6
2	0.10×10^{-3}	1.86	3.35	21887	14060	2200	7.86	28.5
3	0.92×10^{-4}	1.86	3.35	21775	14024	2189	7.85	28.5
6	0.85×10^{-4}	1.85	3.35	21743	13997	2182	7.84	28.4
7	0.78×10^{-4}	1.85	3.34	21717	13953	2173	7.84	28.4
4	0.36×10^{-4}	1.82	3.33	22562	13109	2205	7.93	28.4
5	0.36×10^{-4}	1.83	3.33	22323	13371	2205	7.91	28.4
Expt.		1.84	3.29	21311	12500	2130		
Expt. Errors		0.06	0.09			60		

Thallium

1. From table 7.8b we find that the inclusion of the potential reduces the magnitude of the transition matrix element in both cases. The effect of the shielding is larger for the $6p_{\frac{1}{2}} \rightarrow 6p_{3/2}$ transition producing a reduction of about 25% as compared with 13% for the $6p_{\frac{1}{2}} \rightarrow 7p_{\frac{1}{2}}$ one.
2. In table 7.9b there is less percentage change in the PNC E1 transition matrix elements across the range of potentials than for caesium. The $7p_{\frac{1}{2}}$ transition values decrease in magnitude whereas they increase for the $6p_{3/2}$ one.

We will discuss the conclusions that can be drawn about the value of the PNC E1 transition matrix element in the next section.

7.7. The Physics of the Semi–Empirical Approach

As mentioned in section 7.1 the semi–empirical (SE) potential is meant to be modelling the BO corrections so that

$$V_{semp}(r) \mid v_1 > \qquad (7.17)$$

is representing corrections such as the terms in equation (7.1). Because we are fitting the energy levels we are actually modelling more than the BO corrections because they alone do not account for all of the correlation correction. Moreover, we are assuming that the correction potential is the same for all the orbitals which it will not be in practice. The lowest order correction to the eigenvalue of v_1 due to this potential is given by

$$< v_1 \mid V_{semp}(r) \mid v_1 > \qquad (7.18)$$

As mentioned previously, when this potential is included in the HF equation then the modification of an orbital *b* say due to $V_{semp}(r)$ affects orbital *a* via the HF potential so that the equivalent MBPT diagrams that are being modelled are a quite complicated set of self–consistent equations.

In MBPT the corrections to the orbital energies are given by closed diagrams (i.e. ones where there is no net excitation) whereas the corrections to the wavefunctions are open diagrams (ones which give a net excitation). It might be thought that since we are only fitting the energy levels we are only modelling the closed diagrams correctly

Figure 7.3 Vsemp Acting On First Order Excitation

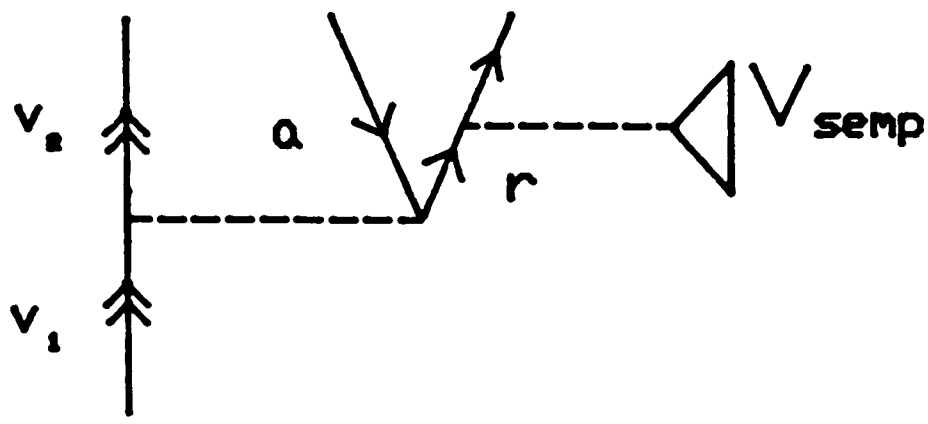

Figure 7.4 PNC Corrections To Brueckner Orbitals

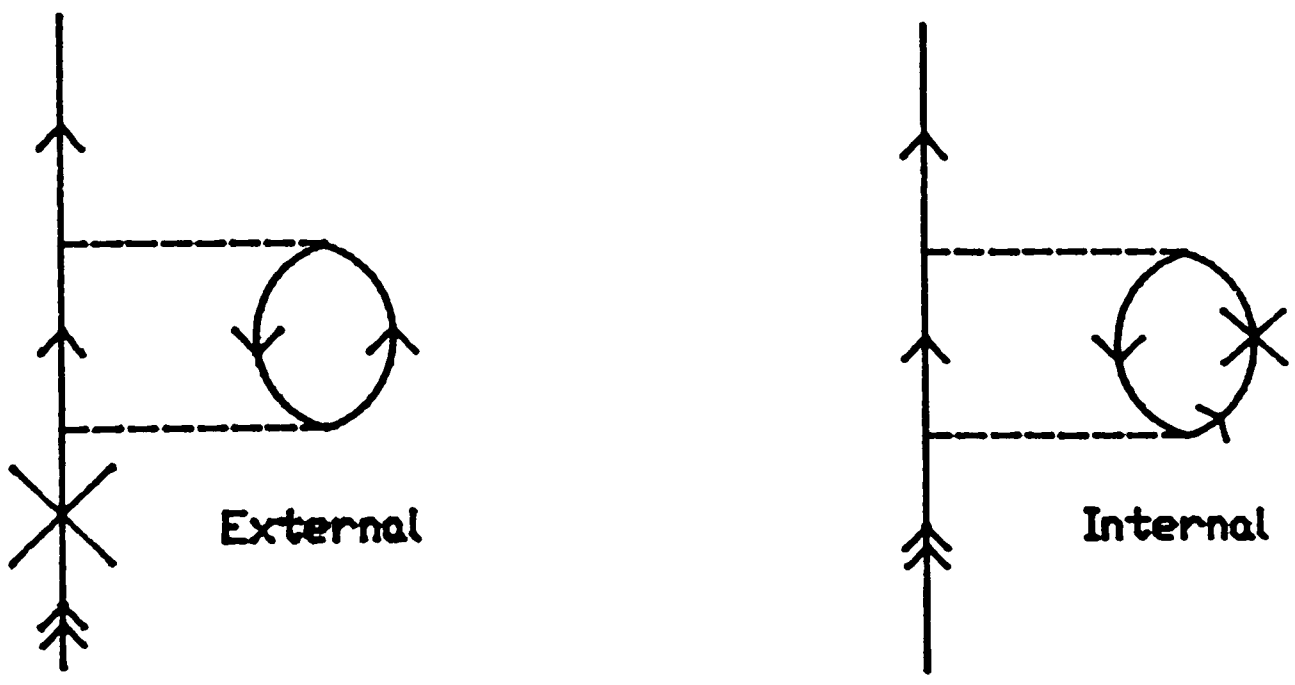

= PNC Interaction

and that there is therefore no reason why our modified wavefunctions should be physically correct. This is not entirely true though since, in our modified HF equations, the energy correction to an orbital *a* say, is contributed to by the modification of the other core orbitals' wavefunctions via the self-consistent HF potential. Since we are only using a spherically symmetric correction potential we can obviously not model all the wavefunction corrections properly. However, it is hoped that by getting the excited state energy levels correct we are also getting the wavefunctions reasonably correct.

When we perform the modified RPA type calculations we are effectively replacing all the orbitals in the MBPT diagrams by the modified orbitals so that we are modelling quite complicated effects. In addition we include the semi-empirical potential acting on the excitation itself which is iterated self-consistently so we are modelling effects such as in figure 7.3. By performing RPA calculations for the transition matrix elements we are including the shielding effects of the photon exactly.

It is not possible with our SE method to model effects that involve internal modifications of the BO corrections. For example, we can model diagrams such as the external PNC interaction but not the internal one (see figure 7.4). However examination of the tables of results of Johnson and Dzuba (see next section) show that these internal structure effects represent small contributions to the PNC transition matrix elements. Thus we can reasonably neglect them.

7.8. Comparison with MBPT Calculations

We have given in tables 7.10 and 7.11 the MBPT calculations of the hyperfine interaction constants, the parity conserving transition matrix elements, the energy levels and the PNC transition matrix elements for caesium and thallium as performed by [Johnson 1988_c] (WJ) and [Dzuba 1987_b] (DZ). WJ has only calculated the second order BO corrections (such as those in figure 7.1 for the valence orbitals). He has included both external and internal PNC corrections but only external photon diagrams. He has not included RPA shielding effects at the photon vertices. DZ on the other hand has done both external and internal photons and PNC interactions and has included shielding at the photon vertices. Both calculations perform finite summations

Table 7.10a

MBPT Caesium Calculations of Dzuba and Johnson

Hyperfine Constants (MHz)

Orbital	Dzuba	Johnson	Our Potential 6	Expt
$6s_{\frac{1}{2}}$	2347 (+30)	2366	2408	2298
$6p_{\frac{1}{2}}$	286 (+2)	---	273	291
$7s_{\frac{1}{2}}$	562 (+7)	574	571	546
$7p_{\frac{1}{2}}$	94.4 (+0.6)	--	87.8	94.3

Parity Conserving E1 Transition Matrix Element Cs $6s_{\frac{1}{2}} \rightarrow 6p_{\frac{1}{2}}$ (atomic units)

Dzuba	Johnson	Our Potential 6	Expt
4.45	4.39	4.52	4.52

Energy Levels (atomic units)

	Dzuba	Johnson	Potential 6	Expt
$6s_{\frac{1}{2}}$	-0.14325	-0.14512	-0.14308	-0.14310
$6p_{\frac{1}{2}}$	-0.09214	-0.09253	-0.09232	-0.09217
$6p_{3/2}$	-0.08961	-0.08997	-0.08990	-0.08964
$7s_{\frac{1}{2}}$	-0.05889	-0.05939	-0.05856	-0.05865

Table 7.10b

MBPT Thallium Calculations of Dzuba

Hyperfine Constants (MHz)

Orbital	Dzuba	Our Potential 6	Expt
$6p_{\frac{1}{2}}$	21321 (+770)	21743	21310.8
$7s_{\frac{1}{2}}$	12564 (+509)	13997	12500
$7p_{\frac{1}{2}}$	2039 (+50)	2182	2130

Parity Conserving E1 Transition Matrix Element (atomic units)

Transition	Dzuba	Our Potential 6	Expt
$6p_{\frac{1}{2}} \rightarrow 7s_{\frac{1}{2}}$	1.72	1.85	1.84 (0.06)
$6p_{\frac{1}{2}} \rightarrow 7s_{\frac{1}{2}}$	3.18	3.35	3.29 (0.09)

Energy Levels (atomic units)

	Dzuba	Potential 6	Expt
$6p_{\frac{1}{2}}$	-0.23309	-0.22307	-0.22446
$6p_{3/2}$	-0.19612	-0.19034	-0.18896
$7s_{\frac{1}{2}}$	-0.10510	-0.10412	-0.10382
$7s_{\frac{1}{2}}$	-0.06510	-0.06843	-0.06436

Table 7.11a

PNC Contributions to MBPT Calculations

Caesium

	Dzuba	Johnson
PNC MBPT/RPA	0.887	0.891
+ Correlation		
External PNC External Radiation		
4d, 5s, 5p	+0.017 (shielding)	+0.0488 (no shielding)
1s to 4p	----	+0.0088
Internal PNC External Radiation		
4d, 5s, 5p	+0.003 (shielding)	+0.0028 (no shielding)
1s to 4p	----	+0.0002
Internal Radiation	+0.003	----
Normalisation Correction	-0.006	---
Total	0.904	0.951

Table 7.11b

PNC Contributions to MBPT Calculations

Thallium

	Dzuba	
	$6p_{\frac{1}{2}} \rightarrow 7p_{\frac{1}{2}}$	$6p_{\frac{1}{2}} \rightarrow 6p_{3/2}$
PNC MBPT/RPA	-9.65	-30.34
+ Correlation		
External PNC External Radiation	+1.79	+7.39
Internal PNC External Radiation	0.00	-3.17
Internal Radiation	-0.2	-0.9
Normalisation Correction	+0.13	+0.6
Semi-Empirical Rescaling	--	-0.06
Total	-7.9	-27.0

of the terms such as in equation (7.2). DZ's sum over excited states includes levels with $l \leq 4$ and the core excitations are calculated for the 4d, 5p and 5s shells. WJ calculates all the core orbital excitations and includes terms with $l \leq 6$.

For the hyperfine calculations DZ only includes excitations diagonal in l for his RPA calculation. To calculate the 2nd order correlation contributions he restricts the excitations to being diagonal in κ (i.e. diagonal in j and l). In table 7.10 we have given in parenthesis the error in DZ's RPA hyperfine calculation through only including the diagonal l terms (this is calculated simply by comparing it with our RPA answer which agrees very well with the corresponding calculations of WJ). Thus for caesium the $6s_{\frac{1}{2}}$ hyperfine value with this correction is very close to WJ's. It is not known what the error is in only including the κ diagonal excitations for the correlation corrections so that one cannot evaluate the internal hyperfine contributions by comparing WJ's and DZ's (corrected) values. In the case of thallium the error is actually quite significant and including the correction factor actually makes the $6p_{\frac{1}{2}}$ answers worse than our semi-empirical hyperfine calculations. It is quite likely that the 'κ diagonal error' will correct for some of this but even so the claimed accuracy of DZ's hyperfine constants for thallium is highly misleading.

As regards the PNC calculations we have given the breakdown of the various contributions in tables 7.11a and 7.11b. For caesium there is a big difference in the external PNC corrections. This is presumably due to the fact that WJ has not included shielding at the photon vertex. As can be seen from 7.11 the internal PNC contributions are small for caesium but for the $6p_{\frac{1}{2}} \rightarrow 6p_{3/2}$ Tl transition they are about 10% of the final answer.

It might be thought that since our SE potential was originally designed to model the external BO contributions, the change in our PNC HF value for the PNC E1 transition matrix element when the SE potential is added (see table 7.8a) should equal WJ's external PNC correction in table 7.11a. However, by inluding the potential in the HF equation we have effectively iterated the BO correction to all orders. As mentioned in [Dzuba 1987b] this has the effect of reducing the correlation correction as we have found.

It is worth noting the values of the known quantities as calculated by MBPT. DZ's estimations for his hyperfine values look better than they are since he has made the approximations mentioned above in his hyperfine calculations. It should be noted that MBPT to this level of approximation over–estimates the hyperfine $s_{\frac{1}{2}}$ values and under–estimates the $p_{\frac{1}{2}}$ values, though not as much as some of our semi–empirical answers. The magnitude of the parity conserving $6s_{\frac{1}{2}} \rightarrow 6p_{\frac{1}{2}}$ transition is under–estimated by between 2% and 3% whereas the semi–empirical approach obtains almost exact agreement. Thus our semi–empirical approach obtains better values of the transition matrix elements at the expense of the hyperfine calculations, though some of our potentials give good $s_{\frac{1}{2}}$ values. We shall discuss our hyperfine calculations and their relevance to the PNC transition matrix element in the next section. It should be mentioned in passing that we obtain better energies than the MBPT calculations but this is only to be expected since we fitted them in the first place. Our outer core orbital energies are worse than the unmodified HF values as mentioned previously (see table 7.4).

7.9. Estimating a Value of the PNC Transition Matrix Elements

We now need to give our estimates of the PNC E1 transition matrix elements for the Cs $6s_{\frac{1}{2}} \rightarrow 7s_{\frac{1}{2}}$ and the Tl $6p_{\frac{1}{2}} \rightarrow 7p_{\frac{1}{2}}$ and $6p_{\frac{1}{2}} \rightarrow 6p_{3/2}$ transitions.

The purpose of calculating the experimentally known values was so that we should know how much weight to put on our PNC answers. In order to do this we need to discuss the relationship between the PNC E1 transition matrix element and the other known physical quantities that we have calculated.

The PNC E1 matrix element is calculated in the same manner as the parity conserving ones except that each contributing orbital is replaced one at a time by its PNC counterpart. One would therefore expect that the PNC matrix elements would be affected in a similar manner to the parity conserving one. Comparing tables 6.7 and 6.8 with 6.14 shows that the contributions from the core excitations are similarly distributed (i.e. for the length gauge the outer core electrons give the most significant contributions). However, the PNC orbital depends on the weak interaction which takes place at the nucleus so one would expect the PNC matrix element to depend on the

electronic wavefunction at the nucleus. It is for this reason that the hyperfine constants have been calculated as these are also dependent on the nuclear wavefunction to a certain extent. However there are several reasons why one should not rely too heavily on the hyperfine interaction constants as measures of the PNC E1 transition matrix element:

1. As can be seen from table 6.10 the contributions from the core excitations are not distributed as the transition matrix element ones are. Instead there are significant contributions from all the $s_{\frac{1}{2}}$ excitations including the innermost ones.
2. The hypefine interaction does depend on the density of the wavefunction at the nucleus so that to lowest order and in the non-relativistic limit the $6p_{\frac{1}{2}}$ hyperfine constant will depend on the square of the density of the $6p_{\frac{1}{2}}$ wavefunction. However once other MBPT terms have been included there will be no direct correspondence between the wavefunction density and the hyperfine constant.
3. The hyperfine constants depend far more on higher order MBPT corrections than the transition matrix elements in general. The correlation corrections required are quite large for Cs. Although they appear to be less for Tl this is because there are many cancellations of contributing terms.

We shall therefore give the parity conserving transition matrix elements more weight in our evaluation of the PNC ones.

As mentioned earlier the eigenvalues of our outer core orbitals are rather inaccurate. It might be thought that since the outer core excitations give the main contribution to the transition matrix elements getting the energy denominators wrong would introduce a large error. However, matching the energy levels exactly is not a guarantee of producing physically accurate results. [W. Johnson 1985, 1986] initially started a program of calculations that included several local semi-empirical potentials in the initial Hamiltonian. These gave good energy level fits (including the core orbitals) and better zeroth order results than the V_{N-1} HF ones but when higher order perturbations were added their behaviour was somewhat erratic. The reason for this is that when MBPT is performed there are in general correction terms according to the zeroth order Hamiltonian used. When using a V_{N-1} HF zeroth order Hamiltonian these correction terms vanish identically. If some other starting Hamiltonian is used

then these correction terms correct for the fact that a different Hamiltonian was used and one will eventually get back to the V_{N-1} HF MBPT result. If one examines the energy denominators in our calculations they are in fact little different from the V_{N-1} HF ones since the dominating core energies are little changed. Thus, even though we have fitted the excited state energies we are not actually changing the energy denominators much at all; we are instead modifying the wavefunctions by modelling the central correlation effects. The fact that we are using a semi-empirical potential to model correlation effects rather than the entire electronic potential means that we have not 'departed far' from the V_{N-1} HF MBPT convergence path and higher order corrections to our approximation are not likely to be important for the transition matrix elements. The fact that our parity conserving E1 transition matrix elements are so close to the experimental values indicates that the poor core orbital fits are not actually a problem.

It might be argued that we are obtaining PNC matrix elements that do not vary much with the electronic potential because all our semi-empirical potentials are so similar with the same asymptotic r^{-4} behaviour. We tried potentials that varied with r differently but found that the fits with the experimental energy levels were much worse. There seemed to be a natural 'resonance' with the r^{-4} type potential. We have used potentials with different inner r dependence but as we have shown this does not seem to affect the transition matrix elements.

Caesium

For caesium potentials 3, 6 and 7 all match the experimental error range for the $6s_{\frac{1}{2}} \rightarrow 6p_{\frac{1}{2}}$ transition. The $6p_{3/2}$ one is not matched by potential 7. For these three potentials the PNC matrix element varies between 0.885 and 0.890. If we disregard potentials 4 and 5 which have relatively large errors for the parity conserving values then the PNC values varies between 0.885 and 0.902 a variation of less than 2% whereas the hyperfine values vary by up to 6%. Thus we have clearly obtained a PNC transition matrix element that is quite stable and not very dependent on the hyperfine values.

From table 7.11 we know that the internal BO contributions that we have not modelled are very small for caesium and their omission is unlikely to introduce much error.

Neglecting potentials 4 and 5, for the hyperfine calculations we have systematically over-estimated the $s\frac{1}{2}$ constants and under-estimated the $p\frac{1}{2}$ ones. This may be due to a systematic over-estimation of the $s\frac{1}{2}$ wavefunction nuclear density and an under-estimation of the $p\frac{1}{2}$ one. On the other hand it could be due to internal or residual correlation effects not included in the calculation. The fact that the PNC matrix element varies much less than the hyperfine values leads us to believe that this 'systematic' is probably not serious.

It is possible to rescale the PNC matrix element by the geometric mean of the $A_{hyp}(6s\frac{1}{2})$ and $A_{hyp}(6p\frac{1}{2})$ in order to try and minimise possible errors from inaccurate wavefunction densities at the nucleus. The justification for this is that the hyperfine constants depend on the square of the nuclear density whereas the weak interaction Hamiltonian, which is mainly between $s\frac{1}{2}$ and $p\frac{1}{2}$ states will depend on the product of the densities at the nucleus of the $s\frac{1}{2}$ and $p\frac{1}{2}$ wavefunctions. If we therefore define

$$X_{hyp} \equiv \left[A_{hyp}(6s\tfrac{1}{2})\ A_{hyp}(6p\tfrac{1}{2}) \right]^{\frac{1}{2}} \qquad (7.18)$$

then the rescaled matrix element is given by

$$PNC_{res} \equiv \frac{PNC_{SE}}{X_{hyp}} \qquad (7.19)$$

where PNC_{SE} is our semi-empirical PNC value and PNC_{res} is the rescaled value. This should have less dependence on the nuclear density though, as mentioned earlier, the hyperfine constants and PNC matrix elements are made up of complicated combinations of their interaction matrix elements and (7.19) will only be approximately independent of the wavefunction at the nucleus. We have calculated the rescaled matrix elements in table 7.12. From this we see that even potentials 4 and 5 agree with the others when rescaled. The rescaled matrix element does not have a trend in it as the unrescaled one did. Neglecting 4 and 5 because of their poor parity conserving transition matrix elements, we can take an average value for $PNC_{res.}$ of 1.102 with a

Table 7.12

Rescaled PNC E1 Transition Matrix Elements For Cs $6s_{\frac{1}{2}} \rightarrow 7s_{\frac{1}{2}}$

Potential	X_{hyp}	PNC E1	PNC E1/X_{hyp} x 10^3
4	768.9	0.858	1.116
5	783.3	0.868	1.108
7	805.1	0.885	1.099
6	811.9	0.889	1.097
3	811.9	0.890	1.096
1	810.1	0.902	1.113
2	812.1	0.898	1.106
Expt.	819.0		

spread of 0.017 from largest to smallest. We can then estimate the correct PNC matrix element by multiplying our mean value by the experimental one to give 0.903 ± 0.01.

The trouble with this method is that it assumes that the residual correlation corrections effect X_{hyp} and the PNC matrix element in the same way. If this is the case then we would expect the rescaled value to be more accurate; however, as mentioned above, the hyperfine constants are far more dependent on correlation effects than the transition matrix elements (both parity conserving and PNC) and the rescaling method might actually be less accurate than the un-rescaled one. Having said that the values for X_{hyp} in table 7.12 are actually quite close to the experimental value with the error for potential 6 say being 0.9%. Thus we can feel confident that although we have not reproduced the hyperfine constants accurately our PNC transition matrix elements should be reliable.

With these considerations in mind we shall estimate the PNC E1 transition matrix element to be 0.895. Estimating the error is always very difficult, whether for an *ab initio* calculation or a semi-empirical one. Numerical errors are likely to be very small ~ 0.2%. The spread in the parity conserving transition matrix element is ~ 0.1%. The spread in our PNC values is less than 1%. The errors in the hyperfine values are 11% at worst but for the reasons mentioned above this is probably due to residual correlation effects which are far more important in the hyperfine calculation than for the transition matrix elements. The error in X_{hyp} is less than 1%. We shall opt for an error of 3% though we feel this is probably a little pessimistic. Our final value for the caesium $6s_{\frac{1}{2}} \rightarrow 7s_{\frac{1}{2}}$ PNC E1 transition matrix element is therefore $0.895(1 \pm 0.03)$ in units of 10^{-11} $(-iea_0\ Q_W/N)$.

Thallium

For thallium the large experimental errors in the parity conserving transition matrix elements means that it is harder to assess the accuracy of the semi-empirical parity conserving calculations. All the potentials give values which are within the quoted experimental range. For the $6p_{\frac{1}{2}} \rightarrow 7s_{\frac{1}{2}}$ transition the spread in our values includes the experimental result in the middle of the range whereas for the $6p_{3/2} \rightarrow$

$7s_{\frac{1}{2}}$ one they are all larger than the quoted result, but by less than 2% at worst.

The hyperfine results have a 'systemmatic' over–estimation of the $p_{\frac{1}{2}}$ values and an under–estimation of the $s_{\frac{1}{2}}$. The variation in the hyperfine values is far greater than in the PNC transition matrix elements. There is no obvious relationship between an X_{hyp} type of function and the PNC matrix elements so that rescaling techniques cannot be used. The reason why this is so might be to do with the fact that the semi–empirical potential is acting far further out in thallium than in caesium and is probably less likely to affect the wavefunction near the nucleus. The semi–empirical X_{hyp}'s are over–estimated by about 6% or 7% which could be significant, though the fact that there seems to be little correlation between them is promising. From [Dzuba 1987_b] we find that there are significant internal contributions for the $6p_{\frac{1}{2}} \rightarrow 6p_{3/2}$ PNC transition amounting to about 10% of the final answer (see table 7.11.b). Since we are not modelling such effects this means that our answer for this transition is going to be less reliable. For the $6p_{\frac{1}{2}} \rightarrow 7p_{\frac{1}{2}}$ transition Dzuba finds a large cancellation so that two terms of size 0.09 cancel.

These factors confirm the fact that although thallium is a single–valence system it has large correlation terms with many cancellations. It is therefore harder to make accurate calculations for thallium than for caesium. The fact that our PNC transition matrix elements seem quite stable and relatively independent of the semi–empirical potential is encouraging. For the $6p_{\frac{1}{2}} \rightarrow 7p_{\frac{1}{2}}$ transition we shall take our estimate to be -7.85×10^{-11} $(-iea_0Q_W/N)$ and for the $6p_{\frac{1}{2}} \rightarrow 6p_{3/2}$ transition -28.4×10^{-11} $(-iea_0Q_W/N)$. The estimation of the errors is perforce rather *ad–hoc* but we estimate about 5% for the $7p_{\frac{1}{2}}$ transition. For the $6p_{3/2}$ one the slight displacement of the parity conserving transition matrix elements from the experimental mean and the large internal contributions in Dzuba's calculation leads us to assign a larger error of 7%.

7.8. Conclusion

We have tried seven semi-empirical potentials, choosing the parameters by fitting the excited states to the experimental ones. We have then incorporated these potentials into our RPA calculations of the transition matrix elements and for the hyperfine dipole interaction constants. The parity conserving transition matrix elements are accurately reproduced. The hyperfine constants are not so accurately reproduced but they depend more on residual correlation effects than the transition matrix elements. Our estimate of the PNC E1 transition matrix element for the caesium $6s_{\frac{1}{2}} \rightarrow 7s_{\frac{1}{2}}$ transition is $0.895(1 \pm 0.03) \times 10^{-11}$ $-iea_0(Q_W/N)$. For the thallium $6p_{\frac{1}{2}} \rightarrow 7p_{\frac{1}{2}}$ transition we estimate $-7.85(1 \pm 0.05) \times 10^{-11}$ $-iea_0(Q_W/N)$ and for the $6p_{\frac{1}{2}} \rightarrow 6p_{3/2}$ transition we estimate $-28.4(1 \pm 0.07) \times 10^{-11}$ $-iea_0(Q_W/N)$.

CHAPTER 8: The Full Open Shell Equations of Motion

8.1 Introduction

So far we have solved the EOM/RPA for caesium and thallium and modelled certain correlation effects by adding a semi-empirical potential to the equations. These correlation effects were thought to contain the major physical effects not so far included in the EOM/RPA. In deriving the EOM/RPA we made several approximations which we are now going to examine. Whilst still only considering single particle excitations in the expression for the excitation operator we shall evaluate all the diagrams that are obtained in deriving the Full Open Shell EOM (EOM/FOS). We shall solve the EOM/FOS in order to verify the assumption that the extra terms represent small physical effects. We shall also attempt to identify the MBPT terms that the extra terms correspond to.

8.2 The Open Shell Equations of Motion

The Open Shell EOM were derived by defining the excitation operator by

$$|J_1M_1\rangle = \sum_{M_0,Q} U^K_Q \; |J_0M_0\rangle\langle KQ, J_0M_0|J_1M_1\rangle \qquad (8.1)$$

with the subsidiary condition

$$(U^K_Q)^\dagger \; |J_0M_0\rangle = 0 \qquad (8.2)$$

We also defined the projection operator P^K_Q in terms of its hermitian adjoint

$$\langle J_1M_1| = \sum_{Q',M_0'} \langle J_1M_1|KQ', J_0M_0'\rangle\langle J_0M_0| \; (P^K_{Q'})^\dagger \qquad (8.3)$$

With these definitions we obtained the Open Shell EOM

$$\sum_{\substack{Q,Q'\\M_0,M_0'}} \langle J_1M_1|KQ', J_0M_0'\rangle\langle J_0M_0'| \; [(P^K_{Q'})^\dagger \; , \; H \; , \; U^K_Q] \; |J_0M_0\rangle\langle KQ, J_0M_0|J_1M_1\rangle$$

$$= \qquad (8.4)$$

$$\omega \sum_{\substack{Q,Q'\\M_0,M_0'}} \langle J_1M_1|KQ', J_0M_0'\rangle\langle J_0M_0'| \; [(P^K_{Q'})^\dagger \; , \; U^K_Q] \; |J_0M_0\rangle\langle KQ, J_0M_0|J_1M_1\rangle$$

The normalisation condition is given by

$$\sum_{\substack{Q,Q' \\ M_0,M_0}} \langle J_1 M_1 | KQ', J_0 M_0' \rangle \langle J_0 M_0' | \, [(U^K_{Q'})^\dagger \, , \, U^K_Q] \, | J_0 M_0 \rangle \langle KQ, J_0 M_0 | J_1 M_1 \rangle = 1 \tag{8.5}$$

The reduced transition matrix element is given by

$$\langle J_1 || \, T^\lambda \, || J_0 \rangle = \sum_{\substack{Q,Q' \\ M_0,M_0'}} [J_1]^{\frac{1}{2}} \, (-1)^{J_1 - J_0 + \lambda} \tag{8.6}$$

$$\langle J_1 M_1 | KQ', J_0 M_0' \rangle \langle J_0 M_0' | \, [(U^K_Q)^\dagger \, , \, T^\lambda{}_\mu] \, | J_0 M_0 \rangle \langle \lambda\mu, J_0 M_0 | J_1 M_1 \rangle$$

There are implicit assumptions in the above equations concerning the rank of the projection operator and whether the rank of the excitation operator should be summed over. We will discuss this later in this chapter.

8.2.1 The EOM/FOS Approximations

In deriving the EOM/RPA we made several approximations:

1. The ground state was a Slater determinant of V_{N-1} HF eigenfunctions.
2. The positive valence excitation was taken to be simply the V_{N-1} HF initial state to final state excitation.
3. The negative valence excitations were neglected
4. The transition frequency ω was taken to be the difference between the eigenvalues of the single particle states involved in the transition.
5. Only four of the commutator diagrams that have valence excitation contributions were considered.

We are now going to re-derive the radial equations but without making all of the above approximations. This will lead to more complicated equations but should give some insight into the formalism of the EOM as compared with MBPT, say.

1. In this chapter we are still going to use the V_{N-1} HF ground state; the validity of this is discussed later.

2. We shall treat both the positive and the negative valence excitations fully, solving for each.

3. We shall now also treat ω as a variable to be solved for.

4. We are also going to consider all diagrams that are obtained using the single particle approximation.

8.2.2. The Single Particle Approximation

With the single particle approximation for the excitation operator we have for U:

$$U = \sum_{a,r} a^{\dagger}_r a_a Y_{ar} - a^{\dagger}_a a_r Z_{ar} + \sum_{x,v} a^{\dagger}_x a_v Y_{xv} - a^{\dagger}_v a_x Z_{vx} \qquad (8.7)$$

where we have used the same notation as before, i.e.

letter	orbital type
a,b,c...	core
p,q,r...	excited (including valence)
x,y,z	excited (excluding valence)
v,n	valence
i,j,k,l	any

(8.8)

Since we are now solving for valence excitations we need to have valence projection terms as well as the core ones that were given in chapter four (4.12).

$$a^{\dagger}_v a_x P^{+}_{vx}$$

and (8.9)

$$a^{\dagger}_x a_v P^{-}_{xv}$$

8.2.1 The EOM/FOS Diagrams

Using the single particle approximation for the excitation operator as given above we are now ready to assign the orbitals to the commutator diagrams. The commutator diagrams are topologically the same as before (table 4.1). In addition to the core diagrams of the EOM/CS we can now assign valence orbitals to the diagrams in all possible ways. Because we are dealing with single valence systems we can only

Table 8.1. Extra V+(a) Diagrams (exchange diagrams not shown)

g_{2+}	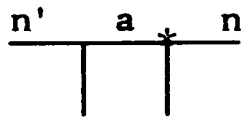	$\omega \langle n\|a^+\rangle \|n\rangle$
a_{2+}	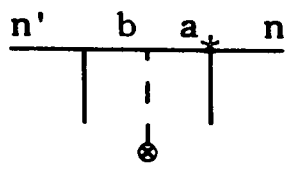	$\epsilon_a \langle n\|a^+\rangle \|n\rangle$
b_{1+}	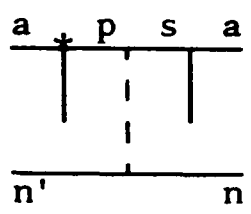	$\langle n\|r_{12}^{-1}(1-P_{12})\|n\rangle\|a^+\rangle$
b_{3+}	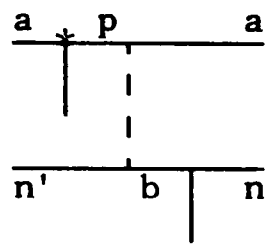	$\langle b^-\|n\rangle\langle n\|r_{12}^{-1}(1-P_{12})\|b\rangle\|a\rangle$
b_{4+}	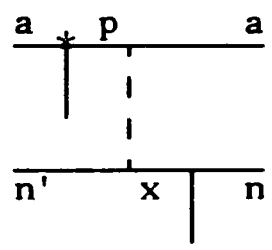	$\langle n\|r_{12}^{-1}(1-P_{12})\|v^+\rangle\|a\rangle$
b_{5+}	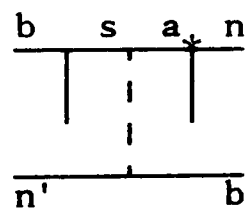	$\|n\rangle\langle b^-n\|r_{12}^{-1}(1-P_{12})\|ab\rangle$
d_{2+}	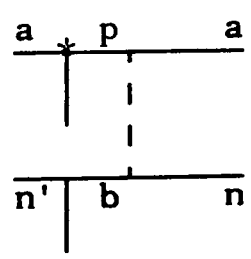	$\langle n\|b^+\rangle\langle b\|r_{12}^{-1}(1-P_{12})\|n\rangle\|a\rangle$
d_{3+}	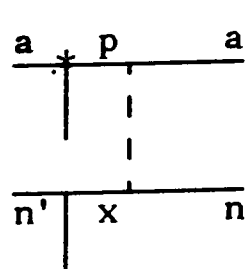	$\langle n^-\|r_{12}^{-1}(1-P_{12})\|n\rangle\|a\rangle$

d_{4+}

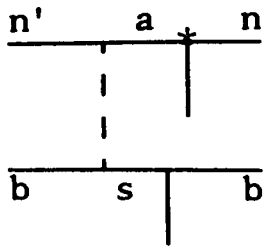

$$|n\rangle\langle nb|r_{12}^{-1}(1-P_{12})|ab^{+}\rangle$$

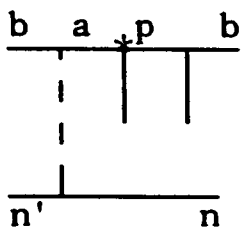

e_{6+} plus e_{7+} +

$$|b^{+}\rangle\langle bn|r_{12}^{-1}(1-P_{12})|an\rangle$$

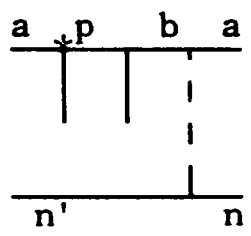

e_{8+}

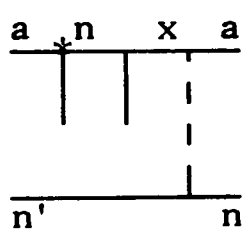

$$|n\rangle\langle n^{-}n|r_{12}^{-1}(1-P_{12})|an\rangle$$

e_{9+}

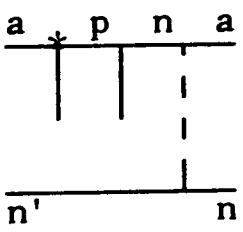

$$|n^{+}\rangle\langle nn|r_{12}^{-1}(1-P_{12})|an\rangle$$

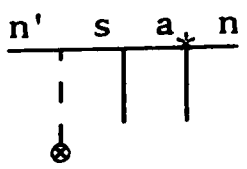

e_{10+} plus e_{11+} +

$$|n\rangle\ \epsilon_n\ \langle n|a^{+}\rangle$$

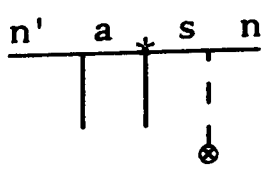

Table 8.2. Extra $V^-(a)$ Diagrams (exchange diagrams not shown)

g_2^-	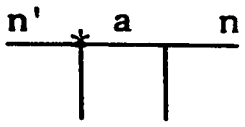	$\omega \langle n\|a^-\rangle \|n\rangle$
a_2^-	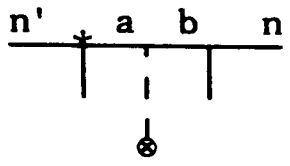	$\epsilon_a \langle n\|a^-\rangle \|n\rangle$
b_1^-	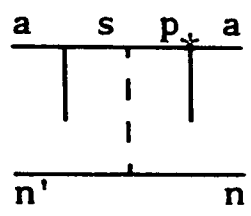	$\langle n\|r_{12}^{-1}(1-P_{12})\|n\rangle\|a^-\rangle$
b_3^-	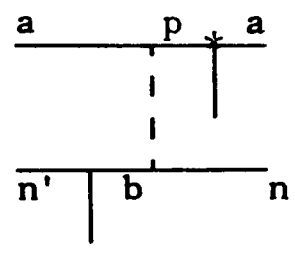	$\langle n\|r_{12}^{-1}(1-P_{12})\|b\rangle\|a\rangle\langle b^+\|n\rangle$
b_4^-	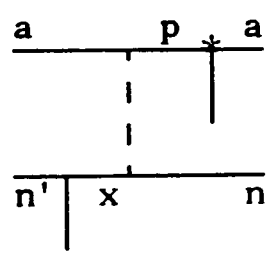	$\langle n\|r_{12}^{-1}(1-P_{12})\|n^-\rangle\|a\rangle$
b_5^-	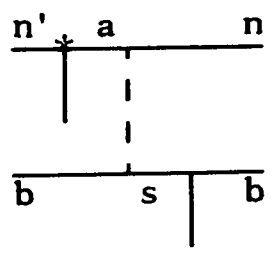	$\|n\rangle\langle b^+n'\|r_{12}^{-1}(1-P_{12})\|ba\rangle$
d_2^-	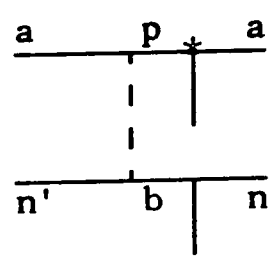	$\langle n\|b^-\rangle\langle b\|r_{12}^{-1}(1-P_{12})\|n\rangle\|a\rangle$
d_3^-	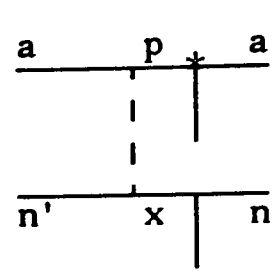	$\langle v^+\|r_{12}^{-1}(1-P_{12})\|n\rangle\|a\rangle$

d_4^-

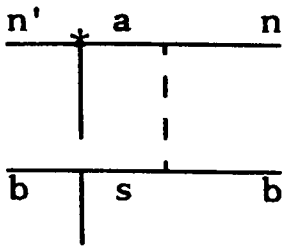

$$|n\rangle\langle nb|r_{12}^{-1}(1-P_{12})|ab^-\rangle$$

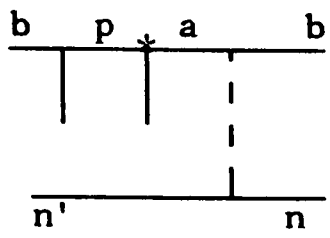

e_6^- plus e_7^- +

$$|b^-\rangle\langle bn|r_{12}^{-1}(1-P_{12})|an\rangle$$

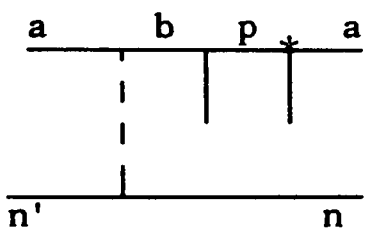

e_8^-

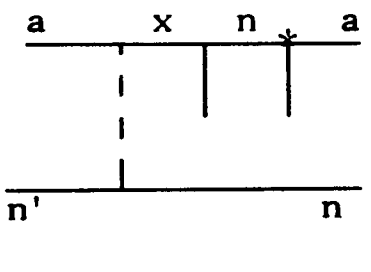

$$|n\rangle\langle n^-n|r_{12}^{-1}(1-P_{12})|an\rangle$$

e_9^-

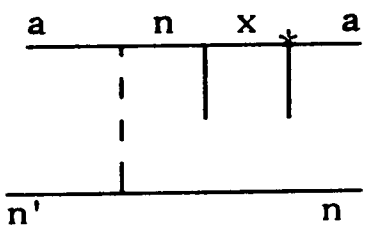

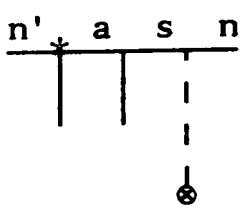

e_{10}^- plus e_{11}^- +

$$|n\rangle\ \epsilon_n\ \langle n|a^-\rangle$$

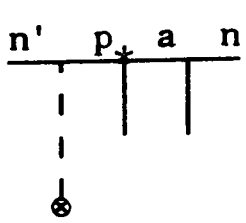

Table 8.3. $V^{+}(n)$ Diagrams

b1v+

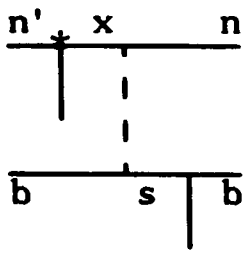

$\langle b|r_{12}^{-1}(1-P_{12})|b^{+}\rangle|n\rangle$

d1v+

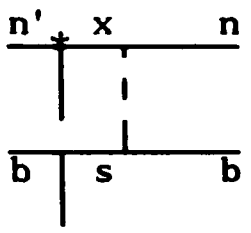

$\langle b^{-}|r_{12}^{-1}(1-P_{12})|b\rangle|n\rangle$

e5v+

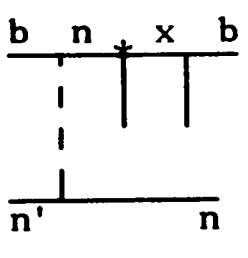

$\left[|b^{+}\rangle - |n\rangle\langle n|b^{+}\rangle\right] \times$

$\langle bn|r_{12}^{-1}(1-P_{12})|nn\rangle$

e7v+

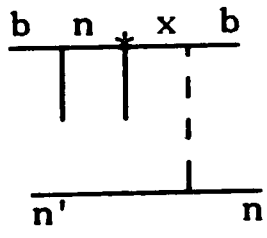

$\langle n|r_{12}^{-1}(1-P_{12})|n\rangle|b\rangle\langle b^{-}|n\rangle$

Table 8.4. $V^{-}(n)$ Diagrams

b1V-

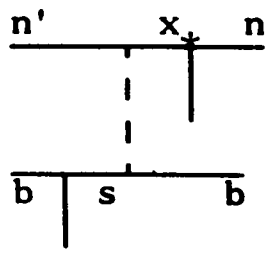

$\langle b|r_{12}^{-1}(1-P_{12})|b^{-}\rangle|n\rangle$

d1V-

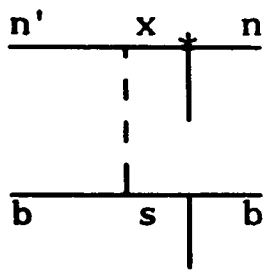

$\langle b^{+}|r_{12}^{-1}(1-P_{12})|b\rangle|n\rangle$

e5V-

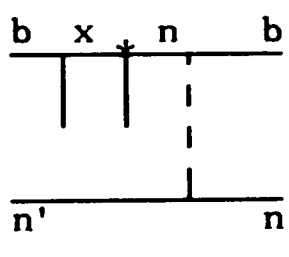

$\left[|b^{-}\rangle - |n\rangle\langle n|b^{-}\rangle\right] \times$

$\langle bn|r_{12}^{-1}(1-P_{12})|nn\rangle$

e7V-

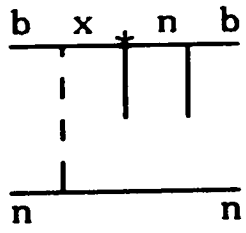

$\langle n|r_{12}^{-1}(1-P_{12})|n\rangle|b\rangle\langle b^{+}|n\rangle$

have one valence orbital on either end of a diagram. The complete list of diagrams containing valence assignments that contribute to the positive core excitation equations are given in table 8.1 and the negative equations in table 8.2. We have only included the direct diagrams in the table but have given the direct and exchange parts of the contribution to the equations on the right-hand side. Sometimes the exchange contribution to the equations is obtained by exchanging the end orbital assignments for that diagram, sometimes the exchange part of the equation comes from the exchanging of assignments from a different diagram. The assignment of valence states to the projection operator vertices as in (8.9) gives the positive and negative valence excitation equations. The diagrams with these assignments are given in tables 8.3 and 8.4. In all four tables the (rather obscure) labelling of the diagrams refers to the topology of the commutator diagrams from which they came.

It should be remembered that these are the additional diagrams that have valence assignments: there are the EOM/CS diagrams to be included as well. We now have a set of diagrams that belong to different excitation equations; the particular equation that a diagram belongs to is given by the particular projection operator in the diagram. We now have four different types of equation: the positive and negative core excitation equations and the positive and negative valence excitation equations.

8.2.4. The EOM/FOS Equations

In analogy with the core excitations we define the positive and negative valence exctations by

$$|n^{+}\rangle = \sum_{x} |x\rangle Y_{xn} \qquad (8.10)$$

$$|n^{-}\rangle = \sum_{x} |x\rangle Z^{*}_{xn} \qquad (8.11)$$

Using these definitions together with the usual definitions of the core excitations (equations (4.24) and (4.25)) we can collect together the terms for the different excitation equations by looking at their projection operators. For example, all the diagrams with projection operator P^{+}_{ap} give the positive core excitation equations. The equations will have the same basic form on the left-hand side as before i.e.

$$(\epsilon_a \pm \omega - h_0 - V_{hf})|a^{\pm}\rangle = |rhs\rangle \qquad (8.12)$$

The right-hand side will be made up of the core diagrams as for the EOM/CS and in addition there will be the extra diagrams with the valence assignments. We shall denote the sum of all these terms on the right-hand side by a potential $V^{\pm}(i)$ where the $\pm$ refers to the positive or negative excitation equation and the i is either a for the core orbital excitation equation of orbital a, or n for the valence excitation equation of orbital n. We shall treat the projection operator as before, i.e. write it as

$$P^{+}_{ap} = \langle \eta_a \mid p \rangle \qquad (8.13)$$

and similarly for the other projection operators. We use the closure relationship as before to obtain the orthogonality terms (see equation (4.31) and associated text). Doing all this leaves us with the positive and negative core and valence excitation equations

$$(\epsilon_a \pm \omega - h_0 - V_{hf})|a^{\pm}\rangle = V^{\pm}(a)|a\rangle - \sum_b |b\rangle\langle b|V^{\pm}(a)|a\rangle \qquad (8.14)$$

where $V^{\pm}(a)$ is given by

$$V^{\pm}(a)|a\rangle = \sum_{b^{\pm}} \langle b|r_{12}^{-1}(1-P_{12})|b^{\pm}\rangle|a\rangle + \langle b^{\mp}|r_{12}^{-1}(1-P_{12})|b\rangle|a\rangle + \text{additional terms in table 8.1 or 8.2} \qquad (8.15)$$

For the valence excitations we obtain

$$(\epsilon_n \pm \omega - h_0 - V_{hf})|n^{\pm}\rangle = V^{\pm}(n)|n\rangle - \sum_{i=b,v} |i\rangle\langle i|V^{\pm}(n)|n\rangle \qquad (8.16)$$

where $V^{+}(n)$ consists of all the terms in table 8.3 and $V^{-}(n)$ consists of all the terms in table 8.4. The sum over i in the orthogonalisation term is over all the core states and the valence states.

Table 8.5 EOM/FOS Normalisation Diagrams

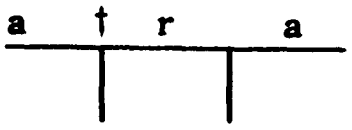

$$\langle a^{+} \mid a^{+} \rangle$$

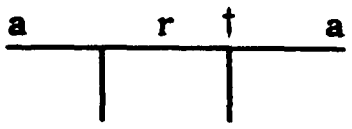

$$-\langle a^{-} \mid a^{-} \rangle$$

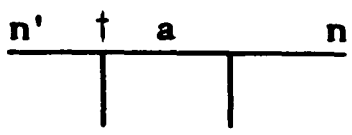

$$\langle n \mid a^{-} \times a^{-} \mid n \rangle$$

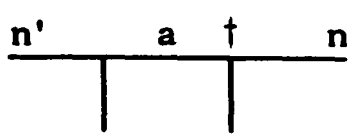

$$-\langle n \mid a^{+} \times a^{+} \mid n \rangle$$

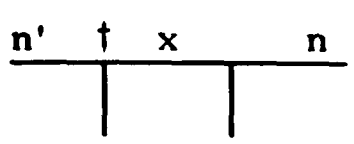

$$\langle n^{+} \mid n^{+} \rangle$$

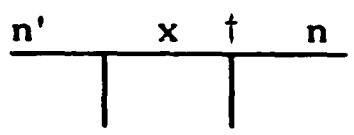

$$-\langle n^{-} \mid n^{-} \rangle$$

Table 8.6 EOM/FOS Transtion Matrix Element Diagrams

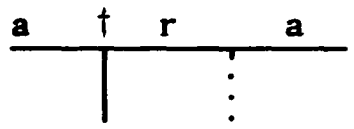

$$\langle a^{+} \mid T^{\lambda} \mid a \rangle$$

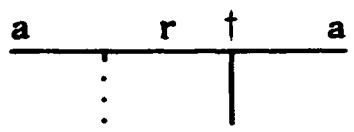

$$\langle a \mid T^{\lambda} \mid a^{-} \rangle$$

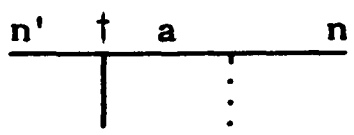

$$-\langle n \mid a^{-} \times a \mid T^{\lambda} \mid n \rangle$$

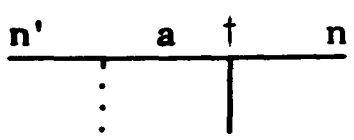

$$-\langle a^{+} \mid n \times n \mid T^{\lambda} \mid a \rangle$$

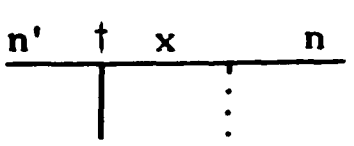

$$\langle n^{+} \mid T^{\lambda} \mid n \rangle$$

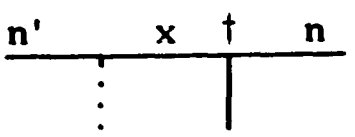

$$-\langle n \mid T^{\lambda} \mid n^{-} \rangle$$

8.2.3. The EOM/FOS Normalisation and Transition Matrix Element Diagrams

We can now assign valence orbitals to the normalisation and transition matrix element diagrams in a similar way to the EOM commutator diagrams. The extra terms for the normalisation are given in table 8.5. The EOM/FOS normalisation condition is given by

$$\sum \quad \langle a^+|a^+\rangle - \langle a^-|a^-\rangle + \langle n^+|n^+\rangle - \langle n^-|n^-\rangle$$

$$+ \langle n|a^-\rangle\langle a^-|n\rangle - \langle n|a^+\rangle\langle a^+|n\rangle \quad = \quad 1 \qquad (8.17)$$

where the summation is over all excitations and occupied orbitals.

The extra terms for the transition matrix element are given in table 8.6. The EOM/FOS expression for the transition matrix element is

$$\langle 1|T|0\rangle \quad = \quad \sum \quad \langle a^+|T|a\rangle + \langle a|T|a^-\rangle + \langle n^+|T|n\rangle + \langle n|T|n^-\rangle$$

$$- \langle n|a^-\rangle\langle a|T|n\rangle - \langle n|T|a\rangle\langle a^+|n\rangle \qquad (8.18)$$

8.2.6. The Positive Valence Excitation Equation

Consider the positive valence excitation equation (8.16) which we shall write as

$$(\epsilon_n + \omega - h_0 - V_{hf})|n^+\rangle \quad = \quad |rhs\rangle - \sum_{i=b,v} |i\rangle\langle i|rhs\rangle \qquad (8.19)$$

where $|rhs\rangle$ represents the $V^+(n)|n\rangle$ terms in table 8.3. This equation is effectively a type of Sternheimer equation as described in chapter three. What it represents is

$$|n^+\rangle \quad = \quad \sum_x \frac{|x\rangle\langle x|rhs\rangle}{\epsilon_n + \omega - \epsilon_x} \qquad (8.20)$$

Since $\omega \simeq \epsilon_{v2} - \epsilon_n$ then the dominant contribution will be for $x = v_2$ i.e. the single particle resonant transition. This is why we approximated $|n^+\rangle$ by $|v_2\rangle$ in the EOM/RPA. When solving for $|n^+\rangle$ numerically care should be taken because of this resonance. It is equivalent to the homogeneous solution mixing discussed in chapter five since, in the approximation that $\omega = \epsilon_{v2} - \epsilon_n$, $|v_2\rangle$ is just the homogeneous solution of the left-hand side of (8.19).

As mentioned in chapter five in practice we solve the equations by having a local RSCF potential approximation to V_{hf} on the left-hand side of the equation and

correcting for this on the right-hand side. This way the homogeneous solution that can be mixed into the equation for $|n^+\rangle$ is the local single particle resonant excited state. We can overcome this in the same way that we did in solving for the original HF orbitals, namely by expressing $|n^+\rangle$ as the local RSCF excited state plus an orthogonal correction

$$|n^+\rangle = |v_{2,RSCF}\rangle + |\delta n^+\rangle$$

$$\langle v_{2,RSCF}|\delta n^+\rangle = 0 \qquad (8.21)$$

The numerical equation for the positive excitation is then of the form

$$(\epsilon_n + \omega - h_0 - V_{rscf})|n^+\rangle = (V_{hf} - V_{rscf})|n^+\rangle + |rhs\rangle - \sum_{i=b,v} |i\rangle\langle i|rhs\rangle \qquad (8.22)$$

Substituting equation (8.21) into this we obtain

$$(\epsilon_n + \omega - h_0 - V_{rscf})|\delta n^+\rangle = |RHS\rangle - \lambda |v_{exc,RSCF}\rangle \qquad (8.23)$$

where

$$|RHS\rangle = (V_{hf} - V_{rscf})|n^+\rangle + |rhs\rangle - \sum_{i=b,v} |i\rangle\langle i|rhs\rangle \qquad (8.24)$$

and λ is given by

$$\lambda = (\epsilon_n + \omega - \epsilon_{v2,RSCF}) = \langle v_{2,RSCF}|RHS\rangle \qquad (8.25)$$

Thus we can find omega from equation (8.25), since ϵ_n and $\epsilon_{v2,RSCF}$ are both known, simply by taking the overlap of the entire right-hand side of equation (8.22) with the local resonant excited state. Because in equation (8.23) we are now only solving for the correction to the valence excitation that is orthogonal to the resonant RSCF excited state, there will be no homogeneous solution mixing problems.

8.2.7. The Radial EOM/FOS

In deriving the radial equations for the EOM/FOS we have the three contributing factors as before: the diagram phase factor, the angular summation contribution and the radial functions themselves. The process is the same as for the EOM/RPA except

that we need the angular reductions for the positive and negative valence excitations.

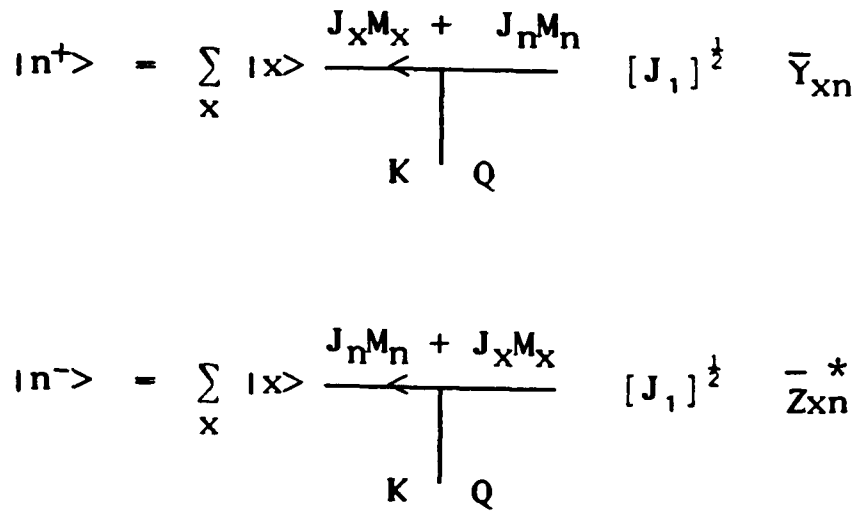

(8.26)

where the lines over the amplitudes indicate that they are reduced ones (i.e. they have no dependence on magnetic quantum numbers). Similarly we need the angular reductions for the valence projection operators

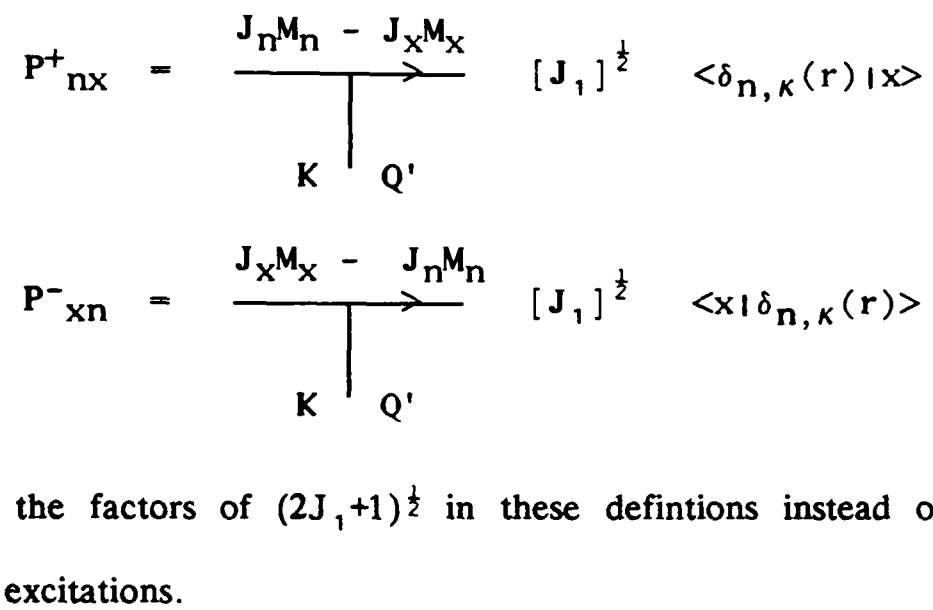

(8.27)

(8.28)

Note the factors of $(2J_1+1)^{\frac{1}{2}}$ in these defintions instead of the $(2K+1)^{\frac{1}{2}}$ used for the core excitations.

Producing the angular diagrams is done in the same way as for the EOM/RPA with the diagrams being topologically identical as before: the Coulomb interaction 3J symbols are inserted together with the excitation and projection reduction 3J symbols. The coupling Clebsch–Gordan coefficients have to be included also. The magnetic quantum numbers are then summed over for all states except the J_1M_1 state. Using the usual diagrammatic technique this corresponds to joining together all the lines that are summing over the same variable. The diagrams can then be simplified as before. The angular factors for all the EOM/FOS diagrams have been checked by computer by [S.A. Blundell].

8.2.8. An Example of EOM/FOS Diagram Evaluation

As an example we shall consider the exchange part of diagram e_7v^+ which contributes to the positive valence excitation equation.

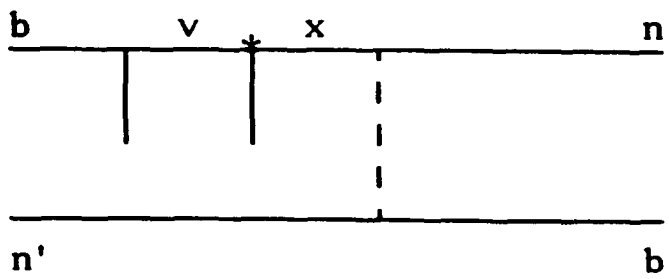

(8.29)

we are using the notation as given in (8.8); we have labelled the outer valence orbitals by n and n' which correspond to the angular momentum states $|J_0M_0>$ and $|J_0M_0'>$ in equation (8.4) respectively.

Phase

This follows the same rules as before (see section 4.2.10). The diagram is an exchange diagram with a commutator diagram factor of $-\frac{1}{2}$ which contains a negative excitation, is part of the $V^+(n)$ term and is part of a positive excitation equation. We therefore obtain $-1 \times -\frac{1}{2} \times -1 \times +1 \times +1 = -\frac{1}{2}$ for the phase factor.

Angular Diagram

We make all the assignments mentioned above, including the Clebsch-Gordan coefficients from equation (8.4) and join together all the lines that we are summing over for each variable. After this we obtain

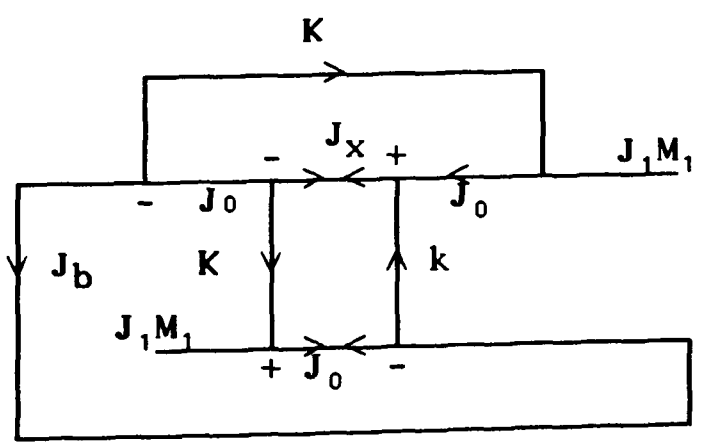

$$[K]^{\frac{1}{2}} \; [J_1]^{3/2} \qquad (8.30)$$

When evaluated this gives

$$(-1)^{k+J_b-J_0}[K,J_1]^{\frac{1}{2}} \begin{Bmatrix} J_0 & J_b & K \\ J_1 & k & J_0 \\ K & J_0 & J_1 \end{Bmatrix} X^k(\kappa_1,\kappa_0,\kappa_0,\kappa_b) \qquad (8.31)$$

Radial Part

There is the usual Slater integral part. When we put in the expression for the projection operator we obtain a Z^k function (see chapter four) and the radial valence function. In addition in equation (8.29) it should be noted that the excitation operator is between b and v. This corresponds to the overlap between the negative excitation of b and the valence orbital. The full radial expression is therefore

$$[b^-|n]\ Z^k(nb;r)\ r\ R_n(r) \qquad (8.32)$$

Total Diagram

The final expression for the diagram is therefore given by

$$-\tfrac{1}{2}\ (-1)^{k+J_b-J_0}[K,J_1]^{\frac{1}{2}} \begin{Bmatrix} J & J_b & K \\ J & k & J \\ K & J_0 & J \end{Bmatrix} X^k(\kappa_1,\kappa_0,\kappa_0,\kappa_b)\ [b^-|n]\ Z^k(nb;r)\ r\ R_n(r) \qquad (8.33)$$

8.3 Results

We can evaluate the exact expressions for all the diagrams as described above. The form of the equations is given in Appendix 2 for the positive and negative core and valence excitations. We thus have a set of self-consistent radial differential equations which are of the forms of equations (8.14) to (8.16). We solved the EOM/FOS numerically for the caesium $6s_{\frac{1}{2}} \rightarrow 6p_{\frac{1}{2}}$ transition and for the $6s_{\frac{1}{2}} \rightarrow 6p_{3/2}$ transition. The results obtained are

Transition	Reduced E1 transition matrix elements		
	EOM/RPA	EOM/FOS	Expt.
$6s_{\frac{1}{2}} \rightarrow 6p_{\frac{1}{2}}$	-4.97	-5.09 -6.12	-4.52 (0.01)
ω	0.04175	0.03796	0.05093
$6s_{\frac{1}{2}} \rightarrow 6p_{3/2}$	7.01	6.95 8.90	6.63(0.01)
ω	0.04358	0.040267	0.05346

The two values in the EOM/FOS column correspond to the length and velocity gauges. For the EOM/RPA calculation these are equivalent. We can note several things about these results though a full discussion of the physics involved will be given later.

1. The additional FOS terms affect the transition matrix elments for the two transitions calculated in different ways: the $6s_{\frac{1}{2}}$ transition result (for the length gauge) changes by 2.4%; the $6p_{3/2}$ values changes by 0.9%; the $6p_{\frac{1}{2}}$ transition answer is actually made worse (i.e. further from the experimental answer) when the extra terms are added. The $6p_{3/2}$ transition result is slightly improved.
2. The values for ω are worse than the EOM/RPA values (which just equal the difference in the HF eigenvalues).
3. Length/velocity equivalence no longer holds. The extra terms affect the velocity gauge more than the length one.

8.4 PNC EOM/FOS

The extension of the parity conserving EOM/FOS to the PNC case follows exactly the same lines as it did for the EOM/RPA. The only difference is that there are many more diagrams and thus many many more PNC terms since each parity conserving orbital is replaced in turn by its PNC counterpart. There will be PNC positive and negative valence excitations to solve for as well. The form of the equations is given in Appendix two.

When the PNC EOM/FOS were solved we obtained

Transition	Reduced PNC E1 transition matrix elements		
	PNC EOM/RPA	PNC EOM/FOS	Expt
$6s_{\frac{1}{2}} \rightarrow 7s_{\frac{1}{2}}$	0.891	0.869 0.893	--
ω	0.07218	0.07198	0.05346

From the results of the PNC EOM/FOS calculation it should be noted that

1. The value for ω is slightly improved
2. The PNC E1 transition matrix element is decreased by 2.5% (considering the length gauge answer).

8.5. Analysis of Extra Diagrams

To get an idea of what the additional diagrams physically represent we can replace the excitations in each term by their 'lowest order' values and derive the equivalent MBPT diagram that represents the resulting expression. For example the positive valence excitation is just the single particle resonant excited state in lowest order. The additional diagrams fall into two basic categories: those dealing with Exclusion Principle violation (EPV) and those that are the valence contribution to two particle excitations

8.5.1. Exclusion Principle Diagrams

In any MBPT correction diagram the Exclusion Principle forbids the existence of two identical particles at once. In solving RPA type equations by coupled self-consistent methods such as we have used there are implicitly included certain terms which are forbidden by the Exclusion Principle. These EPV diagrams involve the same valence state appearing in the sum over the excited states for the core excitations as is actually 'driving' the excitation in the first place. For an example of EPV diagrams see figure 8.1. Diagrams such as *a* are included in RPA calculations. They would be cancelled by diagrams such as *b* which is not included in an RPA

Figure 8.1 MBPT EPV Diagrams

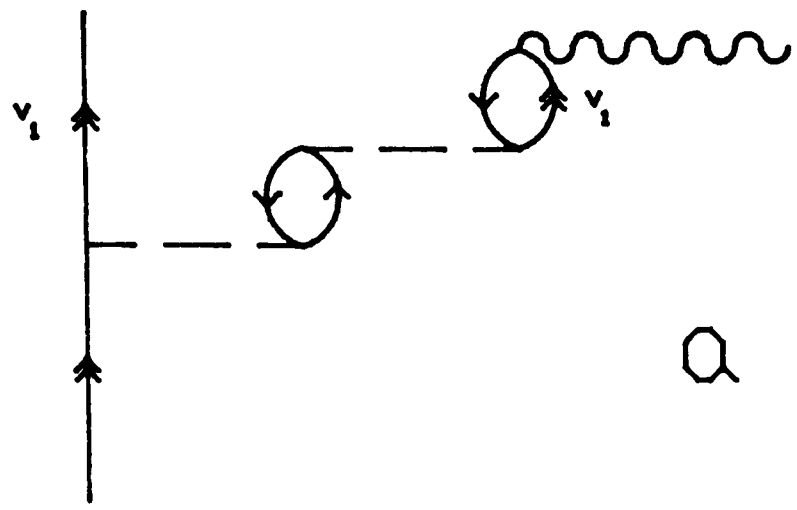

a

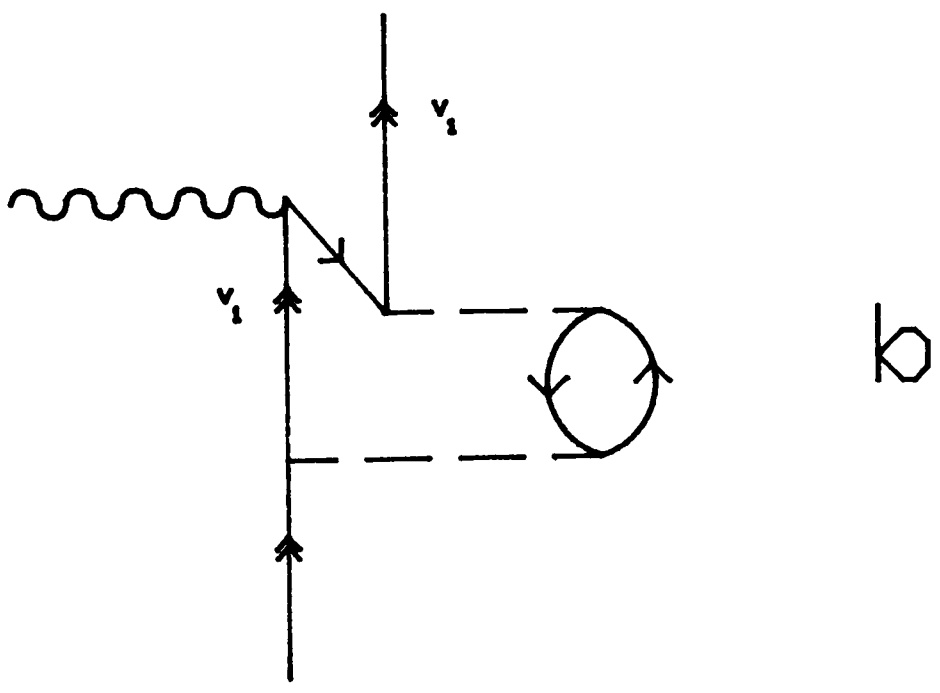

b

Diagrams a and b cancel

formalism. The EOM/FOS diagrams that are concerned with these EPV effects are diagrams d_4, d_2, b_5, b_3, g_2, a_2, e_{10} and e_{11} as given in table 8.1. We have given the equivalent lowest order MBPT type diagram that these EOM/FOS terms represent in figure 8.2. From this it can be seen that these diagrams are directly concerned with the EPV parts of the EOM/RPA diagrams. The creation/annihilation operator formalism will ensure that these extra diagrams are actually removing the original EPV terms.

The first diagram in figure 8.2, which corresponds to the four EOM diagrams mentioned in the figure, will not contribute in lowest order because the direct and exchange EPV terms will cancel each other; they will contribute in the higher order expressions though where there is no exchange between the EPV orbitals. It should be noted that their sum is equivalent to the MBPT diagram without the energy denominator. What these diagrams are effectively doing are orthogonalising the right-hand side of the core excitation equation to the valence orbital with an angular multiplicative factor.

Diagram e_9 is the EPV diagram associated with the diagrams b_1, e_6 and e_7. It should be remembered with all these EPV removal diagrams that there are also the additional matrix element diagrams of table 8.6 and equation (8.18) which contain overlaps of the core excitations with the valence orbitals. These will also be contributing to the valence orbital EPV 'book keeping'.

8.5.2. Valence Contributions to Two Particle Effects

The other main type of additional EOM/FOS diagram is concerned with the valence orbital contributions to two particle excitations. In figure 7.1 in chapter 7 we gave the lowest order two particle excitation effects. The second type of diagram gives contributions such as those in 7.1 except that instead of there being a double sum over excited states the valence orbital is used for one of the excited states. Thus there is only a single excited state sum which is why this type of diagram appears in the single excitation approximation. Diagrams b_1, e_6 and e_7 represent such effects. We have given the lowest order MBPT representation in figure 8.3.

The positive and negative valence excitations are also two particle valence

Figure 8.2 EOM EPV Correction Diagrams

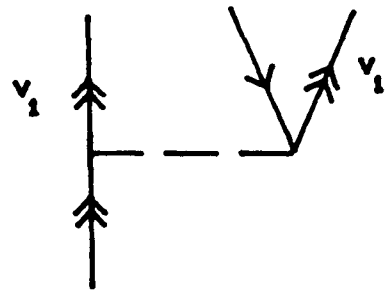

$\times \quad (E_a + w - E_n)$

Diagrams g2 a2 e10 and e11

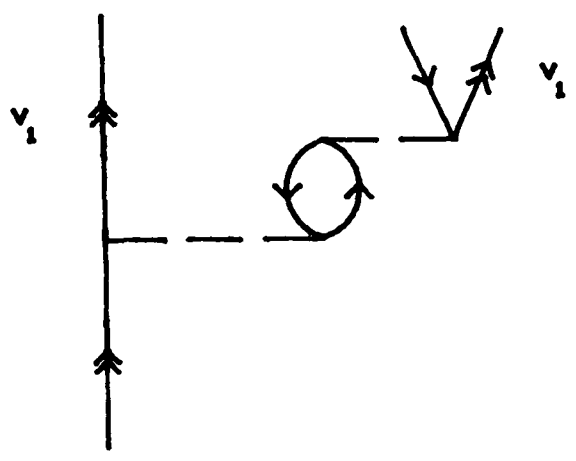

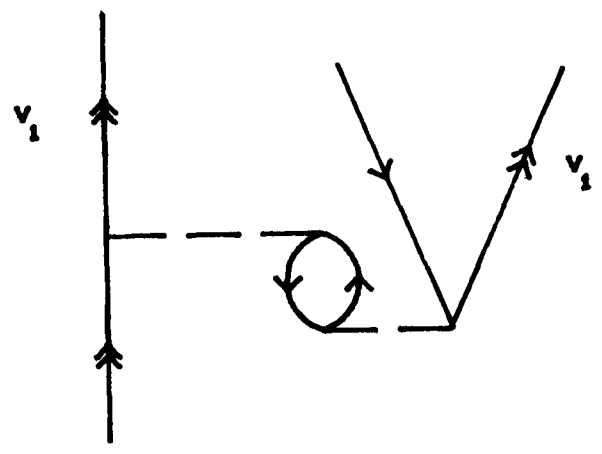

Diagram d4

Diagram b5

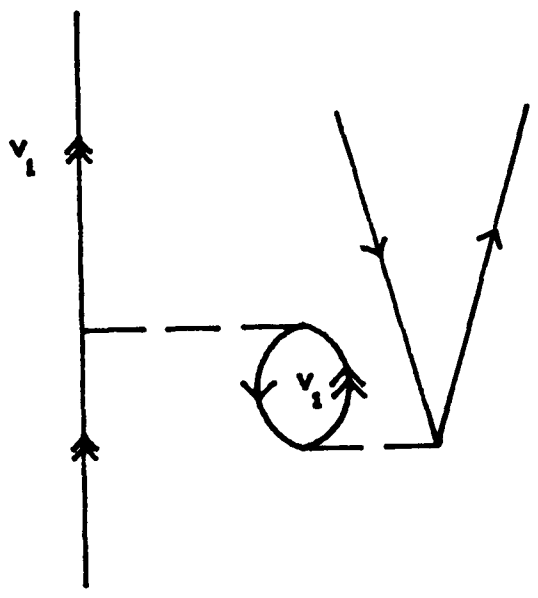

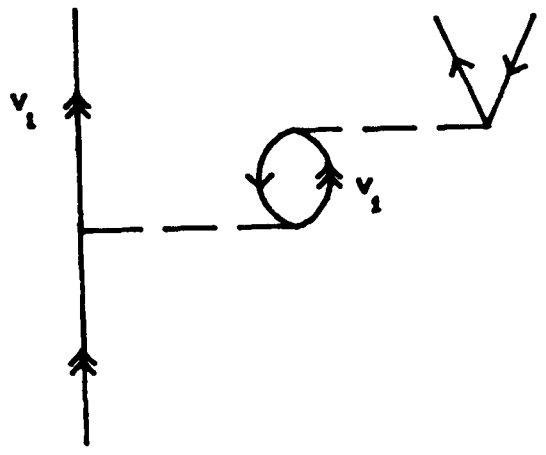

Diagram b3

Diagram d2

Figure 8.3 Valence 'Two Particle' Effects

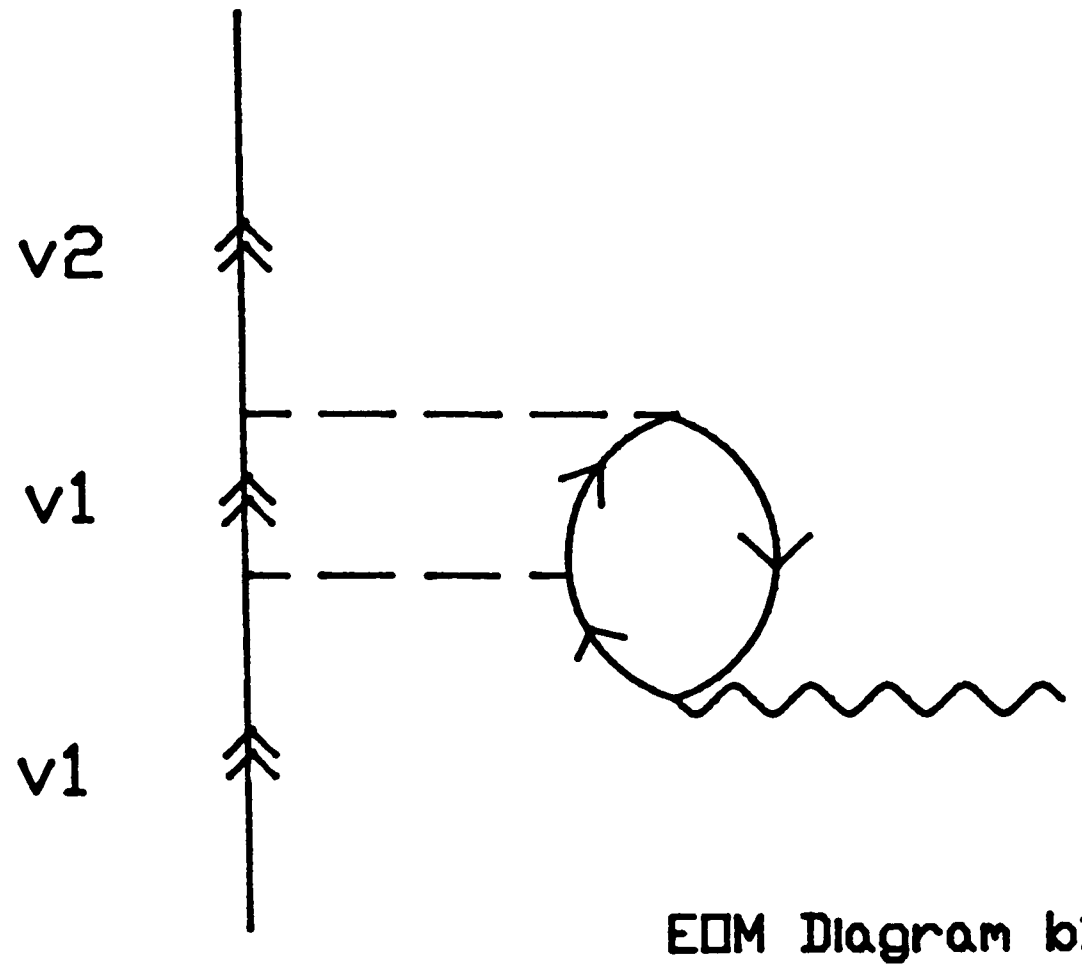

EOM Diagram b1

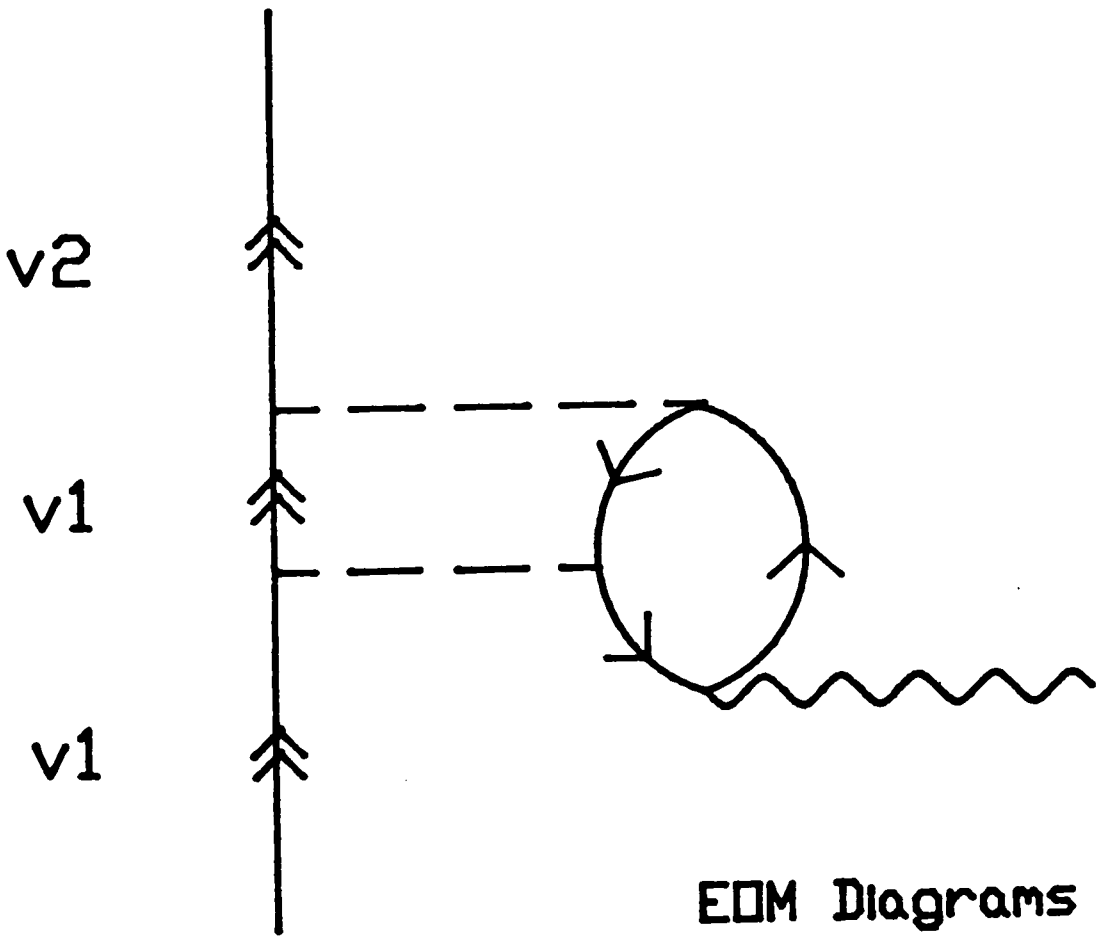

EOM Diagrams e6 and e7

Figure 8.4 Positive and Negative Valence Excitation Diagrams

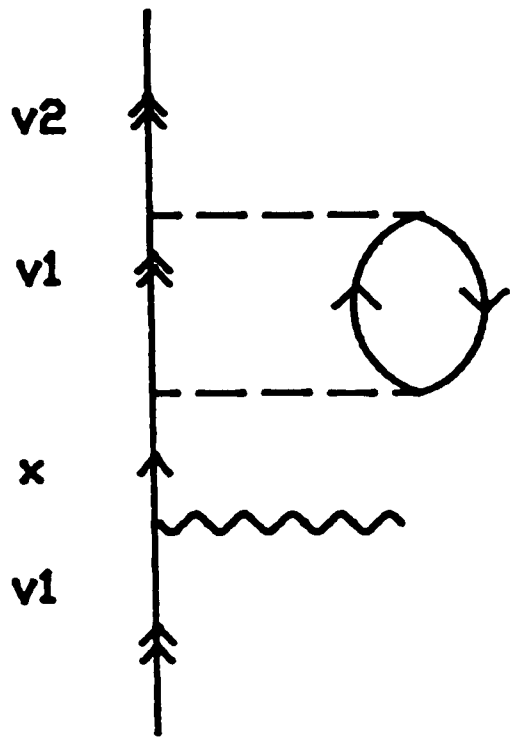

EOM diagram b1v+

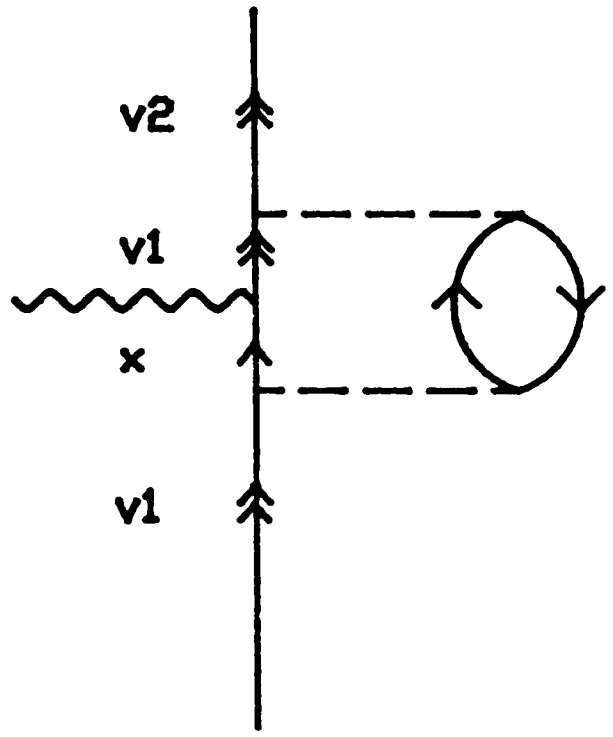

EOM diagram d1v-

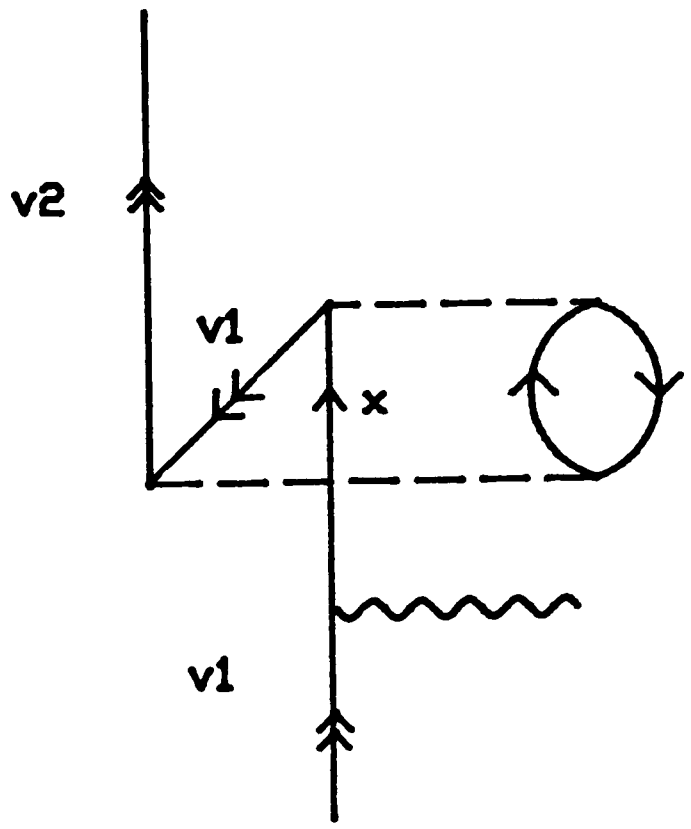

EOM diagram d1v+

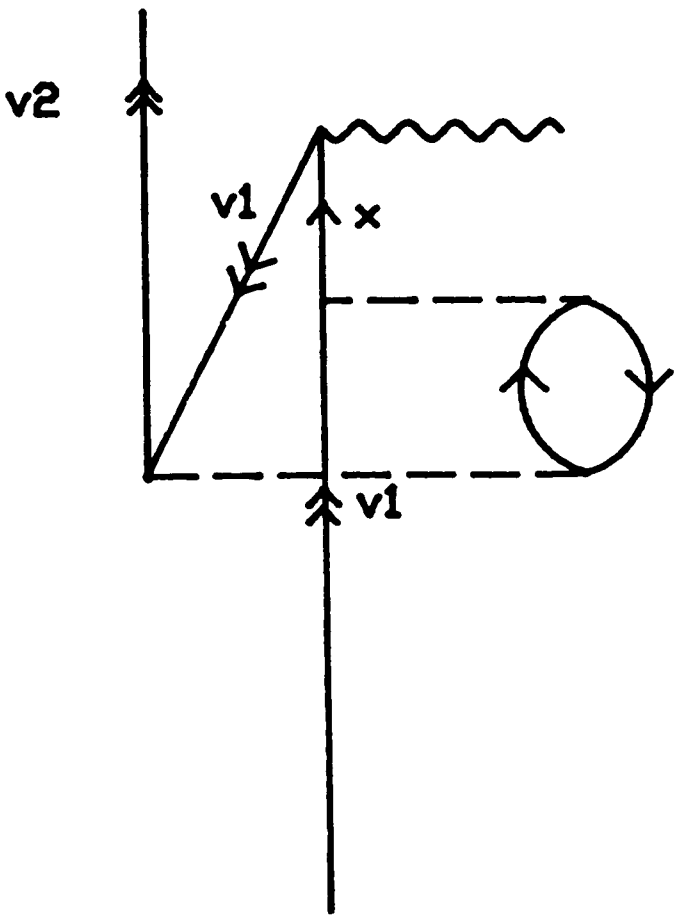

EOM diagram b1v-

contribution effects. We have given the MBPT equivalent representation in figure 8.4. It is interesting to note that the lowest order MBPT representation for diagram 'd₁v+' is not actually an allowed MBPT diagram and has no direct equivalent in a MBPT calculation. At first sight this might seem worrying. However, in the next section when we compare the EOM/FOS with MBPT we shall see how this is resolved.

8.6. Comparison Between MBPT and EOM/FOS

From the above analysis it can be seen that MBPT and EOM/FOS are not identical in that there are some diagrams which do not occur in MBPT. However there are several other differences in the formalism of EOM/FOS from MBPT which means that there should not necessarily be a direct correspondence:

1. ω is not fixed at $\epsilon_{v_2} - \epsilon_{v_1}$ as it is for a MBPT calculation; instead it is solved for. In MBPT ω appears in the energy denominators of the correction diagrams. The corrections to ω can be expressed as the overlap between the valence orbital and the right-hand side of the valence excitation equation (see section 8.2.6). In MBPT, the corrected denominator can be expanded as a series of diagrams consisting of the uncorrected diagrams multiplied by unconnected diagrams that are closed (i.e. they only have valence orbitals on the ends). There is an important theorem in MBPT called the linked diagram theorem (LDT) (see [Lindgren and Morrison]) that basically says that these disconnected or 'unlinked' diagrams cancel with certain other diagrams if the EPV diagrams are included in all the diagrams. The EPV terms will cancel because of the creation/annihilation commutation rules. Thus MBPT only calculates the linked diagrams and includes EPV terms. EOM on the other hand has no LDT and explicitly removes the EPV diagrams. The ω correction terms in the EOM correspond to unlinked diagrams and so are not included in the MBPT formalism.

2 The EOM/FOS transition matrix element is normalised whereas there is no normalisation for MBPT. The reason for this is that the unlinked diagrams of the MBPT transition matrix element cancel the normalisation correction terms when the calculation is done to all orders. If, as in practice, the calculation is of finite order then this cancellation is only approximate.

3. There are angular coupling coefficients included in the diagrams so that U^K_Q is correctly coupled to the ground state. MBPT does not need to do this as Ω (see chapter 3) is a scalar operator. Incomplete expressions for Ω will not necessarily be angular momentum eigenstates though.

Thus EOM/FOS is not identical in set up to MBPT. Each method has its own way of dealing with the EPV diagrams. MBPT includes EPV diagrams explicitly as some of them cancel out the 'unlinked diagrams'. The EOM explicitly includes terms to cancel out the EPV diagrams and solves for ω as well. The two methods should give identical results when carried out to all orders and for all complexities.

As regards the forbidden MBPT diagrams one has to consider the nature of the approximation schemes for MBPT and EOM. The former expands the answer in terms of Coulomb matrix elements and one hopes that the higher the number of matrix elements (i.e. the order of the MBPT calculation) the smaller the contribution. The EOM on the other hand is making approximations in the complexities of the ground state and the excitation operator. For the EOM/FOS we have no correlation effects in the ground state yet we have certain valence 'two particle' effects in the excitation operator. The extra diagrams are all concerned with valence orbital effects yet our ground state core orbitals do not 'see' the valence orbital when being solved for in the V_{N-1} HF equation. When two particle effects are included in the excitation operator they will cancel out or modify the valence 'two particle' effects that have been included so far. Thus the two particle excitations will take care of the 'MBPT disallowed' EOM/FOS diagrams. Quite how this is done is not easy to see, just as it is not easy to see exactly how the EPV diagrams are taken care of. But the nature of the creation/annihilation operator formalism mean that the details are 'taken care of' exactly. The two particle excitation formalism is in principle straightforward but leads to very complicated EOM diagrams because of the commutation relationships. For further discussion on correlation in the EOM see [Mckoy]. If the exact fully correlated ground state is used and all the possible excitation terms included then the correct answer must be obtained just as if a MBPT calculation is done to all orders. One never knows without calculating them how important the terms are that are being

left out. It seems to be that for the EOM/FOS one is including certain terms which are compensated for to a large degree by two particle ground state and excitation effects. So we actually get a worse answer by including just the extra single particle terms of the EOM/FOS.

8.7. The Choice of Rank K of the Excitation Operator

In chapter four we merely stated that we chose K to equal the rank of the transition operator without any justification other than the fact that only core excitations of this rank will contribute to the transition matrix element. There is no intrinsic reason however why the valence excitations should have K=1. For the $J=\frac{1}{2}$ to $J=\frac{1}{2}$ transitions, K can only equal 1 or 0 but for the caesium $6s_{\frac{1}{2}}$ to $6p_{3/2}$ transition, for example K can legitimately be 2 as well. The EOM/RPA result is independent of the choice of K but some of the extra valence terms in the EOM/FOS have K's in them in six J symbols etc. and it is not obvious that there is this independence. The fact that the closed core is spherically symmetric means that the tensor rank of any interaction with the core cannot be change by having any number of core interactions with other core orbitals. Only the rank 1 core excitations can contribute to the final transition matrix element. When the extra diagrams are added to produce the EOM/FOS there is now the possibility that rank 0 core excitations can contribute via a second (exchange) interaction with the non-symmetric valence orbital.

The conclusion from all this is that for a rigorous EOM/FOS calculation the rank K of the excitation operator U^K_Q should be summed over. However the rank 0 core excitations can only contribute via two interactions with the valence orbital so only contribute in higher orders. It is not clear how the other ranks contribute but it is thought that they are not likely to be large contributions.

8.8. Conclusions

We have re-examined the approximations made for the EOM/FOS and evaluated all the terms that are produced in the single particle approximation for the excitation operator. The extra terms are either concerned with the Exclusion Principle violating terms that are implicit in the EOM/RPA equations or represent the valence

contribution to certain two particle effects. Using a V_{N-1} HF ground state we have solved the EOM/FOS for caesium parity conserving and PNC transitions. However the results for the parity conserving transitions are either little better than the EOM/RPA or in fact worse. It is thought that the reason for this is that the extra terms for the EOM/FOS are in fact largely compensated for by the inclusion of two particle effects in the ground state and in the excitation operator.

CHAPTER 9: Conclusion

9.1 Introduction

In this last chapter we shall give a summary of the current atomic PNC situation. In section 9.2 we describe the current status of atomic PNC experiments giving the latest published results. The theory situation is reviewed in section 9.3. Taking the results from experiment and theory we give the latest atomic estimate of Q_W from these results. In 9.5 we describe the outlook for PNC experiments and theory calculations in the future. The findings of this thesis are summarised in section 9.6.

9.2 Summary of PNC Experimental Situation

PNC experiments have been carried out on four heavy elements: lead, bismuth, thallium and caesium. Other elements such as samarium are currently being investigated ([Davies]). There are two basic experimental approaches to PNC measurements: optical rotation and fluorescence.

9.2.1. Optical Rotation

This method is used for bismuth, lead and thallium experiments. These atomic PNC experiments basically involve the interference between an M1 transition and a weak interaction induced PNC E1 one. This interference results in a difference in the atom's response to left and right circularly polarised light. In an optical rotation experiment a plane polarised light beam (which can be considered to be the superposition of left and right circularly polarised beams) is passed through a vapour of the element and the rotation of the plane of polarisation of the beam is measured. The rotation is very small due to the small size of the weak interaction that is causing it; typical values are of the order of 10^{-7} radians. This poses tremendous experimental problems. However the last quoted result for the Oxford experiment on the bismuth 876 nm transitition had an error of 10% and the group is expecting a result of a few percent in the near future.

The optical rotation experiments measure a dimensionless quantity R which is given by

$$R = Im \frac{< f \,||\, E1_{pnc} \,||\, i >}{< f \,||\, M1 \,||\, i >} \qquad (9.1)$$

This can also be calculated *ab initio* where the E1 PNC transition matrix element is given in units of the weak charge Q_W. The M1's can either be obtained experimentally or calculated *ab initio*. Using (9.1) the value of Q_W can be extracted.

9.2.2. Fluorescence Experiments

These are used for caesium and thallium PNC measurements. The latest caesium PNC experiment by [Noecker et al.] is the most accurate atomic PNC experiment done to date with a claimed accuracy of 2%. It involves the $6s\frac{1}{2}$ to $7s\frac{1}{2}$ transition which is a doubly forbidden M1 transition which acquires a PNC E1 amplitude due to the weak force as discussed in previous chapters. The transition is excited with circularly polarised light in an atomic beam placed in an enhancement cavity; perpendicular electric and magnetic fields are applied to the region so that one is effectively measuring the interference between the PNC E1 transition and the Stark Effect induced transition. The magnetic field Zeeman splits the levels. The PNC asymmetry reverses with the E and B field directions, the circular polarisation of the light and with the particular Zeeman component being examined. The decay of the upper level (via an intermediate level) is monitored synchronously with the systematic variation of the parameters mentioned above. The method's great strength is in the number of permutations of the parameters with which to detect the PNC amplitude. The experiment has also quoted an amplitude for the spin dependent weak interaction though the error range includes the possibility of it being zero.

Table 9.1. Summary of Atomic PNC Experimental Situation

Bismuth 876 nm

Location		R	Claimed % Error
Oxford	[Macpherson et al.1987]	-10.0 ± 1.0	10%
Seattle	[Hollister et al. 1981]	-10.4 ± 1.7	16%

Bismuth 648 nm

Location		R	Claimed % Error
Oxford	[Taylor et al. 1987]	-9.3 ± 1.4	15%
Moscow	[Birich et al. 1984]	-7.8 ± 1.8	23%
Novosibirsk	[Barkov et al. 1981]	-20.2 ± 2.7	13%

Lead 1.28 μm

Location		R	Claimed % Error
Seattle	[Emmons et al. 1983]	-9.9 ± 2.5	25%

Caesium 539 nm

Location		$Im(E1_{pnc})/\beta$ (mV / cm)	Claimed % Error
Boulder	[Noecker et al. 1988]	-1.576 (34)	2%
Boulder	[Gilbert et al. 1986]	-1.650 (130)	8%
Paris	[Bouchiat et al. 1986]	-1.560 (170) (120)	13%

Thallium 293 nm

Location		E1 PNC (10^{-11} iea_0)	Claimed % Error
Berkeley	[Drell et al. 1985]	-0.76 ± 0.14	19%

9.2.3. Summary of Atomic PNC Experiments

In table 9.1 we give the latest atomic PNC experimental results. It should be noted that the results of different groups in general agree (and we have only quoted the most accurate in some cases). However there is a notable exception, namely the bismuth 648 nm transition. This has not been resolved yet and additional experimental measurements are required.

It should also be noted that the caesium experiments are the most accurate; this is partly due to the fact that the theoretical calculations for caesium are more accurate than for the other elements and consequently more effort has been put into the experiments. However, PNC experiments for other elements will soon be achieving a few percent accuracy.

9.3 Summary of PNC Theory Situation

The PNC theory calculations are making rapid progress. The many body problem is now fairly well understood and it is a matter of calculation of the most important MBPT terms. The main problem is the estimation of the errors of the calculation. The numerical errors can be estimated by using grid extrapolations and using checks such as length/velocity agreement where appropriate. However the estimation of the error due to the MBPT terms left out or the use of a semi–empirical potential is not easily quantifiable. In the calculations of Johnson the values of known physical quantities, such as parity conserving E1 transition matrix elements and the hyperfine dipole interaction constant, are used as a yardstick to estimate the error of the PNC E1 matrix element. There is no necessary reason why the PNC value has to behave in the same manner as these other values (see chapter 7) but there is little else to go on.

We have given the various PNC theory results in tables 9.2 and 9.3. The two most extensive MBPT calculations on the Cs $6s\frac{1}{2} \rightarrow 7s\frac{1}{2}$ transition are those of [Johnson 1988_c] and [Dzuba 1987_b, 1988] (see table 9.2 and chapter 7). Recently, semi–empirical calculations have been performed by Bouchiat (see next section). The

Table 9.2

Comparison of PNC Theory Calculations (units = $-1ea_0(Q_W/N)x10^{-11}$)

Cs PNC $6s_{\frac{1}{2}} \rightarrow 7s_{\frac{1}{2}}$

Dzuba	Johnson	Bouchiat	Ours
0.90(1±0.02)	0.951(1±0.05)	0.935±0.02±0.03	0.895(1±0.04)

Tl PNC $6p_{\frac{1}{2}} \rightarrow 7p_{\frac{1}{2}}$

Dzuba	PNC RPA	Others	Ours
-7.9(1±0.06)	-9.56_f	-8.0_a	-7.85(1±0.05)
	-9.71_g	$-8.7(1\pm0.21)_b$	
	-9.66_h	-10.0_c	
		-6.2_k	

Tl PNC $6p_{\frac{1}{2}} \rightarrow 6p_{3/2}$

Dzuba	PNC RPA	Others	Ours
-27.0(1±0.03)	-30.38_h	-36_d	-28.4(1±0.07)
		-25.2_e	
		$-28.7(1\pm0.2)_i$	
		-36.6_j	

a: [Sushkov et al.]
b: [Neuffer and Commins]
c: [Plummer and Grant]
d: [Neuffer and Commins]
e: [Henley et al.]
f: [Martensson-Pendrill]
g: [Johnson 1986]
h: this work.
i: [Novikov et al]
j: [Henley and Wilets]
k: [Bouchiat and Bouchiat]

Table 9.3

Comparison of PNC Theory Calculations (units = $-iea_0(Q_W/N)\times10^{-11}$)

Pb 1.28 μm

Dzuba [c]	Others
10.4 ± 0.8	-11.4 [a]
	-13 [b]

Bi 876 nm

Dzuba [c]	Others
10.4 ± 1	-14 [b]
	-12 [d]
	-8.3 [e]
	-10.9 [f]

a: [Botham et al]
b: [Novikov et al]
c: [Dzuba 1988]
d: [Harris et al]
e: [Martensson et al]
f: [Plummer] (D.Phil. thesis Oxford) 1984

only extensive calculations done on the thallium PNC transitions have been by [Dzuba 1987_b] (see tables 9.2). We have quoted the PNC RPA calculations for the thallium transitions by way of comparison. The other quoted calculations for the thallium transitions are all various semi-empirical calculations. Dzuba has also done calculations on lead and bismuth ([Dzuba 1988], see table 9.3). Most of the other calculations for these elements are semi-empirical calculations. In both cases Dzuba's answers are in good agreement with experiment.

9.3.1. Bouchiats Semi-Empirical Calculations

We have discussed Dzuba's and Johnson's calculations already in chapter seven. We shall now outline a semi-empirical calculation performed by [Bouchiat and Piketty 1986] (BC). They consider the rescaled matrix element of the weak Hamiltonian between $s_{\frac{1}{2}}$ and $p_{\frac{1}{2}}$ states for each n level. They perform first order perturbation corrections to these rescaled quantities only. They then use the experimental value for each X_{hyp} (see chapter seven) to give the estimate for the weak interaction matrix element. These calculated quantities are then put in an expression for the PNC transition matrix element that involves the weak interaction matrix elements, the parity conserving matrix elements and energy denominators. Experimental values are used for these last two quantitites. This expression for the PNC transition matrix element involves a finite sum over the $n = 6$ to $n = 8$ states. They use semi-empirical Norcross potential calculations to estimate the contribution from the other n levels. BC has also performed an earlier semi-empirical calculation using a fitted local potential and correction factors for the PNC transitions (see [Bouchiat *et al.* 1983]).

In both these calculations a local Norcross potential is used to model the electronic potential. As we mentioned in chapter 7 although these give good lowest order results their behaviour as higher order terms are added is not very predictable. BC's calculations are not fully relativistic and do not treat the shielding to all orders as we have done. It involves the use of a variety of correction factors to produce fits

to physically known quantities.

9.3.2. This Calculation

The semi–empirical results of this thesis, when compared with the other results quoted in table 9.2 are close to those of the Russian group which are the most extensive MBPT calculations done to date. The Russian's tend to use various approximate methods which make it difficult to appraise their results sometimes (see chapter 7 for their hyperfine calculations for example). There has been some debate recently over the large difference between Johnsons' result and Dzuba's for the caesium $6s\frac{1}{2} \rightarrow 7s\frac{1}{2}$ PNC transition. Our semi–empirical calculation seems to indicate that the iteration of the correlation potential and the shielding of the external photon in the correlation corrections accounts for most of this difference. Whilst it is always difficult to assess the accuracy of any calculation, including a semi–empirical one, our calculations seem to agree with the Russian group's PNC calculations for the caesium and thallium PNC transitions. Ultimately, only a rigorous *ab initio* MBPT calculation or equivalent will achieve the accuracy required to compete with high energy particle physics determination of $\sin^2\theta_W$. However semi–empirical methods give important indications of results, especially when a new area is being investigated as was the case when PNC calculations were first started. Though the result of this thesis cannot claim to be the most accurate one performed, it 'adds more grist to the mill' to the resolution of the current discrepancies in MBPT results.

9.4 Atomic Estimate of Q_W

The level of accuracy of atomic PNC and experiment is not yet high enough to compete with the high energy determination of $\sin^2\theta_W$. The current world average value is (see [Amaldi *et al*])

$$\sin^2\theta_W = 0.230 \pm 0.005 \qquad (9.2)$$

Without radiative corrections Q_W is given by

$$\frac{-Q_W}{N} = 1 - \frac{Z}{N}\left(1 - 4\sin^2\theta_W\right) \qquad (9.3)$$

Adding radiative corrections gives (see [Amaldi et al], [Marciano and Sirlin])

$$\frac{-Q_W}{N} = 0.9793 - \frac{Z}{N}\left(0.9793 - 3.8968\sin^2\theta_W\right) \qquad (9.4)$$

Using (9.3) in (9.4) gives us the values of Q_W for the atomic transitions of interest

Element	$-Q_W$ ($\sin^2\theta_W = 0.230 \pm 0.005$)
$^{133}_{55}Cs$	71.8 ± 1.1
$^{205}_{81}Tl$	114.7 ± 1.6
$^{208}_{82}Pb$	116.6 ± 1.6
$^{209}_{83}Bi$	116.5 ± 1.6

(9.5)

In the atomic determination of the weak charge the most accurately measured PNC experiment is the Cs $6s_{\frac{1}{2}} \rightarrow 7s_{\frac{1}{2}}$ transition. There have been three accurate measurements as given in table 9.1. The experiments measure the ratio of the PNC E1 transition matrix element to β, where β is the vector stark polarisability. [Bouchiat and Guena 1988] have determined β by measuring the ratio (M_1^{hf}/β), where M_1^{hf} is the M1 transition induced by the off-diagonal hyperfine interaction. They use a theoretical value for M_1^{hf} to obtain a value for β of

$$\beta = (27.17 \pm 0.35)\ a_0^3 \qquad (9.6)$$

To extract Q_W from the values of β, the theory value for $E1_{pnc}$ and the experimental value for $E1_{pnc}/\beta$ we have a conversion formula

$$\frac{(E1_{pnc})_{theory}}{\beta} \quad Q_W \times 0.65926 = \left[\frac{E1_{pnc}}{\beta}\right]_{expt} \tag{9.8}$$

where the PNC E1 theory number is in units of $-iea_0(Q_W/N)\times10^{-11}$, β is in units of a_0^3 atomic units, and the experimental ratio is in units of mV/cm. Using tables 9.1 and 9.2 for the Cs PNC values will give different estimations of Q_W according to which values are taken. We shall use our value of $0.895(1\pm0.03)\ -iea_0(Q_W/N)\times10^{-11}$; for the experimental value we shall use the most accurate value obtained, i.e. 1.576(34) mV/cm. We thus obtain for Q_W:

$$Q_W = 71.8 \pm 1.8 \pm 2.1 \tag{9.9}$$

where the first error is due to the experimental determination of β and $(E1_{pnc}/\beta)$ (with the errors added in quadrature) and the second is due to the theory error. This is in good agreement with the quoted value for Q_W for caesium given in (9.5). Using Dzuba's more accurate value of $0.90(1\pm0.02)\ -iea_0(Q_W/N)\times10^{-11}$ gives instead 72.2 with a theory error of ± 1.4 instead of ± 2.1.

Using (9.4) and our value of Q_W we can obtain a value for $\sin^2\theta_W$

$$\sin^2\theta_W = 0.230 \pm 0.009 \tag{9.10}$$

which is in excellent agreement with equation (9.2).

We have not given the Q_W's for the other PNC transitions as the errors in the experimental and theoretical values are far larger than for the Cs $6s\frac{1}{2} \rightarrow 7s\frac{1}{2}$ transition. [Dzuba 1988] has calculated them using his theory results and all the answers agree to within the error ranges.

9.5 Outlook for Atomic PNC

We have already achieved a claimed accuracy of 2% from one atomic PNC experiment. Other experiments will soon be achieving this sort of accuracy. In the next few years much more extensive theory calculations will be done, though there will always be the problem of estimating the error in a MBPT calculation.

The advent of relativistic pair function techniques will enable the calculation of all single and two particle excitation contributions which should give an accuracy that will easily make atomic PNC determinations of Q_W competitive with high energy determinations. The outlook for this field is very promising indeed. With more powerful computing resources such as transputers and parallel processing techniques becoming available it should soon be possible to do very extensive theory calculations. With the experimental accuracy getting to the level of being able to measure the spin-dependent effects such as anapole moments, there is much still of interest in this field.

9.6. Conclusion of Thesis

The Equations of Motion method has been successfully applied to an atomic system and results obtained using the EOM/RPA equations that agree with the equivalent MBPT/RPA calculations done by other groups. The additional single particle excitation terms have been calculated so that we can claim to have done a complete single particle excitation calculation (for rank 1 excitations with a V_{N-1} HF ground state) for caesium including the removal of Exclusion Principle violating diagrams. The extra terms were found to have a small effect for the parity conserving E1 $6s_{\frac{1}{2}} \rightarrow 6p_{3/2}$ transition. For the $6s_{\frac{1}{2}} \rightarrow 6p_{\frac{1}{2}}$ transition the extra terms actually make the answer slightly worse. In the case of the Cs $6s_{\frac{1}{2}} \rightarrow 7s_{\frac{1}{2}}$ PNC transition the effect was to reduce the amplitude slightly. However the poor parity conserving amplitudes indicate that this answer is not reliable. The reason for this is that the extra terms in the EOM/FOS include the valence orbital contribution to some two particle effects but neither the ground state nor the excitation operator have two particle effects in

them. It is felt that the two particle excitations need to be included fully for an accurate answer to be obtained.

To estimate correlation effects we included a semi-empirical potential in the EOM/RPA and obtained the following results

Cs $6s_{\frac{1}{2}} \rightarrow 7s_{\frac{1}{2}}$	$0.895(1\pm0.03) \times 10^{-11}$	$(-iea_0Q_W/N)$
Tl $6p_{\frac{1}{2}} \rightarrow 7p_{\frac{1}{2}}$	$-7.85(1\pm0.05) \times 10^{-11}$	$(-iea_0Q_W/N)$
Tl $6p_{\frac{1}{2}} \rightarrow 6p_{3/2}$	$-28.4(1\pm0.07) \times 10^{-11}$	$(-iea_0Q_W/N)$

This is in good agreement with the most extensive MBPT theory calculation done to date by Dzuba. Thus it has been shown that a semi-empirical method can successfully model complex correlation effects in a simple manner and can include PNC effects as well.

The next stage of calculations to be undertaken will be concerned with pair equation techniques for calculating two particle excitations since these constitute the main effects not yet accounted for. Non-relativistic pair equation techniques have already been used to calculate all one and two particle effects to all orders in lithium by [Lindgren]. It is hoped to extend this to a relativistic formalism which includes PNC effects in the near future.

As regards the EOM the next stage is to include correlation effects in the ground state as well as two particle excitations in the excitation operator. Though the formalism is straight-forward in principle, in practice this will involve many complex EOM diagrams and it is not certain how these can be simply and effectively managed.

APPENDIX 1: Creation and Annihilation Operators

These are operators that 'create' or 'destroy' single particle basis states. They obey the fermion anti-commutation rules:

$$\begin{aligned} [\, a^{\dagger}_i \,,\, a^{\dagger}_j \,]_- &= 0 \\ [\, a_i \,,\, a_j \,]_- &= 0 \\ [\, a_i \,,\, a^{\dagger}_j \,]_- &= \delta_{ij} \end{aligned} \qquad \text{(A1.1)}$$

where the anti-commutator brackets are defined by:

$$[\, x \,,\, y \,]_- \equiv x\, y + y\, x \qquad \text{(A1.2)}$$

and where $a^{\dagger}_i$ creates state $|i\rangle$ from the vacuum state $|0\rangle$ and a_i annihilates it:

$$\begin{aligned} a^{\dagger}_i \,|0\rangle &= |i\rangle \\ a^{\dagger}_i \,|i\rangle &= 0 \\ a_i \,|i\rangle &= |0\rangle \\ a_i \,|0\rangle &= 0 \end{aligned} \qquad \text{(A1.3)}$$

It is thus possible to express a single particle determinant in terms of creation operators acting on a vacuum state.

$$|\alpha\rangle = a^{\dagger}_a\, a^{\dagger}_b\, a^{\dagger}_c\, a^{\dagger}_d\, a^{\dagger}_e\, a^{\dagger}_f \ldots . |0\rangle \qquad \text{(A1.4)}$$

Because of the commutation relations (A1.1) the determinant $|\alpha\rangle$ is anti-symmetric with respect to the interchange of any two orbitals and is zero if any two orbitals are the same.

We can also write expressions for replacing one or more core orbitals in a determinant by an excited state. We write the replacement of a core orbital a by an excited orbital r as:

$$|{}^{r}_{a}\alpha\rangle = a^{\dagger}_r\, a_a\, |\alpha\rangle \qquad \text{(A1.5)}$$

and if a is replaced by r and b by s we have:

$$|{}^{rs}_{ab}\alpha\rangle = a^{\dagger}_r\, a^{\dagger}_s\, a_b\, a_a\, |\alpha\rangle \qquad \text{(A1.6)}$$

To see that this is the correct order for the creation and annihilation operators the full expression for $|\alpha\rangle$ should be written out and the annihilation operators 'moved' along the creation operators by means of the commutation relationships until

they can 'annihilate' the appropriate orbital; if the correct replacement excited orbital is then moved into its place it will be found that the correct phase is obtained with the operators in the order given in (A1.6).

We can similarly express operators in terms of creation and annihilation operators. A single particle operator $\underline{f}$ say can be written as:

$$\underline{f} = \sum_{j,i} a^{\dagger}_j \, a_i \, \langle j|\underline{f}|i\rangle \qquad \text{(A1.7)}$$

Similarly a two particle operator can be written

$$\underline{g} = \sum a^{\dagger}_i \, a^{\dagger}_j \, a_k \, a_l \, \langle i\,j|\underline{g}|l\,k\rangle \qquad \text{(A1.8)}$$

APPENDIX 2: The Equations Used in this Thesis

Space prevents us from giving the exact expressions for the radial equations. They can be found in the micro-fiche at the end of the thesis. The notation used is as for chapter 8. We have included the semi-empirical potential; for the unmodified equations $V_{semp}(r) = 0$.

HF

$$\left[\epsilon_a - h_0 - V_{hf} \right] |a\rangle = V_{semp}(r)|a\rangle$$

$$\langle 1|T|0\rangle = \langle v_2|T|v_1\rangle$$

HYPERFINE

$$\left[\epsilon_a - h_0 - V_{hf} \right] |a^+_{hyp}\rangle = V_{hyp}|a\rangle + V_{semp}(r)|a^+_{hyp}\rangle + \sum_b \left[\langle b^+_{hyp}|g_{12}|b\rangle + \langle b|g_{12}|b^+_{hyp}\rangle\right]|a\rangle$$

- orthogonality terms

The hyperfine constant is given by

$$A_{hyp} = \sum_a \langle v_1\ a|g_{12}|v_1\ a^+_{hyp}\rangle + \langle v_1\ a^+_{hyp}|g_{12}|v_1\ a\rangle$$

V_{hyp} is given by

$$\langle \kappa_1|V_{hyp}|\kappa_2\rangle = -\alpha\ (\kappa_1 + \kappa_2)\ \langle \kappa_1|C^k|\kappa_2\rangle \int (P_1Q_2 + P_2Q_1)\ r^{-2}\ dr$$

EOM/CS

$$\left[\epsilon_a \pm \omega - h_0 - V_{hf} \right]|a^\pm\rangle = V^\pm_{CS}(a)|a\rangle + V_{semp}(r)|a^\pm\rangle - \text{orthog.}$$

where

$$V^\pm_{CS}(a)|a\rangle = \sum_b \left[\langle b|g_{12}|b^\pm\rangle + \langle b^\mp|g_{12}|b\rangle\right]|a\rangle$$

where the transition matrix element is given by

$$\langle 1|T|0\rangle = \frac{\sum_{a^{\pm}} \langle a^{+}|T|a\rangle + \langle a|T|a^{-}\rangle}{\sum_{a^{\pm}} \langle a^{+}|a^{+}\rangle - \langle a^{-}|a^{-}\rangle}$$

EOM/RPA

$$\left[\epsilon_a \pm \omega - h_0 - V_{hf} \right] |a^{\pm}\rangle = V^{\pm}_{RPA}(a)|a\rangle + V_{semp}(r)|a^{\pm}\rangle - \text{orthog.}$$

where

$$V^{+}_{RPA}(a)|a\rangle = \langle v_1|g_{12}|v^{+}\rangle|a\rangle + V^{+}_{CS}(a)$$

$$V^{-}_{RPA}(a)|a\rangle = \langle v^{+}|g_{12}|v_1\rangle|a\rangle + V^{-}_{CS}(a)$$

with

$$|v^{+}\rangle = \frac{|v_2\rangle}{\langle v_2, RSCF|v_2\rangle}$$

and

$$\langle 1|T|0\rangle = \frac{\langle v^{+}|T|v_1\rangle + \sum_{a^{\pm}} \langle a^{+}|T|a\rangle + \langle a|T|a^{-}\rangle}{\langle v_2|v_2\rangle + \sum_{a^{\pm}} \langle a^{+}|a^{+}\rangle - \langle a^{-}|a^{-}\rangle}$$

EOM/FOS

$$\left[\epsilon_a + \omega - h_0 - V_{hf} \right] |a^{+}\rangle = V^{+}_{RPA}(a)|a\rangle + V_{semp}(r)|a^{+}\rangle - \text{orthog.} + \text{terms in table 8.1}$$

$$\left[\epsilon_a - \omega - h_0 - V_{hf} \right] |a^{-}\rangle = V^{-}_{RPA}(a)|a\rangle + V_{semp}(r)|a^{-}\rangle - \text{orthog.} + \text{terms in table 8.2}$$

$$\left[\epsilon_v + \omega - h_0 - V_{hf} \right] |v^{+}\rangle = V_{semp}(r)|v^{+}\rangle + \text{table 8.3} - \text{orthog.}$$

$$\left[\epsilon_v - \omega - h_0 - V_{hf} \right] |v^{-}\rangle = V_{semp}(r)|v^{-}\rangle + \text{table 8.4} - \text{orthog.}$$

the transition matrix element is given by

$$\langle 1|T|0\rangle = \frac{M_{fos}}{M_{norm}}$$

where

$$M_{fos} = \langle v^+|T|v_1\rangle + \langle v|T|v^-\rangle + \sum_{a^\pm} \langle a^+|T|a\rangle + \langle a|T|a^-\rangle - \langle v|a^-\rangle\langle a|T|v\rangle - \langle v|a+\rangle\langle a|T|v\rangle$$

and

$$M_{norm} = \langle v^+|v^+\rangle - \langle v^-|v^-\rangle + \sum_{a^\pm} \langle a^+|a^+\rangle - \langle a^-|a^-\rangle + \langle v|a^-\rangle\langle a^-|v\rangle - \langle v|a^+\rangle\langle a^+|v\rangle$$

<u>PNC HF</u>

$$\left[\epsilon_a - h_0 - V_{hf} \right] |a^{pnc}\rangle = V_{semp}(r)|a^{pnc}\rangle + h^{pnc}|a\rangle + V_{hf}{}^{pnc}|a\rangle$$

$$\langle 1|T|0\rangle = \langle v_2|T|v_1{}^{pnc}\rangle - \langle v_2{}^{pnc}|T|v_1\rangle$$

<u>PNC EOM</u>

$$\left[\epsilon_i \pm \omega - h_0 - V_{hf} \right] |i^\pm\rangle = V^\pm(i)|i^{pnc}\rangle + V^{\pm pnc}(i)|i\rangle + V_{semp}(r)|a^{\pm pnc}\rangle + h^{pnc}|i^\pm\rangle + V_{hf}{}^{pnc}|i^\pm\rangle - \text{orthog.}$$

where 'i' is either a core or a valence orbital and $V^\pm(i)$ is the appropriate potential according to which PNC EOM equation is required (i.e. CS, RPA or FOS). The transition matrix element is given by

$$\langle 1|T|0\rangle = \frac{\sum_{a^\pm} - \langle a^{+pnc}|T|a\rangle + \langle a^+|T|a^{pnc}\rangle - \langle a^{pnc}|T|a^-\rangle + \langle a|T|a^{-pnc}\rangle + \ldots}{\sum_{a^\pm} \langle a^+|a^+\rangle - \langle a^-|a^-\rangle + \ldots}$$

where the '...' signifies the inclusion of the other terms appropriate to the PNC equation being solved.

APPENDIX 3: Length–Velocity Equivalence

Since in this thesis we are concerned mainly with transition matrix elements we need to discuss gauge considerations for the dipole operator. The electric dipole operator in the length gauge is given by $\underline{D}_L = -\underline{r}$ (in atomic units, see appendix 5). The velocity gauge operator is given by $\underline{D}_V = i\ c\ \underline{\alpha}\ /\ \omega_{fi}$ (where $\omega_{fi} = E_f - E_i$). Consider the atomic Hamiltonian

$$H = c\ \underline{\alpha}\ .\ \underline{p} \quad + c^2\ (\beta - I) + V_{nuc}(r) + V_{elec.} \tag{A3.1}$$

where V_{elec} is an approximation to the exact $\sum r_{ij}^{-1}$ term. We can write down the commutator relationship between $\underline{D}_V$ and $\underline{D}_L$:

$$c\ [\ \underline{\alpha}\ .\ \underline{p}\ ,\ -\underline{r}\ ] = i\ c\ [\ \underline{\alpha}\ .\ \underline{\nabla}\ ,\ \underline{r}\ ] = i\ c\ \underline{\alpha} \tag{A3.2}$$

$$\underline{D}_V = \ 1/\omega_{fi}\ [\ (H - V_{elec}), \underline{D}_L\ ] \tag{A3.3}$$

Now we can write equation (A3.3) as

$$\underline{D}_V = \ 1/\omega_{fi}\ ([\ H, \underline{D}_L\ ] - [\ V_{elec}, \underline{D}_L\ ]) \tag{A3.4}$$

By taking matrix elements between the initial and final states the first term can be shown to equal the length gauge dipole operator so we are left with the expression

$$\langle f|\underline{D}_V|i\rangle = \ \langle f|\underline{D}_L|i\rangle + \ 1/\omega_{fi}\ \langle f|[\ V_{elec.}, -\underline{r}\ ]|i\rangle \tag{A3.5}$$

So provided that the electronic interaction part of the Hamiltonian commutes with $\underline{r}$ then the length gauge and the velocity gauge are equivalent. If the exact expression for V_{elec} is used then there is gauge equivalence as one would expect from gauge invariance arguments. A local potential such as for the RSCF calculations of chapter 3 will have length/velocity equivalence but in the case of the Hartree–Fock potential we get:

$$\langle x|[\ V_{hf}, \underline{r}\ ]|y\rangle = \ \sum_b\ (\ \langle b|\langle x|r_{12}^{-1}|b\rangle \underline{r}|y\rangle \ - \langle x|\underline{r}\langle b|r_{12}^{-1}|y\rangle|b\rangle\ ) \tag{A3.6}$$

Thus the HF potential does not commute with $\underline{r}$ because of the exchange terms and so there is no length/velocity equivalence for the HF equation. When using RPA type equations (such as the Equations of Motion) this equivalence returns (see [Botham]).

APPENDIX 4: The Model Independent Approach

As an alternative to the standard model predictions for the weak force coupling constants (as given in chapter 2) the latter can be regarded as model independent parameters to be determined by experiment.

Due to the fact that the nucleons act coherently in the atom we define a weak charge Q_W which is what is determined in the atomic physics approach to PNC experiments. The equation for the weak charge can be expressed in terms of the quark-lepton coupling coefficients, giving a linear equation relating the up and down quark constants.

$$\begin{aligned} Q_W &= Z\, C_{1p} + N\, C_{1n} \\ &= [\ (2\,Z + N)\, C_{1u} + (Z + 2N)\, C_{1d}\ ] \end{aligned} \qquad \text{(A4.1)}$$

where

$$\begin{aligned} C_{1u} &= 1/3\ (\ 2\, C_{1p} - C_{1n}\ ) \\ C_{1d} &= 1/3\ (\ 2\, C_{1n} - C_{1p}\ ) \end{aligned} \qquad \text{(A4.2)}$$

are the quark-lepton coupling constants. Rearranging (A3.1) we obtain a linear relationship between the coupling constants with Q_W as a parameter.

$$C_{1d} = -\frac{(1 + 2\ Z/N)}{(2 + Z/N)}\ C_{1u} - \frac{Q_W/N}{(2 + Z/N)} \qquad \text{(A4.3)}$$

In the SLAC experiment (see chapter one, [Prescott *et al.* 1978,1979]) the individual quarks act incoherently and the combination

$$C_{1d} = 2\ C_{1u} - 0.9 \pm 0.24 \qquad \text{(A4.4)}$$

is obtained. By plotting the lines C_{1d} vs. C_{1u} given in equations (A4.4) and (A4.3) for both the upper and lower limits of the intersection constants, areas of allowed C_{1d} vs. C_{1u} combinations are obtained. Since the standard model predicts the coupling constants as well we can also obtain a third line as a parameterised function of Θ_W. As can be seen from figure A4.1 the three approaches are entirely consistent and the high energy and the atomic physics lines are nearly orthogonal.

Figure A4.1

Allowed regions (90% confidence limit) in C_{1u}–C_{1d} from the SLAC eD experiment and atomic parity violation (taken from [Almaldi *et al*]).

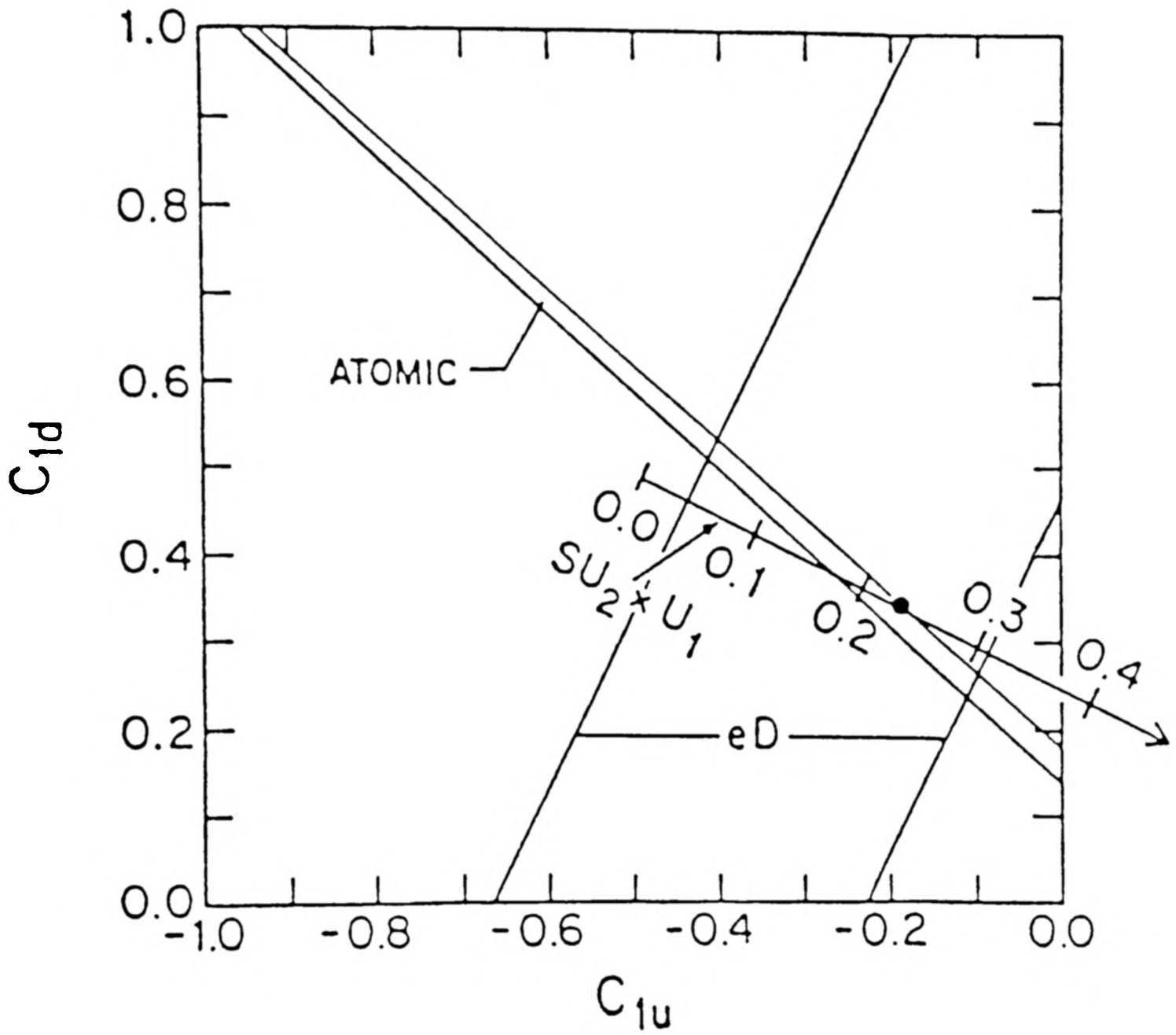

APPENDIX 5: The Units Used in this Thesis

For the atomic equations we employ atomic units

$$e = m_e = \hbar = 4 \pi \epsilon_0 = 1 \qquad \text{(A5.1)}$$

Thus the unit of length is a_0, given by

$$a_0 = \frac{4 \pi \epsilon_0 \hbar^2}{m_e e^2} = 1 \qquad \text{(A5.2)}$$

Using the definition of α

$$\alpha = \frac{e^2}{4 \pi \epsilon_0 c \hbar} \qquad \text{(A5.3)}$$

we obtain the unit of velocity as being α c. Thus $c = 1/\alpha$ in atomic units.

The unit of energy is the Hartree, which is given by

$$1H = 2 h c R_\infty = \frac{m_e e^4}{(4 \pi \epsilon_0)^2 \hbar^2} = 1 \qquad \text{(A5.4)}$$

For the particle physics equations (mainly in chapter 2) we use natural units:

$$\hbar = c = 1 \qquad \text{(A5.5)}$$

If, in addition we use the Heaviside–Lorentz system the we have $\epsilon_0 = 1$. For details see [Aitchison and Hey].

APPENDIX 6: The Runge-Kutta Method

For solving our equations numerically we employ the Runge-Kutta method, a standard technique for solving the equations as written in (5.27), i.e. equations of the form

$$\frac{d\ y(x)}{dx} = f(x,y) \qquad \text{(A6.1)}$$

The Runge-Kutta method expresses $y(x_n+h)$ (where h is the step size) as a Taylor expansion about $y(x_n)$.

$$y(x+h) = y(x) + h\ y'(x) + (h^2/2!)\ y''(x) + (h^3/3!)\ y'''(x) + O(h^4) \qquad \text{(A6.2)}$$

We wish to express y(x+h) in terms of functions of x and y which do not involve derivatives:

$$y(x+h) = y(x) + h\ \Phi\ (x,y) \qquad \text{(A6.3)}$$

so that

$$\begin{aligned}\Phi(x,y) &= y'(x) + (h/2!)\ y''(x) + (h^2/3!)\ y'''(x) + O(h^3) \\ &= f(x,y,) + (h/2!)\ f'(x,y) + (h^2/3!)\ f''(x,y) + O(h^2)\end{aligned} \qquad \text{(A6.4)}$$

The standard expression for $\Phi(x,y)$ when the required accuracy in y(x+h) is $O(h^3)$ is

$$\begin{aligned}\Phi(x,y) &= \sum_{i=1}^{4} c_i\ k_i \\ k_1 &= f(x,y) \\ k_i &= f\left(x + ha_i, y + \sum_{s=1}^{i-1} b_{is}\ k_s\right)\end{aligned} \qquad \text{(A6.5)}$$

Thus there are a series of *c*, *b* and *a* coefficients to be determined. These are found by expanding $\Phi(x,y)$, using the Taylor expansion, up to the required order in h and comparing coefficients with equation (A6.4).

The resulting equations for the coefficients are:

$$
\begin{aligned}
& c_1 + c_2 + c_3 + c_4 && = 1 \\
& c_2 a_2 + c_3 a_3 + c_4 a_4 && = 1/2 \\
& c_2 b_{11} + c_3 (b_{21} + b_{22}) + c_4 (b_{31} + b_{32} + b_{33}) && = 1/2 \\
& c_2 a_2^2 + c_3 a_3^2 + c_4 a_4^2 && = 1/3 \qquad \text{(A6.6)} \\
& c_2 b_{21}^2 + c_3 (b_{21} + b_{22})^2 + c_4 (b_{31} + b_{32} + b_{33})^2 && = 1/3 \\
& c_2 a_2 b_{11} + c_3 a_3 (b_{21} + b_{22}) + c_4 a_4 (b_{31} + b_{32} + b_{33}) && = 1/3 \\
& c_3 b_{22} a_2 + c_4 b_{32} a_2 + c_4 b_{33} a_3 && = 1/6 \\
& c_3 b_{22} b_{11} + c_4 (b_{32} b_{11} + b_{33} b_{21} + b_{33} b_{22}) && = 1/6
\end{aligned}
$$

There is obviously an infinite set of solutions as there are more coefficients to be determined than there are restrictions so we are free to chose to a certain extent the paramters that we use. We use

$$
\begin{aligned}
& c_1 = 1/6 \qquad c_2 = 1/3\ (1 - 1/\sqrt{2}\ ) \qquad c_3 = 1/3\ (1 + 1/\sqrt{2}) \qquad c_4 = 1/6 \\
& a_2 = 1/2 \qquad a_3 = 1/2 \qquad\qquad a_4 = 1 \\
& b_{11} = 1/2 \qquad b_{21} = -1/2\ (1 - 2/\sqrt{2}) \qquad b_{22} = (1 - 1/\sqrt{2}) \\
& b_{31} = 0 \qquad\quad b_{32} = -1/\sqrt{2} \qquad\quad b_{33} = (1 + 1/\sqrt{2})
\end{aligned}
\qquad \text{(A6.7)}
$$

With this choice of coefficients we are able to calculate $y(x_{n+1})$ from $y(x_n)$.

Credits

The original computer codes for the HF, PNC HF and TDHF were written by Ann-Marie Martensson-Pendrill. The Full Open Shell Equations of Motion program was origianlly written by S.A. Blundell and myself. All the programs in this thesis have been re-written by me; the hypefine interaction program was written by my from scratch. I also wrote all the semi-empirical versions of the programmes.

S.A. Blundell and Prof. P.G.H. Sandars set out the formalism for the EOM as presented in this thesis, based on the original paper by [Rowe]. I worked out the negative valence excitation theory and diagrams and re-wrote the EOM/FOS to include them. The angular parts to all the diagrams have been checked by computer by S.A. Blundell.

REFERENCES

Aitchison I.J.R., Hey A.J.G., 1982, *Gauge Theories in Particle Physics*, Adam Hilger

Amaldi U., et. al., 1987, CERN preprint number UPR-0331T

Armstrong L. Jr., 1978, 'Relativistic Effects in Highly Ionized Atoms' in *Structure and Collisions of Ions and Atoms,* ed. Sellin I.A., Topics in Current Physics, Vol 5 (Springer, Berlin, Heidelberg, New York)

Baird P.E.G., et. al., 1976, *Nature*, 264, 528

Bard Y., 1974, *Non linear parameter estimation*, Academic Press

Barkov L.M., Zolotorev M.S., 1980, *Sov. Phys.* JETP, 52, 360

Bearden J.A. and Burr A.F., 1967, *Rev. Mod. Phys.*, 39, 125

Bethe H. and Salpeter E., 1957, *Quantum Mechanics of One- and Two-electron Atoms* (Berlin: Springer)

Birich G.N., Bogdanov, Yu.V., Kanorskii S.I., Sobel'man I.I., Sorokin, V.N., Struk I.I., Yukov E.A., 1984, *Sov. Phys.* JETP, 60, 442

Bleany B.I., Bleany B., 1983, *Electricity and Magnetism*, O.U.P.

Blundell S.A., 1987, private communication.

Boston E., Sandars P.G.H., 1987, Private communication (to be published)

Botham C.P., 1984, D. Phil. Thesis, Oxford

Botham C.P., Blundell S.A., Martensson-Pendrill A.-M., Sandars P.G.H., *Phys. Scr.*, 1987, 36, 481

Bouchiat C., Piketty C.A., Pignon D., 1983, *Nucl. Phys.* B, 221, 68

Bouchiat M.A., Bouchiat C., 1974, *Journal De Physique*, 35, 899

Bouchiat M.A., Bouchiat C., 1975, *Journal De Physique*, 36, 493

Bouchiat M.A., Pottier L., 1984, *Atomic Physics 9*, Ed. Van Dyck, Fortson, Washington, World Scientific

Bouchiat M.A. et. al., 1984, *Phys Lett.*, B134, 463

Bouchiat M.A., Guéna J., Pottier L., Hunter L., 1986, *J. Physique*, 47, 1709

Bouchiat C. and Piketty C.A., 1986, *Europhys. Lett.*, 2 (7), 511

Bouchiat M.A., Guéna J., 1988, *J. Phys. France*, 49, 2037

Brimicombe M.W.S.M, 1976, D. Phil Thesis, Oxford

Brown G.E., 1964, *Unified Theory of Nuclear Models*, (North-Holland: Amsterdam)

Brown G.E.,Ravenahall D.G., 1951, *Proc. Roy. Soc. London*, A 208, 552

Case Studies in Atomic Physics IV, 1975, chapters 3 and 4, ed. McDaniel E.W. and McDowell M.R.C., (North–Holland: Amsterdam)

Chiarella C., Reichel A., *Math. of Comput.*, 22, 137

Commins E.D., Bucksbaum P.H., 1983, *Weak interactions of Leptons and Quarks*, C.U.P.

Das B.P., et. al., 1982, *Phys. Rev. Lett.*, 49, 32

Parpia F.A., Perger W.F., Das B.P., 1988, *Phys. Rev. A*, 37, 4034

Davies I.O.G., 1986, D. Phil Thesis, Oxford

Dembczynski J., Arcimowicz B., Stachowska E., Rudnicka–Szuba H., 1983, *Z. Phys. A*, 310, 27

Drell P.S., Commins E.D., 1985, *Phys. Rev. A*, 32, 2196

Dydak F., 1986, CERN preprint EP/86–121

Dzuba V.A., Flambaum V.V., Sushkov O.P., 1983, *J. Phys.* B, 16, 715

Dzuba V.A., Flambaum V.V., Sushkov O.P., 1984, *J. Phys.* B, 17, 1953

Dzuba V.A., Flambaum V.V., Silvestrov P.G., Sushkov O.P., 1985, *J. Phys.* B, 18, 597

Dzuba V.A., Flambaum V.V., Khriplovich I.B., 1986, *Z. Phys. D*, 1, 243

Dzuba V.A., Flambaum V.V., Silvestrov P.G. Sushkov O.P., 1987_a, *J. Phys.* B, 20, 1399

Dzuba V.A., Flambaum V.V., Silvestrov P.G. Sushkov O.P., 1987_b, *J. Phys.* B, 20, 3297

Dzuba V.A., Flambaum V.V., Silvestrov P.G. Sushkov O.P., 1988, *Europhys. Lett.*, 7 (5), 413

Emmons P.E., Reeves J.E., Fortson E.N., 1983, *Phys. Rev. Lett.* 51, 2089

Emmons P.E., 1984, Ph.D Thesis, Washington

Fermi E, 1934, *Z. Phys.*, 88, 161

Flambaum V.V., Khriplovich I.B., 1980, *Sov. Phys.* JETP, 52, 835

Flambaum V.V., Khriplovich I.B., Sushkov O.P., 1984, *Phys. Lett.*, 146B, 367

Fortson E.N., Wilets L., 1980, *Adv. Atom. Mol. Phys.*, 16, 319

Gilbert S.L., Weiman C.E., 1986, *Phys. Rev. A*, 34, 792

Glashow S.L. et. al., 1970, *Phys. Rev.* D2, 1285

Grangier P., Slusher R.E., Yurke B., LaPorta A., 1987, *Phys. Rev. Lett.*, 59, 2153

Harris M.J., Loving C.E., Sandars P.G.H., 1978,*J. Phys. B*, 11, L749

Hasert F.J., et. al., 1973, *Phys. Rev. Lett.* 46B, 138

Hegstrom R.A., 1979, *Private Communication to P.G.H. Sandars*

Henley E. and Wilets L., 1976, *Phys. Rev A*, 14, 1411

Henley E., Klapish M., Wilets L., 1977, *Phys. Rev. Lett.*, 39, 994

Heully J.-L., Martensson-Pendrill A.-M., 1983, *Physica Scripta*, 27, 291

Hinds E.A., 1979, *Proc. Int. Workshop on Neutral Currents*, Ed. Williams, Cargèse

Hinds E.A., 1980, *Phys. Rev. Lett.*, 44, 374

Hollister J.H., Apperson G.R., Lewis L.L., Emmons T.P., Vold T.G., Fortson E.N., 1981, *Phys. Rev. Lett.*, 51, 2089

Hung P.Q. & Sakurai J.J., 1981, *Am. Rev. Nucl. Part. Scr.*, 31, 375

Hunt R.G., 1979, D. Phil Thesis, Oxford

Johnson W.R., Guo D.S., Idrees M., Sapirstein J., 1985, *Phys. Rev.* A, 32, 2093

Johnson W.R., Guo D.S., Idrees M., Sapirstein J., 1986, *Phys. Rev.* A, 34, 1043

Johnson W.R., Idrees M., Sapirstein J., 1987, *Phys. Rev.* A, 35, 3220

Johnson W.R., Blundell S.A., Sapirstein J., 1988_a, *Phys. Rev.* A, 37, 307

Johnson W.R., Blundell S.A., Sapirstein J., 1988_b, *Phys. Rev.* A, 37, 2764

Johnson W.R., Blundell S.A., Liu Z.W., Sapirstein J., 1988_c, *Phys. Rev.* A, 37, 1395

Jucys A.P., Levinson I.B., Vanagas V.V., 1962, *Mathematical Apparatus of the Theory of Angular Momentum*, (Israel Program for Scientific Translations, Jerusalem), English translation.

Khriplovich I.B., Novikov V.N., Sushkov O.P., 1976, *Sov. Phys.* JETP, 44, 872

Kim J.E., et. al., 1981, *Rev. Mod. Phys.* 53(2), 211

Kogelnik H.W., Ippen E.P., Dienes A., Schank C.V., 1972, IEEE J.Q.E, QE-8, 373

Koopmans T., 1933, *Physica*, 1, 104

Lee T.D., Yang C.N., 1956, *Phys. Rev*, 104, 254

Levy L.P., Williams W.L., 1982, *Phys. Rev. Lett.*, 48, 607

Lindgren I., 1985, *Phys. Rev. A*, 31, 1273

Lindgren I. and Morrison J., 1986, *Atomic Many-Body Theory*, (Springer series on Atoms and Plasmas)

Lindroth E.C., *Pair Correlation in Atomic Systems - Towards a Relativistic Treatment*, D. Phil. thesis, Goteborg, Sweden

Lynn B.W., 1982, Columbia U. PhD Thesis

Lynn B.W., 1984, *Atomic Physics* 9, Ed. Van Dyck, Fortson, Washington, World Scientific

Macpherson M.J.D., 1988, D.Phil. Thesis, Oxford

Macpherson M.J.D, Stacey D.N., Baird P.E.G., Hoare J.P., Sandars P.G.H., Tregidgo K.M.J., Wang Guowen, 1987, *Europhys Lett*, 4, 811

Malvern A.R., 1974, D. Phil Thesis, Oxford

Mandl F., Shaw G., 1984, *Quantum Field Theory*, Wiley

Marciano W.J., Sirlin A., 1983, *Phys. Rev.* D, 27, 552

Martensson-Pendrill A.M., 1985, *J. Physique*, 46, 1949

Martensson-Pendrill A.M., 1986, *preprint*, Chalmers University

Martensson-Pendrill A.-M., 1987, *Physica Scripta*, 36, 122

Martensson A.M., Henley E.M. and Wilets L., 1981, 24, 308

McKoy V., 1980, *Physica Scripta*, 21, 238

Moore C.E., 1971, *Atomic Energy Levels*, Natl. Bur. Stand. Ref. Data Ser., Vol. III.

Neuffer D.V. and Commins E.D., 1977, *Phys Rev A*, 16, 844

Norcross D.W., 1973, *Phys. Rev. A*, 7, 606

Noecker M.C., Masterson B.P., Weiman C.E., *Phys. Rev. Lett.*, to be published.

Novikov V.N., Sushkov O.P., Khriplovich I.B., 1976, *Sov. Phys.* JETP, 44, 872

Novikov V.N., Sushkov O.P., Flambaum V.V., Khriplovich I.B., 1977, *Sov. Phys.* JETP, 46, 420

Perkins D.H., 1982, *Introduction to High Energy Physics*, Addison Wesley.

Plummer E., 1984, D.Phil thesis, Oxford

Plummer E.P. and Grant I.P., 1975, *J. Phys. B: At. Mol. Phys.*, 18, L315-20

Prescott C.Y., et. al., 1978, *Phys. Rev. Lett.*, 77B, 347

Prescott C.Y., et. al., 1979, *Phys. Rev. Lett.*, 84B, 524

Press, Flannery, Teukolsky, Vetterling, 1986, *Numerical Recipes*, C.U.P.

Roberts G.J, et. al., 1980, *J. Phys.* B, 13, 1389

Romanek K.M., Hildebrand O., Gobel E., 1977, *Opt. Comm.*, 21, 16

Rose M.E., 1961, *Relativistic Electron Theory*, (Wiley J. and Sons, inc.)

Rowe D.J. and Ngo-Trong C., 1975, *Rev. Mod. Phys.*, 47 no.2, 471

Rubbia C. et. al., 1983, *Phys. Lett.*, 126B, 398

Rubbia C. 1985, *Rev. Mod. Phys*, 57, 699

Salam A., 1968, *Elementary Particle Physics*, ed. Svartholm, Stockholm

Sandars P.G.H.S., 1977, *J. Phys.* B., 10, 2983

Sandars P.G.H.S., 1984, *Atomic Physics* 9, Ed. Van Dyck, Fortson, Washington, World Scientific

Sandars P.G.H.S., 1985, *Tests of Electroweak Theories*, Ed. B.W. Lynn, C. Verzegnassi, World Scientific

Schwartz C., 1955, *Phys. Rev.* 97, 380; see also [Case Studies] p150

Selby D.R., 1981, D. Phil Thesis, Oxford

Senior J., 1985, *Optical Fibre Communications: Principles and Practice*, Prentice Hall

Shabanova L., Monakov Yu. and Khlyustalov A., 1979, *Opt. Spect.* 47, 3

Snyder A.W., 1981, *Proc.* IEEE, 69, 6

Sucher J., 1980, *Phys. Rev. A*, 22, 348

Sushkov O.P., Flambaum V.V., Khriplovich I.B., 1976, *Sov. Phys.-JETP*, 44, 872

Sushkov O.P., 1987, *Proc.* IX *Vavilov Conference on Nonlinear Optics*, to be published in Kvantovaya Electronika

t'Hooft G., 1971, *Nucl. Phys.*, B33, 173

Taylor J.D., 1984, D. Phil Thesis, Oxford

Taylor J.D., Baird P.E.G., Hunt R.G., Macpherson M.J.D., Nowicki G., Sandars P.G.H., Stacey D.N., 1987, *J. Phys.* B., 20, 5423

Topping, 1960, *Errors of observation and their treatment*, Chapman Hall

Trainor T.A., 1979, *Proc. Int. Workshop on Neutral Currents*, Ed. Williams, Cargèse

Tregidgo K.M.J., 1984, D. Phil Thesis, Oxford

Tregidgo K.M.J., Baird P.E.G., Macpherson M.J.D., Palmer C.W.P., Sandars P.G.H., Stacey D.N.S., Thompson R.C., *J. Phys.* B, 19, 1143

Ulrich R., Simon A., 1979, *App. Opt.* 18, 224

Varnham, Payne, Barlow, Tarbox, 1984, *Opt. Lett.*, 9, 306

Veltman M., 1983, *Proc. International Europhysics Conference on High-Energy Physics,* Ed. Guy, Costain, R.A.L., 880

Weast R.C., 1974, *Handbook of Physics and Chemistry*, CRC Press

Weinberg S, 1967, *Phys. Rev. Lett.*, 19, 1264

Wu C.S., et. al., 1957, *Phys. Rev.*, 105, 1413

Yang K.H., 1976, *Ann. Phys. (NY)*, 101, 62

Zel'dovich Y.B., 1959, *Sov. Phys.* JETP, 9, 682

Zel'dovich Y.B., 1957, *Sov. Phys.* JETP, 6, 1184

ॐ परमात्मने नमः

इति